SYNTHESIS, CHARACTERIZATION AND CAPILLARY ELECTROPHORETIC USE OF NEW, SINGLE-ISOMER HEXASULFATED a-CYCLODEXTRINS

A Dissertation

by

SHULAN LI

Submitted to the Office of Graduate Studies of
Texas A&M University
in partial fulfillment of the requirements for the degree of

DOCTOR OF PHILOSOPHY

May 2004

Major Subject: Chemistry

SYNTHESIS, CHARACTERIZATION AND CAPILLARY ELECTROPHORETIC USE OF NEW, SINGLE-ISOMER HEXASULFATED a-CYCLODEXTRINS

A Dissertation

by

SHULAN LI

Submitted to Texas A&M University
in partial fulfillment of the requirements
for the degree of

DOCTOR OF PHILOSOPHY

Approved as to style and content by:

Gyula Vigh (Chair of Committee)	Manuel P. Soriaga (Member)
Marvin W. Rowe (Member)	Victoria J. DeRose (Member)
Emile A. Schweikert (Head of Department)	Edward A. Funkhouser (Member)

May 2004

Major Subject: Chemistry

ABSTRACT

Synthesis, Characterization and Capillary Electrophoretic Use of New, Single-isomer Hexasulfated α-Cyclodextrins. (May 2004)

Shulan Li, B.S., Shandong University of Building Material;

M.S., Shandong University

Chair of Advisory Committee: Dr. Gyula Vigh

The first three, pure, single-isomer, 6-*O*-sulfo α-cyclodextrins, the sodium salts of hexakis(6-*O*-sulfo)-α-CD (HxS), hexakis(2,3-di-*O*-methyl-6-*O*-sulfo)-α-cyclodextrin (HxDMS) and hexakis(2,3-di-*O*-acetyl-6-*O*-sulfo)-α-cyclodextrin (HxDAS) have been synthesized, analytically characterized and utilized as chiral resolving agents in capillary electrophoresis. The purity of each synthetic intermediate and of the final product was determined by HPLC-ELSD and indirect UV-detection capillary electrophoresis. The structural identity of each intermediate and final product was verified by 1D and 2D NMR, and mass spectrometry.

HxS, HxDMS and HxDAS have been used to separate a series of neutral, basic, ampholytic and acidic enantiomers in pH 2.5 and pH 9.5 aqueous and acidic methanol background electrolytes using capillary electrophoresis. Rapid separations with satisfactory peak resolution values were obtained for most of the analytes, indicating that HxS, HxDAS and HxDMS can serve as chiral resolving agent for a wide range of analytes. The observed separation patterns follow the predictions of the CHArged Resolving agent Migration (CHARM) model. The separation patterns observed with HxS, HxDAS and HxDMS as chiral resolving agent were compared with those of (1) β-cyclodextrin analogues, such as, heptakis(6-

O-sulfo)-β-cyclodextrin (HS), heptakis(2,3-di-*O*-acetyl-6-*O*-sulfo)-β-cyclodextrin (HDAS) and heptakis(2,3-di-*O*-methyl-6-*O*-sulfo)-β-cyclodextrin (HDMS); (2) γ-cyclodextrin analogues, such as, octakis(6-*O*-sulfo)-γ-cyclodextrin (OS), octakis(2,3-di-*O*-acetyl-6-*O*-sulfo)-γ-cyclodextrin (ODAS) and octakis(2,3-di-*O*-methyl-6-*O*-sulfo)-γ-cyclodextrin (ODMS). The effects of the structure of the analytes, and those of the pH and the solvent of the background electrolyte were also studied.

To my husband, Xiaodong, my daughter, Tong, my parents, Peiqiao and Qinying, and parents-in-law, Chuntian and Baorong for their unconditional support.

ACKNOWLEDGMENTS

I would like to express my deep gratitude to my advisor Professor Gyula Vigh for his great support and guidance during my studies at Texas A&M University. His patience and help made this work possible. His enthusiasm and brightness at work and his high requirements encouraged me to do my best in my studies. I really appreciate the time and efforts of my committee members: Dr. DeRose, Dr. Rowe, Dr. Soriaga, and Dr. Funkhouser. The help from the Chemistry Department is also greatly appreciated. I would like to thank my co-workers for their kind help and friendship: Dr. Ivan Spanik, Dr. Arne Kolberg, Nellie Fleisher, Dawn Kirby Maynard, Wenhong Zhu, Brent Busby, Adriana Salinas, Silvia Sanchez-Vindas, Kinsley Nzeadibe, Sanjiv Lalwani, Ann Hwang, Peniel Lim, Omar Maldonado, Evan Shave, Brian Sinajon, Roy Estrada, and Ilson Steidel. Finally, I would like to thank the funding agencies for their support: the Texas Advanced Research Program, J&W Scientific Inc., Beckman-Coulter Instruments, and CereStar Incorporated.

TABLE OF CONTENTS

CHAPTER Page

CHAPTER Page

LIST OF FIGURES

FIGURE Page

FIGURE Page

FIGURE Page

FIGURE Page

FIGURE Page

LIST OF TABLES

CHAPTER I

INTRODUCTION

1.1 Enantiomers Separation and Capillary Electrophoresis

For many synthetic, biological organic compounds and widely prescribed drugs, chirality is one of their important properties [1]. When a chiral environment is absent, the enantiomers cannot be differentiated because they have the same physical and chemical properties. However, enantiomers can be distinguished in a chiral environment, such as in biological systems, including human bodies [2], which can lead to different pharmacokinetic, pharmacologic and toxicologic properties for the enantiomers. For some of the chiral drugs, one of the enantiomers exhibits the desired biological or pharmaceutical activity, which the other enantiomer can be inactive, or have side effects, even toxic effects. Therefore, the pharmacological effects and metabolic pathways for each enantiomer of a new chiral drug must be studied before it is approved for use in humans [3,4]. Since enantiomeric separation on an analytical scale is required both for monitoring the enantiomeric purity of the chiral drug, and for performing drug metabolism, pharmacokinetic and clinical studies, separation techniques play an important and essential role [5].

Different techniques can be used for enantiomer separations, such as gas chromatography (GC) [6], high performance liquid chromatography (HPLC), including both reversed phase and normal phase HPLC [7-21], supercritical fluid chromatography (SFC)

This dissertation follows the style and format of Journal of Chromatography A.

[22,23], capillary electrochromatography (CEC) [22-26], and capillary electrophoresis (CE)[27-35]. Though the separation efficiency of capillary GC is high, it is limited to the analysis of volatile analytes or their derivatives. Compared to CE, HPLC has lower separation efficiency and requires larger amounts of chiral resolving agents. SFC with a chiral stationary phase has the same disadvantages as HPLC. The use of CE for enantiomer separation has attracted considerable attention as a result of its distinct separation mechanism, high separation efficiency, versatility, low running costs, rapid method development, speed of analysis, small sample volumes, and low consumption of chiral resolving agents and solvents [33, 36-46]. There are indirect and direct CE enantiomer separation methods. Compared to the indirect CE method, which needs to introduce another chiral center into the target analyte to form two diastereomers, the direct CE method simply requires the addition of a chiral selector to the BGEs [26, 33, 46].

1.1.1 Generation of EOF and Its Roles

The electroosmotic flow (EOF), which acts as the pump in HPLC but without the mechanical complexity of HPLC pump, is one of the advantages of CE [47]. The EOF is generated due to the partial dissociation of silanol groups on the inner surface of the fused silica capillary which creates immobile negative surface charges. In order to maintain electric neutrality, the immobile SiO^- groups attract mobile cations from the background electrolytes (BGEs). Some of the cations from the BGEs are attracted strongly and form the compact (Stern) layer. The less-tightly held cations in the diffuse (Gouy-Chapman) layer are farther out into the solution. Thus, a double layer is formed, and the potential at the shear plane between these two layers is known as the zeta (ζ) potential [48]. During a CE run, when potential is applied

across the capillary, charged particles outside the shear plane move with a constant velocity. The solvated mobile cations in the diffuse layer migrate toward the cathode dragging along their hydrate layer (bulk solvent). Since the SiO^- groups can not move, an unbalanced bulk flow, the electroosmotic flow (EOF) arises. The radial velocity profile of electroosmotic flow is plug-like, not parabolic as with pressure driven flow [49]. This eliminates the most significant band broadening mechanisms (parabolic flow profile, multiple flow paths) that limit column efficiency in HPLC and provides CE with an order of magnitude higher separation efficiency than HPLC. When the reciprocal of the Debye-Huckel parameter, 1/k, called the thickness of the double layer, is much smaller than the radius of a capillary r, the electroosmotic flow velocity ν^{eo} depends on the permittivity of the medium (ε), the dielectric constant (ε_0), the zeta potential of the capillary wall (ζ), the dynamic viscosity of the medium (η) and the applied electric field strength (E). The relationship between these parameters can be described by the following formula [47]:

$$n^{eo} = -ze_0eE/h \tag{1}$$

Here, the negative sign means that when ζ is negative, the bulk flow is toward the negative electrode. The ζ potential, whose value depends on the surface charge density (σ), ionic strength (I), the permittivity of the medium (ε) and the dielectric constant (ε_0), can be written as [47]:

$$z = -s(RT/e_0eIF^2)^{1/2}/h \tag{2}$$

Thus,

$$\mu^{eo} = \nu^{eo}/E = -\varepsilon\zeta/\eta = \varepsilon(\varepsilon_0 \varepsilon RT/IF^2)^{1/2}/\eta \quad (3)$$

i.e. EOF mobility depends on the ionic strength (I) and the viscosity of the solution. Since viscosity changes around 2 % /°C, it is mandatory to control the temperature in capillary electrophoresis.

In CE, separation of the charged analytes depends on their mobility (μ) difference in the applied electric field, which is proportional to their charge to hydrodynamic size ratios:

$$\mu = z/(6\pi\eta r) \quad (4)$$

where z is the charge number of the analyte, r is the hydrodynamic radius of the analyte ion, and η is the viscosity of the solution. Charged molecules migrate with the observed mobility (μ^{obs}) which is a combination of their electrophoretic mobility (μ^{eff}) and the non-selective electroosmotic mobility (μ^{eo}):

$$\mu^{obs} = \mu^{eff} + \mu^{eo} \quad (5)$$

Since non-charged molecules have zero effective mobilities, they will arrive the detector at the same time by migrating with the electroosmotic flow (EOF), a charged agent need to be used to separate neutral components from each other in CE.

1.1.2 Role of Background Electrolytes

The major purposes of BGEs are to conduct the electric current for the separation of analytes and to regulate the pH. Suitable BGEs must contain enough ions (including cations or

anions) to transport the electric current, and also must have significant buffering capacity at the selected pH [50]. When a voltage is applied across the capillary and generates an electric current, the temperature of the solution increases due to generation of Joule heat. The increased temperature of the solution will change the properties of the BGEs (such as viscosity, EOF, etc.). Joule heat will also cause temperature differences (ΔT) between the walls and the center of the capillary [51]. ΔT depends on the electric field strength (E), the conductivity of the solution (k)and the capillary radius (r) [51]:

$$\Delta T \sim E^2 k r^2 \quad (6)$$

The temperature difference leads to extra peak broadening which in turn decreases separation efficiency and peak resolution. According to Equation 6, low-conductive BGEs, which can bring low currents, are preferred.

The mobility of EOF mainly depends on the pH and ionic strength of the BGEs. Analyte mobility (μ) also strongly depends on the ionic strength (I) and the charge of the analyte (z) [52-54].

$$m = exp(-0.77(zI)^{1/2}) \quad (7)$$

where, $$I = 0.5 \Sigma c_i z_i^2 \quad (8)$$

and c_i is the concentration of the component i of the BGE, and z_i is the charge of the component. Higher BGEs ionic strength will lower both the analyte and EOF mobilities.

1.2 Chiral Resolving Agents and Charged Cyclodextrins

By adding a chiral resolving agent to the BGEs to provide enantioselective intermolecular interactions, the enantiomers may form diastereomeric complexes with the chiral resolving agent in a dynamic equilibrium process. If the complexation constants of the enantiomers with the chiral resolving agent are different, enantiomer separations in CE can be achieved. The chiral resolving agents can be crown ethers [55-57], macrocyclic antibiotics [58-62], cyclopeptides [63, 64], proteins [65, 66], chiral surfactants (including amino acid based surfactants, bile salts and glycosidic surfactants) [67, 68], chiral calixarenes [69], polysaccharides and cyclic carbohydrates [70, 71], cyclodextrins (CD) [33, 36, 72-74], etc. Among all the resolving agents that were used, CDs proved to be the most useful [33, 36, 72-74]. Native CDs are relatively cheap, stable, have low toxicity, are relatively soluble in aqueous BGEs, and are transparent above 210 nm which makes UV detection possible [33, 36, 72-74]. Native CDs are neutral, cyclic, nonreducing oligosaccharides obtained from enzymatic degradation of starch, and consist of six (α-), seven (β-), and eight (γ-) D(+)-glucopyranose units bonded through α-(1,4) linkages to form truncated cones with relatively hydrophobic cavities and hydrophilic exteriors. The crystallographic diameter of the hydrophobic cavity is 0.57, 0.78, and 0.95 nm for α-, β-, and γ- CD, respectively [75]. The secondary hydroxyl groups are located on the wider side of the cone, while the primary hydroxyl group are located on the narrow side of the cone. CDs can form inclusion complexes with a wide range of small molecules. Chiral recognition in CDs comes from the five asymmetric chiral carbons on each glucose units [72]. Depending on the inner diameter of the cavity of the CDs and the size of the analytes, analytes can form host-guest complexes in dynamic equilibrium with CDs through full or partial inclusion into cavities of the CDs. Formation and stabilization of the host-guest

inclusion complexes is influenced by the steric parameters of the analytes, and by the possibility of creating intermolecular interactions, such as hydrogen bonding, Van der Waals interactions, metal coordination, Coulombic interactions, and hydrophobic interactions between substituents of the analyte and the CDs [76]. The interaction strength of the two enantiomers with the host-cyclodextrin molecule will be different from each other, which leads to different complex formation constants. This, in turn, leads to different electrophoretic mobilities and possibly CE separation.

The hydroxyl groups of CDs can be chemically modified to enhance the hydrophobicity of the CD by alkylation or to improve their solubility by adding polar or nonpolar groups to the CDs. Derivatization of α-, β-, and γ-CDs can change their chiral recognition ability and their physicochemical properties (such as, their solubilities in selected solvents).

Native CDs and their neutral derivatives, such as, 2,6-dimethyl-, 3,6-dimethyl-, 2,3,6-trimethyl- [77, 78], 2,3-diacetyl-, 2,3- hydroxyethyl, 2,3-hydroxypropyl- [26, 79], cyanoethyl [80], mono-3-phenylcarbamoyl [81], have been used extensively as chiral resolving agents in CE. They can not be used to separate neutral analytes since neutral analytes have zero effective mobility. Charged cyclodextrin derivatives provide at least two important advantages over neutral CDs. First, both neutral analytes and charged analytes can be enantioresolved with charged CDs. Second, the introduction of ionic groups onto the CD rim or connected to it via a short alkyl chain enhances the solubility of charged CDs in aqueous media [74, 82]. Charged cyclodextrin derivatives, including weak and strong electrolyte cationic and anionic derivatives have been used as chiral resolving agents to separate neutral analytes. Though weak electrolyte CDs, including anionic carboxymethyl-, carboxyethyl-, succinyl-, phosphate- [83, 84] and cationic methylamino-, ethylamino-, mono-6-amino-6-deoxy, mono-6-β-aminoethylamino-6-

deoxy- [76, 85-87] derivatives, can provide special selectivity for certain analytes, their charge number depends on the pH and can only be used in a limited pH range. The zwitterionic CDs derivatives [88-89], for example mono-6-δ-glutamylamino-6-deoxy-β-CD [88], also behave as weak electrolytes CDs derivatives and their charge depends on the pH of the buffer.

Strong electrolyte CDs, including cationic and anionic derivatives can be used over the entire working pH range of CE and make optimization of enantiomer separations possible. However, cationic CDs, such as quaternary ammonium-β-CD, 2-hydroxy-3-trimethylammoniumpropyl-β-CD, 6-tris(hydroxyethylamino)-β-CD, 2-hydroxypropyltrimethyl ammonium β-CD [90-92] adsorb on the negatively-charged wall of the fused silica capillary and act as a stationary phase, which reduces the separation efficiency. Therefore permanently-charged, anionic CDs, including sulfoethyl ether-, sulfopropyl ether-, sulfobutyl ether- [93-96], and sulfated-CDs [97, 98], which cannot adsorb on the negatively charged wall, have attracted attention.

Most commercially available charged CDs are randomly substituted, which means that they are complex mixtures of different isomers with different substitution positions and different degrees of substitution. The effective mobilities of the CD isomers differ when their degree of substitution is different. The complexation rates of the different CD isomers are also slightly different, consequently kinetic band broadening can occur, and lead to decrease of separation efficiency. Each CD isomer may have their own selectivity for a given pair of enantiomers. Mixtures of CD isomers may reduce, cancel or enhance the overall separation selectivity of a CE system. With resolving agent mixtures, fundamental molecular-level studies, such as NMR, crystallographic, and molecular modeling studies, which can help the understanding of the chiral recognition process are not possible. Compositional variation in the randomly substituted

CDs in different batches can cause unpredictable separations [99-101]. All these problems make rational experimental design difficult. Therefore, it is very important to synthesize single isomer charged CDs with control over both the degree and the site of substitution. Since 1997, Vigh and coworkers synthesized, purified and characterized a family of single-isomer CDs and used them for CE enantiomer separations, including heptakis(6-sulfo)-β-CD [102], heptakis(2,3-diacetyl-6-sulfo)-β-CD [103], heptakis(2,3-dimethyl-6-sulfo)-β-CD [104], octakis(6-sulfo)-γ-CD [105, 106], octakis(2,3-diacetyl-6-sulfo)-γ-CD [107-109], octakis(2,3-dimethyl-6-sulfo)-γ-CD [110-112] and heptakis(2-methyl-3,6-di-sulfo)-β-CD [113].

1.3 Theoretical Background and CHARM Model

Several research groups have developed theoretical models to describe CE enantiomer separations [114-118]. Wren and Rowe's model [117] related the mobility to the concentration of CD selectors:

$$Dm_{ep} = m_A - m_B = [C](m_f - m_c)(K_B - K_A)/\{1 + [C](K_A + K_B) + K_A K_B [C]^2\} \quad (9)$$

where, $\Delta\mu_{ep}$ is the difference in the apparent electrophoretic mobility of the enantiomer pair, μ_A and μ_B, μ_f is the electrophoretic mobility of the analyte in free solution, μ_c is the electrophoretic mobility of the analyte-chiral resolving agent complex, K_A and K_B are equilibrium constants, and [C] is the concentration of the chiral resolving agent. Selectivity, which was expressed as the mobility difference, depends not only on the chiral discrimination ability of the chiral resolving agent (expressed by the two binding constants K_A, K_B), but also

on the mobility difference between the free and complexed forms of the enantiomers. In 1994, Goodall [118] proposed another theoretical model to consider both mobility differences and resolution. However, these models were only suitable for neutral analytes and charged chiral resolving agents.

In 1994, Vigh's group introduced a multiple-equilibria-based model, called the CHArged Resolving agents Migration model (CHARM model) [119], for rational, predictable design of separation with charged chiral resolving agents for the enantiomers of chiral weak electrolytes (including weak acids and weak bases) and neutral analytes as a function of both pH and the concentration of the single-isomer, permanently-charged cyclodextrins. According to this paper, peak resolution and separation selectivity depend on the pH of the BGEs, the EOF rate, the charge number of the resolving agent, the effective charge number of the analytes and the CD concentration. Resolution of the two enantiomer
peaks was expressed as [115, 119]:

$$Rs \sim [(\alpha-1)[(\alpha+b)(1+b)(Z_1)(Z_2)]^{½} / \{[(\alpha+b)^3(Z_1)]^{½}+[\alpha(1+b)^3 Z_2]^{½}\} \quad (10)$$

Here, k is the Boltzman constant, e_o is the electric charge, T is the absolute temperature, l is the capillary length from injector to the detector, E is the electric field strength, α is separation selectivity which can be defined as the mobility ratio of two enantiomers:

$$\alpha = m_1^{eff}/m_2^{eff} \quad (11)$$

and β is the normalized electroosmotic flow mobility, defined as:

$$b = m^{eo} / m_2^{eff} \qquad (12)$$

Thus, peak resolution depends on α, β and Z^{eff}. If all the other parameters are kept constant, the higher the Z^{eff} , the higher the resolution. It also shows that initially, peak resolution increases linearly with α. The α value depends on the ionic mobilities of the free and complexed analytes, the binding constants, the pH of the BGEs, and the concentration of the chiral resolving agent. Another key to the development of enantiomer separations is to optimize the β term by using a coated capillary and / or appropriate background electrolyte constituents. Under identical α and Z^{eff}, peak resolution increases towards infinitely high values as β approaches -1. As long as the CD shows any selectivity for the enantiomers, peak resolution can be improved by optimizing β at the expense of increased analysis time.

Because α-, β-, and γ- cyclodextrins and their corresponding derivatives have different cavity sizes, their complexation strength with analytes will be different. Since single isomer, sulfated α-CDs have not been made yet, this dissertation will discuss the synthesis, analytical characterization and applications of a new class of single-isomer sulfated cyclodextrins, hexakis(2,3-di-*O*-acetyl-6-*O*-sulfo)-α-CD (HxDAS), hexakis(2,3-di-*O*-methyl-6-*O*-sulfo)-α-CD (HxDMS) and hexakis(6-*O*-sulfo)-α-CD (HxS).

CHARTER II

SYNTHESIS AND CHARACTERIZATION*

Single isomer CDs, sulfated β- and γ-CD derivatives, are now commercially available. In this work, the first three single-isomer, 6-sulfated α-CDs, the sodium salts of hexakis(2,3-di-*O*-acetyl-6-*O*-sulfo)-α-CD (HxDAS), the sodium salts of hexakis(6-*O*-sulfo)-α-CD (HxS), and the sodium salts of hexakis(2,3-di-*O*-methyl-6-*O*-sulfo)-α-CD (HxDMS) have been synthesized on a large scale and analytically characterized.

2.1 Materials and General Methods

Except for native α-CD, which was purchased from Cargill (Hammond, IN, USA), all chemicals used in this work were obtained from Aldrich Chemical Company (Milwaukee, WI, USA). For the α-CD intermediates, progress of the reaction was monitored by thin layer chromatography (TLC), using Silica-60 plates (E. M. Science, Gibbstown, NJ). The developed plates were visualized by dipping them into an α-naphthol staining solution (mix 26.25 g of α-naphthol, 315 ml of 100% ethanol, 105 ml of concentrated sulfuric acid, and 66 ml of distilled water) and heating for 10 min at 100°C.

The purity of the intermediates was determined by analytical isocratic HPLC using a Programmable Solvent Module 126 (Beckman-Coulter, Fullerton, CA), a Sedex Model 55

---

* Part of this chapter is reprinted with permission from: S. L. Li and Gy. Vigh, Electrophoresis, 24 (2003) 2487-2498; Copyright 2003 - Wiley -VCH.

evaporative light scattering detector (S.E.D.E.R.E., Alfortville, France), and an AD 406 data acquisition system operated under Gold 8.1 software control (Beckman-Coulter) running on a 486DX4 personal computer (Computer Associates, College Station, TX). The separations were obtained on a 4.6mm I. D. × 250mm column packed with a 5μm Zorbax ODS stationary phase (Agilent, Newport, DE). The purity values reported in this dissertation were calculated on the assumption that the response factors of the evaporative light scattering detector were the same for all CD isomers. The progress of the sulfation reaction and the purity of the sulfated α-CD products were monitored by indirect UV detection CE using a P/ACE 2000 system (Beckman-Coulter), at 214 nm and 10 kV applied potential, on a 26.4 / 19.6 cm long, 26μm I. D. bare fused silica capillary column (Polymicro Technologies, Phoenix, AZ). The cartridge coolant of the P/ACE 2000 was thermostated at 20°C.

The molecular weight of the intermediates was obtained by high resolution MALDI-TOF-MS. A Voyager Elite XL TOF mass spectrometer equipped with delayed extraction capability (PerSeptive Biosystems, Framingham, MA) in reflectron mode, with an acceleration voltage of 25 kV, 70% grid voltage, 0.035% guide wire voltage, and a delay of 180 μs, was used to collect high-resolution mass spectra. The analytes were spotted onto a Teflon target using the dried droplet method [120]. The matrix was prepared by dissolving 10 mg 2,4,6-trihydroxyacetophenone in 1mL acetonitrile [121].

The molecular weight of products HxDAS, HxS, and HxDMS were obtained by ESI-TOF-MS with a Vestec Model 201-A single quadrupole mass spectrometer equipped with a Vestec electrospray ion source (PerSeptive Biosystems). The sample was prepared at a concentration of 4 mg/mL in an ACN : water 1:1 (v/v) solvent mixture.

^{1}H and ^{13}C NMR spectra were measured on UnityPlus 300 and 500 spectrometers with a quad nucleus (^{1}H / ^{19}F / ^{31}P / ^{13}C) probes, which employed Solaries 2.4 and Vnmrx 5.3 b softwares. The proton (H) and carbon (C) assignments were based on the ^{1}H-^{1}H 2D COSY (Correlation Spectroscopy) and ^{1}H-^{13}C HETCOR (Heteronuclear Chemical Shift Correlation) spectra.

The single crystal structure was obtained with a Bruker SMART 1000 X-ray Diffractometer (Bruker AXS, Madison WI) to collect diffraction data, and the structure was solved by the SHELXTL program suite [122]. Crystal structure figures and solvent-accessible surfaces were obtained with the Insight II program, and the Connolly algorithm as implemented in Insight II [123].

2.2 Synthesis and Characterization of HxDAS, HxS and HxDMS

Regioselective protection methods for the 2,3,6-hydroxyl groups of native α-CD were used to synthesize, hexakis (2,3-di-*O*-acetyl-6-*O*-sulfo)-α-cyclodextrin (HxDAS), hexakis (6-*O*-sulfo)-α-cyclodextrin (HxS), and hexakis (2,3-di-*O*-methyl-6-*O*-sulfo)-α-cyclodextrin (HxDMS)according to the scheme shown in Figure 1. The details of the synthetic procedures are outlined in Appendix.

2.2.1 Hexakis(6-*O*-*tert*-butyldimethylsilyl)-a-Cyclodextrin

According to a modified procedure of Takeo [102, 124], the primary hydroxyl groups at the sixth position of the glucopyranose units of native α-CD (1) were protected by reacting them with *tert*-butyldimethylchlorosilane in DMF and CH_2Cl_2 to produce hexakis (6-*O*-*tert*-butyldimethylsilyl)-α-CD (intermediate (2)). The progress of the reaction was monitored by

TLC, using aluminum-backed Silica 60 plates and 50:10:1 $CHCl_3$: CH_3OH : H_2O as running solvent, giving an R_f=0.42 for intermediate (2). The purity of (2) was analyzed by isocratic non-aqueous reverse phase HPLC, using a 4.6mm × 250mm Zorbax C18 column and a 20: 80 EtOAc : CH_3OH mobile phase at 2mL / min at ambient temperature. Intermediate (2) with purity > 99 % was obtained using methylethylketone (MEKT) as the recrystallizing solvent. Figure 2 shows a non-aqueous, reversed-phase HPLC separation of (2) after recrystallization and its corresponding MEKT mother liquor. The HPLC method can detect as little as 0.1% impurity.

The structure of intermediate (2) was characterized by high resolution ^1H and ^{13}C NMR spectroscopy. The peak assignments for ^1H and ^{13}C NMR were determined from the 1-dimensional ^1H and ^{13}C NMR spectra, coupled with 2-dimensional ^1H-^1H COSY and ^1H-^{13}C HETCOR NMR spectroscopy (^1H NMR data in $CDCl_3$: δ 4.90 (doublet, 6 H-1, J_{1-2} = 2.5 Hz); δ 4.03 (triplet, 6 H-3, J_{3-2} = 8.7 Hz, J_{3-4} = 8.7 Hz); δ 3.94 (doublet, 6 H-6, $J_{6-6'}$ = 11.6 Hz); δ 3.84 (doublet, 6 H-5, J_{5-4} = 8.7 Hz); δ 3.76 (doublet, 6 H-6', $J_{6'-6}$ = 11.6 Hz); δ 3.63, 3.59 (12 H-2, 4); δ 0.89 (singlet, 6 **$(\underline{CH_3})_3$**C); δ 0.06, 0.05 (two sets of singlet, 6 **$(\underline{CH_3})_2$**Si); ^{13}C NMR data in $CDCl_3$: δ 101.78 (C-1); δ 81.53 (C-4); δ 74.60 (C-2); δ 73.25 (C-3); δ 72.46 (C-5); δ 62.20 (C-6); δ 26.21 ($(\underline{C}H_3)_3C$); δ 18.65 ($(CH_3)_3\underline{C}$); δ -4.93, -4.97 ($(\underline{C}H_3)_2Si$)). ^1H - ^1H COSY and ^1H - ^{13}C HETCOR NMR spectra in Figures 3 and 4 show only those proton and carbon contours that are related to the glucose unit. The *tert*-butyldimethylsilyl group portions are omitted, since their chemical shift are far away from those of the glucose unit, and can be

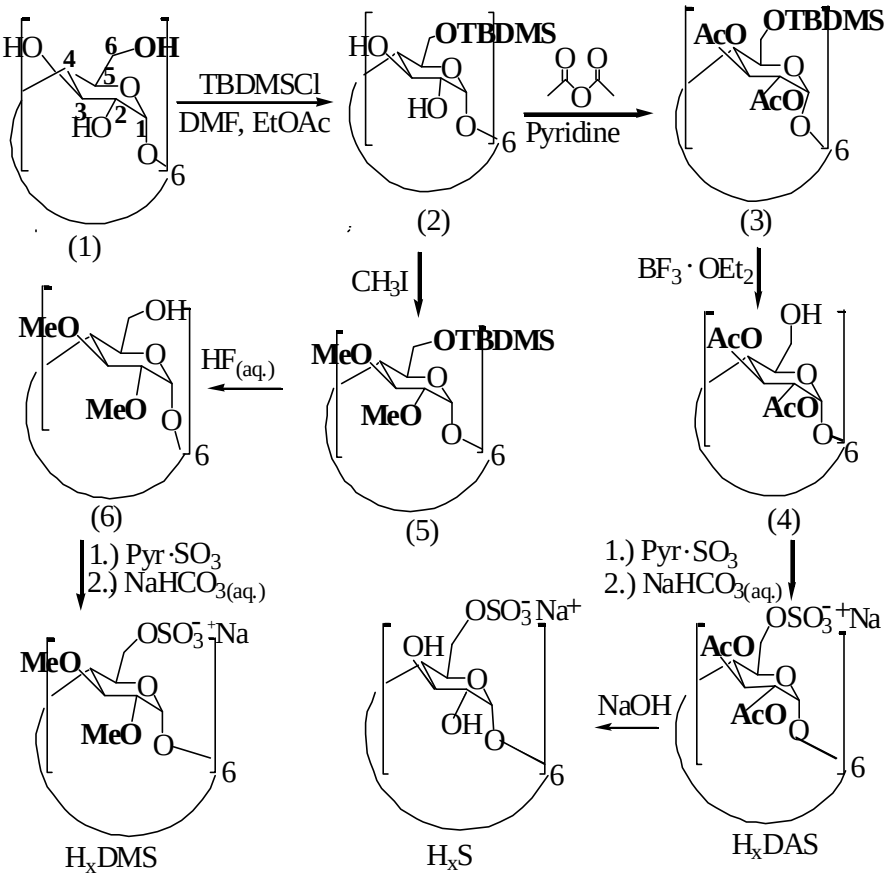

Figure 1. Synthesis scheme for hexakis(2,3-di-*O*-acetyl-6-*O*-sulfo)-α-CD (HxDAS), hexakis(6-*O*-sulfo)-α-CD (HxS), and hexakis(2,3-di-*O*-methyl-6-*O*-sulfo)-α-CD (HxDMS).

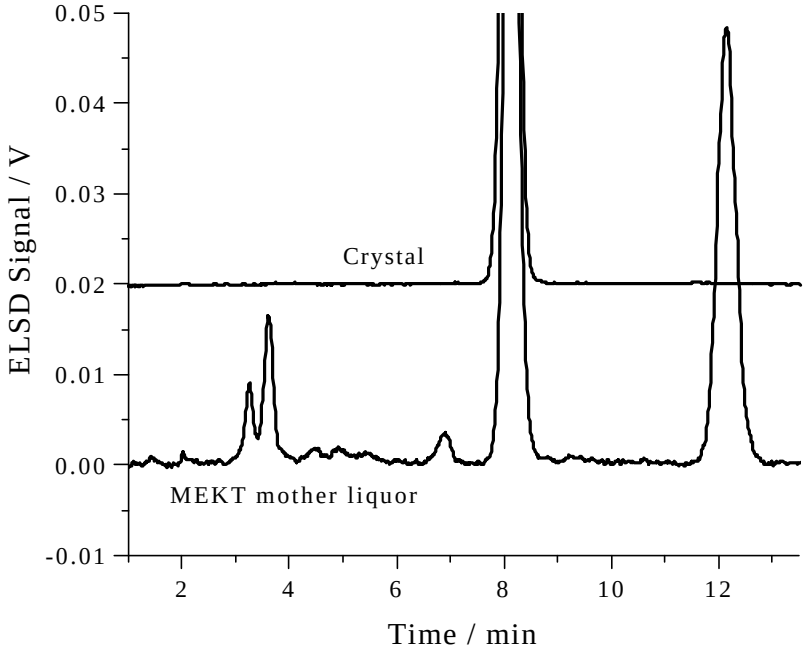

Figure 2. Chromatograms of crystalline (2) and its mother liquor. Purity of the product > 99 %. Conditions: EtOAc : MeOH = 80 : 20, F = 2mL / min, C18 column.

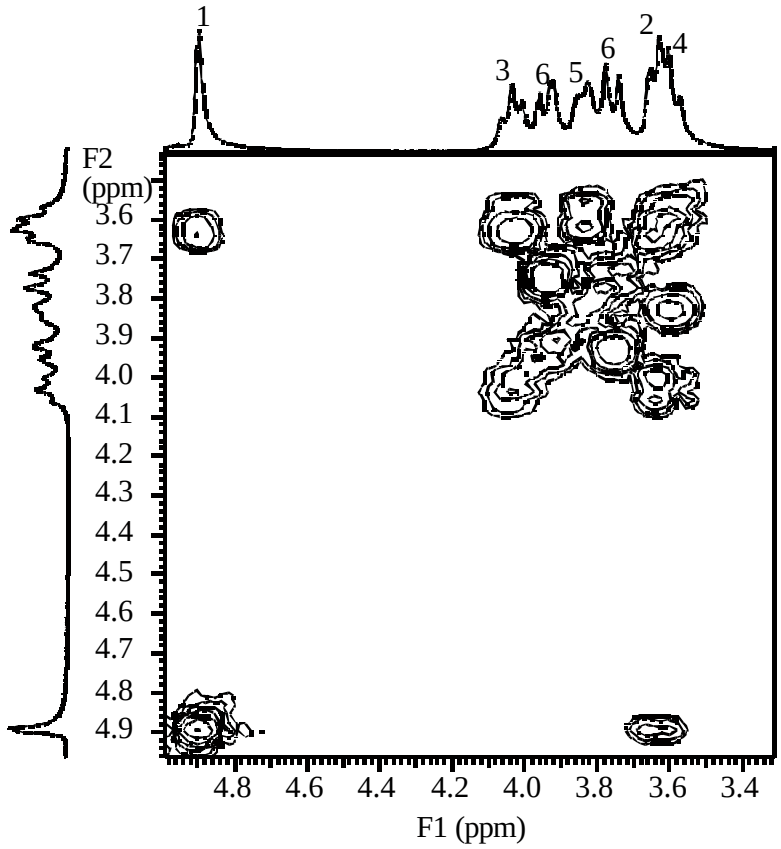

Figure 3. 2D COSY of (2) in $CDCl_3$ using 300 mHz NMR.

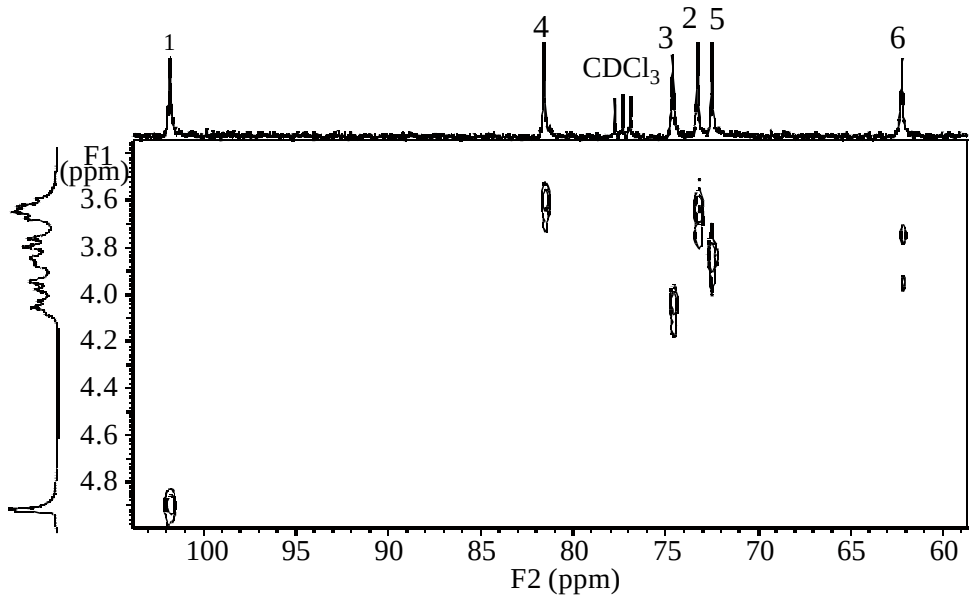

Figure 4. 2D HETCOR of (2) in $CDCl_3$ using 300 mHz NMR.

unambiguously assigned.

High resolution MALDI-TOF-MS was used to determine the molecular weight of intermediate (2). The MALDI-TOF-MS of the Na^+ and K^+ ion-adduct portion of intermediate (2) is shown in Figure 5: the calculated molecular weight values of the Na^+ and K^+ ion-adducts of the parent molecule, 1681.43 and 1697.53, agree well with the value obtained using MALDI-TOF-MS, 1680.89 and 1696.88 for the Na^+, K^+ ion-adducts, respectively, indicating the presence of six *tert*-butyldimethylsilyl groups on intermediate (2).

To prove structural identity, a single crystal of intermediate (2) was grown by dissolving intermediate (2) in ethanol to obtain a saturated solution, followed by evaporation of the solvent at room temperature in air to give white, transparent, single crystals suitable for x-ray diffraction analysis. The crystal structure of intermediate (2) is shown in Figure 6, indicating that the *tert*-butyldimethylsilyl ether groups are located on C6 in each of the six glucose subunits. The Connolly surface rendering of intermediate (2) demonstrated that this intermediate has a large hydrophobic surface.

2.2.2 Hexakis(2,3-di-*O*-acetyl-6-*O*-*tert*-butyldimethylsilyl)-a-Cyclodextrin

Hexakis(2,3-di-*O*-acetyl-6-*O*-*tert*-butyldimethylsilyl)-α-CD (3), was obtained by complete acetylation of the 2,3-hydroxyl groups of intermediate (2) with acetic anhydride in ethyl acetate solvent. The progress of the reaction was monitored by TLC, using Silica 60 plates and 4:1 toluene : EtOH as running solvent, giving an R_f = 0.56 for intermediate (3). Using DMF as the recrystallizing solvent, intermediate (3) with a purity > 99 % was obtained,

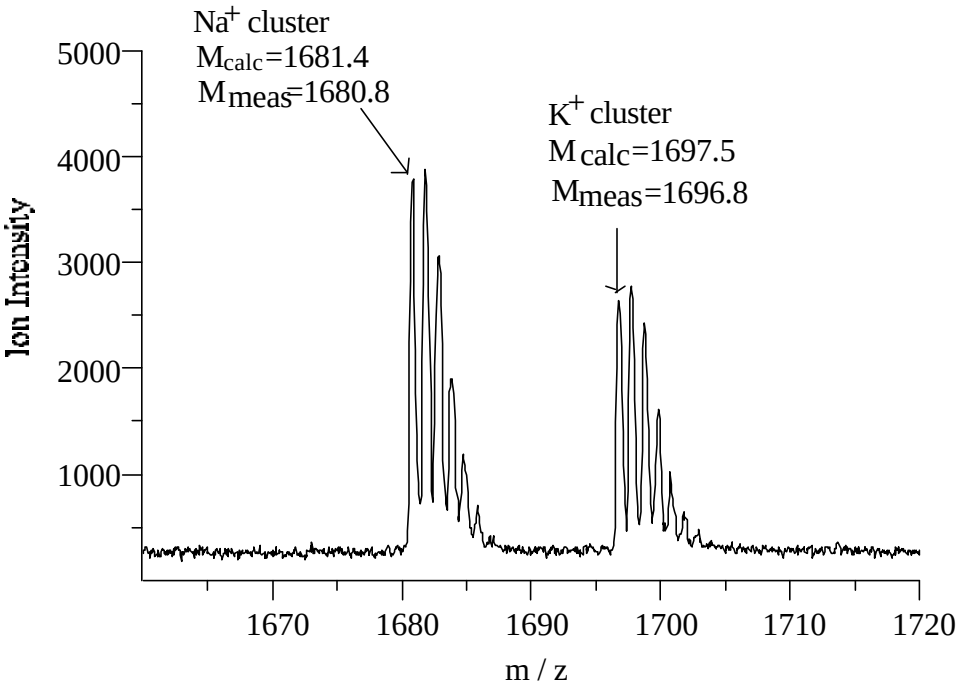

Figure 5. MALDI-TOF-MS spectrum of (2).

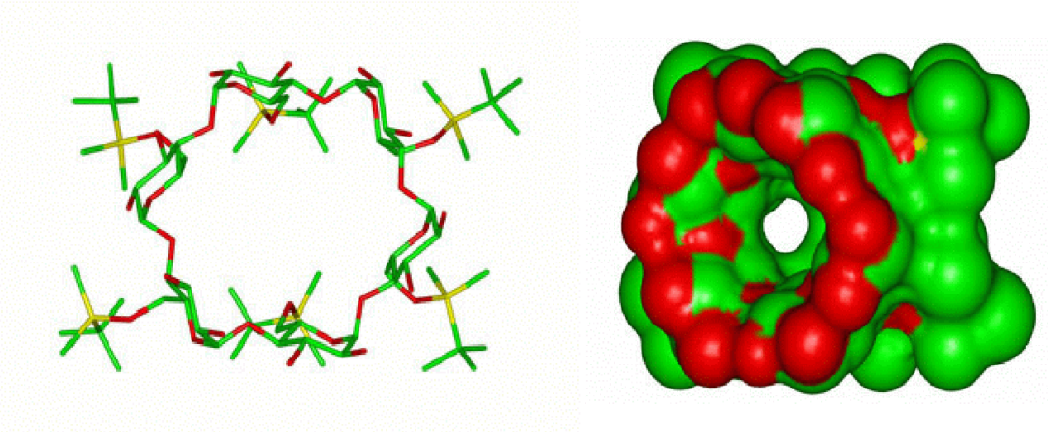

Figure 6. X-ray crystal structure of (2) and the Connolly surface rending.

as determined by isocratic analytical HPLC, using a 4.6mm × 250mm Zorbax C18 column and a 20 : 80 EtOAc : CH_3OH mobile phase at 2mL / min, at ambient temperature. Figure 7 shows the chromatogram of intermediate (3) after recrystallization and its DMF mother liquor.

The ^{1}H and ^{13}C NMR chemical shifts and peak assignments for intermediate (3) were also determined from the 1-dimensional ^{1}H and ^{13}C NMR spectra, coupled with 2-dimensional ^{1}H-^{1}H COSY and ^{1}H-^{13}C HETCOR NMR spectroscopy (^{1}H NMR data in $CDCl_3$: δ 5.47 (doublet of doublet, 6 H-3, J_{3-2} = 10.3 Hz, J_{3-4} = 8.9 Hz); δ 5.10 (doublet, 6 H-1, J_{1-2} = 3.4 Hz); δ 4.68 (doublet of doublet, 6 H-2, J_{2-1} = 3.4 Hz, J_{2-3} = 10.3 Hz); δ 4.12 (doublet of doublet, 6 H-6, J_{6-5} = 2.0 Hz, $J_{6-6'}$ = 11.9 Hz); δ 4.02 (triplet, 6 H-4, J_{4-3} = 8.9 Hz, J_{4-5} = 8.9 Hz); δ 3.91 (doublet, 6 H-5, J_{5-4} = 8.9 Hz); δ 3.70 (doublet, 6 H-6', $J_{6'-6}$ = 11.9 Hz); δ 2.07, 2.05 (two sets of singlet, 6 CO$\underline{CH_3}$ on C2 and 6 CO$\underline{CH_3}$ on C3); δ 0.89 (singlet, 6 $\underline{(CH_3)_3}C$); δ 0.06, 0.05 (two sets of singlet, 6 $\underline{(CH_3)_2}Si$); ^{13}C NMR data in $CDCl_3$: δ 171.05, 169.91 ($\underline{C}OCH_3$ on C2 and $\underline{C}OCH_3$ on C3); δ 96.78 (C-1); δ 75.52 (C-4); δ 72.35 (C-5); δ 72.09 (C-3); δ 71.67 (C-2); δ 62.26 (C-6); δ 26.20 ($(\underline{C}H_3)_3C$); δ 21.27, 21.10 (CO$\underline{C}H_3$ on C2 and CO$\underline{C}H_3$ on C3); δ 18.60 ($(CH_3)_3\underline{C}$); δ -4.67, -4.95 ($(\underline{C}H_3)_2Si$)). 2D ^{1}H-^{1}H COSY and ^{1}H-^{13}C HETCOR NMR spectra, which show those proton and carbon contours that are related to the glucose units, are shown in Figures 8 and 9, respectively.

Figure 10 shows the MALDI-TOF-MS of the Na^+ and K^+ ion-adduct portion of intermediate (3). The calculated molecular weight values of the Na^+ and K^+ ion-adducts of the parent molecule, 2183.95 and 2199.93, agree well with the value obtained using high

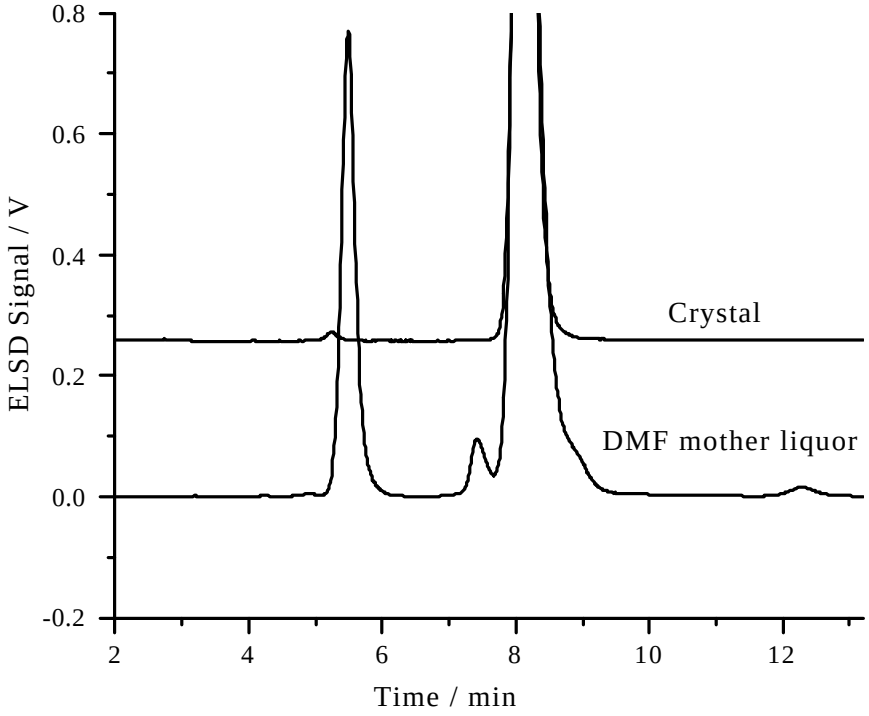

Figure 7. Chromatograms of crystalline (3) and its mother liquor. Purity of the product > 99 %. Conditions: EtOAc : MeOH = 20 : 80, F = 2mL / min, C18 column.

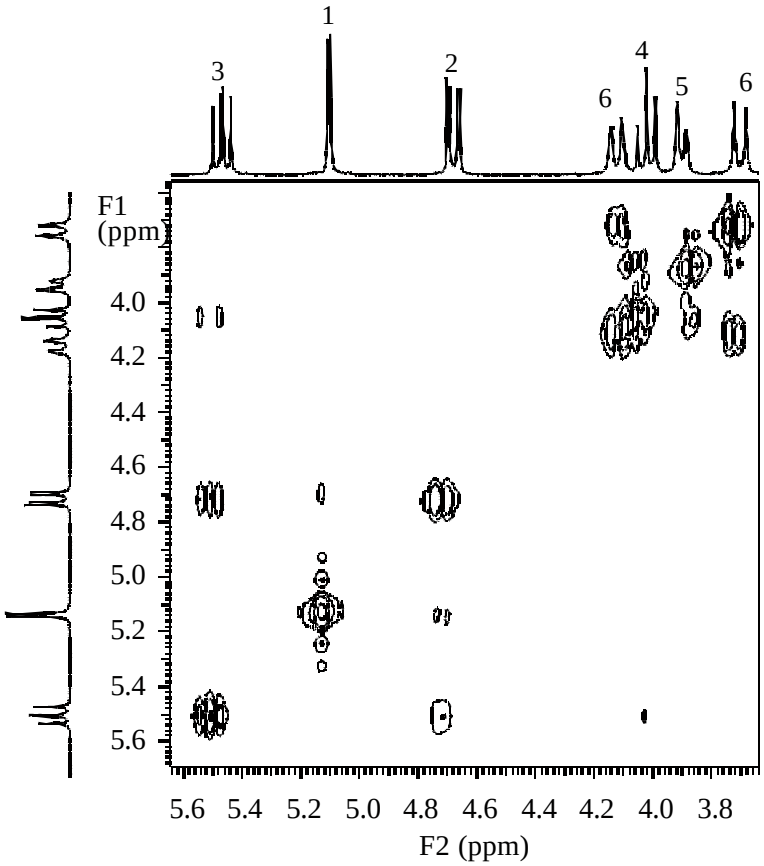

Figure 8. 2D COSY of (3) in $CDCl_3$ using 300 mHz NMR.

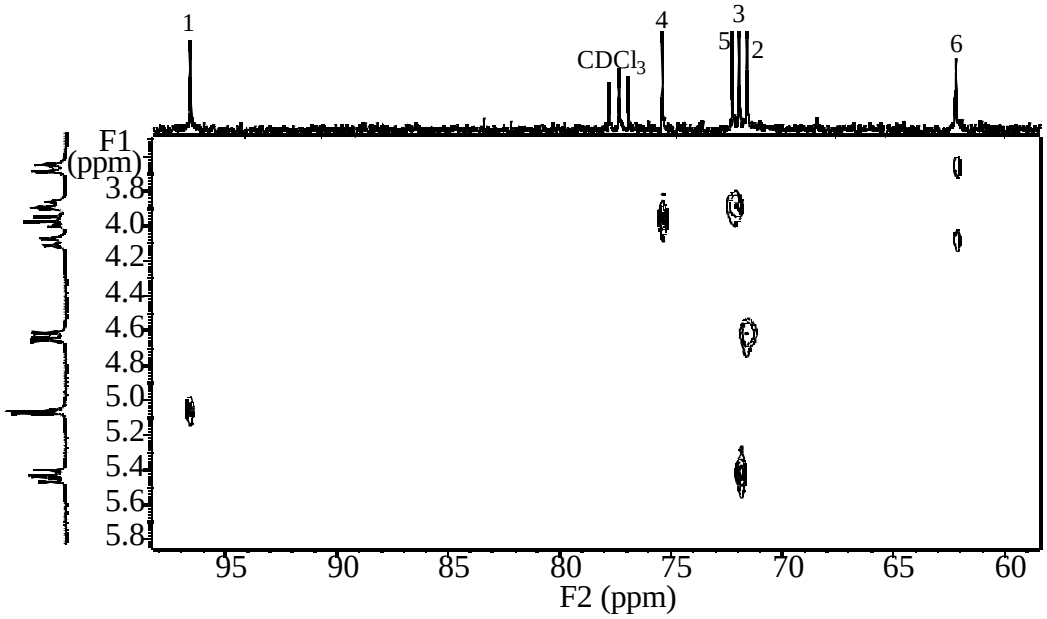

Figure 9. 2D HETCOR of (3) in $CDCl_3$ using 300 mHz NMR.

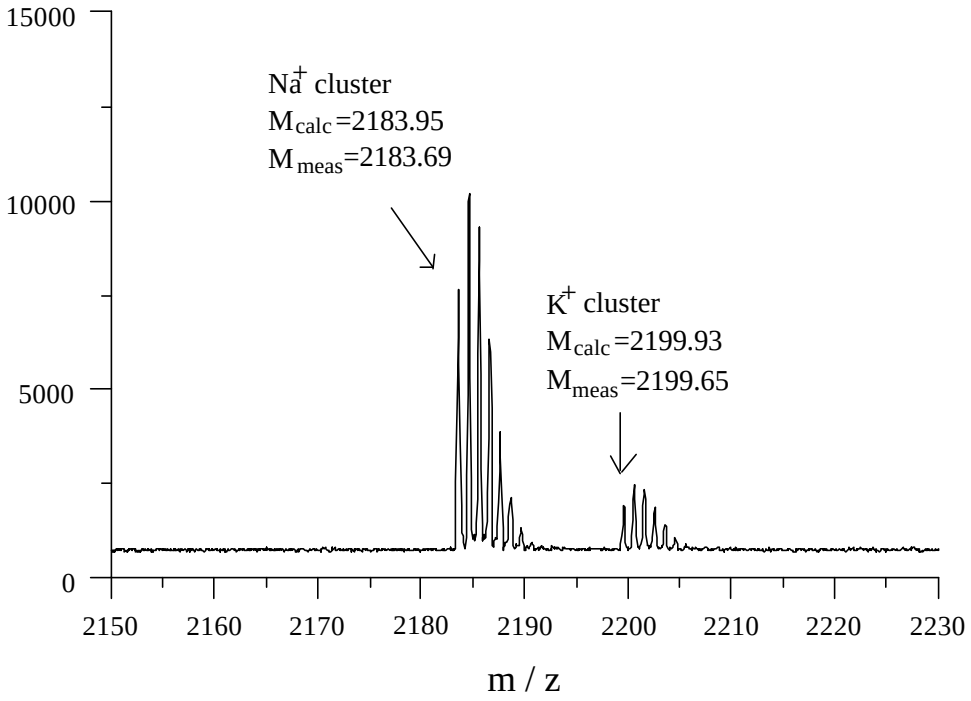

Figure 10. MALDI-TOF-MS spectrum of (3). The measured m/z values agree well with the m/z values calculated for the monoisotopic sodium and potassium adducts.

resolution MALDI-TOF-MS: 2183.69 and 2199.65, respectively, indicating the presence of six *tert*-butyldimethylsilyl groups and twelve acetyl groups on intermediate (3).

2.2.3 Hexakis(2,3-di-*O*-acetyl)-a-Cyclodextrin

In the third step, the *tert*-butyldimethylsilyl protecting groups at the sixth position were removed from intermediate (3) with BF_3·EtOEt complex in CH_2Cl_2 to produce hexakis(2,3-di-*O*-acetyl)-α-CD (intermediate (4)). The progress of the reaction was monitored by TLC, using Silica 60 plates and 50 :10 :1 $CHCl_3$: CH_3OH : H_2O as running solvent, giving an R_f=0.33 for intermediate (4). Intermediate (4) with a purity > 99 % was obtained by recrystallization from acetone as determined by isocratic analytical HPLC, using a 4.6mm × 250mm Zorbax C18 column and a 48 : 52 H_2O : CH_3OH mobile phase with 1.5mL / min rate, at temperature 40°C. Figure 11 shows the chromatogram of intermediate (4) after recrystallization and its corresponding acetone mother liquor.

The ^1H and ^{13}C NMR chemical shifts and peak assignments were determined from the 1D ^1H and ^{13}C NMR spectra, coupled with 2D ^1H - ^1H COSY and ^1H - ^{13}C HETCOR NMR spectroscopy (^1H NMR data in $CDCl_3$: δ 5.43 (triplet, 6 H-3, J_{3-2} = 8.8 Hz, J_{3-4} = 8.8 Hz); δ 5.09 (doublet, 6 H-1, J_{1-2} = 2.7 Hz); δ 4.81 (doublet of doublet, 6 H-2, J_{2-1} = 2.7 Hz, J_{2-3} = 8.8 Hz); δ 4.02, 3.90 and 3.81 (24 H-4, 5, 6); δ 2.06, 2.04 (two sets of singlet, 6 CO$\underline{CH_3}$ on C2 and 6 CO$\underline{CH_3}$ on C3); ^{13}C NMR data in $CDCl_3$: δ 170.97, 170.00 ($\underline{C}OCH_3$ on C2 and $\underline{C}OCH_3$ on C3); δ 96.95 (C-1); δ 77.09 (C-4); δ 72.66 (C-5); δ 71.83 (C-3); δ 70.92 (C-2); δ 61.55 (C-

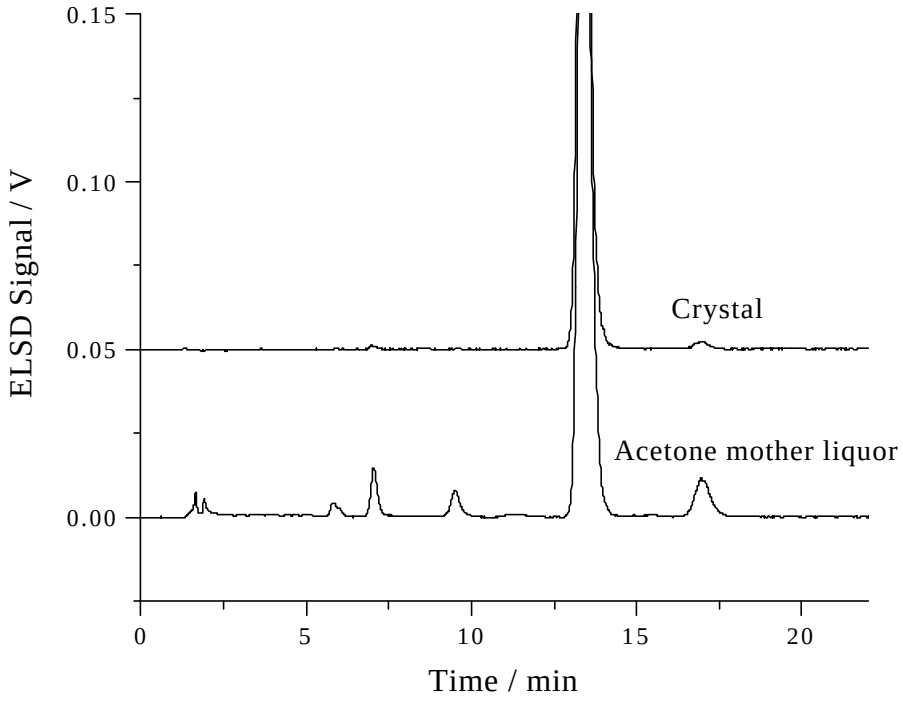

Figure 11. Chromatograms of crystalline (4) and its mother liquor. Purity of the product > 99 %. Conditions: H_2O : MeOH = 48 : 52, F = 1.5mL / min, T = 40°C, C18 column.

6); δ 21.07, 20.99 ($CO\underline{C}H_3$ on C2 and $CO\underline{C}H_3$ on C3)). Since all the acetyl groups are easily assigned, Figures 12 and 13 show 2D ^1H - ^1H COSY and ^1H - ^{13}C HETCOR NMR spectra of those proton and carbon contours that are related to the glucose unit of intermediate (4).

The calculated molecular weight values of the Na^+ and K^+ ion-adducts of the parent molecule, 1499.43 and 1515.41, agree well with the values obtained using high resolution MALDI-TOF-MS, 1498.85 and 1515.65, respectively, as shown in Figure 14, indicating that the six *tert*-butyldimethylsilyl groups on intermediate (4) were removed completely, but the 12 acetyl groups still remained on intermediate (4).

2.2.4 Hexakis(2,3-di-*O*-acetyl-6-*O*-sulfo)-a-Cyclodextrin

Finally, intermediate (4) was sulfated at the sixth positions of the glucopyranose units using sulfur trioxide-pyridine complex in the presence of DMF and anhydrous pyridine. Indirect UV detection CE with a 20 mM para-toluenesulfonic acid (pTSA) / β-alanine (pH 3.5) background electrolyte with (-) to (+) polarity was used to monitor the progress of the reaction and to assay the purity of the target material. The reaction was quenched by slowly adding a hot saturated sodium bicarbonate solution to obtain the sodium salt of hexakis(2,3-di-*O*-acetyl-6-*O*-sulfo)-α-CD (HxDAS). Using isopropanol induced precipitation, HxDAS was obtained with a calculated purity of 97.8 % (assuming identical response factors). The electropherogram is shown in Figure 15.

The ^1H and ^{13}C NMR chemical shifts and peak assignments were determined from the 1D ^1H and ^{13}C NMR spectra, coupled with 2D ^1H - ^1H COSY and ^1H - ^{13}C HETCOR NMR

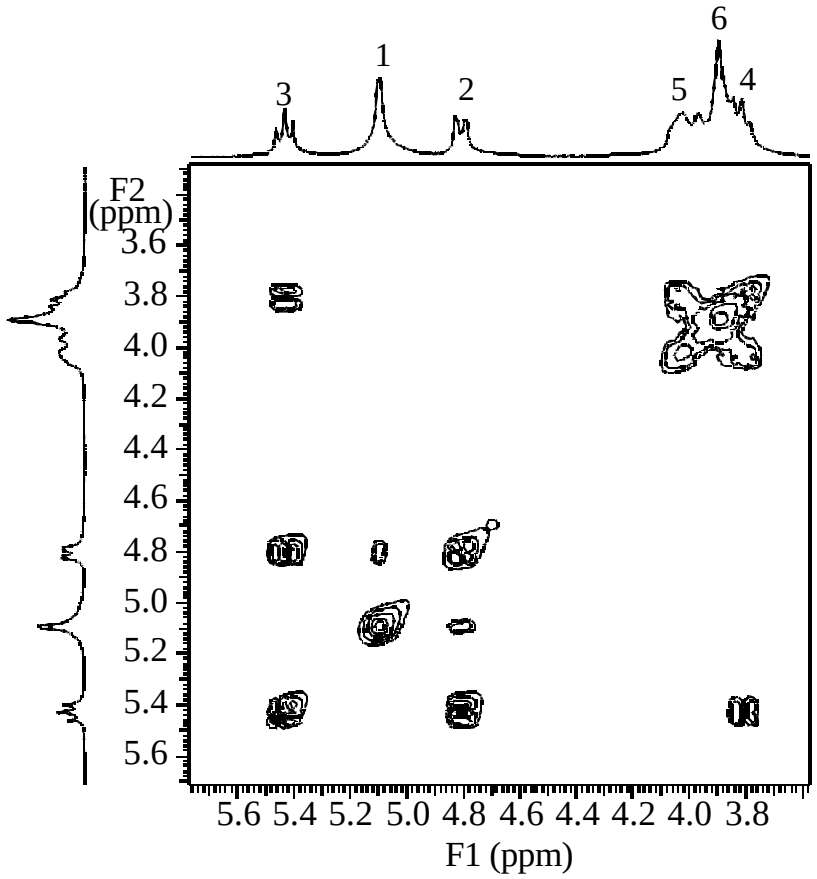

Figure 12. 2D COSY of (4) in $CDCl_3$ using 300 mHz NMR.

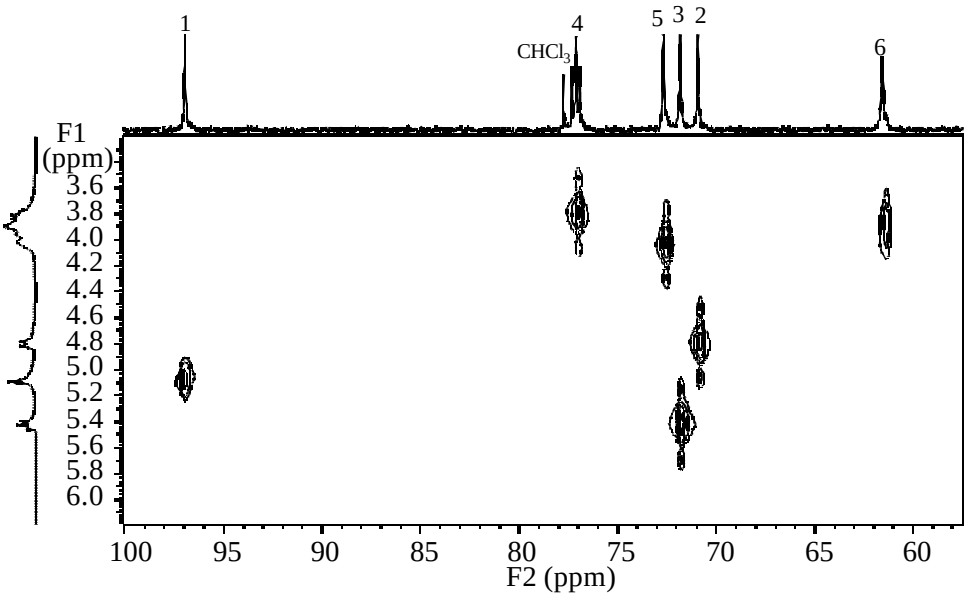

Figure 13. 2D HETCOR of (4) in $CDCl_3$ using 300 mHz NMR.

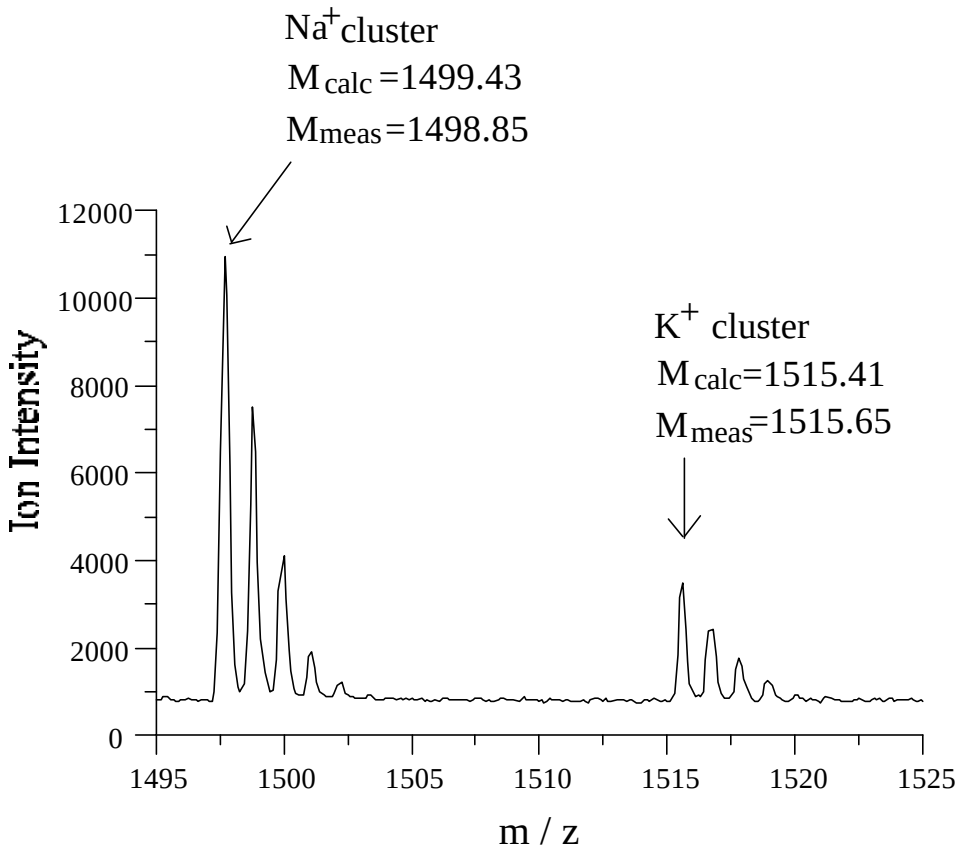

Figure 14. MALDI-TOF-MS spectrum of (4). The measured m/z values agree well with the m/z values calculated for the monoisotopic sodium and potassium adducts.

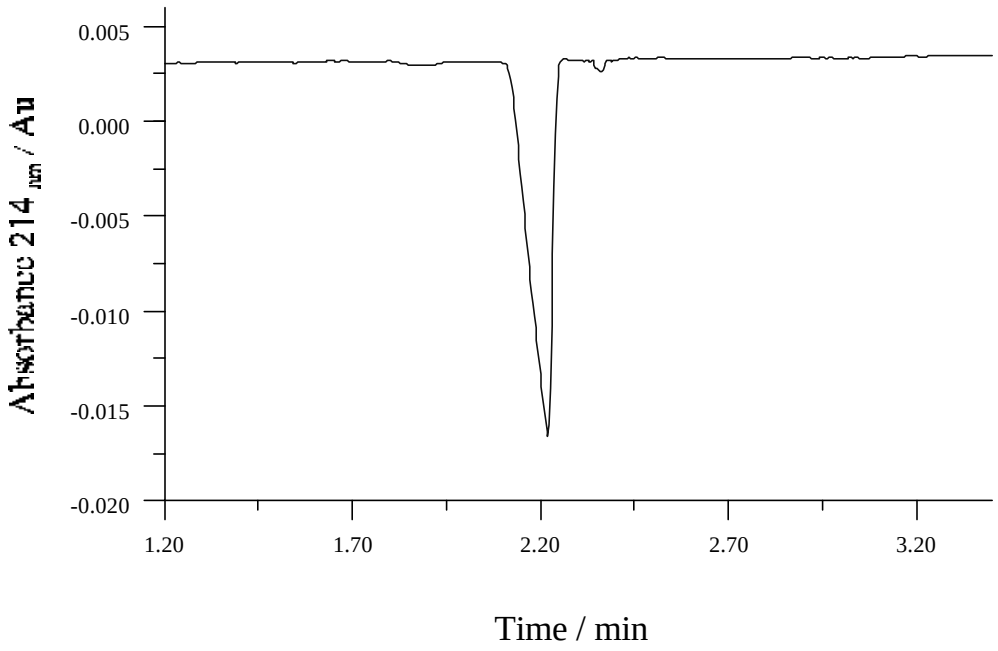

Figure 15. Indirect UV detection CE electropherogram of HxDAS. Purity > 97.8 %. Conditions: 20 mM pTSA / β-alanine, pH = 3.5, (-) to (+) polarity, Lt / Ld =26.4 / 19.6 cm, 10 kV, 214 nm, T = 20ºC.

spectroscopy (^{1}H NMR data in D_2O: δ 5.36 (triplet, 6 H-3, J_{3-2} = 8.5 Hz, J_{3-4} = 8.5 Hz); δ 5.18 (doublet, 6 H-1, J_{1-2} = 2.9 Hz); δ 4.81 (doublet of doublet, 6 H-2, J_{2-1} = 2.9 Hz, J_{2-3} = 8.5 Hz); δ 4.44 (doublet, 6 H-6, $J_{6-6'}$ = 11.5 Hz); δ 4.25 (doublet, 6 H-6', $J_{6'-6}$ = 11.5 Hz); δ 4.14 (doublet, 6 H-5, J_{5-4} = 8.5 Hz); δ 4.02 (triplet, 6 H-4, J_{4-5} = 8.5 Hz, J_{4-3} = 8.5 Hz); δ 2.02, 2.01 (two sets of singlet, 6 CO$\underline{CH}_3$ on C2 and 6 CO$\underline{CH}_3$ on C3); ^{13}C NMR data in $CDCl_3$: δ 173.28, 173.03 ($\underline{C}OCH_3$ on C2 and $\underline{C}OCH_3$ on C3); δ 96.78 (C-1); δ 75.58 (C-4); δ 71.77(C-3); δ 71.02 (C-2); δ 70.35 (C-5); δ 66.97 (C-6); δ 20.64, 20.58 (CO$\underline{C}H_3$ on C2 and CO$\underline{C}H_3$ on C3)). 2D ^{1}H - ^{1}H COSY and ^{1}H - ^{13}C HETCOR NMR spectra of HxDAS, in Figures 16 and 17, show the ^{1}H - ^{1}H and ^{1}H - ^{13}C connectivities, respectively.

The measured m/z value of 1067.05 obtained using high resolution positive ion-mode ESI-TOF-MS (Figure 18) agrees well with the m/z value calculated for the monoisotopic disodium adduct, $[C_{60}H_{78}O_{60}S_6Na_8]^{2+}$, 1067.03, indicating that the sulfation process was successful.

2.2.5 Hexakis-6-*O*-sulfo-α-Cyclodextrin

The second product, the sodium salt of hexakis(6-*O*-sulfo)-α-CD (HxS)**,** was obtained by reacting HxDAS with a 500 mM aqueous sodium hydroxide solution. Indirect UV detection CE with a 20 mM TEMED / phthalic acid (pH 5.5) background electrolyte with (-) to (+) polarity was used to monitor the progress of the reaction and to assay the purity of the target material. Using methanol-induced precipitation, HxS with a calculated purity of 98 % (assuming identical response factors) was obtained (electropherogram shown in Figure 19).

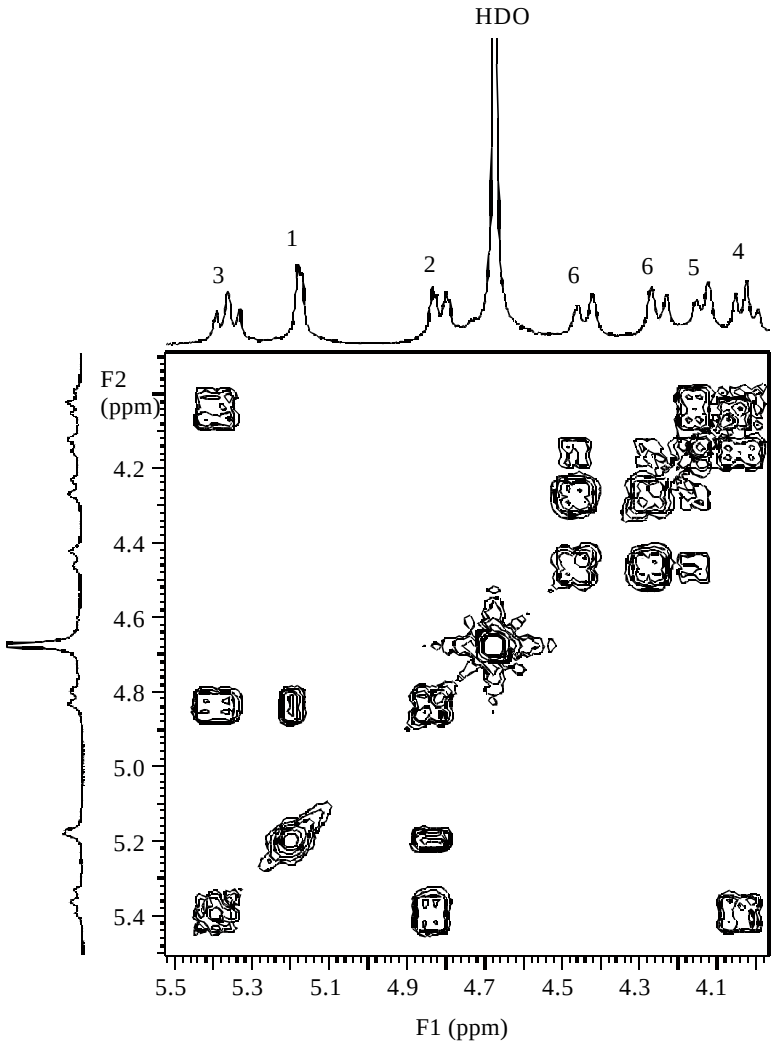

Figure 16. 2D COSY of HxDAS in D_2O using 300 mHz NMR.

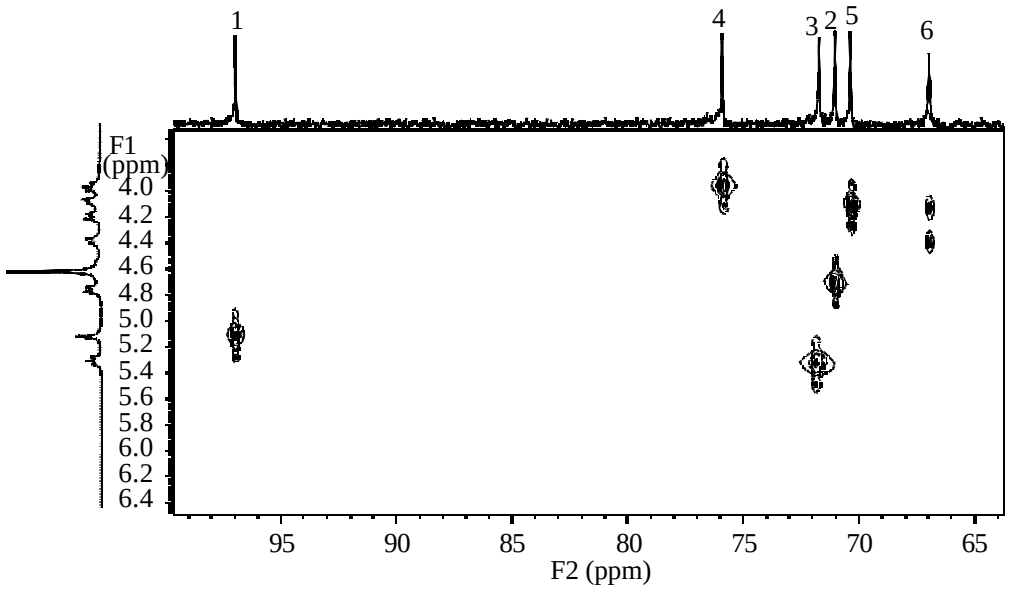

Figure 17. 2D HETCOR of HxDAS in D_2O using 300 mHz NMR.

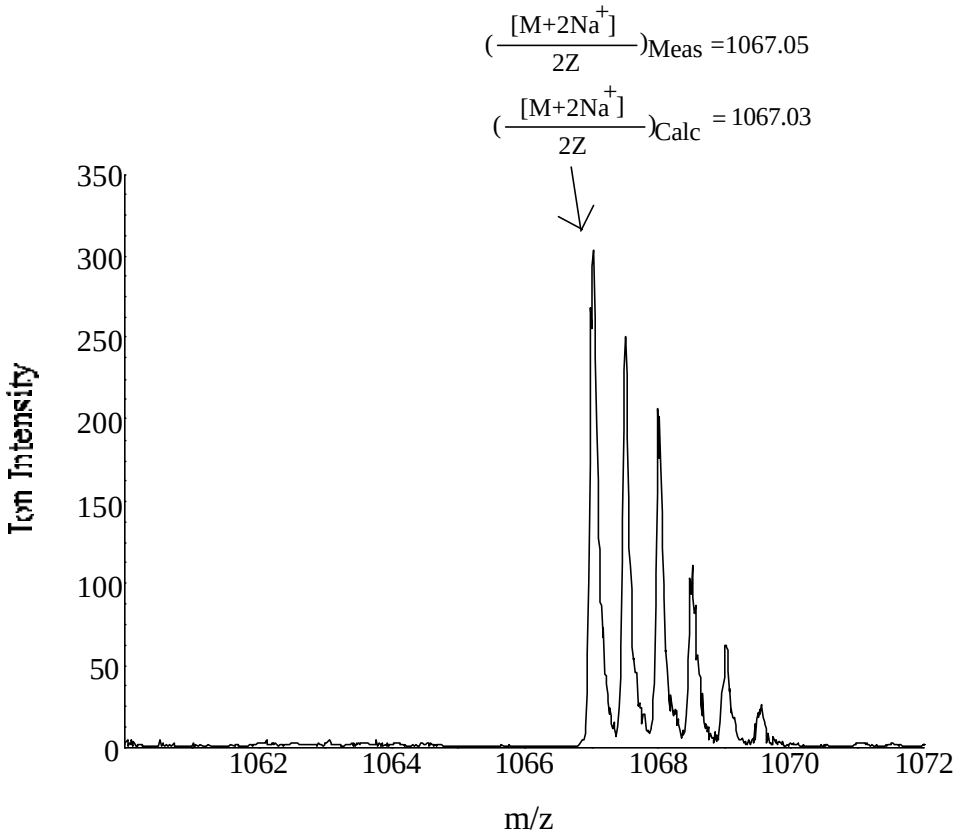

Figure 18. High resolution ESI-TOF-MS spectrum of HxDAS. The measured m/z value of 1067.05 agrees well with the m/z value calculated for the monoisotopic disodium adduct, $[C_{60}H_{78}O_{60}S_6Na_8]^{2+}$, 1067.03.

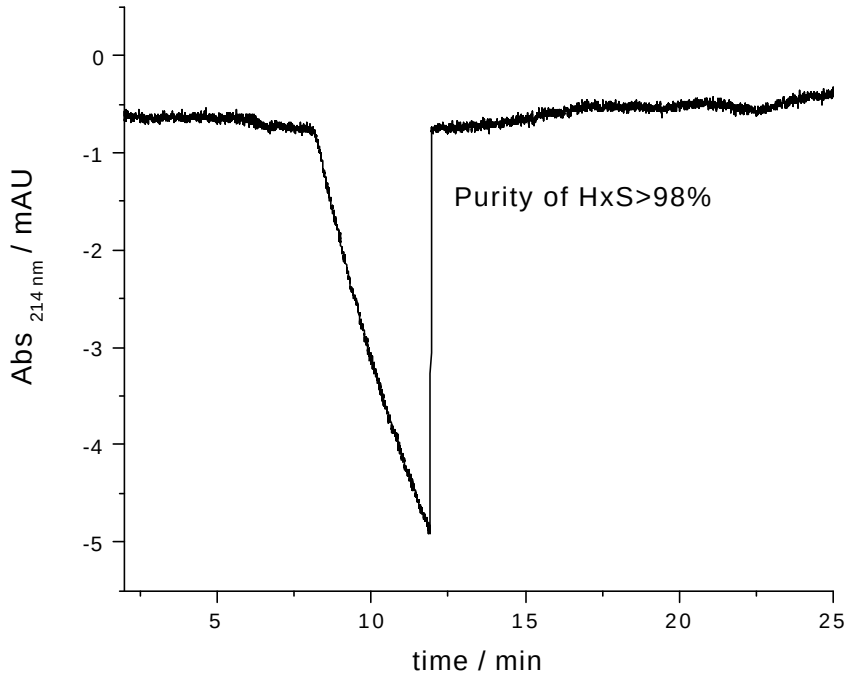

Figure 19. Indirect UV detection CE electropherogram of HxS. Purity > 99 %. Conditions: 20 mM TEMED / phthalic acid, pH = 5.5, (-) to (+) polarity, Lt / Ld = 26.4 /19.6 cm, 214 nm, 10 kV, T = 20ºC.

The ^{1}H and ^{13}C NMR chemical shifts and peak assignments were determined from the 1D ^{1}H and ^{13}C NMR spectra, coupled with 2D ^{1}H - ^{1}H COSY and ^{1}H - ^{13}C HETCOR NMR spectroscopy (shown in Figures 20 and 21, respectively) (^{1}H NMR data in D_2O: δ 5.22 (doublet, 6 H-1, J_{1-2} = 3.2 Hz); δ 4.54 (doublet, 6 H-6, $J_{6-6'}$ = 9.2 Hz); δ 4.38 (doublet 6 H-6', $J_{6'-6}$ = 9 .2Hz); δ 4.22 (doublet, 6 H-5, J_{5-4} = 9.9 Hz); δ 4.09 (triplet, 6 H-3, J_{3-2} = 9.9 Hz, J_{3-4} = 9.9 Hz); δ 3.79 (triplet, 6 H-4, J_{4-3} = 9.9 Hz; J_{4-5} = 9.9 Hz); δ 3.75 (doublet of doublet, 6 H-2, J_{2-1} = 3.2 Hz, J_{2-3} = 9.9 Hz); ^{13}C NMR data in $CDCl_3$: δ 101.22 (C-1); δ 80.65 (C-4); δ 73.22 (C-3); δ 71.77 (C-2); δ 70.05 (C-5); δ 67.38 (C-6)).

High resolution negative-ion mode ESI-TOF-MS indicated very good agreement between the calculated and measured m/z values: portions of the mass spectra corresponding to HxS ions with three to six negative charges (brought about by the dissociation of three to six Na^+ ions), which are shown in Figure 22. The high agreements indicate that the deacetylation process was successful.

2.2.6 Hexakis(2,3-di-*O*-methyl-6-*O*-t-butyldimethylsilyl)-a-Cyclodextrin

The secondary hydroxyl groups of intermediate (2) were methylated in THF at room temperature using iodomethane and dry NaH for 4 h to obtain hexakis(2,3-di-*O*-methyl-6-*O*-t-butyldimethylsilyl)-α-cyclodextrin (intermediate (5)) with 99 % conversion at the 50 g scale. Reaction progress was monitored using a 5μm Luna C18 RP-HPLC column with a 65:35 MeOH : EtOAc isocratic mobile phase at 2mL / min, at ambient temperature. Intermediate (5) with a purity > 99 % was obtained by using ethanol : H_2O (1:10 v:v) mixture as the

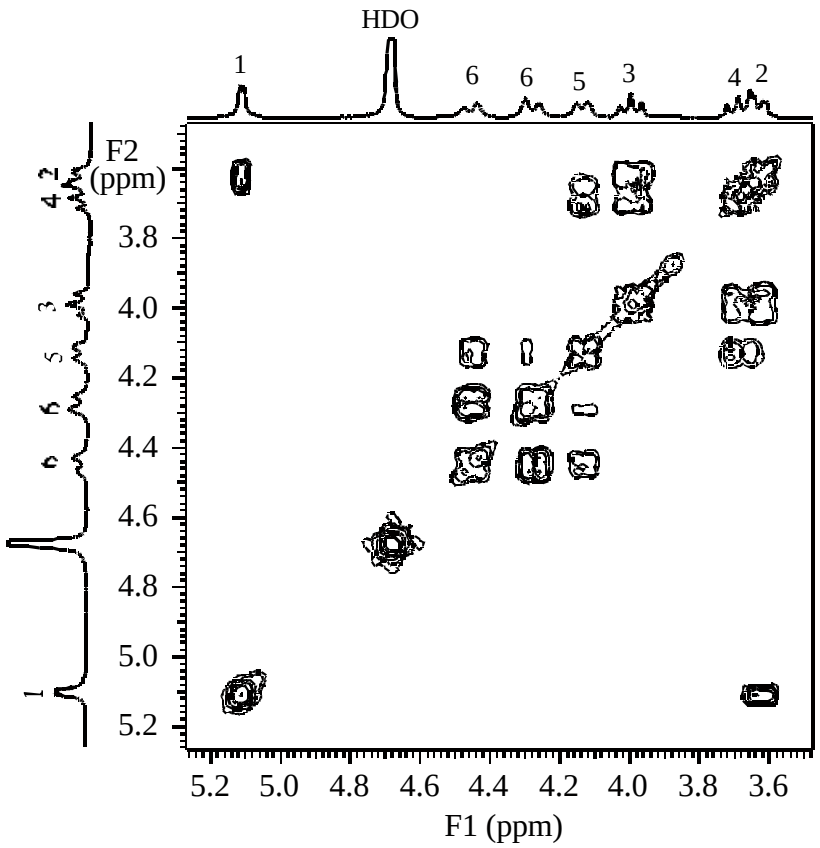

Figure 20. 2D COSY of HxS in D_2O using 500 mHz NMR.

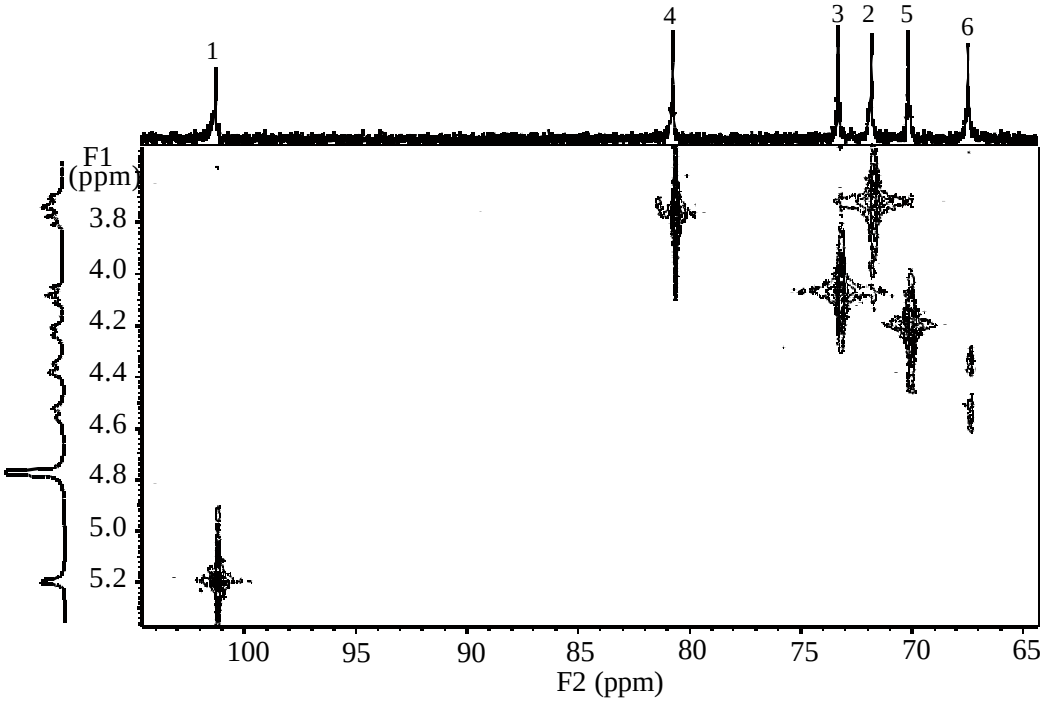

Figure 21. 2D HETCOR of HxS in D_2O using 500 mHz NMR.

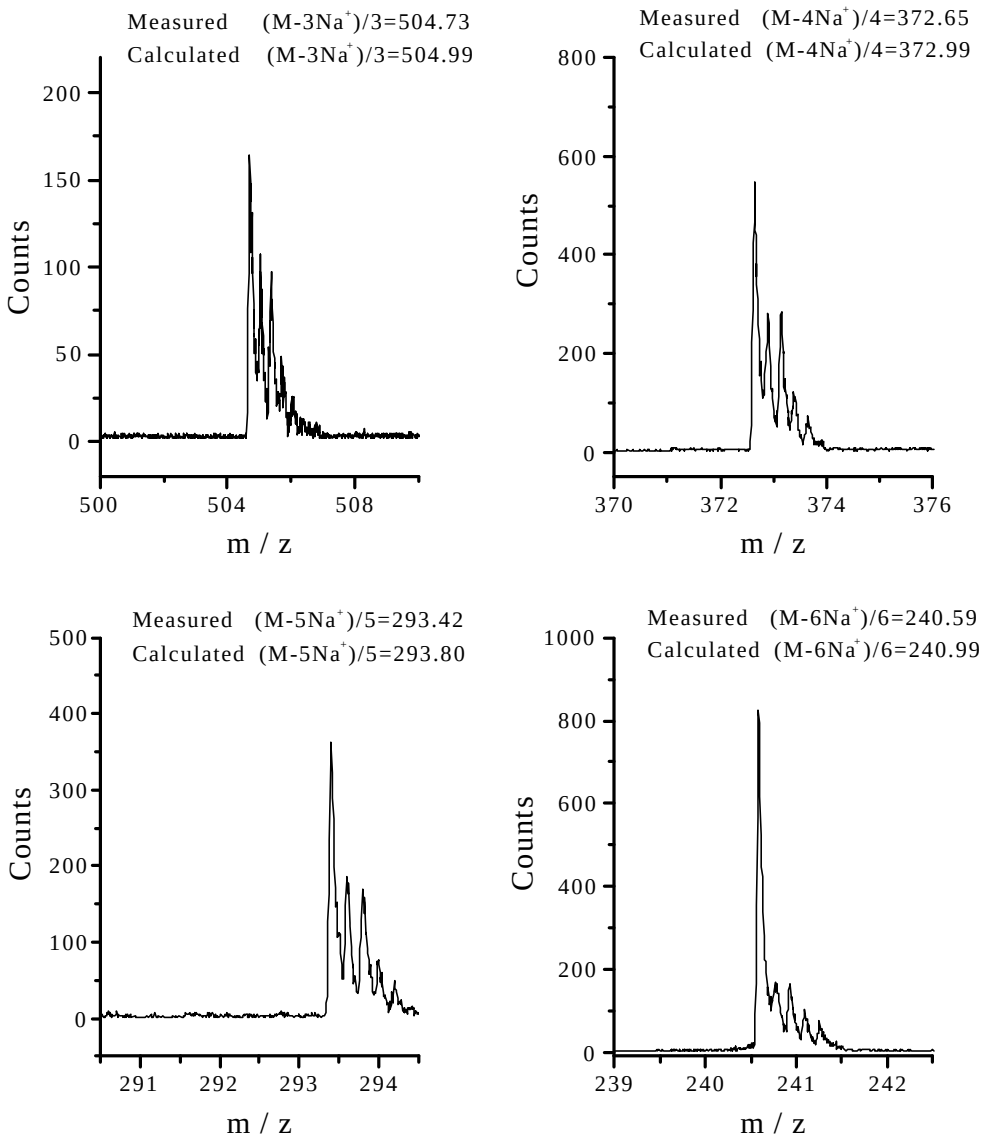

Figure 22. Portions of the high resolution ESI-TOF-MS spectrum of HxS.

recrystallizing solvent to remove trace salt, and pure ethanol was used to remove the over-methylated under-silylated cyclodextrin impurities. Figure 23 shows a non-aqueous, reversed-phase HPLC separation of intermediate (5) after recrystalization and its corresponding ethanol mother liquor. The postulated structure of intermediate (5) was verified by 1D ^{1}H and ^{13}C and 2D ^{1}H - ^{1}H COSY and 2D ^{1}H - ^{13}C HETCOR NMR spectroscopy (^{1}H NMR data in $CDCl_3$: δ 5.03 (doublet, 6 H-1, J_{1-2} = 3.2 Hz); δ 4.07 (doublet of doublet, 6 H-6, J_{6-5} = 2.7 Hz, $J_{6-6'}$ = 11.5 Hz); δ 3.69 (quartet, 12 H-(4+5), J_{4-3} = 9.7 Hz, J_{4-5} = 9.7 Hz); δ 3.63 (doublet, 6 H-6', $J_{6'-6}$ = 11.5 Hz); δ 3.58 (triplet, 6 H-3, J_{3-2} = 9.7 Hz, J_{3-4} = 9.7 Hz); δ 3.05 (doublet of doublet, 6 H-2, J_{2-1} = 3.2 Hz, J_{2-3} = 9.7 Hz); δ 3.65, 3.49 (two sets of singlet, 6 O$\underline{CH_3}$ on C2 and 6 O$\underline{CH_3}$ on C3); δ 0.87 (singlet, 6 $(\underline{CH_3})_3C$); δ 0.03, 0.02 (two sets of singlet, 6 $(\underline{CH_3})_2Si$); ^{13}C NMR data in $CDCl_3$: δ 99.64 (C-1); δ 82.59 (C-2); δ 81.61 (C-3); δ 81.30 (C-4); δ 72.73 (C-5); δ 62.46 (C-6); δ 61.94, 58.11 (O$\underline{C}H_3$ on C2 and O$\underline{C}H_3$ on C3); δ 26.09 ($(\underline{C}H_3)_3C$); δ 18.42 ($(CH_3)_3\underline{C}$); δ -4.72, -4.95 ($(\underline{C}H_3)_2Si$)). Figures 24 and 25, showed the ^{1}H - ^{1}H and ^{1}H - ^{13}C connectivities, respectively. Once again, the structure omitted the *tert*-butyldimethylsilyl group portions.

The Na^+ ion-adduct portion of the high resolution MALDI-TOF mass spectrum of the parent molecule (5) is shown in Figure 26. The measured m/z value of 1848.01 agrees well with the calculated monoisotopic value of $[C_{84}H_{168}O_{30}Si_6Na]^+$, 1847.55.

2.2.7 Hexakis(2,3-di-*O*-methyl)-a-Cyclodextrin

Deprotection of intermediate (5) was accomplished using 48 % HF_{aq} in 100 % ethanol

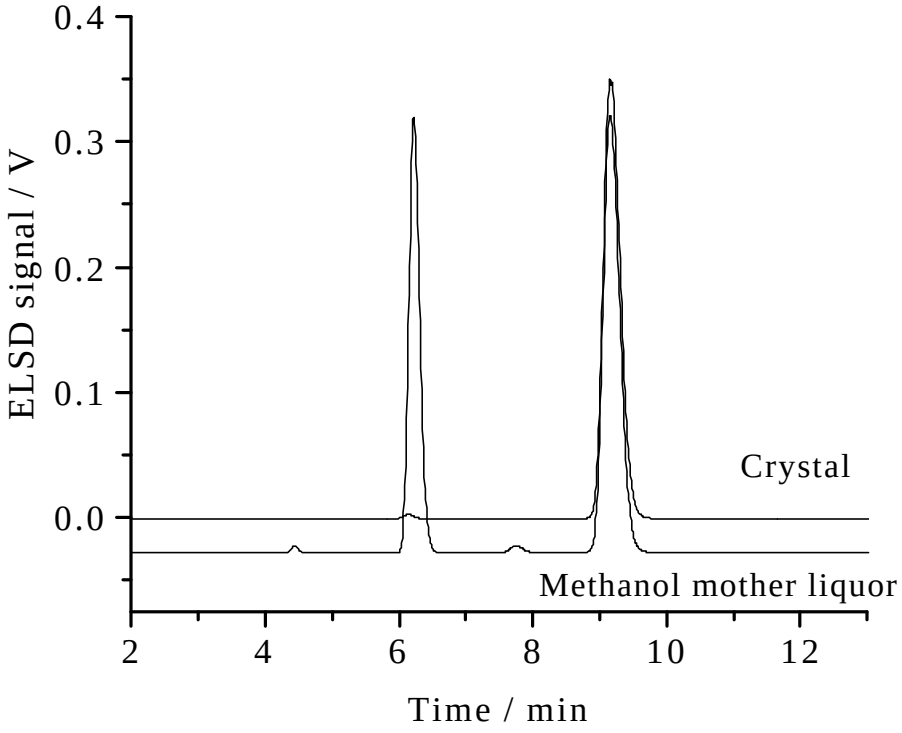

Figure 23. Chromatograms of crystalline (5) and its mother liquor. Purity of the product > 99 %. Conditions: MeOH : EtOAc = 65 : 35, F = 2mL / min, C18 column.

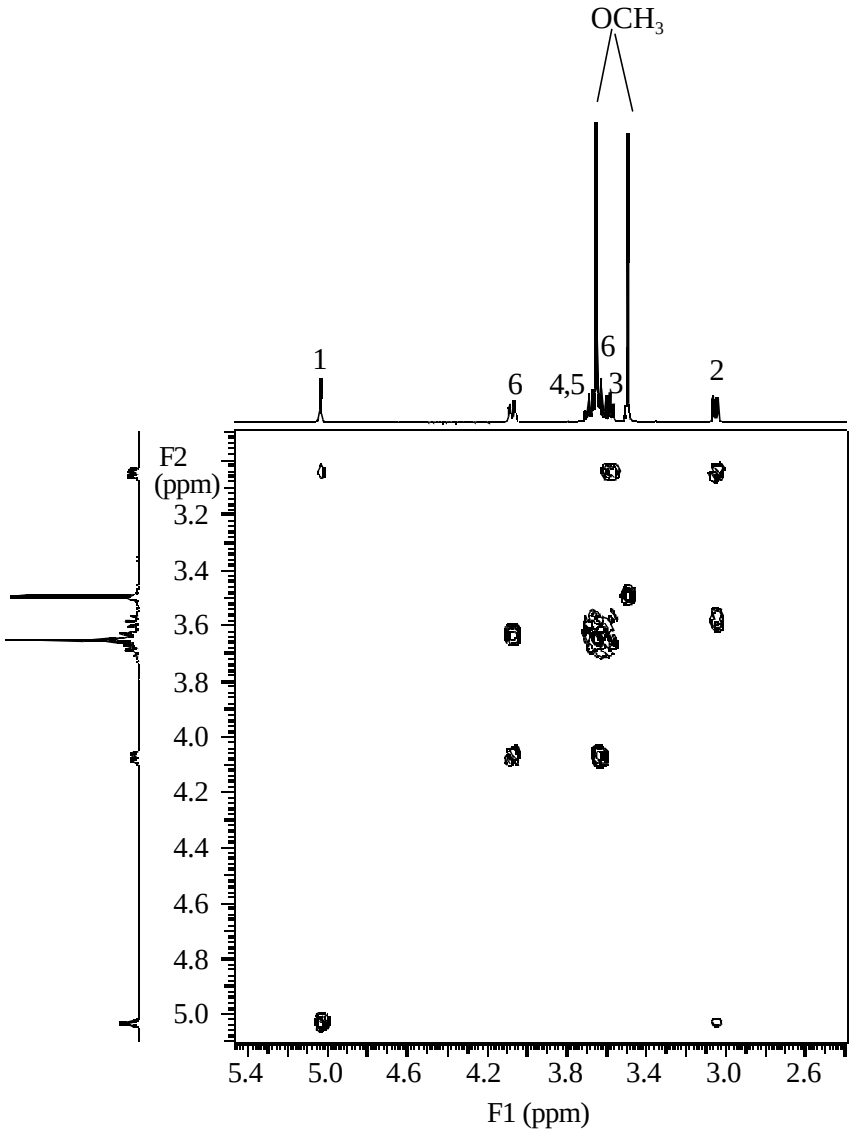

Figure 24. 2D COSY of (5) in $CDCl_3$ using 500 mHz NMR.

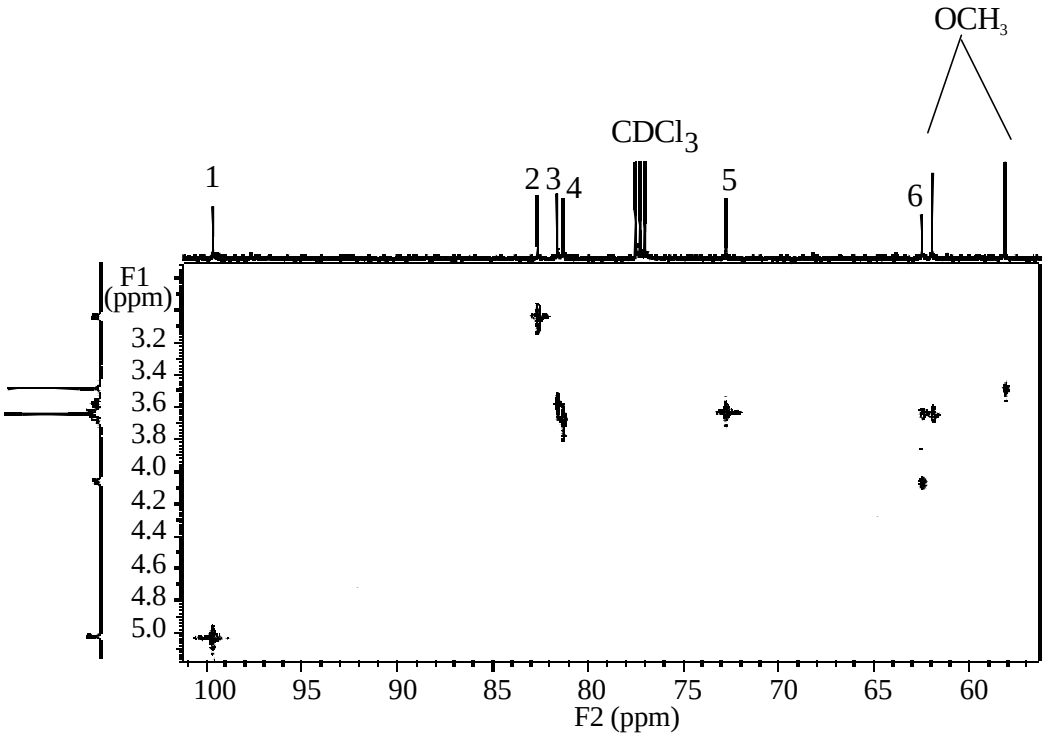

Figure 25. 2D HETCOR of (5) in $CDCl_3$ using 500 mHz NMR.

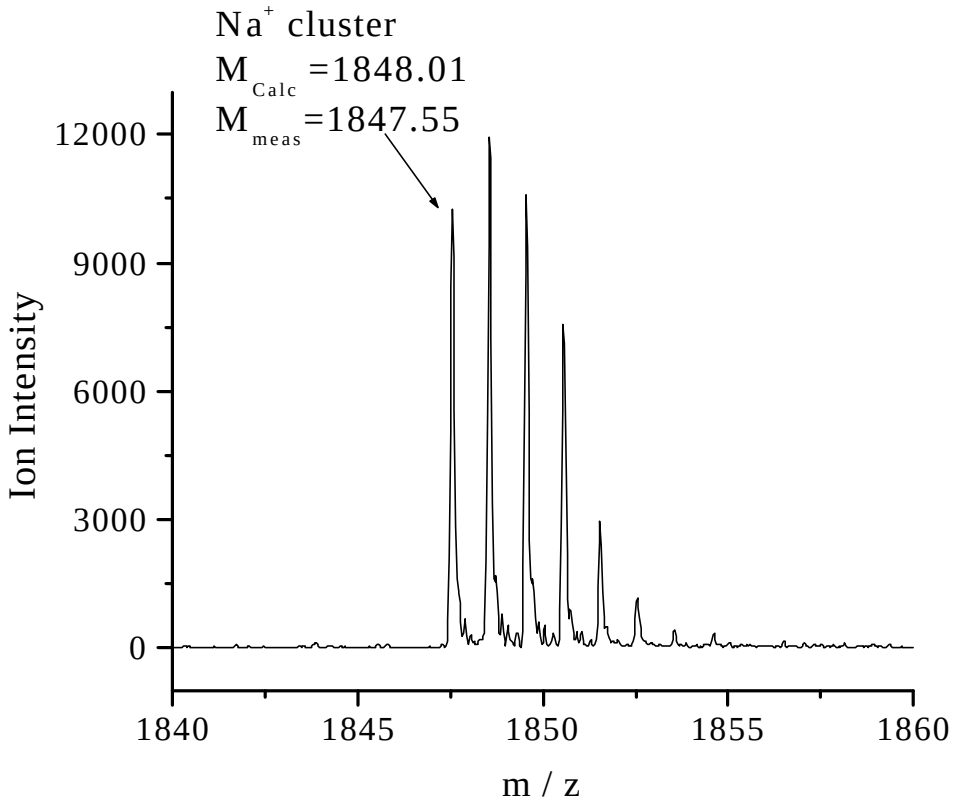

Figure 26. High resolution MALDI-TOF-MS spectrum of (5). The measured m/z value of 1848.01 agrees well with the m/z value calculated for the monoisotopic sodium adduct, $[C_{84}H_{168}O_{30}Si_6Na]^+$, 1847.55.

for 24 h at room temperature to obtain hexakis(2,3-di-*O*-methyl)-α-cyclodextrin (intermediate (6)) with a 99 % conversion at the 200 g scale. The reaction was monitored by TLC with a 50:10:1 $CHCl_3$: MeOH: H_2O mobile phase giving an $R_f = 0.42$ for the target compound. The purity of the product was determined by a 5 μm Luna C18 RP-HPLC column with a 75:25 MeOH : H_2O isocratic mobile phase at 1.2mL / min, with temperature 50°C. The crude material was recrystallized three times from DMF : water : acetone to yield a 99.6% isomerically pure white powder (Figure 27). Assigned 2D ^1H - ^1H COSY and 2D ^1H - ^{13}C HETCOR NMR spectra of intermediate (6) are included in Figures 28 and 29, respectively.

The Na^+ ion-adduct portion of the high resolution MALDI-TOF mass spectrum of the parent molecule (6) is shown in Figure 30. The measured m/z values of 1163.50, 1179.37 agree well with the calculated monoisotopic value of sodium and potassium adduct portions of $[C_{48}H_{84}O_{30}Na]^+$, $[C_{48}H_{84}O_{30}K]^+$, 1163.49, 1179.47, respectively.

2.2.8 Hexakis(2,3-di-*O*-methyl-6-*O*-sulfo)-a-Cyclodextrin

Intermediate (6) was sulfated in DMF at room temperature for 48 h using pyridine sulfur trioxide complex to obtain Hexakis(2,3-di-*O*-methyl-6-*O*-sulfo)-α-cyclodextrin (HxDMS) with a 97% conversion at the 100 g scale. The reaction was monitored by indirect UV detection CE analysis using a 20 mM para-toluene sulfonic acid : 40 mM tris(hydroxymethyl)aminomethane BGE (pH 8.2) with (+) to (-) polarity. Purification of the crude material was accomplished with six precipitations from a 6:1 EtOH : H_2O mixture by dissolving the crude material in a minimum volume of water followed by addition of six times the water volume of ethanol. The final isomeric purity of the white powder obtained was

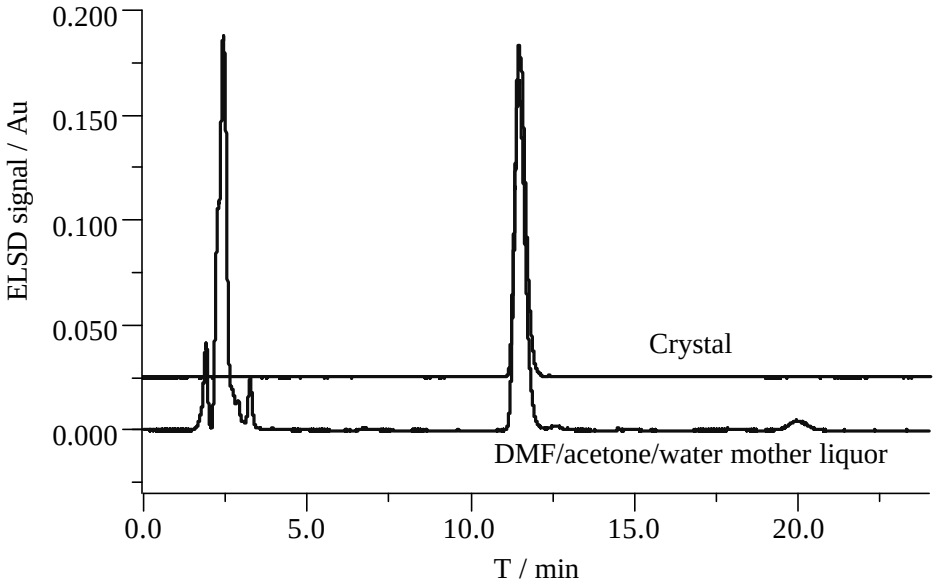

Figure 27. Chromatograms of crystalline (6) and its mother liquor. Purity of the product > 99 %. Conditions: H_2O : MeOH = 25 : 75, F = 1.2mL / min, T = 50°C, C18 column.

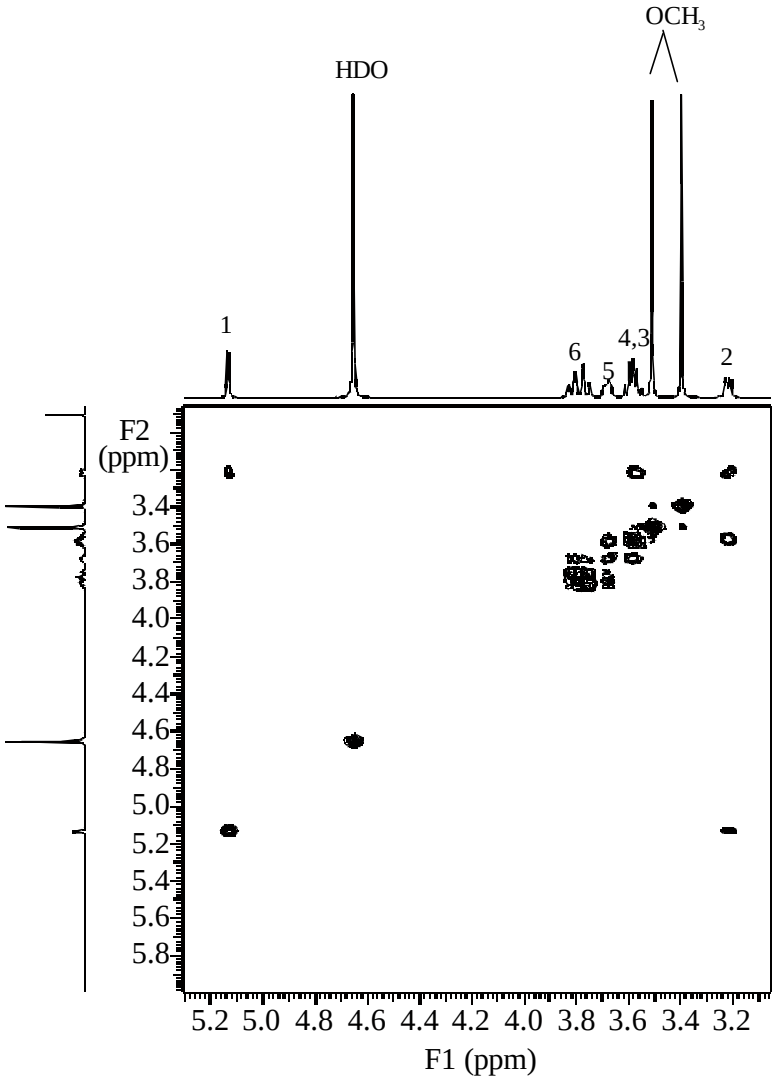

Figure 28. 2D COSY of (6) in $CDCl_3$ using 500 mHz NMR.

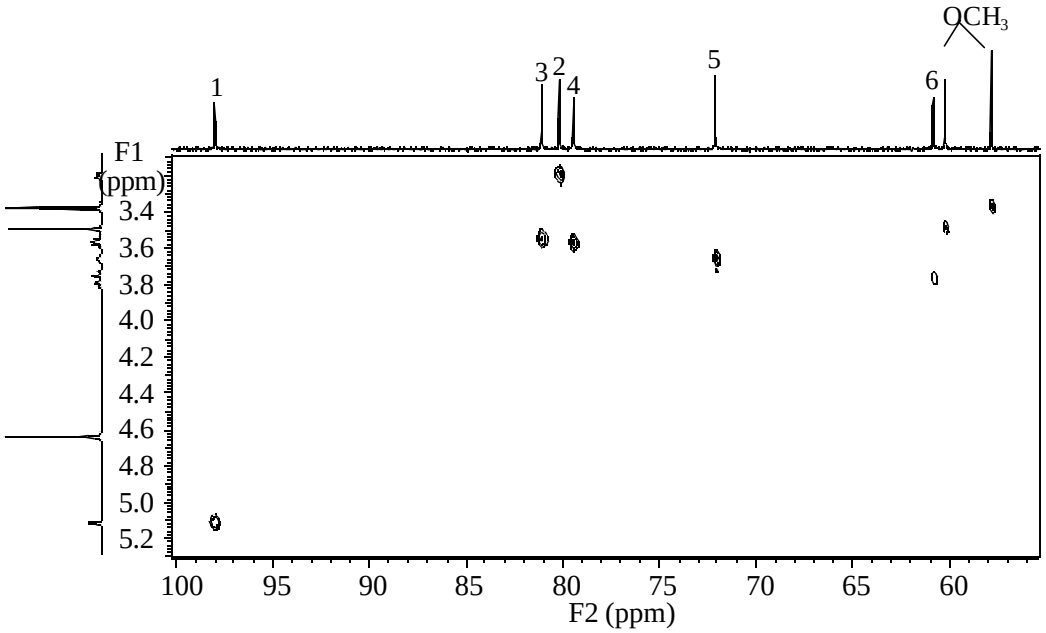

Figure 29. 2D HETCOR of (6) in $CDCl_3$ using 500 mHz NMR.

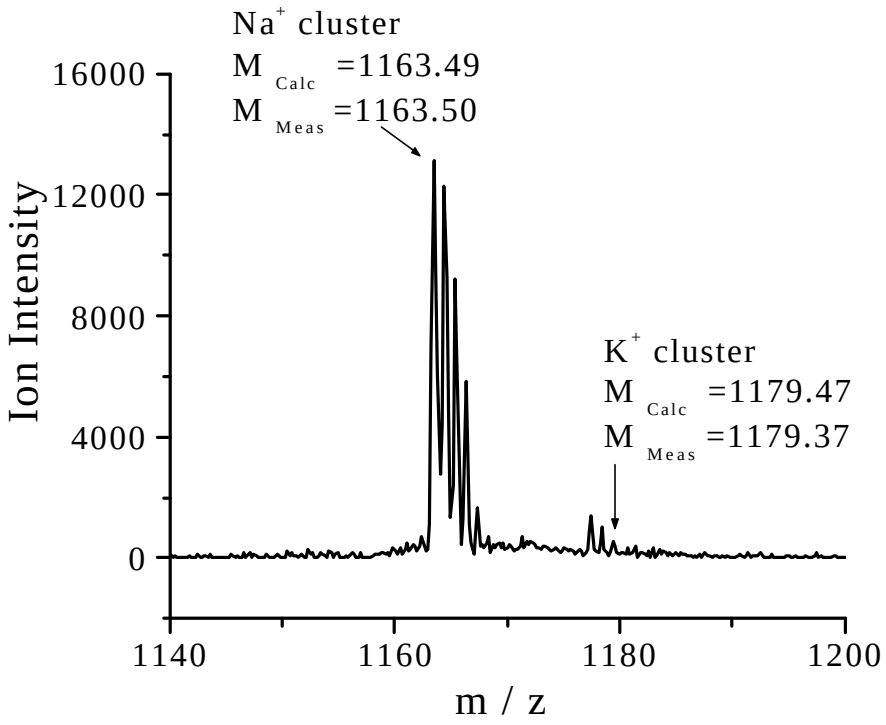

Figure30. High resolution MALDI-TOF-MS spectrum of (6). The measured m/z values agree well with the calculated monoisotopic value of sodium and potassium adduct portions.

found to be > 98 % by indirect UV detection CE as indicated in Figure 31 (assuming identical response factors). The assigned ^{1}H-^{1}H 2D COSY and ^{1}H-^{13}C 2D HETCOR NMR spectra of HxDMS are including in Figures 32 and 33, respectively.

The high resolution ESI-TOF mass spectra of the Na^{+} ion-adduct and Na^{+} ion-loss portion of the parent molecule, HxDMS from which two to five Na^{+} dissociated are shown in Figure 34. The measured m/z values agree well with the calculated values.

2.3 Summary

The sodium salt of hexakis(2,3-di-*O*-acetyl-6-*O*-sulfo)-α-CD (HxDAS), hexakis(6-*O*-sulfo)-α-CD (HxS), and hexakis(2,3-di-*O*-methyl-6-*O*-sulfo)-α-CD (HxDMS) have been synthesized on a large scale via regioselective protecting group chemistry and analytically characterized. Their purity was monitored by isocratic reversed phase HPLC and indirect UV detection CE, respectively. The structural identity of each intermediate and final product was determined by ^{1}H NMR, ^{13}C NMR, ^{1}H-^{1}H 2D COSY NMR, and ^{1}H- ^{13}C 2D HETCOR NMR spectra, mass spectrometry, and x-ray crystallography.

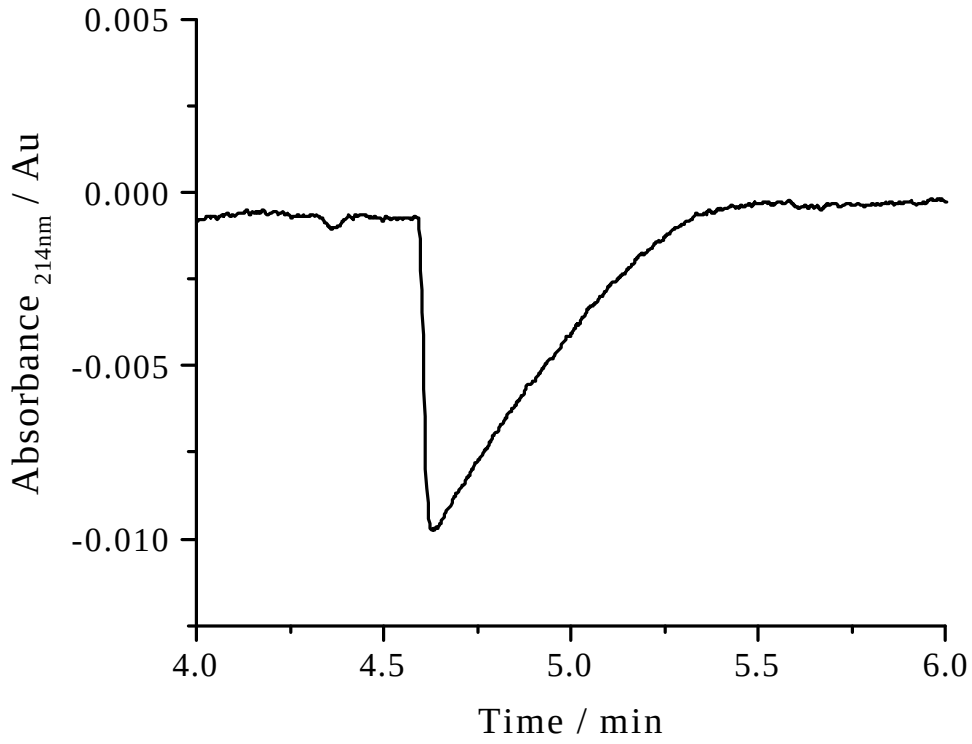

Figure 31. Indirect UV detection CE electropherogram of HxDMS. Purity > 98.9 %. Conditions: 20 mM pTSA / 40 mM Tris, pH = 8.0, (+) to (-) polarity, Lt / Ld =26.4 / 19.6 cm, 214 nm, 10 kV, T = 20ºC.

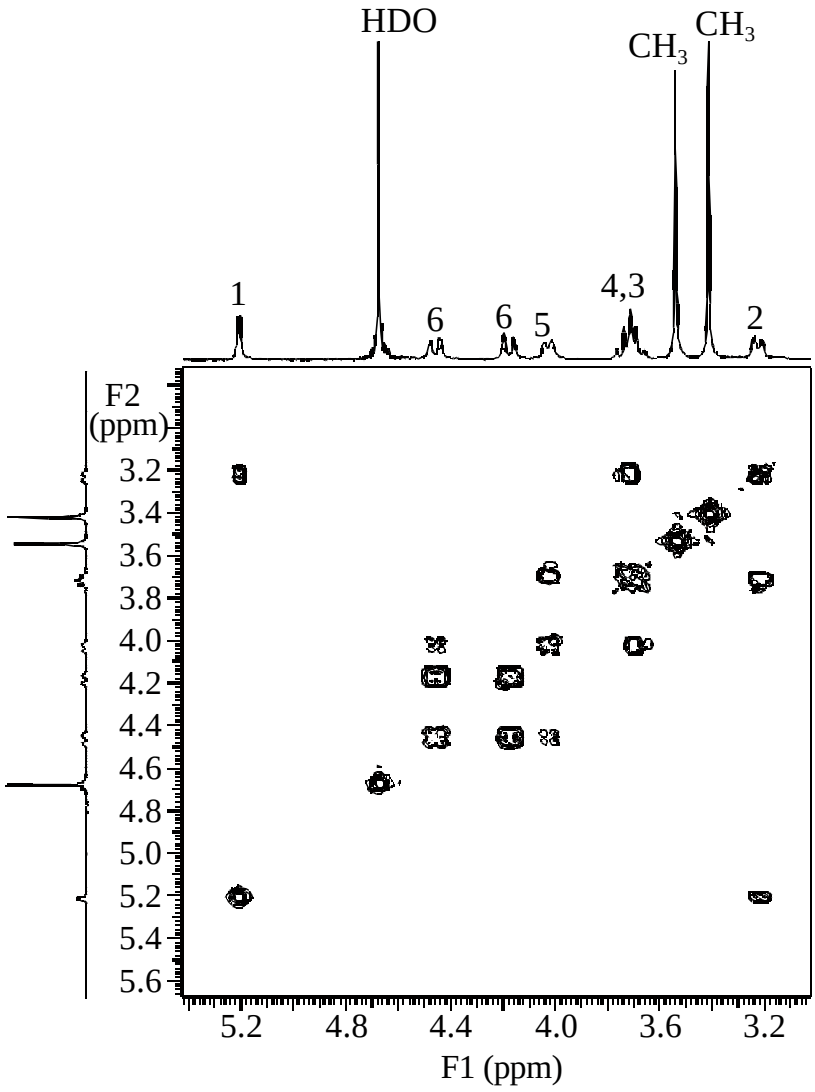

Figure 32. 2D COSY HxDMS in D_2O using 500 mHz NMR.

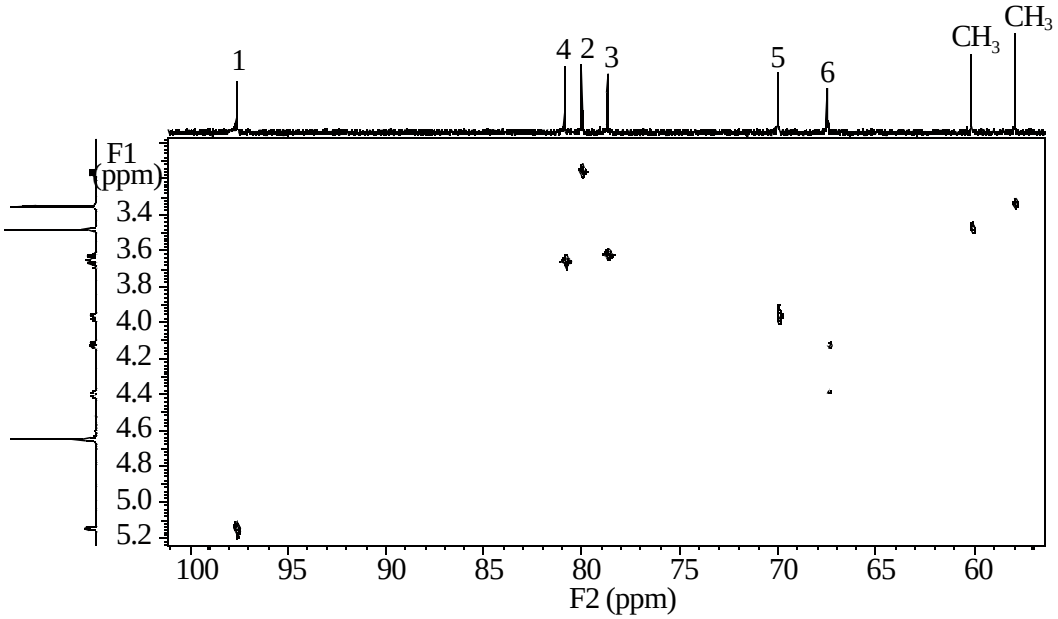

Figure 33. 2D HETCOR HxDMS in D_2O using 500 mHz NMR.

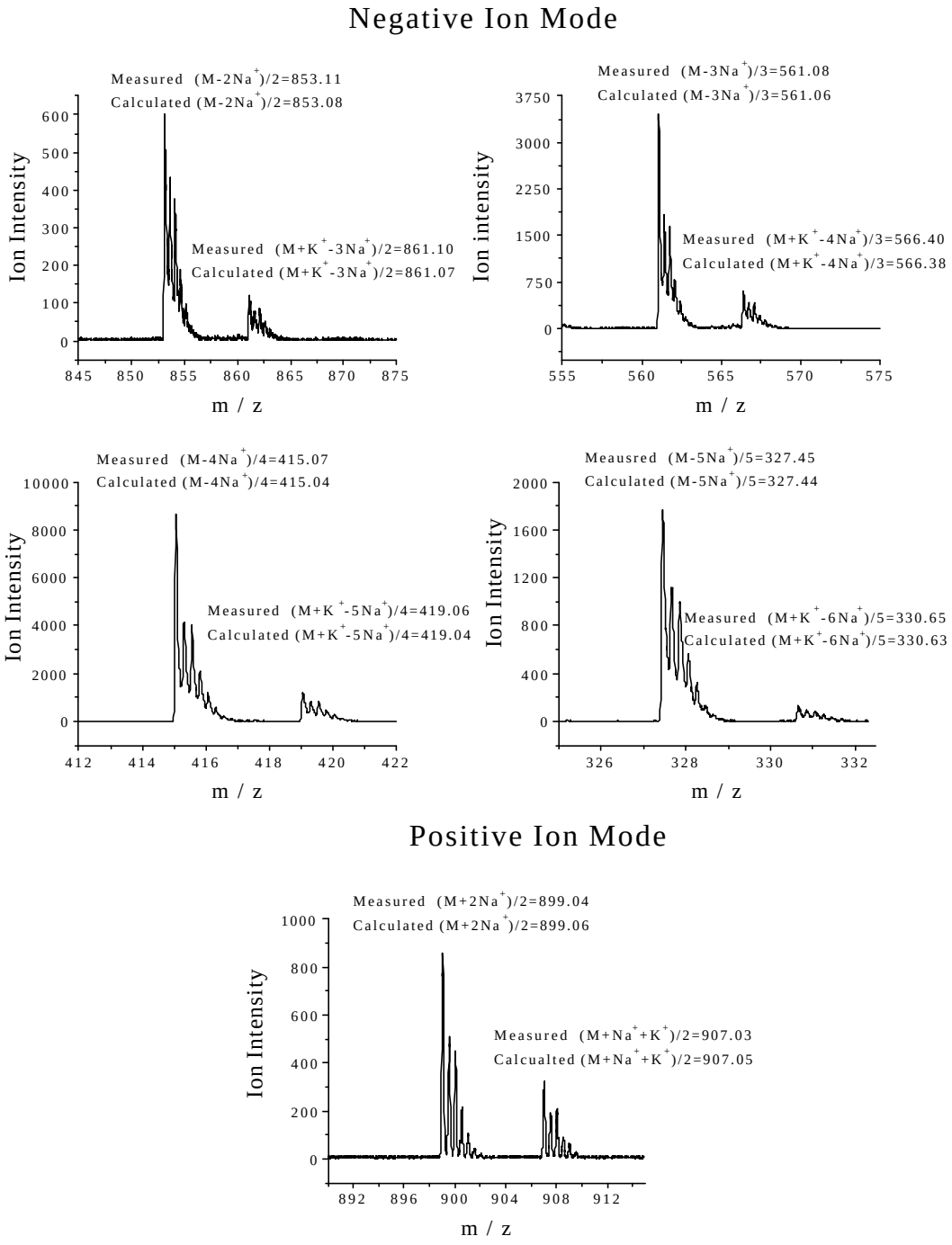

Figure 34. Portions of the high resolution ESI-TOF-MS spectrum of HxDMS.

CHAPTER III

ENANTIOMER SEPARATIONS WITH HxDAS*

The effects of the size of the cyclodextrins, and the polarity of the substituents, on the chiral recognition processes are very significant. Hexakis(2,3-di-*O*-acetyl-6-*O*-sulfo)-α-CD (HxDAS) possesses moderately hydrophobic acetyl substituents at the 2 and 3- positions on each glucose unit of native α-CD. It was the first choice to synthesize and to use as a chiral resolving agent in different BGEs.

3.1 Enantiomer Separations with HxDAS in Low pH BGEs

According to the CHARM model, when a strong electrolyte resolving agent, such as HxDAS is used, only two BGE pH, one at a low pH and another at a high pH are required [119]. According to previous work, low pH BGEs will provide good resolution values because more favorable β values can be obtained than in high pH BGEs. Therefore, investigations of enantiomer separations with HxDAS started in a low pH BGE.

3.1.1 Materials

The analytes were obtained from Sigma (St. Louis, MO). Phosphoric acid, hydrochloric acid and lithium hydroxide were purchased from Aldrich Chemical Company (Milwaukee, WI). Hexakis(2,3-di-*O*-acetyl-6-*O*-sulfo)-α-CD (HxDAS) was synthesized and

---

Part of the material in this chapter is reprinted with permission from:
S. L. Li and Gy. Vigh, Electrophoresis 21 (2003) 2487-2498; Copyright 2003-Wiley-VCH.

analytically characterized in our laboratory as described in Chapter II. Deionized water from a Milli-Q unit (Millipore, Milford, MA) was used to prepare all the solutions that were used in the experiment. The stock buffer was prepared by titrating of 25 mM H_3PO_4 to pH 2.5 with LiOH. The 0-75 mM HxDAS BGEs were prepared immediately prior to use by weighing out the required amounts of the sodium salt of HxDAS into 25mL volumetric flasks and bringing the volumes to mark with the pH 2.5 stock BGE solution.

3.1.2 Finding an EOF Marker

Nitromethane (NM), which proved to have zero effective mobility with the previously tested sulfated CDs was selected for HxDAS as well. Its suitability was determined according to Ref. [125]. Figure 35 shows two detector traces of NM in 50 mM HxDAS BGE during the first and second pressure mobilization steps and in superimposition. The first pass shows the NM position inside the 50 mM HxDAS BGE band before electrophoresis. On both sides of the HxDAS BGE band, there was plain, pH 2.5 H_3PO_4 / LiOH buffer. NM was injected into the 50 mM HxDAS BGE and base BGE portion. The second detector trace shows each analyte after a short electrophoresis step as they are mobilized pass the detector by nitrogen pressure. The relative movement of NM in the 50 mM HxDAS BGE before and after electrophoresis, with respect to NM in the base BGE bands, is identical indicating that NM does not complex with HxDAS. Since NM will have zero effective mobility in all HxDAS BGEs used in this work, it can be used as neutral marker to calculate the electroosmotic flow (EOF) mobilities [125].

3.1.3 CE Conditions

All enantiomer separations were performed on a P/ACE 2000 capillary

electrophoresis instrument using a 27μm i.d., bare fused silica capillary (Polymicro Technologies, Phoenix, AZ, USA) with a total length (Lt) of 26.4 cm, and 19.6 cm from injection to detector (Ld). A window for UV detection was prepared by removing a section of the polyimide coating with a flame, and then wiped clean with a methanol-soaked Kimwipe. All separations were obtained at 2-10 kV applied potential, positive to negative electrode polarity, at 214 nm UV wavelength, and 20°C cartridge coolant temperature. Between runs, the capillary was flushed with deionized water for 4mins, followed by the running buffer for 2mins. The analytes were pressure injected by 2 psi nitrogen for 1 s. All solutions used were passed through a 0.2μm pore size disc filter prior to use.

3.1.4 Materials and Methods

In order to test the hydrolytic stability of HxDAS in the stock BGE, a 50 mM HxDAS solution was prepared, stored in the refrigerator at 4°C for a week and repeatedly analyzed by the indirect UV detection CE method used during the synthesis of HxDAS. Acetate loss was first detected on the third day indicating that BGEs prepared freshly daily were safe to use.

Since NM has zero effective mobility in all HxDAS BGEs used in this work, it can be used as a neutral marker to calculate the electroosmotic flow (EOF) mobility. NM was co-injected with each sample to obtain effective mobilities of the enantiomers as:

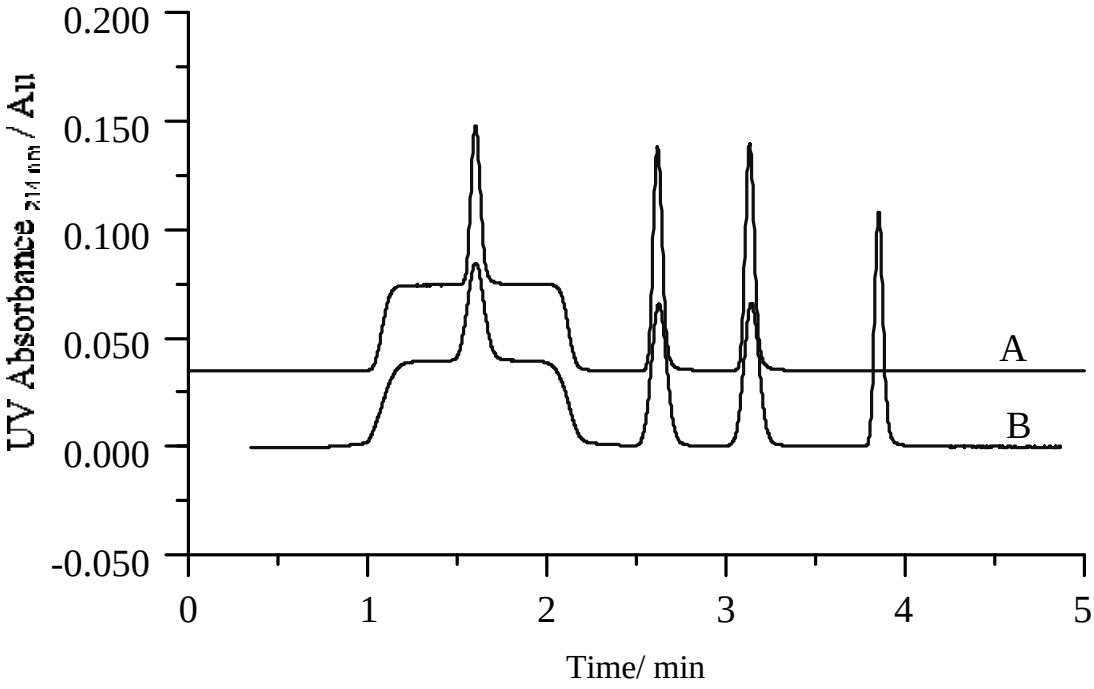

Figure 35. HxDAS does not complex with nitromethane. Trace A shows NM pass through detector before electrophoresis; trace B show NM pass through detector after electrophoresis.

$$m_i^{eff} = m_i^{obs} - m^{EOF} \quad (13)$$

The peak resolution, Rs, values was calculated using the following Equation:

$$Rs = 2(t_2 - t_1)/(w_1 + w_2) \quad (14)$$

where, subscript 2 refers to the enantiomer which has a lower effective mobility in the lowest HxDAS BGE that was used, t_1 and t_2 are the observed migration times of the enantiomers and w_1 and w_2 are the baseline peak widths of the respective enantiomer peaks. According to the Rs equation (see equation 10) [119, 126], the higher the applied electric field, the higher the Rs value that can be obtained. However, due to Joule heating effects, the applied potential must be in the linear region of Ohm's plot. In order to determine the highest potentials where Ohm's plots were still linear, the true electrophoretic currents were measured as a function of the applied potential value over the 0 to 75 mM HxDAS concentration range in 5 mM increment. All effective mobility values of the analytes reported in this dissertation were measured in the linear region of the Ohm's plots. The viscosities of the 0-75 mM HxDAS BGEs were measured using the P/ACE 2000 unit as a viscometer [127]. The results are shown in Figure 36, in which viscosities are plotted as a function of the concentration of HxDAS. The viscosity of the solution increased by about 40 % over the concentration range studied.

3.1.5 Effects of Analyte Mobilities

Since the effective mobilities of the polyanionic analyte-cyclodextrin complexes depend very strongly on the ionic strength of the BGE [119], the measured μ^{eff} values can only be used for qualitative comparison of the migration behavior. The concentration of HxDAS in the

system can affect the μ^{eff} values of the analyte-negatively charged CD complexes through three ways. First of all, the higher concentration of HxDAS used, the higher the mole fraction of the analyte that is present as an analyte-negatively charged CD complex. This, in turn, increases the anionic effective mobility of the analyte species. The second effect is based on the relationship between the mobility of the analyte and the viscosity of the solution, which can be approximated according to Walden's rule [128]:

$$m(C_{HxDAS}) \times h(C_{HxDAS}) = constant \quad (15)$$

where, $\eta(C_{HxDAS})$ refers to viscosity of the solution with a certain concentration of HxDAS. The mobility of the analyte decreases as the viscosity of the solution increases. Figure 36 shows that the higher concentration of HxDAS used in the system, the higher the viscosity of the solution, which will reduce the effective mobility of the analyte.

The third factor is based on the relation between the effective mobility of the analyte and the ionic strength of the solution. Increasing the concentration of HxDAS will significantly increase the ionic strength I, which was expressed as equation 8 [52-54]. The increasing ionic strength, in turn will decrease the μ^{eff} of the charged species, according to the equation 7 when the charge is lesser than or equal to 6 and $I < 0.1$ [52-54].

The mobility of the analyte then can be determined by both increasing the degree of complexation of the analyte with HxDAS and the mobility-reducing effects of both higher ionic strength and higher viscosity as the concentration of HxDAS was increased.

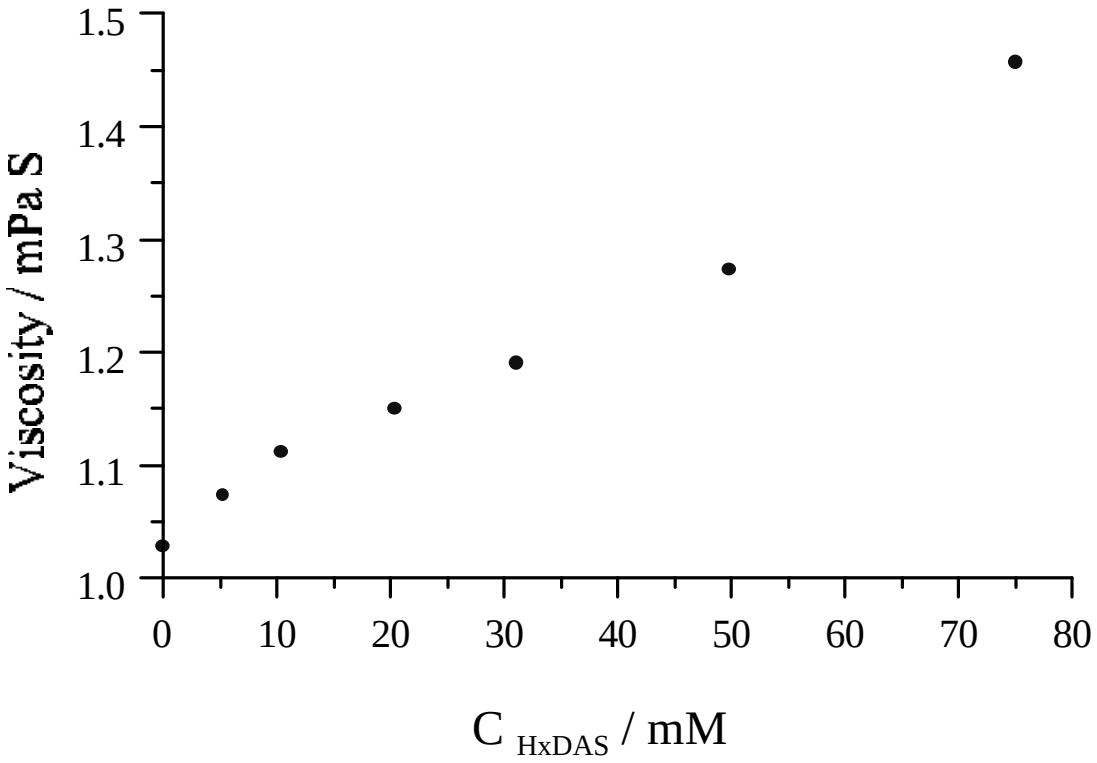

Figure 36. Viscosity of 25 mM H_3PO_4 / LiOH (pH = 2.5) buffers with different concentration of HxDAS.

3.1.6 Results and Discussion

A series of nonionic, weak acid, weak base and ampholytic enantiomers (shown in Figures 37-40, respectively) were separated with the pH 2.5 HxDAS BGEs. Table 1 lists the effective mobilities of the less mobile enantiomers, μ, the separation selectivities, α, the measured peak resolution values, Rs, the corresponding dimensionless EOF mobility values, β, and the injector-to-detector potential drop values, U, for the nonionic, weak acid, weak base and ampholytic enantiomers, respectively. An entry of N/A indicates that a value could not be calculated due to overlap with either a non-comigrating system peak or the neutral marker peak. The applied potential was limited to 8 kV in the 5 mM HxDAS-containing BGE and decreased with increasing HxDAS concentration to 2 kV in the 75 mM HxDAS containing BGE. Over the 5 to 75 mM HxDAS concentration range, the μ^{EOF} values were between (3 to 35)$\times 10^{-5}$ cm^2/Vs.

3.1.6.1 Separation of the Enantiomers of Neutral Analytes

The enantiomers of nine of the sixteen nonionic compounds tested could be separated. For the weakly complexing nonionic analytes, the effective anionic mobilities increased as the concentration of HxDAS is increased, but remained low, only reaching 11x10^{-5} cm^2/Vs, similar to what was observed with the β-CD analog, HDAS [103], and the γ-CD analog, ODAS [107]. Three typical effective mobility plots are shown in the top panel of Figure 41. The increasing degree of complexation of the nonionic analyte with HxDAS overrides the mobility-reducing effects of both higher ionic strength and higher viscosity as the concentration of HxDAS was increased. However, these nonionic enantiomers

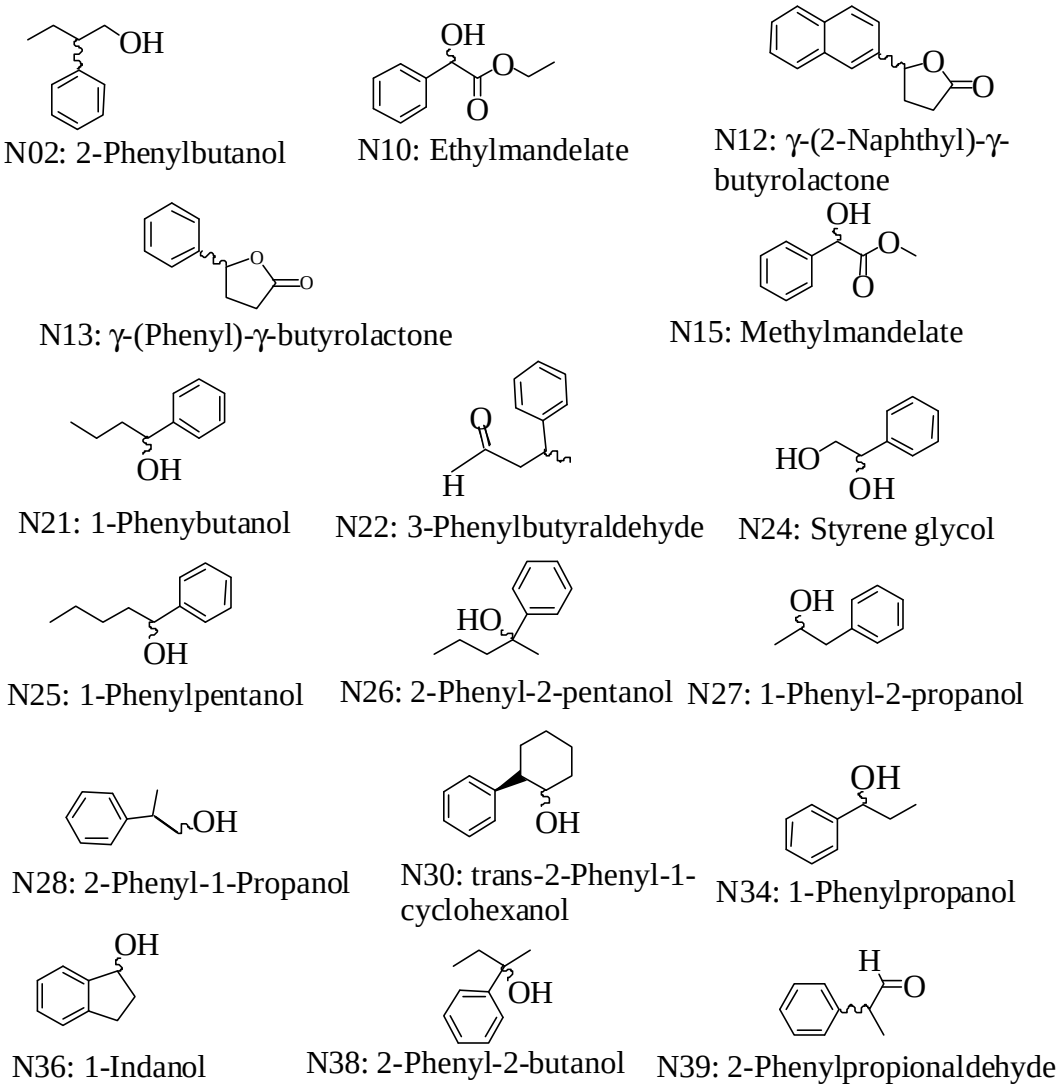

Figure 37. Names and structures of the nonionic analytes.

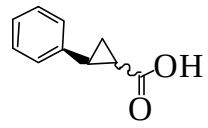

A02: trans- 2-Phenyl-1-cyclopropane carboxylic acid

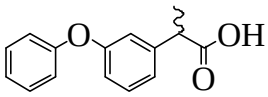

A22: Fenoprofen

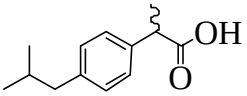

A23: Ibuprofen

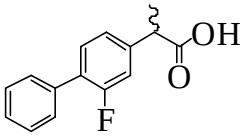

A26: Flurbiprofen

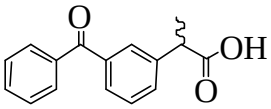

A27: Ketoprofen

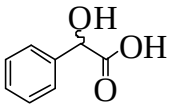

A28: Mandelic acid

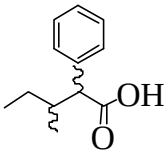

A30: 3-Methyl-2-phenylvaleric acid

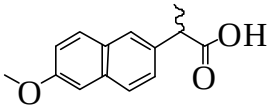

A31: Naproxen

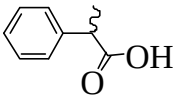

A36: 2-Phenylpropionic acid

Figure 38. Names and structures of the weak acid analytes.

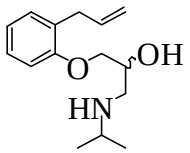

B02: Alprenolol

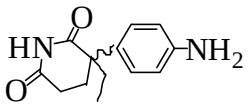

B03: Aminoglutethimide

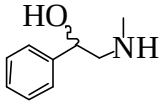

B04: Halostachine

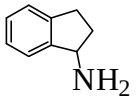

B05: 1-Aminoindan

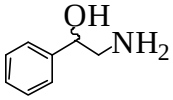

B06: Phenylethanolamine

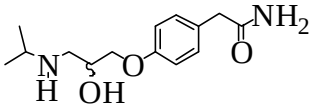

B08: Atenolol

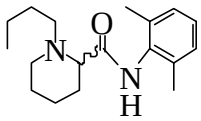

B10: Bupivicaine

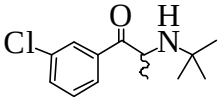

B11: Bupropion

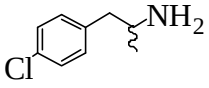

B13: 4-Chloroamphetamine

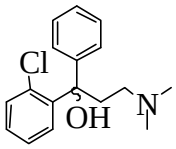

B14: Chlophedianol

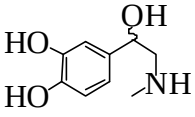

B16: Epinephrine

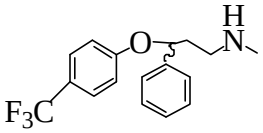

B18: Fluoxetine

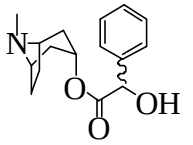

B19: Homatropine

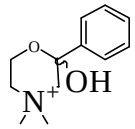

B20: Hemicholinium-15

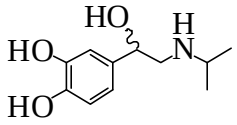

B21: Isoproterenol

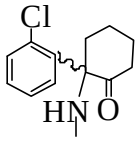

B22: Ketamine

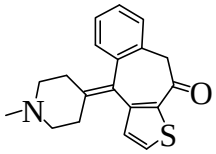

B23: Ketotifen

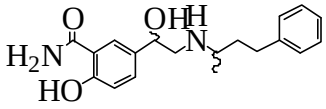

B24: Labetalol

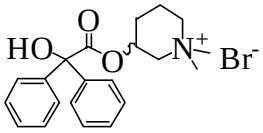

B25: Mepenzolate bromide

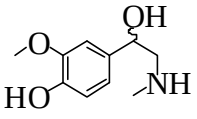

B26: Metanephrine

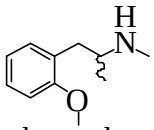

B28: Methoxyphenamine

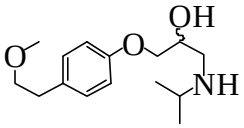

B31: Metoprolol

Figure 39. Names and structures of weak base analytes.

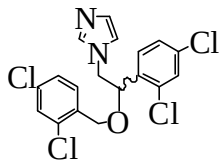

B32: Miconazol

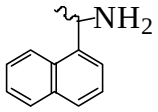

B33: (1-Naphthyl) ethylamine

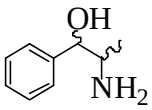

B34: Norephedrine

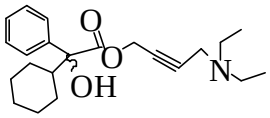

B35: Oxybutynin

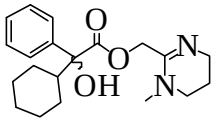

B36: Oxyphencyclimine

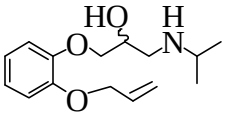

B37: Oxprenolol

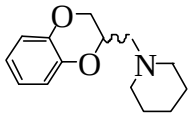

B38: Piperoxan

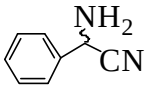

B39: Phenylglycinonitrile

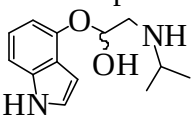

B41: Pindolol

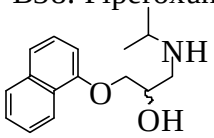

B42: Propranolol

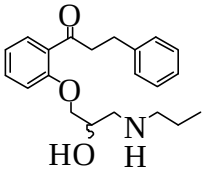

B43: Propafenone

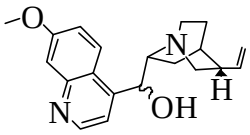

B44: Quinidine

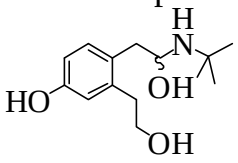

B45: Salbutamol

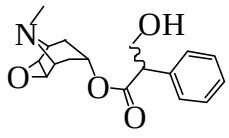

B46: Scopolomine

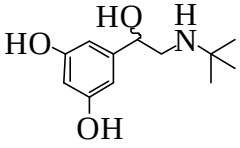

B47: Terbutaline

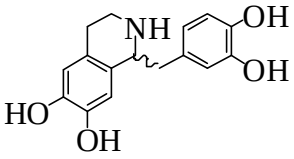

B49: Tetrahydropapaveroline

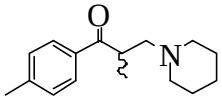

B51: Tolperisone

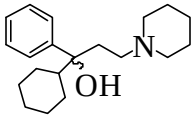

B53: Artane

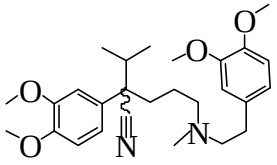

B54: Verapamil

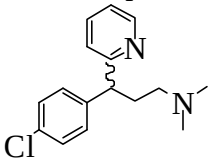

B56: Chlorpheniramine

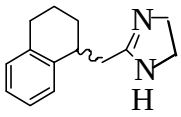

B58: Tetrahydrozoline

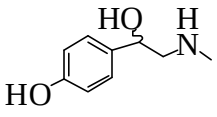

B61: Synephrine

Figure 39. Continued.

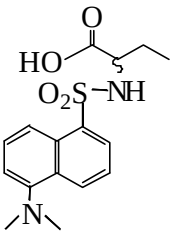

Z01: Dansyl-α-Amino-n-butyric acid

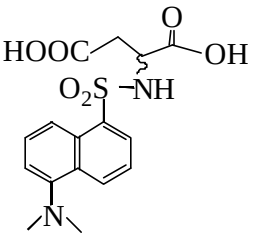

Z02: Dansyl-Aspartic acid

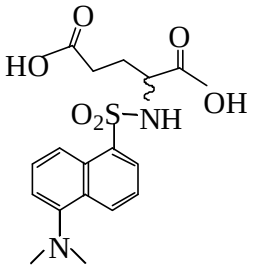

Z03: Dansyl-Glutamic acid

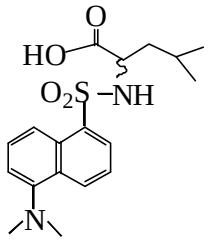

Z04: Dansyl-Leucine

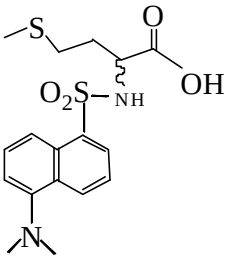

Z05: Dansyl-Methionine

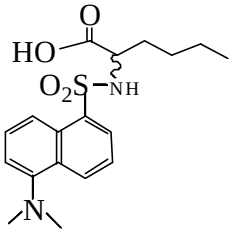

Z06: Dansyl-Norleucine

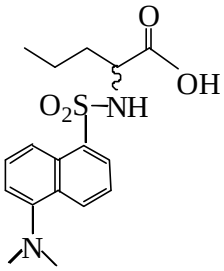

Z07: Dansyl-Norvaline

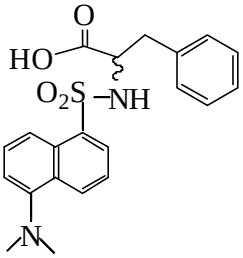

Z08: Dansyl-Phenylalanine

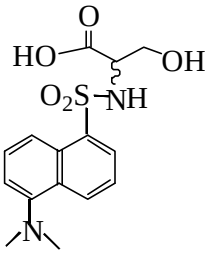

Z09: Dansyl-Serine

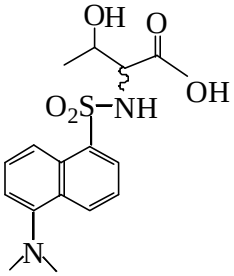

Z10: Dansyl-Threonine

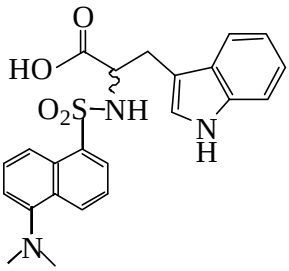

Z11: Dansyl-Tryptophan

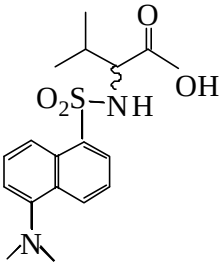

Z12: Dansyl-Valine

Figure 40. Names and structures of ampholytic analytes.

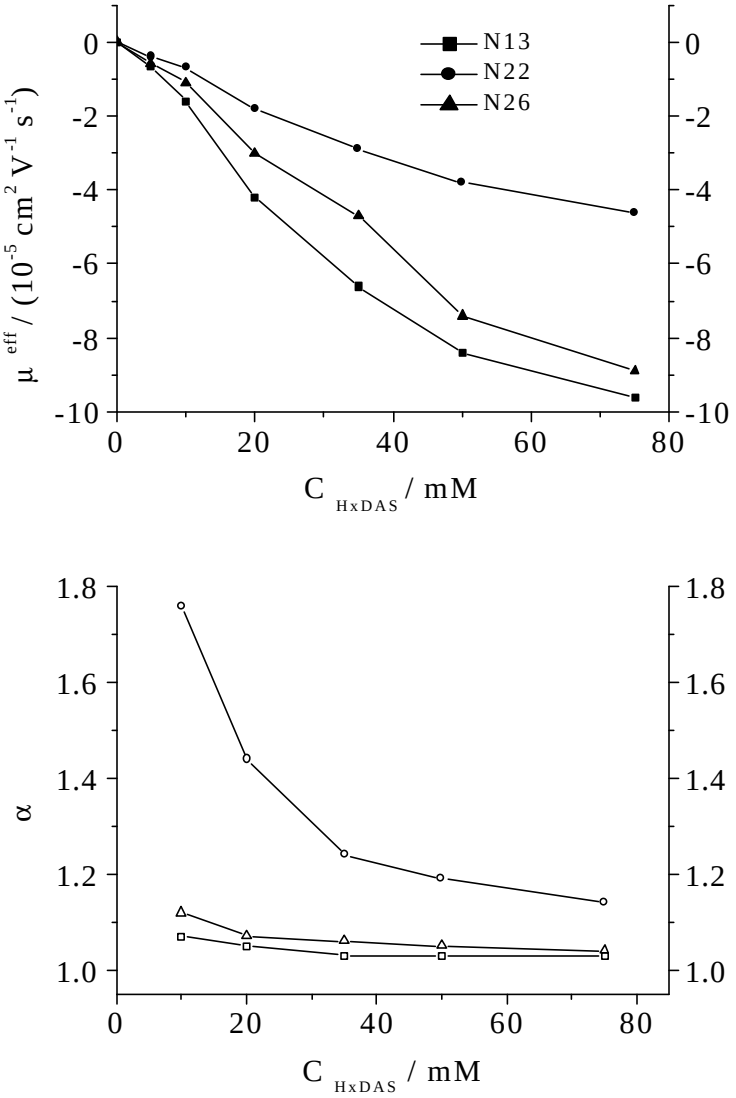

Figure 41. Effective mobilities and separation selectivities for the enantiomers of nonionic analytes in pH = 2.5 BGEs with HxDAS.

Table 1. Separation data in pH=2.5 HxDAS BGEs. (μ, in 10^{-5} cm^2 / Vs units)

HxDAS (mM)		5					10	
U (kV)		8					8	
Analyte	μ	α	β	Rs	μ	α	β	Rs
N02	-0.4	1.00	-24	0	-0.6	1.00	-23	0
N10	N/A				-0.2	1.00	-73	0
N12	-2.0	1.09	-7.2	1.1	-3.6	1.05	-4.0	<0.6
N13	-0.7	1.05	-20	<0.6	-1.6	1.07	-7.8	<0.6
N15	-0.2	1.03	-76	<0.6	-0.4	1.05	-36	<0.6
N21	N/A				N/A			
N22	-0.4	1.29	-26	1.1	-0.7	1.76	-13	1.6
N24	N/A				-0.2	1.00	-62	0
N25	-1.1	1.09	-25	0.8	-4.9	1.07	-3.1	0.8
N26	-0.6	1.06	-19	<0.6	-1.1	1.12	-9.1	0.8
N27	N/A				-0.1	1.00	-77	0
N28	N/A				-0.5	1.00	-12	0
N30	-0.6	1.03	-24	<0.6	-1.0	1.04	-11	<0.6
N34	-0.3	1.00	-37	0	-0.7	1.00	-21	0
N36	N/A				-0.3	1.20	-48	<0.6
N38	-0.2	1.00	-42	0	-0.4	1.00	-33	0
N39	-0.2	1.00	-42	0	-0.5	1.00	-20	0

Table 1. Continued.

HxDAS (mM)			20				35	
U (kV)			8				6	
Analyte	μ	α	β	Rs	μ	α	β	Rs
N02	-2.3	1.00	-7.2	0	-3.5	1.00	-3.2	0
N10	-1.9	1.00	-8.4	0	-2.1	1.00	-5.1	0
N12	-4.4	1.04	-3.7	<0.6	-5.4	1.04	-2.7	0.7
N13	-4.2	1.05	-3.8	<0.6	-6.6	1.03	-3.0	0.7
N15	-0.6	1.17	-21	<0.6	-0.9	1.22	-9.8	<0.6
N21	N/A				N/A			
N22	-1.8	1.51	-4.1	3.8	-2.9	1.48	-2.3	3.5
N24	-0.6	1.00	-24	0	-1.2	1.00	-8.4	0
N25	-7.8	1.03	-2.1	0.9	-9.2	1.02	-1.6	0.7
N26	-3.0	1.10	-4.9	0.7	-4.7	1.09	-3.9	0.7
N27	-1.0	1.00	-16	0	-1.6	1.00	-4.8	0
N28	-0.9	1.00	-7.3	0	-1.3	1.00	-5.2	0
N30	-3.2	1.03	-4.6	<0.6	-3.9	1.03	-3.1	<0.6
N34	-3.6	1.00	-4.2	0	-3.9	1.00	-3.4	0
N36	-1.1	1.18	-4.1	0.8	-1.3	1.11	-4.2	0.7
N38	-2.1	1.00	-7.0	0	-2.5	1.00	-6.4	0
N39	-1.5	1.00	-9.3	0	-1.9	1.00	-4.0	0

Table 1. Continued.

HxDAS (mM)			50				75	
U (kV)			4				4	
Analyte	μ	α	β	Rs	μ	α	β	Rs
N02	-3.9	1.00	-3.7	0	-4.7	1.00	-1.5	0
N10	-2.5	1.00	-4.6	0	-2.8	1.00	-2.9	0
N12	-5.8	1.03	-2.4	<0.6	-4.8	1.04	-2.1	<0.6
N13	-8.4	1.03	-1.8	1.3	-9.6*	1.03	-1.3	<0.6
N15	-1.1	1.27	-9.4	<0.6	-1.2	1.33	-6.7	2.3
N21	-9.0	1.03	-1.6	0.8	N/A			
N22	-3.8	1.42	-4.1	2.5	-4.6*	1.38	-2.4	3.2
N24	-1.6	1.00	-6.0	0	-1.9*	1.00	-5.2	0
N25	-10.9	1.02	-1.7	<0.6	-11.0**	1.00	-0.9	0
N26	-7.4	1.06	-2.6	0.6	-8.9	1.04	-1.3	1.7
N27	-2.3	1.00	-7.7	0	-2.9*	1.00	-2.3	0
N28	-1.7	1.00	-3.2	0	-1.9*	1.00	-4.3	0
N30	-4.5	1.02	-2.0	<0.6	-5.0*	1.02	-2.2	<0.6
N34	-4.3	1.00	-3.6	0	-4.8	1.00	-2.5	0
N36	-2.1	1.00	-4.7	0	-2.9*	1.00	-4.2	0
N38	-2.9	1.00	-5.2	0	-3.2	1.00	-2.2	0
N39	-2.1	1.00	-6.9	0	-2.9	1.00	-4.0	0

* U = 3 kV ** U = 2 kV

Table 1. Continued.

HxDAS (mM)	0					5				10			
U (kV)						8				8			
Analyte	μ	μ	α	β	Rs	μ	α	β	Rs	μ	α	β	Rs
A02	0	-0.8 -3.7	4.63 1.78	-24	10 25	-1.2 -5.1	4.25 1.63	-7.5	26 29				
A22	0	-1.9	1.00	-6.4	0	-3.5	1.00	-1.7	0				
A23	0	-1.7	1.00	-5.8	0	-3.1	1.00	-2.2	0				
A27	0	-1.3	1.00	-5.1	0	-2.0	1.00	-2.3	0				
.A28	0	-1.4	1.00	-7.1	0	-1.8	1.00	-3.6	0				
A29	0	-0.6	1.03	-15	<0.6	-0.9	1.12	-6.2	1.8				
A30	0	-1.3	1.40	-4.2	1.6	-1.9	1.50	-2.7	11				
A31	0	-1.5	1.53	-4.3	2.9	-1.8	1.58	-2.8	3.0				
A32	0	-2.5	1.08	-3.5	<0.6	-3.3	1.12	-2.2	0.9				
A36	0	-0.7	1.00	-9.6	0	-1.6	1.00	-4.1	0				

Table 1. Continued.

HxDAS (mM)			20				30	
U (kV)			8				6	
Analyte	μ	α	β	Rs	μ	α	β	Rs
A02	-1.6 -6.6	4.12 1.47	-9.6	18 20	-1.7 -6.8	3.98 1.41	-3.9	12 15
A22	-3.9	1.00	-5.7	0	-4.1	1.00	-1.5	0
A23	-4.3	1.00	-5.1	0	-4.9	1.00	-1.1	0
A27	-2.5	1.00	-6.8	0	-3.1	1.00	-2.7	0
.A28	-2.3	1.00	-9.1	0	-2.8	1.00	-3.1	0
A29	-1.7	1.08	-4.1	0.9	-2.5	1.07	-3.4	1.0
A30	-2.5	1.47	-4.5	4.8	-3.2	1.44	-3.4	5.3
A31	-2.4	1.59	-2.2	3.1	-2.8	1.57	-2.4	2.9
A32	-3.9	1.08	-1.3	2.4	-4.3	1.07	-1.7	2.3
A36	-2.0	1.00	-3.4	0	-2.3	1.00	-3.9	0

Table 1. Continued.

HxDAS (mM)	0			5			10		
U (kV)	10			8			8		
Analyte	μ	μ	α	β	Rs	μ	α	β	Rs
B02	24.7	9.4	1.08	0.7	<0.6	4.3	1.09	1.7	<0.6
B03	24.3	10.8	1.00	0.3	0	8.3	1.00	0.9	0
B04	33.2	15.7	1.01	0.3	<0.6	14.7	1.02	0.5	<0.6
B06	32.8	16.4	1.01	0.1	<0.6	15.8	1.03	0.5	<0.6
B08	21.1	9.6	1.04	0.5	<0.6	6.9	1.07	1.0	<0.6
B10	19.8	7.5	1.07	0.6	<0.6	5.2	1.15	1.4	0.9
B11	21.7	7.3	1.04	0.6	<0.6	2.1	1.17	4.0	1.1
B12	17.0	-2.1	0.41	-2.3	8.7	-3.4	0.50	-1.7	8.3
B13	27.9	6.0	1.11	0.8	<0.6	3.0	1.30	2.3	0.7
B14	23.4	N/A				2.6	1.00	3.1	0
B16	25.8	9.5	1.04	0.6	0.8	3.9	1.12	2.1	0.8
B18	18.5	-1.5	-0.66	-4.0	7.4	-3.3	0.33	-1.8	3.3
B21	24.1	8.2	1.02	0.6	<0.6	3.6	1.05	2.1	<0.6
B22	25.6	12.5	1.01	0.3	<0.6	9.0	1.01	0.8	<0.6
B23	21.4	N/A				N/A			
B24	18.4	N/A				N/A			
B26	23.7	5.2	1.07	0.9	<0.6	N/A			
B28	28.3	14.7	1.00	0.3	0	9.7	1.01	0.7	<0.6
B31	18.9	6.3	1.05	0.7	<0.6	3.4	1.14	1.9	0.8

Table 1. Continued.

HxDAS (mM)	20				30			
U (kV)	8				7			
Analyte	μ	α	β	Rs	μ	α	β	Rs
B02	2.0	1.18	2.6	1.5	2.2	1.33	4.2	1
B03	5.3	1.00	1.0	0	2.3	1.17	6.4	1
B04	12.0	1.03	0.5	<0.6	11.3	1.03	1.3	<0.6
B06	13.6	1.03	0.5	<0.6	11.4	1.06	1.2	<0.6
B08	4.7	1.11	2.6	<0.6	2.8	1.15	5.6	1
B10	3.6	1.21	3.2	1.1	2.7	1.32	1.6	2.6
B11	2.0	1.11	3.9	0.7	1.8	1.16	2.5	1.6
B12	-9.7	0.54	-1.6	7.6	N/A			
B13	0.5	1.60	14	0.7	-0.6	0.72	-10	0.6
B14	2.4	1.00	6.8	0	N/A			
B16	3.4	1.11	4.5	0.6	3.6	1.14	4.1	<0.6
B18	-4.4	0.46	-4.2	8.0	-4.6	0.58	-2.7	11
B21	4.5	1.04	1.4	<0.6	5.6	1.04	1.8	<0.6
B22	8.2	1.01	1.0	<0.6	7.9	1.01	0.8	<0.6
B23	N/A				N/A			
B24	N/A				N/A			
B26	2.0	1.13	3.8	1.1	2.1	1.15	3.5	1.2
B28	9.0	1.02	0.8	<0.6	8.5	1.02	0.8	<0.6
B31	2.1	1.14	2.7	1.1	1.8	1.15	2.9	1.4

Table 1. Continued.

HxDAS (mM)	40				50			
U (kV)	6				6			
Analyte	μ	α	β	Rs	μ	α	β	Rs
B02	1	1.36	7.5	1.6	0.6	1.61	32	1.1
B03	4.5	1.18	1.6	1.7	4.8	1.53	3.9	2.4
B04	8.9	1.04	2.8	<0.6	10.6	1.03	1.7	<0.6
B06	12.9	1.04	1.4	<0.6	11	1.04	1.7	<0.6
B08	2.5	1.16	2.8	1.5	3.3	1.15	6.3	0.8
B10	2	1.47	3.6	4.1	1.6	1.62	11	2.6
B11	1.6	1.21	4.8	1.4	1.4	1.26	13	0.9
B12	N/A				-7.6	0.65	-2.2	8.2
B13	0.7	1.57	7.5	1.2	0.5	1.4	39	0.9
B14	2.6	1	3	0	1.8	1	10	0
B16	4.2	1.07	1.7	1	4.4	1.09	3.6	0.9
B18	-4.7	0.66	-4.9	4.9	-4.6	0.65	-3.9	7.3
B21	4	1.03	3.5	<0.6	3.6*	1.03	2.9	<0.6
B22	7.8	1.01	1.8	<0.6	9.1	1.01	3.9	<0.6
B23	-7.9	0.99	-1.8	<0.6	-7.4	0.76	-2.5	1
B24	-4	0.89	-3.2	1.5	-3.7	0.97	-3.1	<0.6
B26	1.7	1.2	7	1.3	0.9	1.18	15	1
B28	7.7	1.03	1.5	<0.6	8.2	1.02	2.1	<0.6
B31	1.5	1.19	4.1	2	1.8	1.18	10	0.9

* U = 5 kV

Table 1. Continued.

HxDAS (mM)	0					5			
U (kV)	10					8			
Analyte	μ	μ	α	β	Rs	μ	α	β	Rs
B32	17.7	-2.2	0.87	-3.4	3.5	N/A			
B33	28.3	8.8	1.13	0.5	1.2	5.3	1.19	1.2	1.7
B34	27.5	15.7	1.00	0.2	0	12.3	1.01	0.6	<0.6
B35	18.0	6.9	1.00	0.5	0	4.1	1.05	1.7	0.7
B36	18.9	5.0	1.05	1.0	<0.6	1.6	1.16	5.7	0.9
B37	21.8	7.8	1.07	0.5	0.7	5.5	1.10	1.2	0.7
B38	24.5	4.7	1.26	0.9	3.5	3.3	1.45	1.7	3.6
B39	30.5	16.0	1.03	0.3	<0.6	11.7	1.06	0.5	1.0
B41	23.2	11.6	1.06	0.5	1.0	5.3	1.20	1.6	0.8
B42	24.3	-2.1	0.86	-3.0	1.4	-3.6	0.90	-1.6	1.9
B45	19.5	10.0	1.02	0.4	<0.6	9.3	1.03	1.3	<0.6
B47	21.0	N/A				N/A			
B49	18.6	5.7	1.04	0.9	<0.6	3.1	1.10	2.2	1.2
B51	20.6	8.5	1.04	0.5	<0.6	5.4	1.11	1.2	<0.6
B53	18.1	5.4	1.02	0.7	<0.6	1.3	1.18	5.3	0.7
B54	17.6	N/A				N/A			
B58	25.9	11.6	1.04	0.3	<0.6	8.1	1.05	1.0	<0.6
B61	24.2	10.6	1.02	0.4	<0.6	7.6	1.05	1.2	<0.6

Table 1. Continued.

HxDAS (mM)	20				30			
U (kV)	8				7			
Analyte	μ	α	β	Rs	μ	α	β	Rs
B32	N/A				N/A			
B33	3.9	1.21	1.9	1.5	3.0	1.32	2.8	1.7
B34	11.5	1.01	0.7	<0.6	10.6	1.02	1.0	<0.6
B35	2.9	1.06	2.8	<0.6	2.6	1.08	3.8	0.7
B36	1.0	1.34	6.6	1.4	N/A			
B37	6.4	1.07	2.8	<0.6	3.2	1.11	2.4	1.1
B38	1.2	1.82	6.9	4.2	0.6	2.09	7.2	5.9
B39	11.7	1.06	0.7	1.4	10.9	1.07	0.4	2.1
B41	-0.3	-1.34	-32	1.9	-0.7	-0.18	-4.8	6.0
B42	-4.8	0.93	-1.6	<0.6	-5.1	0.94	-2.5	1.4
B45	7.9	1.04	1.0	<0.6	N/A			
B47	N/A				6.4	1.04	0.6	0.8
B49	1.0	1.24	7.4	1.3	0.4	1.61	8.5	1.7
B51	2.2	1.32	5.2	1.4	1.0	1.59	3.1	3.5
B53	-2.3	0.61	-7.1	<0.6	-4.3	0.93	-3.0	0.9
B54	N/A				N/A			
B58	7.2	1.07	1.1	0.7	5.8	1.08	0.6	0.9
B61	6.8	1.05	1.1	<0.6	5.4	1.09	0.8	<0.6

Table 1. Continued.

HxDAS (mM)	40				50			
U (kV)	6							
Analyte	μ	α	β	Rs	μ	α	β	Rs
B32	N/A				-8.2	0.96	-2.2	1.3
B33	2.0	1.43	3.5	4.0	1.2	1.95	6.6	3.4
B34	9.3	1.03	0.8	0.6	10.9	1.02	1.4	<0.6
B35	2.0	1.10	3.2	0.8	1.8	1.16	8.6	<0.6
B36	-0.9	0.59	-8.8	<0.6	-0.5	0.88	-30	<0.6
B37	2.5	1.24	2.6	3.0	2.4	1.17	6.2	1.1
B38	0.3	4.52	25	5.2	0.5	3.10	30	3.1
B39	9.0	1.09	0.8	1.9	6.2	1.08	1.3	1.6
B41	-1.2	0.52	-5.8	3.3	-1.7*	0.65	-11	1.5
B42	-5.3	0.95	-4.7	0.7	-5.7	0.95	-3.0	1.0
B47	1.4	1.00	14	0.0	1.8	1.00	9.1	0
B45	5.3	1.04	3.6	<0.6	7.7	1.00	1.0	0
B49	-0.2	-0.09	-85	0.8	-0.8	0.57	-20	<0.6
B51	0.3	3.64	25	4.9	0.6*	1.83	17	1.5
B53	-2.5	0.66	-9.1	3.1	-1.3	1.00	-12	0
B54	N/A				-11.8*	0.94	-1.7	2.8
B58	4.6	1.08	3.7	1.0	5.5	1.07	1.5	0.8
B61	4.7	1.20	1.6	2.4	5.7*	1.05	13	<0.6

* U = 5 kV ** U = 3 kV

Table 1. Continued.

HxDAS (mM)	0			10	
U (kV)	10			8	
Analyte	μ	μ	α	β	Rs
Z01	16.0	1.3	1.22	12	<0.6
Z02	13.4	1.1	1.00	16	0
Z03	14.6	0.9	1.00	21	0
Z04	15.3	1.0	1.04	12	<0.6
Z05	15.0	0.8	1.00	14	0
Z06	16.5	0.14	1.90	81	0.7
Z07	16.0	0.6	1.00	18	0
Z08	15.2	0.4	1.00	38	0
Z09	14.7	1.5	1.23	6.3	1.1
Z10	15.4	1.7	1.09	8.8	<0.6
Z11	16.0	-2.5	0.91	-3.2	1.4
Z12	17.6	1.5	1.11	6.1	<0.6
Tryptophan	10.5	5.1	1.04	2.1	<0.6

Table 1. Continued.

HxDAS (mM)			20				35	
U (kV)			8				7	
Analyte	μ	α	β	Rs	μ	α	β	Rs
Z01	1.7	1.12	5.0	0.9	1.9	1.09	5.8	0.7
Z02	1.7	1.00	3.4	0	5.7	1.00	2.3	0
Z03	0.7	1.00	8.4	0	2.2	1.08	4.9	0.6
Z04	1.4	1.09	4.9	0.6	1.5	1.07	4.0	<0.6
Z05	1.1	1.00	5.2	0	1.8*	1.00	5.3	0
Z06	-0.8	0.88	-22	<0.6	-1.4*	0.91	-7.8	<0.6
Z07	0.8	1.00	7.7	0	1.7	1.12	7.0	0.6
Z08	0.2	1.00	12	0	2.4	1.00	3.3	0
Z09	2.0	1.18	3.7	1.1	2.2	1.13	4.9	0.6
Z10	2.2	1.03	3.3	<0.6	0.9*	1.16	11	0.7
Z11	-3.7	0.93	-5.0	0.8	-4.8*	0.96	-2.9	1.1
Z12	0.9	1.31	10	0.7	0.36*	1.49	19	0.9
Tryptop-han	4.7	1.06	1.8	<0.6	4.0*	1.07	1.2	0.6

Table 1. Continued.

HxDAS (mM)			50				75	
U (kV)			4				2	
Analyte	μ	α	β	Rs	μ	α	β	Rs
Z01	1.6	1.06	8.0	<0.6	1.3	1.03	6.0	<0.6
Z02	3.5	1.00	2.4	0	2.7**	1.00	3.8	0
Z03	0.8	1.28	11	1.0	0.4	1.00	25	0
Z04	1.3	1.05	11	<0.6	1.2	1.03	8.3	<0.6
Z05	1.5	1.00	4.9	0	1.4	1.00	7.5	0
Z06	-1.2	0.94	-14	<0.6	-0.4	1.00	-16	0
Z07	0.5	1.42	18	0.9	0.3	1.00	33	0
Z08	2.2	1.00	3.5	0	0.2**	1.00	44	0
Z09	2.1	1.06	5.7	0.7	2.3	1.00	4.7	0
Z10	0.4	1.00	5.7	0	0.5	1.00	20	0
Z11	-3.8	0.97	-5.1	0	-1.9	1.00	-5.2	0
Z12	1.5	1.32	6.1	0.7	1.1	1.08	10	<0.6
Trypto-phan	3.0	1.08	3.9	0.6	2.4	1.00	4.3	0

* U = 6 kV ** U = 3 kV

complexed moderately weakly with HxDAS, which leads to unfavorable β values (in the -70 to -2 range) and, consequently, inadequate peak resolution. The corresponding separation selectivities increase to a maximum and then slowly decrease as the concentration of HxDAS is increased (Figure 41, bottom panel), in agreement with the predictions of the CHARM model [119].

A very small structural change in the nonionic analytes can affect the chiral recognition processes with HxDAS. The small change of the carbon numbers in the long hydrophobic chain that contain the chiral center can affect the separation significantly. For example, the enantiomers of methylmandelate, 3-phenylbutyraldehyde, 1-phenylbutanol, 1-phenylpentanol and 2-phenyl-2-pentanol obtained enantiomer separations in pH 2.5 BGE with HxDAS; however, the enantiomers of ethylmandelate, 2-phenylpropionaldehyde, 1-phenylpropanol and 2-phenyl-2-propanol were not separated in pH 2.5 BGE with HxDAS. Changing the position of the chiral center along a chain while keeping the C number in the long chain constant also affects the chiral recognition processes dramatically. For example, the enantiomers of 1-phenylbutanol were separated, those of 2-phenylbutanol and 2-phenyl-2-butanol were not.

The cavity size of the cyclodextrins affects the enantiomer separations for the neutral analytes significantly. Figure 42 shows the effective mobility plots (top panel) and the corresponding separation selectivities (bottom panel) for methylmandelate with HxDAS, HDAS and ODAS as the chiral resolving agents. The strength of the inter-molecular interactions between methylmandelate and the three CD derivatives follows the order of ODAS ≅ HDAS > HxDAS. This can be explained by considering that the cavity size of ODAS and HDAS are suitable for methylmandelate to dip in.

3.1.6.2 Separation of the Enantiomers of Weak Acids

Of the ten weak acids studied, enantiomer separations were observed for five. Figure 43 shows a few typical effective mobility (top panel) and separation selectivity (bottom panel) plots for some of the weak acid enantiomers. The effective mobilities of the weak acid analytes in the HxDAS-free low pH BGE are initially close to zero and become increasingly anionic as the HxDAS concentration is increased, but only reach values as high as $-(4 - \text{to} - 11)\times10^{-5}$ cm^2/Vs. The observed separation selectivities pass through a shallow maximum at low HxDAS concentrations: whenever there is a separation, the α maximum values are generally much higher (in the $1.1 < \alpha < 1.6$ range) than what were observed with the β- and γ-CD analogs, HDAS [103] and ODAS [107].

3.1.6.3 Separation of the Enantiomers of Weak Bases

Enantiomer separations have been achieved for 35 of the 37 chiral weak bases tested. As with the γ-CD analog, ODAS [107], the weak base enantiomers can be divided into three groups: weakly binding, moderately strongly binding and strongly binding weak bases [113]. We consider a weak base to be a weakly binding weak base when its effective mobility remains cationic over the entire HxDAS concentration range tested [113]. The top panels in Figure 44 show the mobility (left panel) and separation selectivity (right panel) curves for four typical, weakly binding weak base enantiomers. In each case, the initially cationic effective mobility of the weak base is between 18×10^{-5} and 27×10^{-5} cm^2/Vs. As the HxDAS

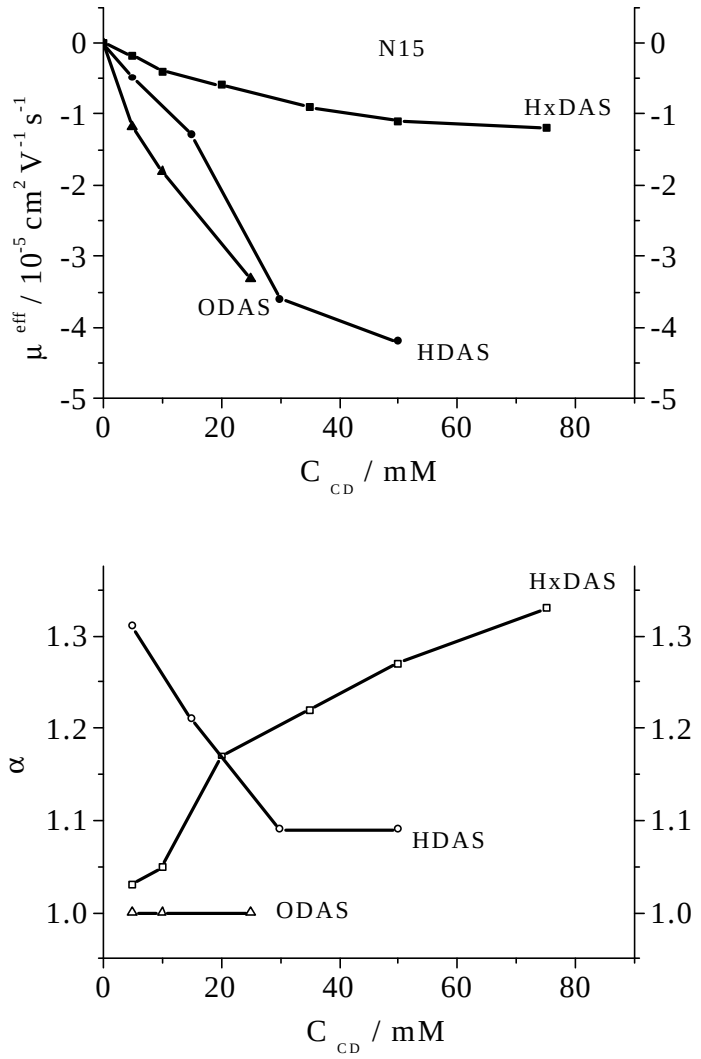

Figure 42. Effects of the cyclodextrin cavity size on the separation for the enantiomers of Methylmandelate in pH = 2.5 BGE with HxDAS, HDAS, ODAS.

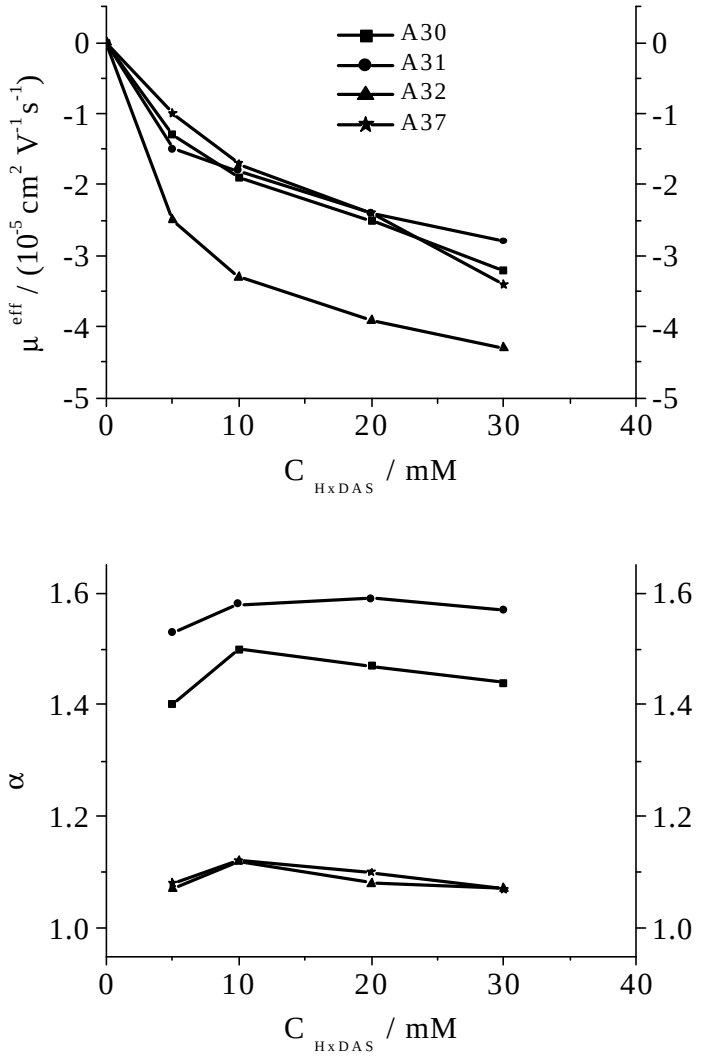

Figure 43. Effective mobilities and separation selectivities for the enantiomers of weak acid analytes in pH = 2.5 BGEs with HxDAS.

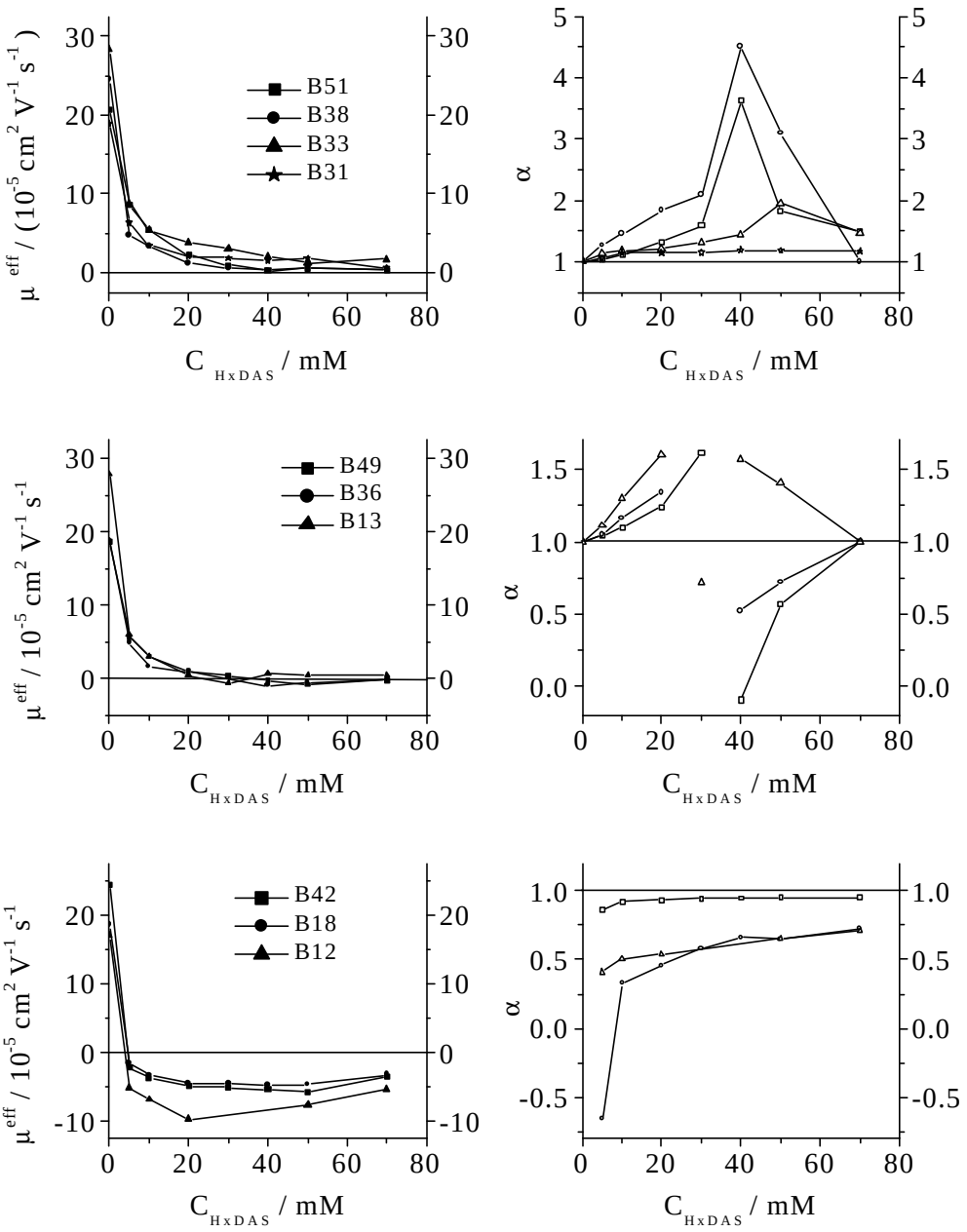

Figure 44. Effective mobilities and separation selectivities for weak base analytes in pH=2.5 BGEs with HxDAS. Weakly binding (top panels), moderately strongly binding (middle panels) and strongly binding (bottom panels).

concentration is increased, the effective mobilities of the weak bases approach zero, but do not become anionic, due to the combined effects of increased complexation with HxDAS and the ionic strength-related differential depression of the mobilities of the free and the complexed forms of the weak base [113]. For the weakly binding weak base enantiomers, separation selectivities pass a maximum as the HxDAS concentration is increased, as predicted by Ref. [113].

For this discussion, we consider a base to be a moderately strongly binding base when the effective mobilities of the enantiomers do become anionic, but remain close to zero [113]. The middle panels in Figure 44 show the mobility (left panel) and separation selectivity (right panel) curves for typical, moderately strongly binding weak bases. Separation selectivities become more favorable as the HxDAS concentration approaches the point where the effective mobility of one of the enantiomers changes from cationic to anionic, as also predicted by Ref. [113].

We consider a weak base to be a strongly binding weak base when its effective mobilities become more anionic than -5×10^{-5} cm^2/Vs in the HxDAS concentration range tested. The bottom panels in Figure 44 show the mobility (left panel) and separation selectivity (right panel) curves for three typical, strongly binding weak bases. As predicted by Ref. [113], their effective mobilities pass an anionic mobility extremum as the HxDAS concentration is increased, caused by the combined effects of increased complexation with HxDAS and the ionic strength-related differential depression of the mobilities of the free and the complexed forms of the weak base [113]. For some of these strongly binding weak bases, the effective mobilities become anionic in the $0 < C_{HxDAS} < 5$ mM range where no measurements were made. Therefore, the $\alpha > 1$ portions of the separation selectivity curves predicted by Ref. [113] are

not observed for them.

The cyclodextrin cavity size also dramatically affects the enantiomer separations for the weak base analytes at pH 2.5 with HxDAS. Figure 45 shows the effective mobility plots (top panel) and the corresponding separation selectivities (bottom panel) for piperoxan (B38) with HxDAS, HDAS and ODAS as the chiral resolving agents. The strength of the interactions between piperoxan and the three CD's derivatives also follows the order of ODAS ≅ HDAS > HxDAS. Piperoxan binds to HxDAS weakly (without crossing the zero mobility line), but it binds to ODAS and HDAS strongly.

3.1.6.4 Separation of the Enantiomers of Ampholytic Analytes

Of the fourteen ampholytic components tested, enantiomer separations were observed for ten. As shown in the top panels of Figure 46, these analytes can also be divided into weakly (in Figure 46, left panels) and strongly binding (in Figure 46, right panels) groups, and their migration (top panels) and separation selectivity (bottom panels) patterns follow trends similar to those of the weak base enantiomers. This is not surprising, because in the pH 2.5 BGE used, almost all of the ampholytic analytes are fully protoned cations.

A small change of the analyte structure, not only affects whether or not a separation is obtained, but it also affects the separation behavior. For example, the structures of Dansyl-leucine (Z04) and Dansyl-norleucine (Z06) are very similar, however, the former complexes with HxDAS weakly, and the latter complexes with HxDAS strongly. Figure 47 shows the effective mobility plots (top panel) and the corresponding separation selectivities (bottom

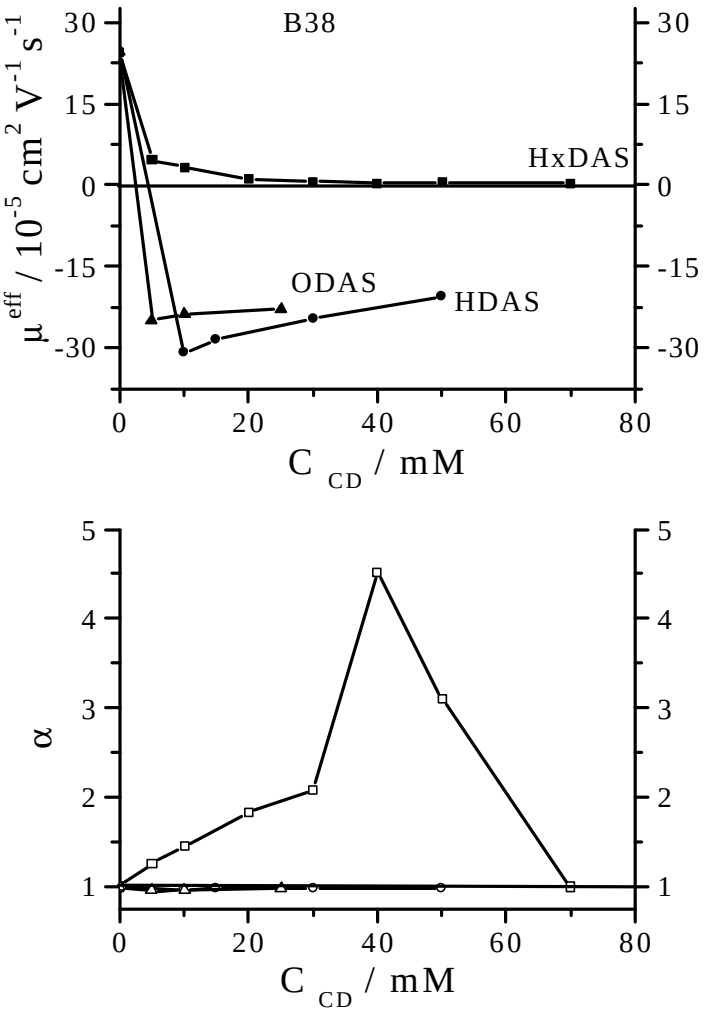

Figure 45. Effects of the cyclodextrin cavity size on the separation of the enantiomers of Piperoxan in pH = 2.5 BGEs with HxDAS, HDAS, ODAS.

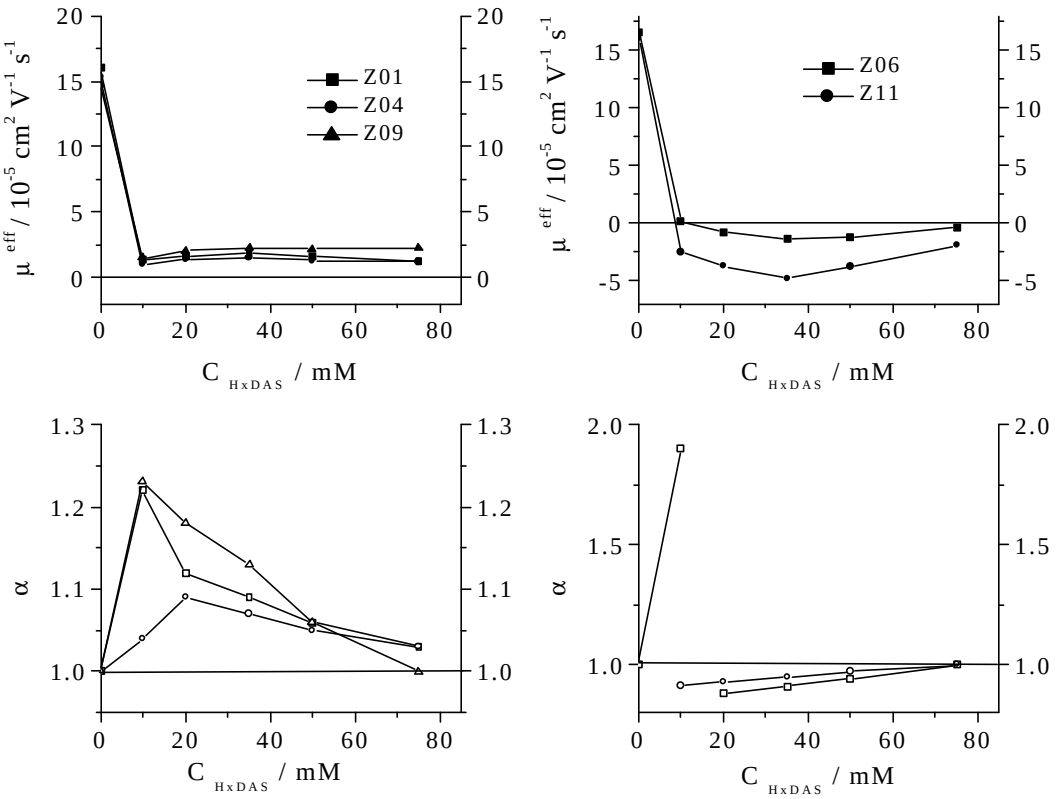

Figure 46. Effective mobilities and separation selectivities for the ampholytic analytes in pH = 2.5 BGEs with HxDAS. Weakly binding (left panels) and strongly binding (right panels).

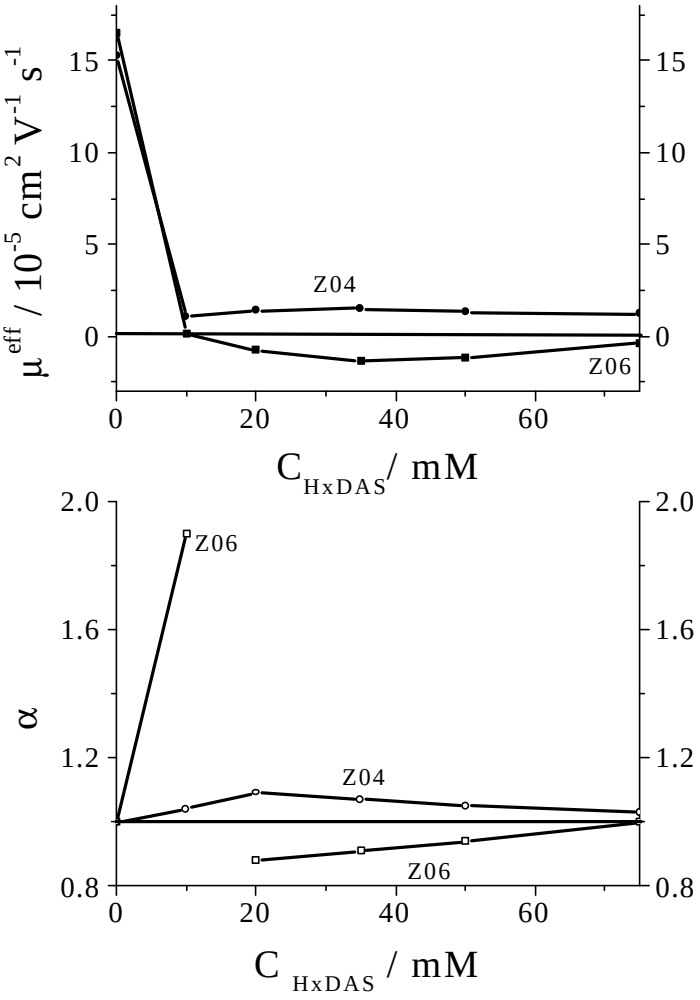

Figure 47. Effects of analyte structure on the separation of the enantiomers of ampholytic analytes in pH = 2.5 BGEs with HxDAS.

panel) for Z04 and Z06 with HxDAS as chiral resolving agent.

The cyclodextrin cavity size also affects the separation of the enantiomers of ampholytic analytes. Figure 48 shows the effective mobility plots (top panel) and the corresponding separation selectivities (bottom panel) for tryptophan with HxDAS, HDAS and ODAS as chiral resolving agents. The strength of the inter-molecular interactions between tryptothan and the three CD derivatives also follow the order: ODAS > HDAS > HxDAS. Tryptophan complexes with HxDAS weakly, but it complexes with ODAS and HDAS strongly, and the inter-molecular interactions between tryptophan and ODAS and HDAS are close to each other.

A few typical enantiomer separations obtained with HxDAS are illustrated in Figure 49 (for nonionic, weak acid and ampholytic analytes) and Figure 50 (for weak base analytes). The numbers under the compound codes (see Figures 37-40) show the concentration of HxDAS (in mM) and the applied potential (in kV) used. When shown, the peak of NM is indicated by N. Adequate peak resolutions were achieved, though with somewhat longer separation times than with HDAS and ODAS, for a number of structurally quite different analytes.

3.2 Enantiomer Separations with HxDAS in High pH BGEs

The previous studies have shown that HxDAS has excellent enantioseparation ability in low pH BGEs. Though the low pH buffer leads to favorable β values and therefore good peak resolution [119], the enantiomers of some of the analytes still cannot be separated at low pH. Therefore, it was interesting to investigate the separation behavior of HxDAS in high pH

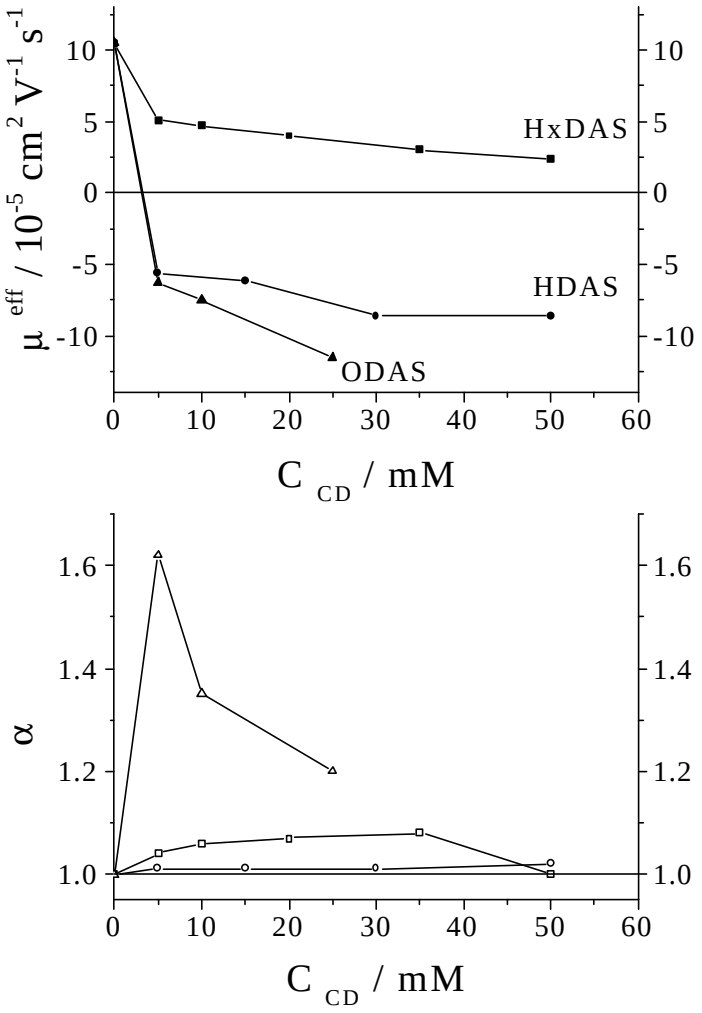

Figure 48. Effects of the cyclodextrin cavity size on the separation of the enantiomers of Tryptophan in pH = 2.5 BGEs with HxDAS, HDAS, ODAS.

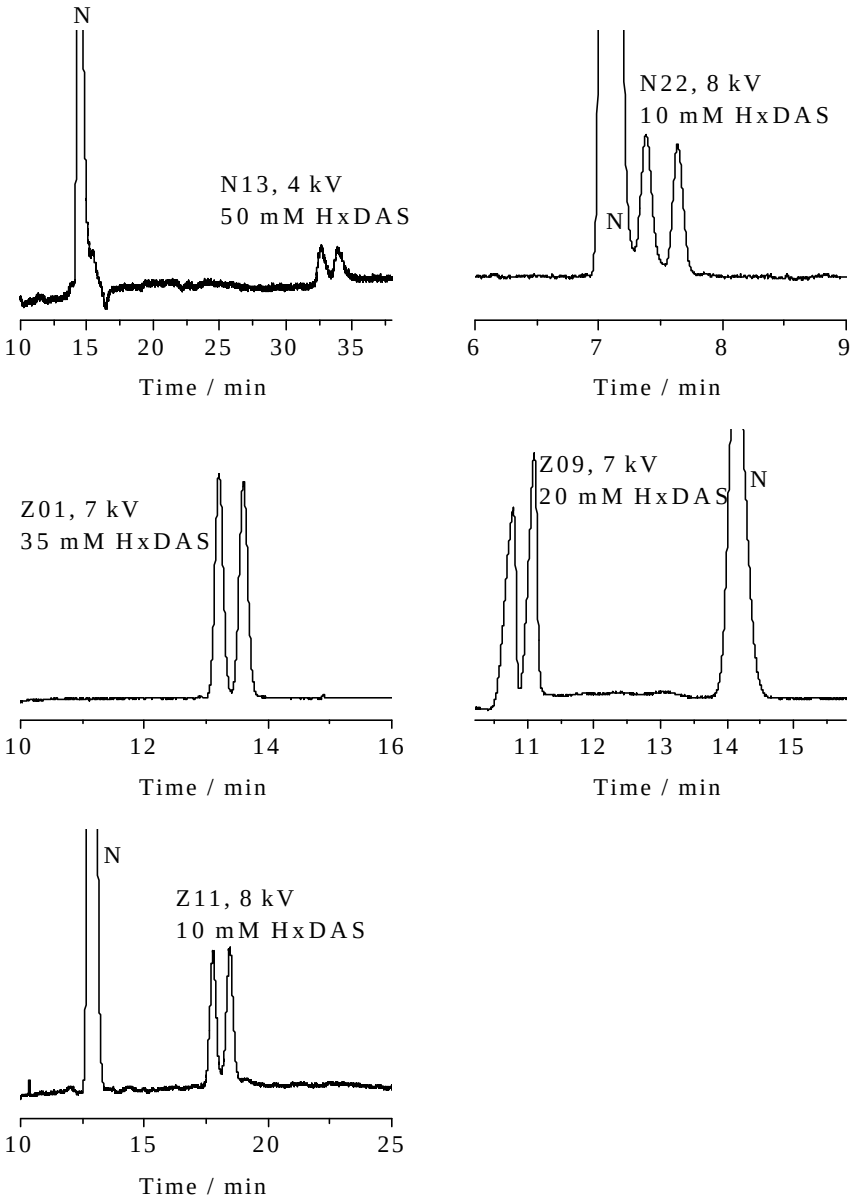

Figure 49. Typical electropherograms of nonionic, ampholytic analytes in pH = 2.5 BGEs with HxDAS.

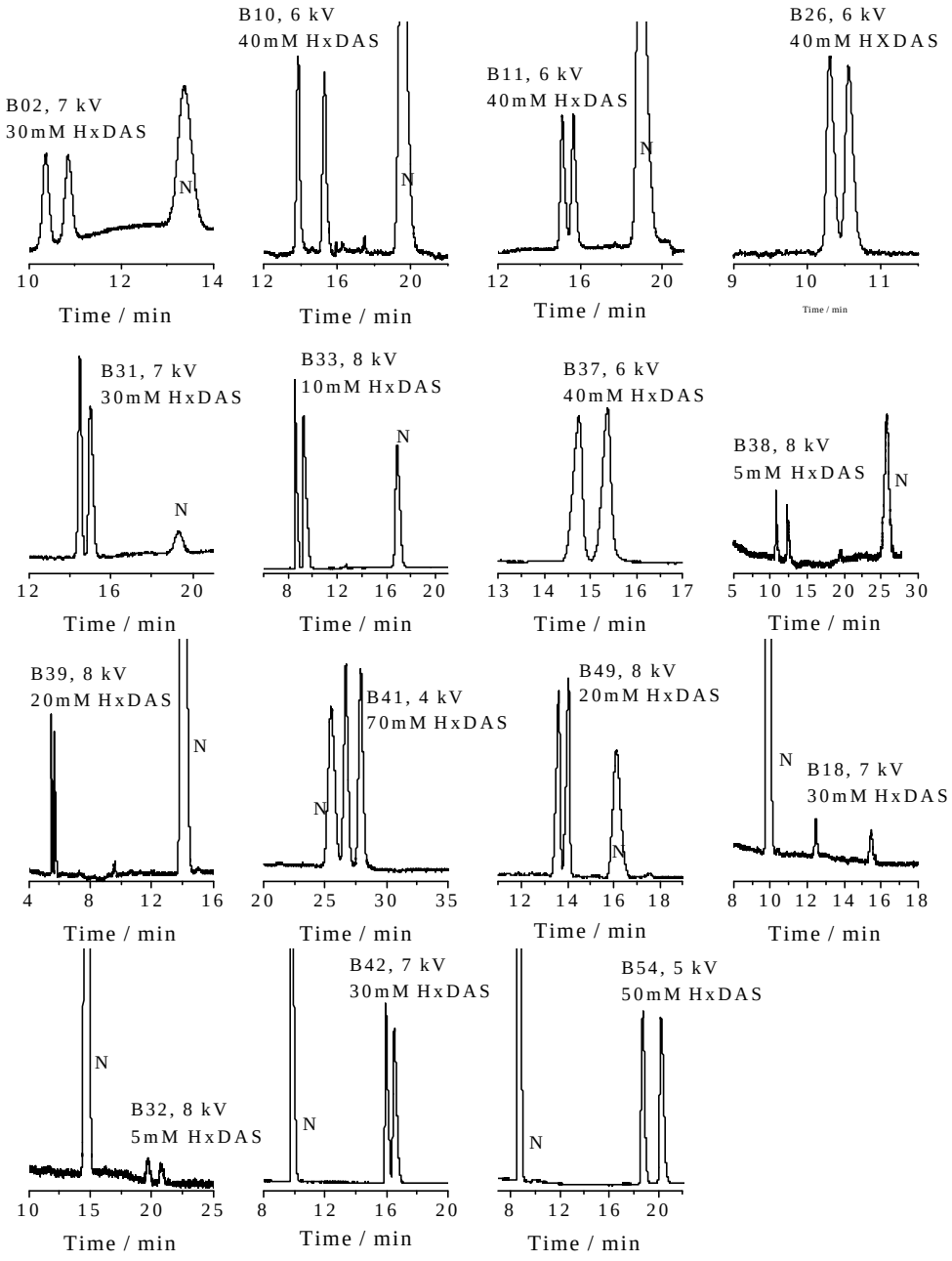

Figure 50. Typical electropherograms of weak base analytes in pH = 2.5 BGEs with HxDAS.

BGEs.

3.2.1 Experimental Conditions and Methods

Dimethylsulfoxide (DMSO) was also found not to complex with HxDAS at high pH. Therefore, it can be used as EOF marker. All CE separations were carried out in 25 mM ethanolamine BGEs adjusted to pH 9.5 with methane sulfonic acid (MSA). The 5 to 50 mM HxDAS BGEs were prepared by weighing out the required amounts of HxDAS into 25mL volumetric flasks and bringing the volumes to mark with the pH 9.5 stock BGE solution. The hydrolytic stability of HxDAS in the high pH stock BGE was also tested. Acetate loss was first detected on the third day indicating that BGEs prepared freshly just prior to use were safe to use. The other experimental details are the same as listed in 3.1.3-3.1.5.

3.2.2 Results and Discussion

HxDAS was used for the separation of the enantiomers of neutral, weak acid, weak base, and ampholytic analytes whose structures are shown in Figures 37-40. The effective mobilities of the slower enantiomer, μ, separation selectivities, α, measured peak resolution values, Rs, corresponding dimensionless EOF values, β, and applied potential drop values, U, for the neutral, weak acid, weak base, and ampholytic analytes are listed in Table 2. An entry of N/A indicates that a value could not be calculated due to overlap with either a non-comigrating system peak or the neutral marker peak. The applied potential was limited to 13 kV in the 5 mM HxDAS-containing BGE. The potential decreased with increasing HxDAS concentration to 4 kV in the 50 mM HxDAS containing BGES.

Over the 5 to 50 mM HxDAS concentration range, the μ^{EOF} values were between

(10 to 35)x10^{-5} cm^2/ Vs.

3.2.2.1 Separation of the Enantiomers of Neutral Analytes

Enantiomer separations were achieved for seven of the twelve nonionic compounds tested. For the weakly complexing nonionic analytes, the effective anionic mobility increased as the concentration of HxDAS increased, but remained low, only reaching 16 x 10^{-5} cm^2 / Vs, similarly to what was observed in low pH BGEs. Four typical effective mobility plots are shown in the top panel of Figure 51. Again, the increasing degree of complexation of the nonionic analyte with HxDAS did override the mobility - reducing effects of both the higher ionic strength and the higher viscosity as the concentration of HxDAS is increased. The nonionic enantiomers complexed moderately weakly with HxDAS, which lead to unfavorable β values (in the range of -60 to -2) and, consequently, inadequate peak resolution. The corresponding separation selectivities increased to a maximum and then slowly decreased as the concentration of HxDAS was increased (Figure 51, bottom panel), in agreement with the prediction of the CHARM model [119].

Again, as with the results obtained in low pH BGE, the structures of the analytes play a very important role in the enantiomer separation process. Very small structural changes of the nonionic analytes can affect the enantiomer separation results with HxDAS. For example, the enantiomers of 1-phenylbutanol (N21) were separated in pH 9.5 BGE with HxDAS, those of 1-phenyl-2-propanol (N27) were not.

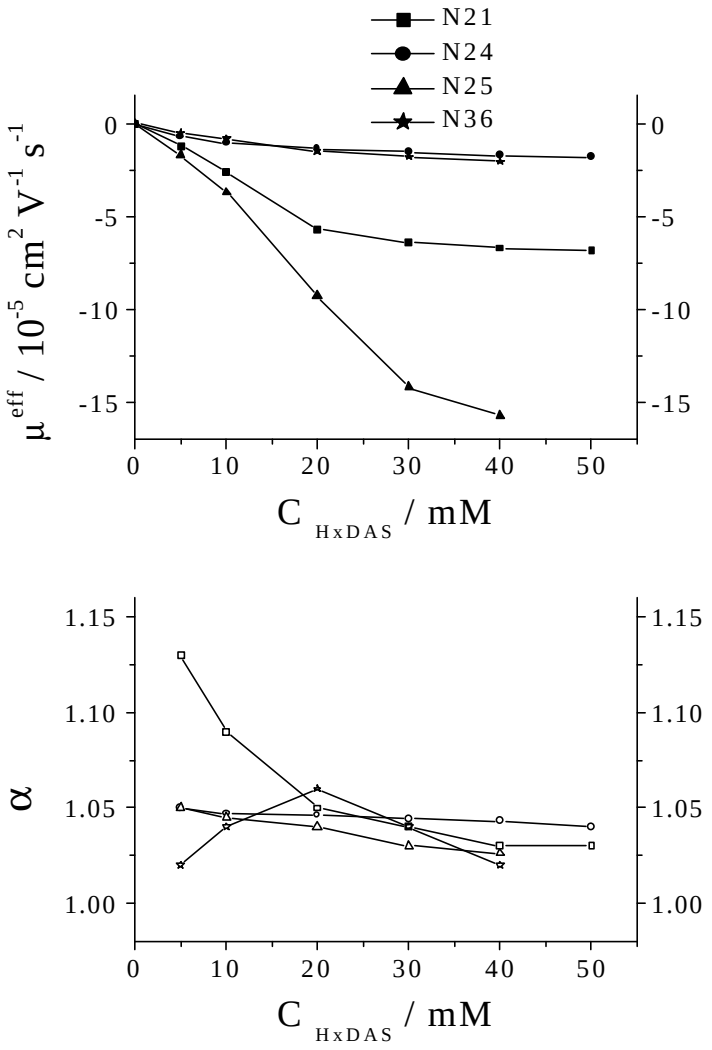

Figure 51. Effective mobility and separation selectivities for the enantiomers of nonionic analytes in pH = 9.5 BGEs with HxDAS.

Table 2. Separation data in pH=9.5 BGEs. (μ in 10^{-5} cm^2 V^{-1} s^{-1} unit)

HxDAS (mM)	0			5			10		
U (kV)			13				12		
Analyte	μ	μ	α	β	Rs	μ	α	β	Rs
N02	0	N/A				-0.9	1.00	-32	0
N21	0	-1.2	1.13	-15	<0.6	-2.6	1.09	-14	<0.6
N24	0	-0.7	1.05	-32	<0.6	-1.1	1.05	-25	<0.6
N25	0	-1.7	1.05	-21	<0.6	-3.7	1.05	-6.5	<0.6
N26	0	-1.0	1.00	-23	0	-2.2	1.00	-10	0
N27	0	-0.6	1.00	-37	0	-1.0	1.00	-23	0
N28	0	-0.5	1.00	-45	0	-1.0	1.00	-25	0
N30	0	-0.7	1.00	-36	0	-1.5	1.00	-17	0
N34	0	-1.0	1.00	-42	0	-2.3	1.00	-19	0
N36	0	-0.5	1.02	-61	<0.6	-0.8	1.04	-27	<0.6
N38	0	-0.7	1.00	-49	0	-1.1	1.00	-17	0
N39	0	-0.6	1.20	-29	<0.6	-1.4	1.27	-25	<0.6

Table 2. Continued.

HxDAS (mM)		20				30		
U (kV)		10				8		
Analyte	μ	α	β	Rs	μ	α	β	Rs
N02	-1.8	1.00	-7.2	0	-2.4	1.00	-10	0
N21	-5.7	1.05	-1.9	2.1	-6.4	1.04	-2.5	<0.6
N24	-1.3	1.05	-10	<0.6	-1.6	1.04	-19	<0.6
N25	-9.3	1.04	-1.6	2.7	-14.2	1.03	-5.4	0.6
N26	-5.9	1.06	-2.6	1.1	-9.1	1.04	-4.8	<0.6
N27	-1.6	1.00	-8.5	0	-2.0	1.00	-11	0
N28	-1.7	1.00	-6.9	0	-2.0	1.00	-11	0
N30	-3.1	1.00	-4.1	0	-3.7	1.00	-8.6	0
N34	-5.2	1.00	1.0	<0.6	-6.0	1.06	-2.8	<0.6
N36	-1.5	1.06	-7.8	<0.6	-1.8	1.04	-8.8	<0.6
N38	-1.9	1.00	-6.0	0	-2.2	1.00	-10	0
N39	-2.3	1.21	-7.1	<0.6	-2.4	1.13	-10	<0.6

Table 2. Continued.

HxDAS (mM)		40				50		
U (kV)		4				2		
Analyte	μ	α	β	Rs	μ	α	β	Rs
N02	-2.9	1.00	-2.7	0	-3.2	1.00	-1.4	0
N21	-6.7	1.03	-1.8	<0.6	-6.8	1.03	-2.5	<0.6
N24	-1.7	1.04	-3.7	<0.6	-1.8	1.04	-32	<0.6
N25	-15.7	1.03	-1.2	2.3	N/A			
N26	-11.0	1.03	-1.4	<0.6	N/A			
N27	-2.3	1.00	-4.1	0	-2.5	1.00	-3.2	0
N28	-2.2	1.00	-4.2	0	-2.2	1.00	-3.4	0
N30	-3.9	1.00	-2.2	0	-4.1	1.00	-1.9	0
N34	-6.2	1.02	-1.3	<0.6	N/A			
N36	-2.1	1.02	-3.0	<0.6	N/A			
N38	-2.4	1.00	-2.4	0	-2.6	1.00	-3.2	0
N39	-2.5	1.05	-8.3	<0.6	N/A			

Table 2. Continued.

HxDAS (mM)	0			5				10	
U (kV)				13				12	
Analyte	μ	μ	α	β	Rs	μ	α	β	Rs
A04	-18.9	-16.8	1.00	-1.4	0	-15.2	1.00	-1.9	0
A22	-21.1	-18.3	1.00	-1.2	0	-15.7	1.00	-1.8	0
A23	-22.7	-17.4	1.00	-1.2	0	-16.1	1.00	-1.6	0
A26	-23.2	-20.5	1.00	-1.1	0	-17.5	1.00	-1.8	0
A27	-19.6	-17.2	1.00	-1.4	0	-15.7	1.00	-2.1	0
A30	-24.0	-9.2	1.03	-2.5	<0.6	-7.4	1.03	-1.9	<0.6
A31	-20.9	-16.2	1.00	-2.4	0	-15.3	1.00	-1.8	0
A36	-23.9	-19.8	1.00	-1.6	0	-18.4	1.00	-1.4	0
Z01	-24.9	-17.6	1.00	-2.1	0	-13.8	1.00	-1.3	0
Z04	-24.6	-16.7	1.00	-2.3	0	-12.1	1.00	-1.4	0
Z05	-21.8	-14.2	1.02	-2.1	<0.6	-11.7	1.03	-1.4	<0.6
Z06	-24.7	-19.6	1.00	-2.2	0	-17.8	1.00	-1.2	0
Z09	-22.7	-19.2	1.00	-2.1	0	-17.8	1.00	-1.4	0
Z10	-21.5	-19.0	1.00	-2.1	0	-17.8	1.00	-1.4	0
Z11	-19.0	-15.8	1.00	-2.3	0	-11.8	1.00	-1.5	0
Z12	-24.3	-16.2	1.00	-2.2	0	-15.1	1.00	-1.4	0

* applied potential U=5 kV

Table 2. Continued.

HxDAS (mM)			20				30	
U (kV)			10				8	
Analyte	μ	α	β	Rs	μ	α	β	Rs
A04	-15.5	1.00	-1.4	0	-16.1	1.00	-1.1	0
A22	-14.4	1.00	-1.6	0	-14.0	1.00	-1.3	0
A23	-14.9	1.00	-1.5	0	-13.9	1.00	-1.2	0
A26	-15.5	1.00	-1.5	0	-13.8	1.00	-1.1	0
A27	-14.5	1.00	-1.6	0	-13.4	1.00	-1.1	0
A30	-11.1	1.02	-1.2	<0.6	-12.1	1.02	-1.2	<0.6
A31	-14.4	1.00	-1.4	0	-13.8	1.00	-1.1	0
A36	-19.3	1.00	-1.1	0	-19.8	1.00	-1.1	0
Z01	-14.3	1.00	-1.7	0	-15.2	1.00	-1.5	0
Z04	-14.0	1.00	-1.7	0	-14.4	1.00	-1.3	0
Z05	-13.1	1.02	-1.8	<0.6	-14.8*	1.01	-1.1	<0.6
Z06	-16.0	1.00	-1.5	0	-13.8	1.00	-1.1	0
Z09	-14.6	1.00	-1.2	0	-12.1	1.00	-1.4	0
Z10	-14.1	1.00	-1.3	0	-12.5	1.00	-1.4	0
Z11	-12.5	1.00	-1.5	0	-13.1	1.00	-1.2	0
Z12	-14.2	1.00	-1.4	0	-13.4	1.00	-1.2	0

* applied potential U=5 kV

Table 2. Continued.

HxDAS (mM)	0		5			10			
U (kV)	14		13			12			
Analyte	μ	μ	α	β	Rs	μ	α	β	Rs
B02	10.4	5.5	1.02	4.5	<0.6	3.0	1.10	5.5	<0.6
B03	8.6	N/A				-0.8	0.92	-8.1	<0.6
B04	12.6	10.3	1.02	2.6	<0.6	9.1	1.04	0.8	0.6
B06	8.6	6.2	1.00	2.8	0	4.5	1.04	0.7	1.2
B08	10.9	5.8	1.06	4.0	0.6	2.6	1.26	2.4	2.7
B11	1.5	N/A				0.9	1.10	3.8	<0.6
B16	9.6	N/A				2.5	1.11	1.8	1.4
B18	10.3	N/A				-2.7	0.68	-1.8	11
B24	7.0	-1.9 -1.9 -1.9	1.00 1.00 1.00	-10	0 0 0	-4.2 -4.4 -4.5	0.87 0.96 0.97	-1.7	6.2 2.1 1.5
B25	18.0	2.4	1.09	8.0	<0.6	-3.0	0.90	-1.5	8.3
B26	6.0	N/A				0.5	1.35	9.0	1.5
B28	21.5	N/A				4.3	1.04	1.1	0.6
B31	10.6	N/A				1.3	1.33	7.6	1.3
B33	9.6	N/A				3.5	1.20	2.7	1.9

Table 2. Continued.

HxDAS (mM)	20				30			
U (kV)	10				6			
Analyte	μ	α	β	Rs	μ	α	β	Rs
B02	0.6	1.33	8.8	<0.6	-0.1	-2.36	-310	2.0
B03	-0.9	0.94	-6.5	<0.6	-1.2	0.92	-10	<0.6
B04	7.5	1.05	1.1	0.8	5.6	1.07	1.7	1.2
B06	3.7	1.05	1.2	1.5	4.2	1.07	1.5	1.9
B08	0.8	1.51	10	1.7	0.6	1.67	20	1.9
B11	0.5	1.43	19	1.2	0.2	2.60	26	0.7
B16	3.0	1.13	2.7	0.7	3.3	1.13	4.1	1.7
B18	-6.6	0.88	-1.4	6.6	-6.5	0.81	-2.0	11
B24	-5.3 -5.4 -5.5	0.92 0.98 0.98	-1.8	3.5 1.2 <0.6	-6.1 -6.2 -6.3	0.92 0.97 0.98	-2.2	3.6 1.0 0.7
B25	N/A				-2.9	0.56	-4.6	1.6
B26	0.4	1.77	19	2.0	0.3	1.80	25	1.4
B28	6.4	1.06	1.1	0.8	5.8	1.05	2.4	0.9
B31	0.8	1.56	15	1.8	0.3	2.13	16	3.3
B33	2.0	1.44	8.3	3.7	0.6	1.69	26	1.3

Table 2. Continued.

HxDAS (mM)	40				50			
U (kV)	5				4			
Analyte	μ	α	β	Rs	μ	α	β	Rs
B02	-0.7	0.41	-10	1.2	-1.0	0.64	-10	2.1
B03	-1.4	0.91	-9.8	<0.6	-1.1	0.90	-9.2	<0.6
B04	4.4	1.09	1.8	1.2	5.6	1.05	1.8	1.3
B06	N/A				3.2	1.08	1.6	1.6
B08	N/A				-1.6	0.88	-6.4	1.0
B11	-0.3	-0.33	-23	1.2	-0.5	0.56	-22	1.0
B16	2.3	1.00	1.4	0	1.0	1.00	8.9	0
B18	-6.3*	0.77	-4.6	9.4	-6.1	0.73	-1.7	9.2
B24	N/A				-5.7 -5.8 -5.9	0.94 0.98 0.98	-1.8	2.8 0.7 0.6
B25	-0.1	-1.92	-16	3.8	0.6	1.00	16	0
B26	0.4	1.00	19	0	0.6	1.00	17	0
B28	4.0*	1.07	3.5	<0.6	3.7	1.06	2.6	1.0
B31	-0.3	0.45	-16	1.5	-0.5	0.77	-20	2.1
B33	1.4	1.45	1.6	2.4	1.8	1.20	1.5	1.0

* U=3 kV

Table 2. Continued.

HxDAS (mM)	0		5			10			
U (kV)	14		13			12			
Analyte	μ	μ	α	β	Rs	μ	α	β	Rs
B34	8.5	5.6	1.00	4.0	0.0	3.3	1.02	1.8	<0.6
B35	8.5	3.6	1.06	8.0	0.7	1.3	1.09	3.5	0.6
B36	16.0	0.5	1.09	19	<0.6	-0.7	0.83	-7.0	1.5
B37	10.5	5.5	1.06	3.6	0.6	2.0	1.11	3.2	1.2
B38	2.3	N/A				0.8	1.13	3.5	<0.6
B41	10.6	1.6	1.38	15	1.0	-0.3	-0.60	-51	3.4
B42	10.1	-2.8	0.83	-7.3	1.0	-4.4	0.89	-1.5	6.7
B45	6.0	N/A				4.9	1.06	1.4	1.3
B49	0.2	N/A				-1.0	0.85	-72	<0.6
B51	7.8	3.2	1.19	8.0	<0.6	0.6	1.83	14	3.3
B53	0.8	N/A				-1.4	0.64	-7.1	2.5
B54	0.0	N/A				N/A			
B56	9.9	N/A				-5.4	0.98	-1.4	0.6
B58	20.2	N/A				6.5	1.07	1.5	1.0
B61	10.4	N/A				5.5	1.05	1.4	0.9

Table 2. Continued.

HxDAS (mM)	20				30			
U (kV)	10				6			
Analyte	μ	α	β	Rs	μ	α	β	Rs
B34	4.8	1.03	2.2	0.7	4.1	1.04	3.5	0.8
B35	0.9	1.23	12	1.0	0.8	1.29	18	0.7
B36	-2.4	0.90	-4.1	1.5	-2.7	0.93	-5.6	1.0
B37	1.5	1.00	10	0	0.8	1.00	17	0
B38	-0.2	-1.62	-7.4	8.9	-0.7	0.30	-23	4.5
B41	-1.7	0.73	-4.1	3.7	-2.2	0.78	-6.3	3.5
B42	-6.4	0.92	-1.4	5.1	-6.7	0.93	-2.3	2.8
B45	3.9	1.08	1.1	1.8	4.3	1.09	3.4	0.9
B49	-1.7	0.90	-4.2	1.4	-1.8	0.93	-8.7	0.7
B51	-0.9	0.30	-4.9	6.2	-1.8	0.50	-17	3.4
B53	-1.6	0.80	-2.1	2.1	-1.6	0.88	-7.5	1.1
B54	N/A				N/A			
B56	N/A				N/A			
B58	3.2	1.12	1.5	1.2	3.7	1.15	4.1	0.6
B61	2.2	1.09	2.1	1.5	2.9	1.13	3.3	1.3

Table 2 Continued.

HxDAS (mM)	40				50			
U (kV)	5				4			
Analyte	μ	α	β	Rs	μ	α	β	Rs
B34	3.4	1.03	2.3	0.7	2.9	1.03	3.2	0.7
B35	-0.2	-1.69	-20	6.0	-0.4	0.57	-24	1.5
B36	-2.7	0.96	-2.8	0.6	-2.4	0.94	-3.1	0.6
B37	0.4	1.00	13	0	0.3	1.00	33	0
B38	-1.4	0.50	-6.2	4.2	-1.3	0.39	-6.6	7.7
B41	-2.4	0.83	-5.3	2.9	-2.7	0.85	-3.4	3.1
B42	N/A				-5.4	0.92	-1.7	2.8
B45	2.5	1.12	4.9	0.8	2.4	1.09	3.9	2.8
B49	-1.7	0.96	-9.9	<0.6	-1.6	0.94	-6.7	<0.6
B51	-2.7	0.64	-4.3	3.9	-2.1	0.61	-7.7	2.8
B53	-1.7	0.96	-2.6	0.7	-1.9	0.97	-4.8	<0.6
B54	N/A				-6.8	0.98	-2.2	1.1
B56	N/A				-6.2	0.99	-2.3	<0.6
B58	1.1	1.18	4.8	0.6	1.1	1.17	6.4	0.9
B61	1.5	1.16	4.0	0.7	1.3	1.12	7.7	0.7

3.2.2.2 Separation of the Enantiomers of Weak Acid and Ampholytic Analytes

Because in the pH 9.5 BGE used almost all of the ampholytic analytes are fully deprotoned anions, the separation behavior of ampholytic analytes are similar to those of the weak acid analytes. Of the ten weak acids and eight ampholytic components studied, enantiomer separation could be obtained only for one ampholytic analytes. This is not surprising, since the β values are unfavorable (-16 to -2), which leads to inadequate peak resolution values. The anionic mobilities are higher at low HxDAS concentration and become lower as the HxDAS concentration is increased. This phenomenon is due to interplay of their increasing complexation with HxDAS and the mobility suppressing effects of the increasing ionic strength and viscosity of the BGE [113]. The corresponding separation selectivity increased to a maximum and then slowly decreased as the concentration of HxDAS was increased, in agreement with the prediction of the CHARM model [119].

3.2.2.3 Separation of the Enantiomers of Weak Bases

Enantiomer separations have been achieved for 29 of the 29 weak bases tested. The effective mobilities and selectivities patterns are similar to those observed in the low pH BGE [129] indicating that pH 9.5 is not high enough to render most of the tested weak base analytes neutral. The weak base enantiomers can also be divided into three groups in the high pH BGEs: weakly binding, moderately strongly binding and strongly binding weak bases. The top panels in Figure 52 show the mobility (left panel) and separation selectivity (right panel) curves for two typical, weakly binding weak bases, while the middle panels show the mobility (left panel) and separation selectivity (right panel) curves for three typical, moderately strongly binding

weak bases. The bottom panels in Figure 52 show the mobility (left panel) and separation selectivity (right panel) curves for four typical, strongly binding weak bases.

The peak resolution values depend not only on the separation selectivities, but also, very sensitively, on the β values and the magnitude of the effective potential drop. Although the dimensionless electroosmotic flow mobilities (the β values) are fairly large, and thus unfavorable, adequate peak resolution values were obtained in less than 10 to 20 min for most of the weak bases studied, as shown in Figure 53. The numbers under the compound codes (see Figures 37) next to the electropherograms indicate the actual HxDAS concentrations (in mM) and effective separation potentials in kV (the actual potential drop between the injection point and the detector window).

3.3 Comparison of Separation Results in High pH and Low pH Aqueous BGEs

3.3.1 Neutral Analytes

The effective mobilities and separation selectivities of the neutral analytes in the high pH BGEs are similar to those in the low pH BGEs. Even though the effective mobilities increase anionically as the HxDAS concentration is increased in both pH BGEs, for some of the neutral analytes, the increase in pH 9.5 BGE with HxDAS is smaller than in the pH 2.5 HxDAS BGEs, indicating that the ethanolamine / MSA buffer components compete with the neutral analytes for the HxDAS more strongly than the H_3PO_4 / LiOH buffer components.

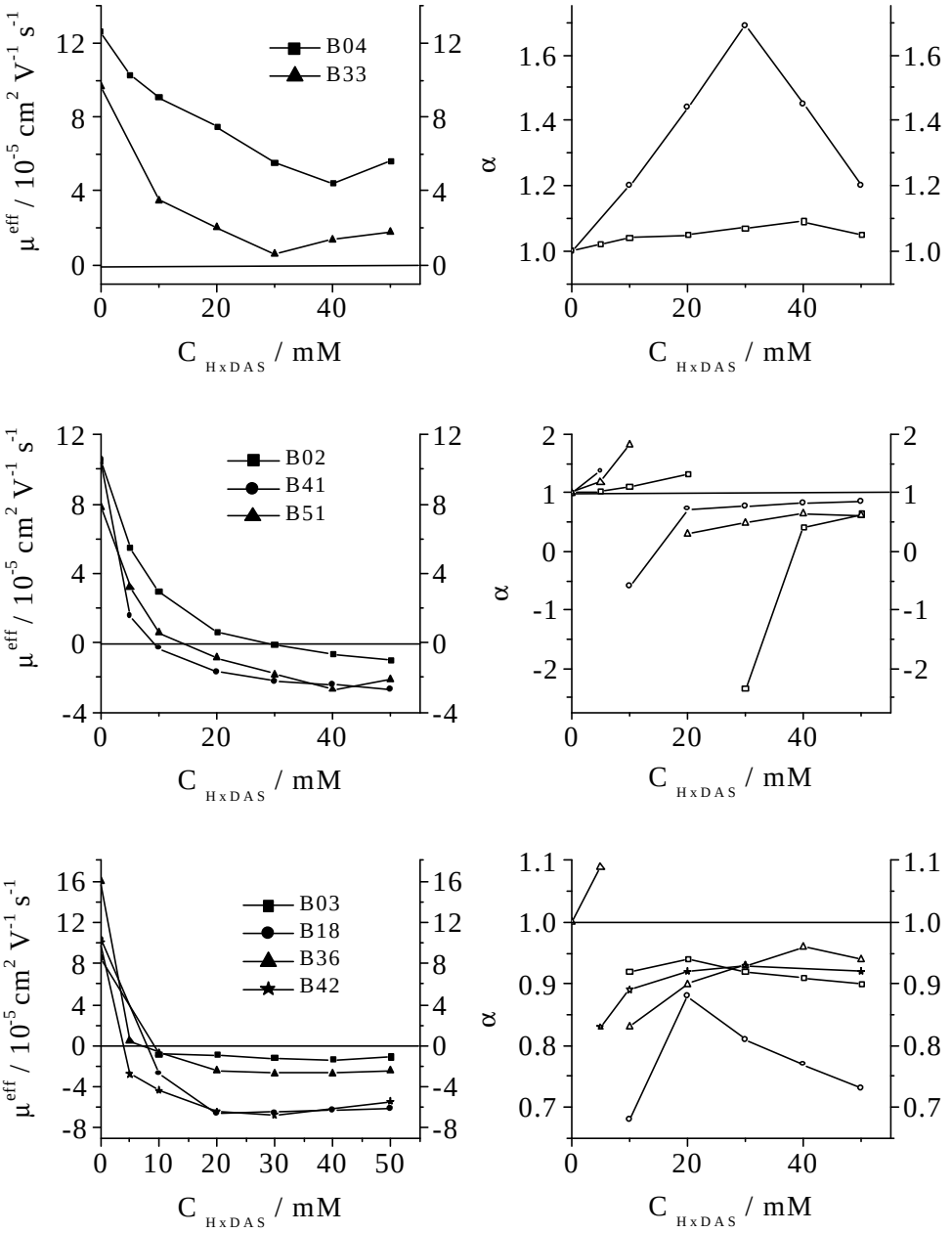

Figure 52. Effective mobility and separation selectivity for the enantiomers of weak base analytes in pH = 9.5 BGEs with HxDAS**.** Weakly binding (top panels), moderately strongly (middle panels) and strongly binding (bottom panels)**.**

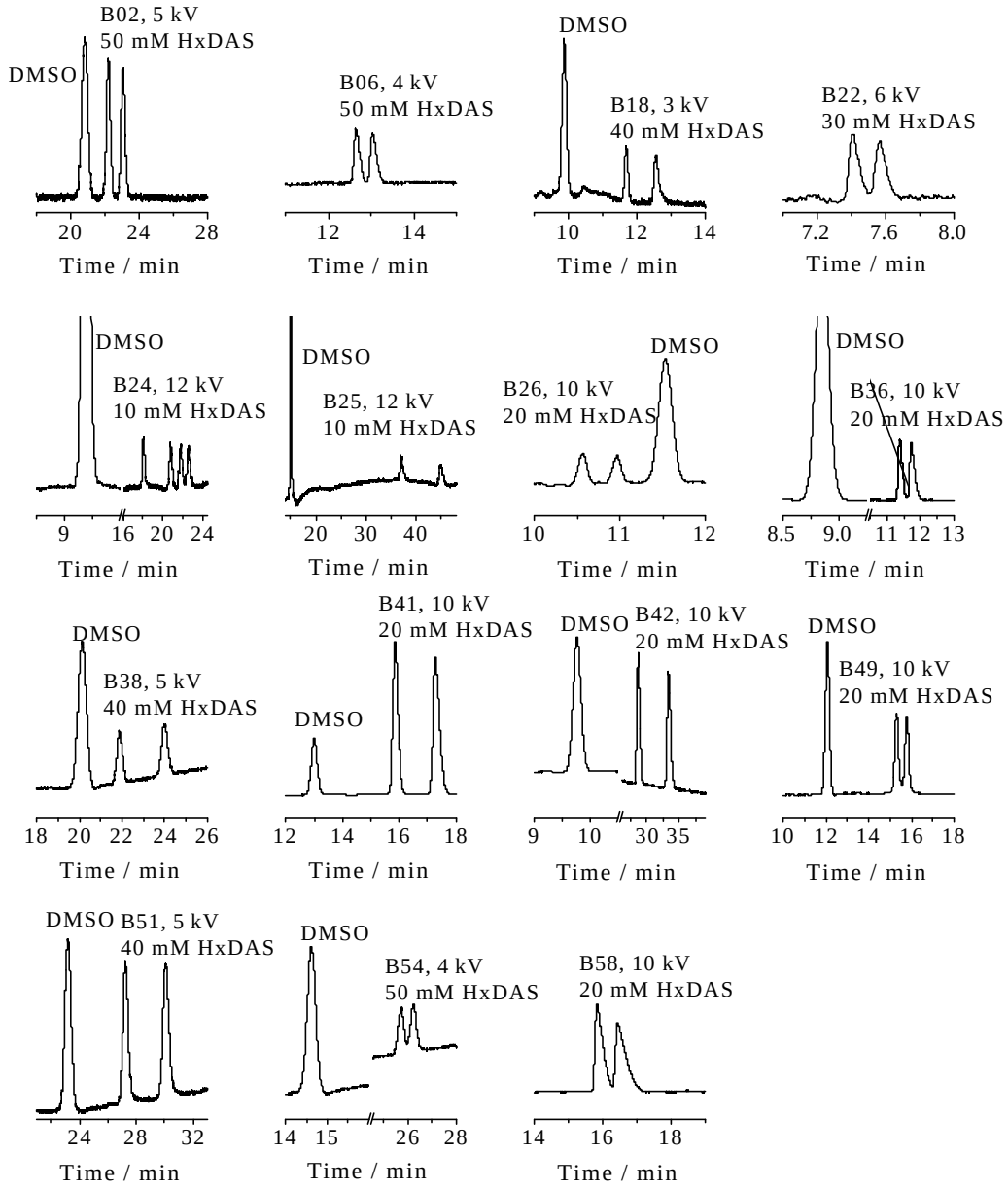

Figure 53. Typical electropherograms of weak base analytes in pH = 9.5 BGEs with HxDAS.

3.3.2 Weak Bases

Since most of the weak bases maintained their cationic mobility in the low pH HxDAS BGEs, the speed with which the separations were completed (generally under 30 min) was due to the aid of the EOF and the weak binding between HxDAS and the enantiomers. The EOF mobility is considerably higher at high pH than at low pH, due to the increased charge density of the capillary wall. The enantiomers are much less cationic at high pH because of their lower degree of protonation. Therefore, separations in the high pH BGEs were also fast. As the HxDAS concentration was increased in the high pH BGEs, the enantiomers typically acquired an anionic effective mobility at considerably lower HxDAS concentrations than in the low pH BGEs, and migrated against the EOF mobility. This led to separation times between 5 and 25 min, depending on the applied potential.

The numbers of enantiomers for which favorable separation selectivity was found in the high pH BGE and in the low pH BGE were almost equal. However, some weak base enantiomers had dramatically different separation selectivity patterns in the high pH versus low pH BGE. For example, labetalol, which could not be separated in the low pH BGE, was baseline separated all four stereoisomers. Figure 54 shows the effective mobility plots (top panel) and the corresponding separation selectivities (bottom panel) for piperoxan (B38) and tolperisone (B51) in both high pH and low pH BGEs with HxDAS as the chiral resolving agent. These weak base analytes were weakly binding with HxDAS in low pH BGEs; however, in high pH BGEs, they showed strongly binding behavior.

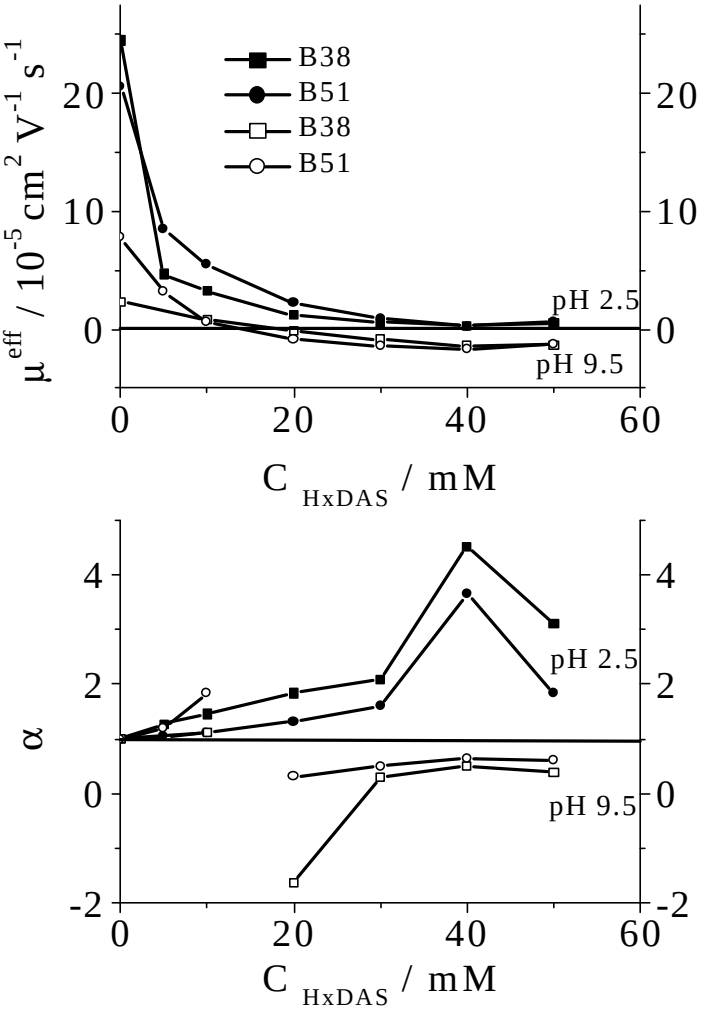

Figure 54. Effects of the background electrolyte pH on the separation of enantiomers of weak base analytes with HxDAS.

3.3.3 Weak Acids

At low pH, the acids became increasingly anionic with increasing HxDAS concentration. Separation selectivities observed for the low pH weak acid separations passed through a maximum at low HxDAS concentration. However, at high pH, the trend in the mobility was opposite from that observed in the low pH separations. The anionic effective mobilities of the enantiomers were high at low HxDAS concentration and became lower as the HxDAS concentration was increased due to both complexation with HxDAS and the mobility suppressing effects of the increasing ionic strength. Separation selectivities were poor at high pH resulting in a lack of separation despite comparable β values to those seen in the low pH measurements.

3.3.4 Ampholytic Analytes

The ampholytic analytes have similar separation behavior to the weak bases in low pH BGE, since almost all of the ampholytic analytes as fully protoned cations. The mobilities and selectivities for these analytes in pH 9.5 BGE with HxDAS followed trends similar to those of the weak acid enantiomers. This is not surprising, because in the pH 9.5 BGE used, almost all of the ampholytic analytes are fully deprotoned anions.

The change of the pH plays a complementary role in the ampholytic analyte enantiomer separations. Figure 55 shows the effective mobility plots (top panel) and the corresponding separation selectivities (bottom panel) for Dansyl-methionine (Z05) and Dansyl-norleucine (Z06) in both high pH and low pH BGEs with HxDAS as the chiral resolving agent. Enantiomer separations were obtained for Z06 in low pH BGE, but the enantiomers of Z05 were not

separated. However, in high pH BGE, the results are opposite, the two enantiomers of Z05 were separated, but those of Z06 were not separated.

3.4 Separation of the Enantiomers of Weak Bases with HxDAS in Acidic Methanol BGE

The use of nonaqueous BGEs in CE can expand the range of enantiomer separations since the solvent properties such as the dielectric constant, viscosity, polarity and autoprotolysis are different, which in turn might change separation selectivity and peak resolution [130-132]. The organic solvents that can be used for nonaqueous CE separation include amides, such as formamide, N-methyl formamide, N, N - dimethyl formamide, N, N-dimethyl acetamide, DMSO, acetonitrile, and methanol [109, 112, 130-139]. Since methanol is UV transparent down to 200 nm, it is advantageous to choose methanol as the solvent. The ε/η ratio for methanol is 61, which is lower than water (90). Because the current generated by CE in methanol will be lower than that in water at a given ionic strength, a higher field strength can be applied, which can effectively shorten the analysis time.

3.4.1 Material and Conditions

An acidic methanolic buffer was prepared from 25 mM H_3PO_4 and 12.5 mM LiOH for use in nonaqueous measurements. The stock buffers were used to prepare the 0-30 mM HxDAS BGEs for CE enantiomer separations. The enantiomers were dissolved in the BGE

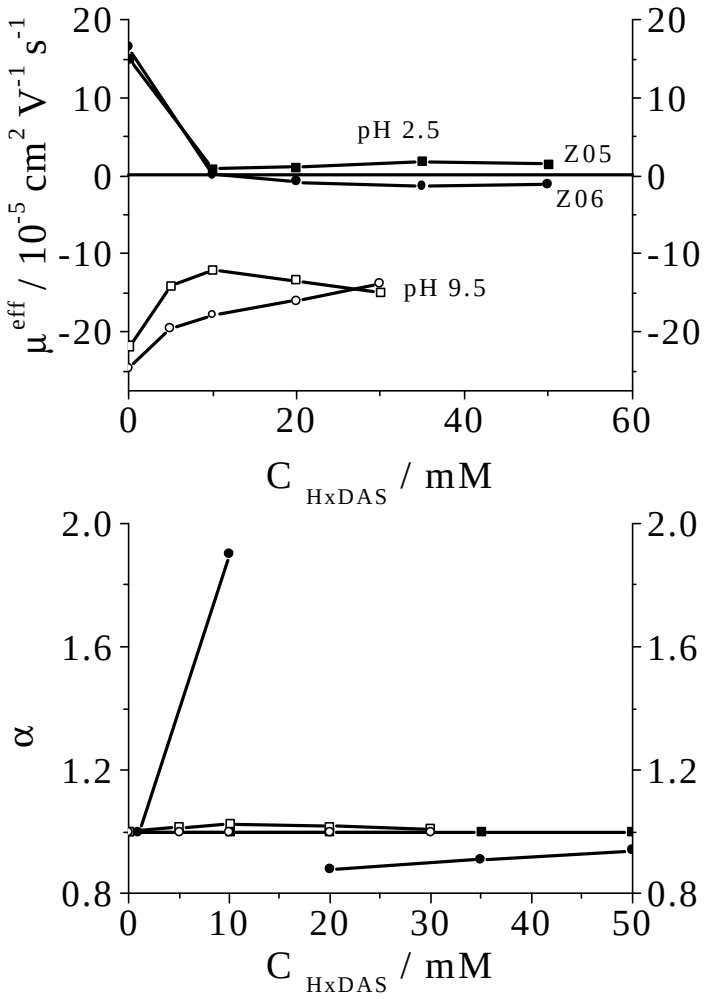

Figure 55. Effects of the background electrolyte pH on the separation of the enantiomers of ampholytic analytes with HxDAS.

and co-injected for 1 s by 2 psi nitrogen with the EOF marker from a solution approximately 0.5 mM in both the analyte and the EOF marker. In order to determine the highest potentials where Ohm's plots were still linear, the electrophoretic current was measured as a function of the applied potential over the 0-30 mM HxDAS concentration range in 5 mM increments. 16 kV was the maximum applied potential that was still in the linear region of Ohm's plots. All subsequent effective mobility measurements were carried out at 16 kV. All measurements were repeated in triplicate.

3.4.2 Results and Discussions

Table 3 lists the effective mobilities of the less mobile enantiomer, μ, the separation selectivity, α, the corresponding normalized electroosmotic flow mobility, β, the peak resolution, Rs, and the injector-to-detector potential drop, U values. Mobility and separation selectivity plots for some of the weak base enantiomers are shown in Figure56.

Enantiomer separations were achieved for twenty eight of the thirty one weak bases. The migration behavior of the weak bases followed one of two mobility patterns. The effective mobilities of the weakly binding weak base analytes remained cationic throughout the HxDAS concentration range, and their cationic effective mobilities decreased at the low HxDAS concentration used and then increased as the HxDAS concentration was increased further. This can be explained by the increasing ionic strength as the concentration of HxDAS was increased: it significantly suppressed the effective mobility of the charged analyte-CD complexes. The separation selectivity patterns were similar to what was seen for the weak

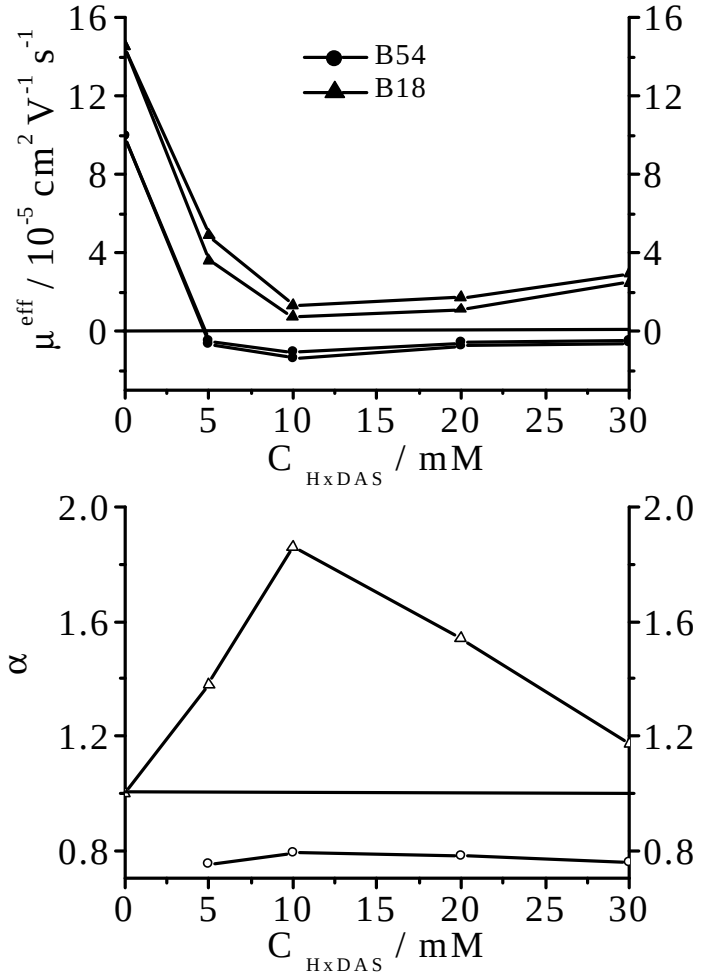

Figure 56. Effective mobility and separation selectivity for the enantiomers of weak base analytes in acidic methanol BGEs with HxDAS.

Table 3. Separation data in acidic methanol HxDAS BGEs. (μ, in 10^{-5} cm^2 / Vs units)

HxDAS (mM)			5				10	
U (kV)			16				16	
Analyte	μ	α	β	Rs	μ	α	β	Rs
B02	9.3	1.02	0.5	<0.6	7.2	1.04	0.6	1.1
B05	15.3	1.16	0.5	8.9	10.7	1.22	0.3	6.3
B06	7.8	1.03	0.7	1.0	7.4	1.05	0.6	1.3
B08	6.3	1.03	0.7	<0.6	4.1	1.07	1.2	0.7
B10	9.7	1.03	0.6	<0.6	7.5	1.05	0.6	1.4
B11	13.2	1.00	2.7	0	11.9	1.02	0.4	<0.6
B12	-2.4	-2.54	-2.2	20	-2.9	-1.41	-1.7	17
B13	6.7	1.03	0.7	<0.6	3.7	1.08	1.4	1.7
B18	4.1	1.20	0.9	1.2	0.7	1.86	6.8	2.6
B20	11.0	1.02	0.4	<0.6	7.3	1.04	0.6	1.1
B22	12.9	1.00	0.3	0	10.6	1.01	0.4	<0.6
B24	3.2 2.9 1.4	1.03 1.10 2.07	41	0.7 1.8 3.6	2.3 2.0 1.2	1.04 1.15 1.37	3.3	1.0 0.7 2.1
B25	5.0	1.02	0.8	<0.6	0.7	1.16	5.9	0.9
B28	12.4	1.00	0.3	0	8.9	1.02	0.4	<0.6

Table 3. Continued.

HxDAS (mM)			20				30	
U (kV)			16				16	
Analyte	μ	α	β	Rs	μ	α	β	Rs
B02	7.9	1.03	0.4	1.0	8.6	1.01	0.2	<0.6
B05	8.0	1.24	0.2	3.8	7.3	1.26	0.2	4.7
B06	7.1	1.06	0.4	0.7	6.7	1.07	0.6	1.0
B08	4.6	1.04	0.5	<0.6	4.9	1.02	0.2	<0.6
B10	8.5	1.04	0.3	0.8	8.6	1.03	0.2	0.9
B11	12.9	1.00	0.2	0	13.4	1.00	0.2	0
B12	-1.3	-3.19	-1.3	38	-1.2	-3.67	-1.4	39
B13	4.0	1.07	0.6	1.5	4.3	1.04	0.2	1.5
B18	1.1	1.54	2.0	1.7	2.5	1.17	0.4	3.8
B20	7.8	1.03	0.3	<0.6	8.0	1.02	0.2	<0.6
B22	9.1	1.02	0.3	<0.6	8.6	1.03	0.2	<0.6
B24	1.6 1.5 1.1	1.06 1.07 1.36	2.4	1.3 0.6 1.4	1.8 1.7 1.5	1.05 1.06 1.13	3.8	1.4 0.6 1.4
B25	1.0	1.12	3.0	0.7	1.3	1.06	0.6	<0.6
B28	9.2	1.01	0.3	<0.6	9.4	1.00	0.2	0

Table 3. Continued.

HxDAS (mM)			5				10	
U (kV)			16				16	
Analyte	μ	α	β	Rs	μ	α	β	Rs
B31	7.0	1.03	1.0	<0.6	5.8	1.05	1.2	1.1
B32	6.5	1.03	1.1	<0.6	5.6	1.04	0.7	1.3
B33	8.9	1.04	0.8	<0.6	6.8	1.06	0.5	0.6
B34	7.4	1.03	1.0	<0.6	5.7	1.05	0.6	1.2
B37	10.1	1.02	0.7	<0.6	9.7	1.03	0.5	<0.6
B38	4.3	1.05	1.7	<0.6	3.8	1.11	1.4	<0.6
B41	9.2	1.02	0.8	<0.6	8.8	1.03	0.6	<0.6
B42	6.6	1.05	1.1	<0.6	6.2	1.08	0.8	0.8
B43	5.1	1.06	1.4	<0.6	4.7	1.07	1.1	1.3
B46	2.5	1.04	2.8	<0.6	2.5	1.00	2.0	0
B49	4.7	1.02	1.5	<0.6	4.1	1.04	1.0	<0.6
B51	9.7	1.02	0.8	<0.6	9.1	1.03	0.5	0.9
B54	-0.6	0.75	-11	<0.6	-1.4	0.79	-3.2	1.2
B56	8.6	1.03	0.8	<0.6	8.0	1.04	0.5	1.0
B35	4.7	1.00	1.6	0	4.2	1.00	1.1	0
B36	7.9	1.00	0.9	0	7.1	1.00	0.7	0
B45	9.6	1.00	0.7	0	9.0	1.00	0.5	0

Table 3. Continued.

HxDAS (mM)			20				30	
U (kV)			16				16	
Analyte	μ	α	β	Rs	μ	α	β	Rs
B31	6.1	1.03	0.3	<0.6	6.4	1.02	0.2	<0.6
B32	5.8	1.04	0.4	1.0	6.1	1.03	0.3	1.1
B33	7.5	1.04	0.3	1.3	8.1	1.02	0.2	0.9
B34	6.6	1.03	0.4	0.9	7.1	1.02	0.3	1.1
B37	9.3	1.04	0.3	<0.6	9.0	1.05	0.2	<0.6
B38	4.1	1.05	0.7	1.6	4.4	1.02	0.5	1.4
B41	8.4	1.04	0.3	<0.6	8.3	1.04	0.1	0.9
B42	6.5	1.05	0.4	1.1	6.8	1.03	0.2	0.8
B43	4.4	1.09	0.7	1.2	4.8	1.05	0.3	1.0
B46	2.9	1.00	0.9	0	3.1	1.00	0.8	0
B49	3.8	1.05	0.8	<0.6	3.6	1.06	0.3	<0.6
B51	8.7	1.04	0.4	1.1	8.5	1.04	0.2	0.7
B54	-0.8	0.78	-5.4	1.0	-0.6	0.76	-2.0	1.0
B56	7.4	1.05	0.4	0.8	7.2	1.06	0.3	0.9
B35	4.4	1.00	1.0	0	4.5	1.00	0.9	0
B36	6.6	1.00	0.4	0	6.4	1.00	0.4	0
B45	8.5	1.00	0.3	0	8.3	1.00	0.4	0

bases in aqueous BGEs. The second mobility pattern is similar to what was seen for strongly binding bases in the aqueous measurements. The effective mobilities of the enantiomers became anionic at a low HxDAS concentration, then decreased at the higher HxDAS concentrations due to the increasing ionic strength. A discontinuity was observed in the separation selectivity patterns of the strongly binding weak bases. These behaviors are shown in Figure 56, bottom panel.

Like in the aqueous BGEs, the cyclodextrion cavity size also affects the enantiomer separation behavior in NACE. Figure 57 shows the effective mobility plots (top panel) and the corresponding separation selectivities (bottom panel) for piperoxan (B38) and propranolol (B42) in acidic methanol BGEs with HxDAS, HDAS and ODAS as the chiral resolving agents. The complexing strength for the two weak base analytes with HxDAS, HDAS and ODAS in acidic methanol BGEs were similar to the results that we obtained in aqueous CE, following the order: ODAS > HDAS > HxDAS.

3.4.3 Comparison of NACE to ACE

There were four weak bases, 1-aminoindan (B05), hemicholinium-15 (B20), propafenone (B43) and scopolomine (B46), which could not be separated in aqueous CE, but could be separated in acidic methanol BGE.

The BGE solvent also affects the separation patterns. Pindolol (B41) and propranolol (B42), which showed particularly strong binding and baseline separation in aqueous BGE, showed weak binding and could not be baseline separated in NACE. In both low pH and high

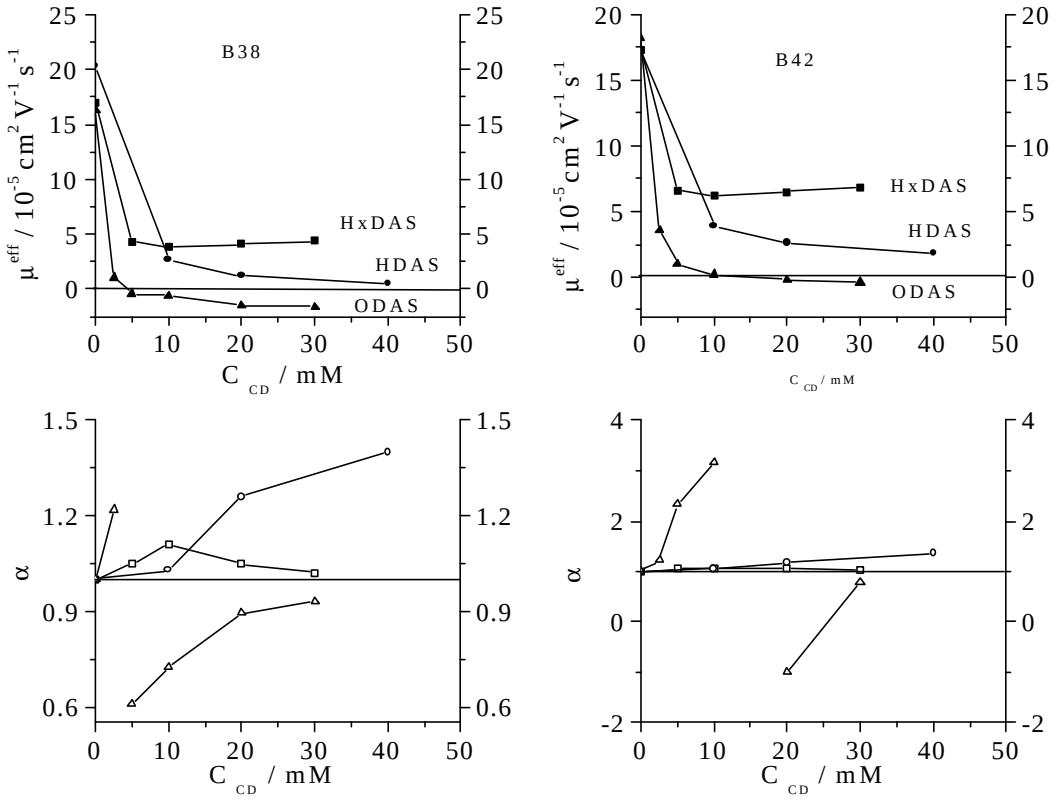

Figure 57. Effects of cyclodextrin cavity size on the separation of the enantiomers of the weak base analytes in acidic methanol BGEs with HxDAS, HDAS, ODAS.

pH aqueous BGEs, fluoxetine (B18) was strongly binding with HxDAS. However, in NACE, it's binding was weak. Figure 58 shows the effective mobility plots (top panel) and the corresponding separation selectivities (bottom panel) for fluoxetine (B18) and propranolol (B42) in acidic aqueous and methanol BGEs with HxDAS as the chiral resolving agent.

Many enantiomers, whose mobilities were measured in both acidic aqueous and acidic methanolic BGEs had a considerably more cationic mobility in the acidic methanolic BGEs than in the low pH aqueous BGEs. These analytes could be separated both in acidic aqueous and acidic methanolic BGEs and showed decreased binding strengths in the acidic methanolic BGE. The same phenomena were observed with HDAS and ODAS containing BGEs. There are two potential reasons leading to this phenomenon. (i) Compared to the aqueous system, the degree of dissociation of the charged HxDAS is significantly suppressed in methanol, so HxDAS behaves more like a neutral cyclodextrin; (ii) Compared to water, methanol acts as a stronger competing agent of analytes, reducing the complexation constants of the HxDAS-analyte complexes compared to those observed in an aqueous BGEs.

Favorable β values lead to baseline separation for the enantiomers of most of the weak base analytes tested in acidic methanol BGEs (Figure 59). The numbers under the compound codes (see Figure 37) next to the electropherograms indicate the actual HxDAS concentrations (in mM) and the effective separation potentials in kV (the actual potential drop between the injection point and the detector window).

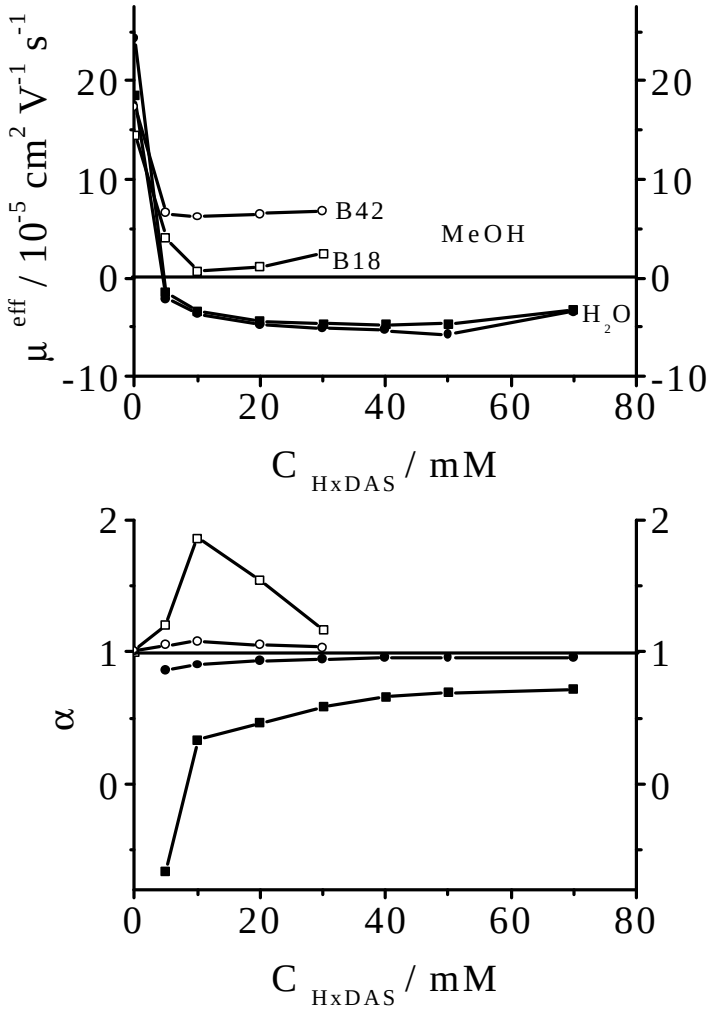

Figure 58. Effects of the BGE solvent on the separation of the enantiomers of the weak base analytes with HxDAS.

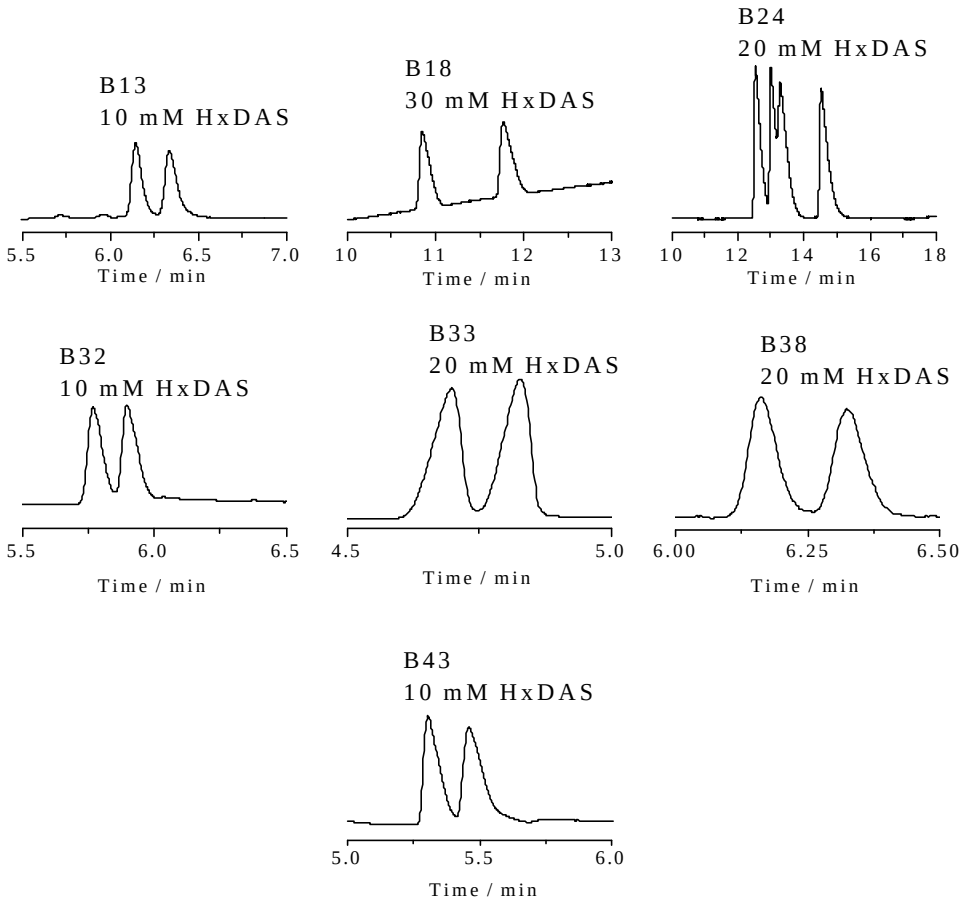

Figure 59. Typical electropherograms of weak base analytes in acidic methanol BGE with HxDAS.

3.5 Summary

The first new, single-isomer, α-CD, HxDAS, has been synthesized on a large scale with a purity > 97.8 % and effectively used for the CE separations of the enantiomers of a large number of neutral, weak acid, ampholytic and weak base analytes in both low and high pH aqueous BGEs as well as for the separation of weak bases in an acidic methanolic BGE. The effective mobilities and separation selectivities followed the predictions of the CHARM model of CE enantiomer separations and led to different peak resolution values than the corresponding β-CD analogue, HDAS, and γ-CD analogue, ODAS. The experimental results show that the chiral recognition process depends on (i) the pH of the BGE; (ii) the type of BGE solvent; (iii) the structure of the analytes; (iv) the size of the CD cavity; and (v) the type of the ions in the background electrolyte.

CHAPTER IV

ENANTIOMER SEPARATIONS WITH HxS

The previous experiments (Chapter III) showed us that HxDAS, which bears moderately hydrophobic acetyl groups at the 2, 3- positions on the glucopyranose units, could be successfully used to separate the enantiomers of neutral, weak base, weak acid and ampholytic analytes in both aqueous (pH=2.5 and pH=9.5) and nonaqueous (acidic methanolic) BGEs. Since different substituents can provide different inter - molecular interactions with chiral analytes, it seemed interesting to investigate the use of hexakis(6-*O*-sulfo)-α-CD (HxS), which contains hydrophilic hydroxyl groups at the 2 and 3- positions on the glucopyranose unit for the separation of pharmaceutically important compounds.

4.1 Separations in Low pH BGEs

According to the predictions of the charged resolving agent migration model (CHARM model) of CE enantiomer separations [119], only two BGEs, one with a low pH and another with a high pH are required to find the best possible separation selectivities for any weak electrolyte and neutral analyte with a strong electrolyte chiral resolving agent, such as HxS. All low pH measurements were carried out in the 25 mM phosphoric acid buffer whose pH was adjusted to 2.5 with LiOH.

4.1.1 Experimental Methods and Conditions

Except for the sodium salt of hexakis(6-*O*-sulfo)-α-cyclodextrin (HxS), which was synthesized as described in Chapter II, all other chemicals were obtained from Aldrich Chemical Company. Details of the other experimental conditions can be seen in Chapter III.

4.1.2 Results and Discussion

A series of neutral, weak acid and weak base enantiomers were separated with the pH 2.5 HxS BGEs. The effective mobilities of the less mobile enantiomers, μ, the separation selectivities, α, the measured peak resolution values, Rs, the corresponding dimensionless EOF mobility values, β, and the injector-to-detector potential drop values, U, are listed in Table 4.

4.1.2.1 Separation of the Enantiomers of Nonionic and Weak Acid Analytes

For the weakly complexing noncharged analytes and weak acid analytes, the effective anionic mobilities increased as the concentration of HxS was increased (top panels in Figure 60), indicating that complexation did override the mobility-reducing effects of both higher ionic strength and higher viscosity. Except for the two lactones, γ-(2-naphthyl)-γ-butyrolactone (N12) and γ-(2-phenyl)-γ-butyrolactone (N13), the increase in μ^{eff} for most noncharged and weak acid analytes is larger with HxS than with HxDAS [129] indicating stronger interactions with HxS than with HxDAS. There are also separation selectivity differences between HxDAS and HxS: α is larger for the enantiomers of γ-(2-phenyl)-γ-butyrolactone (N13), carprofen (A04) and fenoprofen (A22) with HxS than with HxDAS [129]. The differences, brought about by the

removal of the acetyl groups from HxDAS, can be attributed to either size effects or polarity effects.

4.1.2.2 Separation of the Enantiomers of Weak Bases

Effective mobility and separation selectivity curves for some of the weak bases are shown in Figure 61 as a function of the concentration of HxS. Just as with HxDAS (Chapter III), the weak bases can be divided into two groups, weakly binding bases and strongly binding bases, depending on the response of their effective mobilities to the increased HxS concentration.

For the weakly binding bases, the effective mobilities remain cationic even for HxS concentrations as high as 50 mM (left top panel in Figures 61). The corresponding separation selectivities pass a relatively large local maximum (left bottom panel in Figure 61). According to Reference [113], when complexation is weak, the mole fraction of the anionic analyte - HxS complex is small, even for a relatively high HxS concentration. On the other hand, the high HxS concentration leads to a high ionic strength in the BGE. The high ionic strength depresses the mobility of the highly charged anionic complexes (irrespectively of their low mole fraction) much more than that of the free, monoprotonated weak base analytes (irrespectively of their high mole fraction). Consequently, the contribution of the anionic analyte - HxS complex to the effective mobility of the weak base analyte band is smaller than

Table 4. Separation data in pH=2.5 HxS BGEs. (μ, in 10^{-5} cm^2 / Vs units).

HxS (mM)	0		10		
U (kV)	0		12		
Analyte	μ	μ	α	β	Rs
NSA^-	0	-27.8			
N12	0	-1.3	1.00	-3.7	0
N13	0	N/A			
N21	0	-11.3*	1.03	-0.5	1.0
N25	0	-14.0*	1.03	-0.4	1.2
N26	0	-6.61*	1.05	-0.5	2.5
N27	0	-0.8	1.00	-19	0
N28	0	-1.24	1.08	-2.0	0.7
N30	0	-2.62	1.07	-3.9	0.8
N36	0	-1.07	1.00	-3.8	0
A02	0	-8.46*	1.08	-0.7	1.8
A04	0	-3.92	1.03	-3.4	0.7
A22	0	-5.2	1.05	-1.1	0.9
A28	0	-4.9	1.00	-1.2	0
A36	0	-4.1	1.00	-1.3	0

* Polarity (-) to (+), NSA^- as secondary EOF marker

Table 4. Continued.

HxS (mM)		20				30		
U (kV)		10				8		
Analyte	μ	α	β	Rs	μ	α	β	Rs
NSA^-	-28.0				-28.2			
N12	-2.78	1.00	-2.1	0	-3.9	1.00	-1.0	0
N13	N/A				-3.53	1.15	-4.8	1.7
N21	N/A				N/A			
N25	-15.1*	1.01	-0.4	0.8	-16.1*	1.01	-0.6	0.7
N26	-9.9*	1.03	-0.5	1.1	-12.5*	1.01	-0.9	1.2
N27	-1.8	1.00	-3.0	0	-2.92*	1.00	-0.6	0
N28	-2.0	1.05	-2.6	1.0	-2.48*	1.04	-0.2	<0.6
N30	-4.22	1.06	-1.0	1.1	-5.27*	1.04	-0.2	1.2
N36	-2.4	1.00	-2.1	0.0	-3.31*	1.00	-0.5	0
A02	-15.1*	1.05	-0.4	2.3	-19.6	1.03	-2.7	0.7
A04	-8.16*	1.02	-0.8	0.6	-12.9*	1.01	-0.2	0.6
A22	-9.64*	1.04	-0.5	0.7	-13.8*	1.04	-0.2	1.6
A28	-8.66*	1.00	-0.6	0	-11.0*	1.00	-0.1	0
A36	-7.44*	1.00	-0.6	0	-10.4*	1.00	-0.3	0

Table 4. Continued.

HxS (mM)	0					5			
U (kV)	18					14			
Analyte	μ	μ	α	β	Rs	μ	α	β	Rs
B02	24.7	6.6	1.00	3.4	0	5.4	1.00	3.2	0
B03	24.3	5.5	1.02	4.1	<0.6	4.1	1.04	4.6	<0.6
B08	21.1	5.2	1.00	4.2	0	N/A			
B09	21.7	5.7	1.00	3.9	0	2.9	1.00	3.8	0
B10	19.8	6.1	1.00	3.6	0	4.2	1.00	3.4	0
B11	21.7	6.7	1.03	3.4	<0.6	4.5	1.05	7.0	0.6
B13	27.9	6.6	1.00	3.3	0	3.1	1.03	4.4	<0.6
B14	27.3	5.5	1.00	4.2	0	N/A			
B18	18.6	9.9	1.08	1.7	5.3	6.8	1.15	2.2	0.9
B19	24.2	6.3	1.05	2.6	0.6	3.2	1.16	0.8	2.0
B21	24.1	9.0	1.00	1.3	0	N/A			
B22	25.6	6.7	1.00	3.0	0	N/A			
B25	21.9	4.1	1.09	4.0	<0.6	2.0	1.23	5.0	0.6
B26	23.7	4.8	1.00	3.8	0	5.5	1.00	3.0	0
B28	28.3	5.4	1.00	3.9	0	4.7	1.00	3.6	0
B31	18.9	3.6	1.00	5.8	0	1.7	1.00	6.8	0
B32	17.7	4.0	1.00	5.6	0	1.7	1.00	6.8	0
B34	27.5	6.7	1.01	2.4	<0.6	4.6	1.02	3.1	<0.6
B35	18.0	3.4	1.00	6.0	0	4.7	1.00	3.2	0

HxS (mM)	10				
U (kV)	13				
Analyte	μ	α	β	Rs	
B02	5.4	1.00	3.2	0	
B03	4.1	1.04	4.6	<0.6	
B08	N/A				
B09	2.9	1.00	3.8	0	
B10	4.2	1.00	3.4	0	
B11	4.5	1.05	7.0	0.6	
B13	3.1	1.03	4.4	<0.6	
B14	N/A				
B18	6.8	1.15	2.2	0.9	
B19	3.2	1.16	0.8	2.0	
B21	N/A				
B22	N/A				
B25	2.0	1.23	5.0	0.6	
B26	5.5	1.00	3.0	0	
B28	4.7	1.00	3.6	0	
B31	1.7	1.00	6.8	0	
B32	1.7	1.00	6.8	0	
B34	4.6	1.02	3.1	<0.6	
B35	4.7	1.00	3.2	0	

Table 4. Continued.

HxS (mM)	20				30			
U (kV)	12				8			
Analyte	μ	α	β	Rs	μ	α	β	Rs
B02	4.8	1.00	2.6	0	4.4	1.00	2.5	0
B03	3.7	1.06	8.0	<0.6	4.7	1.10	1.5	<0.6
B08	3.9	1.00	2.9	0	4.2	1.00	2.9	0
B09	2.2	1.00	4.8	0	1.5	1.00	6.2	0
B10	3.4	1.00	3.9	0	2.8	1.00	4.3	0
B11	3.7	1.06	0.8	1.5	2.5	1.08	4.4	<0.6
B13	1.2	1.05	8.0	<0.6	-0.6	0.92	-15	0.7
B14	4.3	1.00	4.3	0	10.9	1.00	0.7	0
B18	2.8	1.26	0.9	4.9	0.6	1.58	14	3.8
B19	2.8	1.09	2.7	0.6	2.3	1.06	2.8	1.0
B21	5.5	1.00	2.8	0	3.9	1.00	1.5	0
B22	N/A				2.5	1.09	2.4	<0.6
B25	N/A				0.7	1.60	3.5	3.9
B26	6.2	1.00	2.2	0	7.3	1.00	1.7	0
B28	N/A				4.0	1.00	4.2	0
B31	0.9	1.00	10	0	-0.6	0.74	-9.9	1.1
B32	3.5	1.00	3.2	0	5.9	1.00	1.2	0
B34	3.2	1.06	2.4	<0.6	2.1	1.05	2.7	<0.6
B35	3.6	1.00	2.1	0	2.2	1.00	1.5	0

Table 4. Continued.

HxS (mM)	40				50			
U (kV)	6				5			
Analyte	μ	α	β	Rs	μ	α	β	Rs
B02	5.0	1.00	1.6	0	N/A			
B03	3.5	1.08	1.6	0.9	N/A			
B08	3.7	1.00	2.9	0	3.4	1.00	1.9	0
B09	N/A				-0.3	0.94	-37	<0.6
B10	3.2	1.00	2.8	0	2.3	1.00	2.4	0
B11	1.1	1.11	9.0	<0.6	-0.8	0.95	-11	0.8
B13	-2.2	0.95	-3.8	<0.6	-1.2	0.91	-4.6	<0.6
B14	13.6	1.00	0.9	0	N/A			
B18	-1.6	0.86	-6.9	1.0	-1.1	0.92	-6.4	0.9
B19	1.8	1.03	3.6	0.7	N/A			
B21	3.4	1.00	2.1	0	4.1	1.00	0.8	0
B22	1.4	1.06	8.2	<0.6	N/A			
B25	1.0	1.42	4.0	0.9	1.3	1.32	5.5	1.3
B26	8.3	1.00	1.2	0	N/A			
B28	4.9	1.00	3.4	0	5.6	1.00	0.6	0
B31	-1.4	0.92	-9.8	0.7	N/A			
B32	4.1	1.00	2.4	0	N/A			
B34	1.4	1.03	9.2	<0.6	1.8	1.00	3.2	0
B35	1.6	1.00	2.3	0	N/A			

Table 4. Continued.

HxS (mM)	0			5		10			
U (kV)	14		12			11			
Analyte	μ	μ	α	β	Rs	μ	α	β	Rs
B37	21.8	N/A				4.7	1.04	4.1	<0.6
B38	24.5	6.2	1.02	3.6	<0.6	3.0	1.04	2.8	<0.6
B39	30.5	10.6	1.05	1.4	2.2	4.1	1.15	2.8	2.4
B41	23.2	6.0	1.02	2.3	<0.6	3.8	1.05	1.2	1.2
B42	24.3	6.6	1.00	3.3	0	4.1	1.02	2.1	<0.6
B43	18.8	3.9	1.15	3.4	<0.6	2.2	1.27	40	2.9
B44	35.3	N/A				5.0	1.06	2.1	0.7
B45	19.5					8.1	1.00	2.1	0
B46	22.2					7.7	1.00	2.0	0
B47	35.3	5.6	1.00	3.4	0	3.7	1.00	4.3	0
B48	12.4	N/A				6.6	1.03	2.2	<0.6
B49	18.6					5.1	1.02	3.5	<0.6
B51	20.6	6.6	1.02	1.7	<0.6	1.9	1.06	3.6	0.9
B53	18.1	3.8	1.06	3.0	0.7	-3.3	0.91	-3.8	<0.6
B54	17.6	2.78	1.12	3.8	4.1	1.3	1.20	6.6	1.0
B56	41.7	2.7	1.10	6.4	1.2	1.5	1.17	3.6	0.6
B57	17.0	3.5	1.02	4.8	<0.6	1.7	1.06	3.5	<0.6
B58	25.9	8.1	1.02	2.3	<0.6	3.7	1.06	3.6	0.7
B61	24.2	5.2	1.02	3.6	<0.6	1.72	1.04	5.4	<0.6

Table 4. Continued.

HxS (mM)		20				30		
U (kV)		10				8		
Analyte	μ	α	β	Rs	μ	α	β	Rs
B37	2.6	1.12	3.6	<0.6	1.1	1.35	2.4	1.6
B38	-0.3	0.62	-5.3	1.0	-1.0	0.72	-8.5	1.3
B39	N/A				1.4	1.08	6.2	0.7
B41	N/A				2.5	1.09	1.6	0.9
B42	3.4	1.04	3.1	<0.6	2.2	1.07	8.3	<0.6
B43	N/A				0.2	1.91	28	1.1
B44	1.3	1.17	4.2	2.8	-0.1	0.89	-23	0.8
B45	3.9	1.00	7.0	0	0.7	1.00	9.4	0
B46	3.8	1.00	4.5	0	2.0	1.00	4.0	0
B47	2.2	1.00	4.4	0	1.2	1.00	5.4	0
B48	N/A				2.4	1.08	3.4	0.8
B49	1.8	1.05	5.6	<0.6	-0.7	0.75	-7.1	0.8
B51	N/A				2.8	1.14	5.7	<0.6
B53	N/A				-10.1*	0.95	-1.7	1.1
B54	N/A				-1.7	0.94	-12	0.6
B56	N/A				1.2	1.25	15	<0.6
B57	<-0.1	0.75	-325	1.1	-0.5	0.82	-43	<0.6
B58	4.8	1.11	2.4	1.1	5.3	1.16	4.6	1.1
B61	N/A				2.9	1.06	3.4	<0.6

Table 4. Continued.

HxS (mM)	40				50			
U (kV)	6				5			
Analyte	μ	α	β	Rs	μ	α	β	Rs
B37	0.6	1.28	10	0.9	0.9	1.20	3.4	0.7
B38	-1.6	0.80	-4.3	0.9	-1.0	0.88	-3.0	1.2
B39	2.2	1.04	6.0	0.6	3.2	1.00	1.1	0
B41	N/A				4.1	1.02	0.8	<0.6
B42	N/A				1.6	1.08	1.9	<0.6
B43	-0.3	0.83	-6.6	0.8	-1.2	0.95	-2.5	<0.6
B44	-1.5	0.91	-2.5	0.6	N/A			
B45	0.5	1.00	6.5	0	N/A			
B46	3.6	1.00	1.6	0	N/A			
B47	3.0	1.00	3.3	0	2.1	1.00	2.8	0
B48	2.7	1.07	4.2	<0.6	N/A			
B49	-2.1	0.82	-4.2	<0.6	N/A			
B51	3.7	1.11	2.4	<0.6	3.5	1.09	0.8	<0.6
B53	-8.0	0.90	-2.1	0.9	-6.3	0.86	-3.2	0.8
B54	-2.5	0.96	-2.9	0.6	-2.1	0.93	-2.1	0.7
B56	1.7	1.12	3.2	<0.6	2.3	1.04	2.4	<0.6
B57	-0.3	0.89	-50	0.7	-0.3	0.86	-38	<0.6
B58	4.6	1.12	1.3	0.9	3.4	1.07	1.4	0.7
B61	3.6	1.05	2.4	<0.6	3.1	1.03	1.8	<0.6

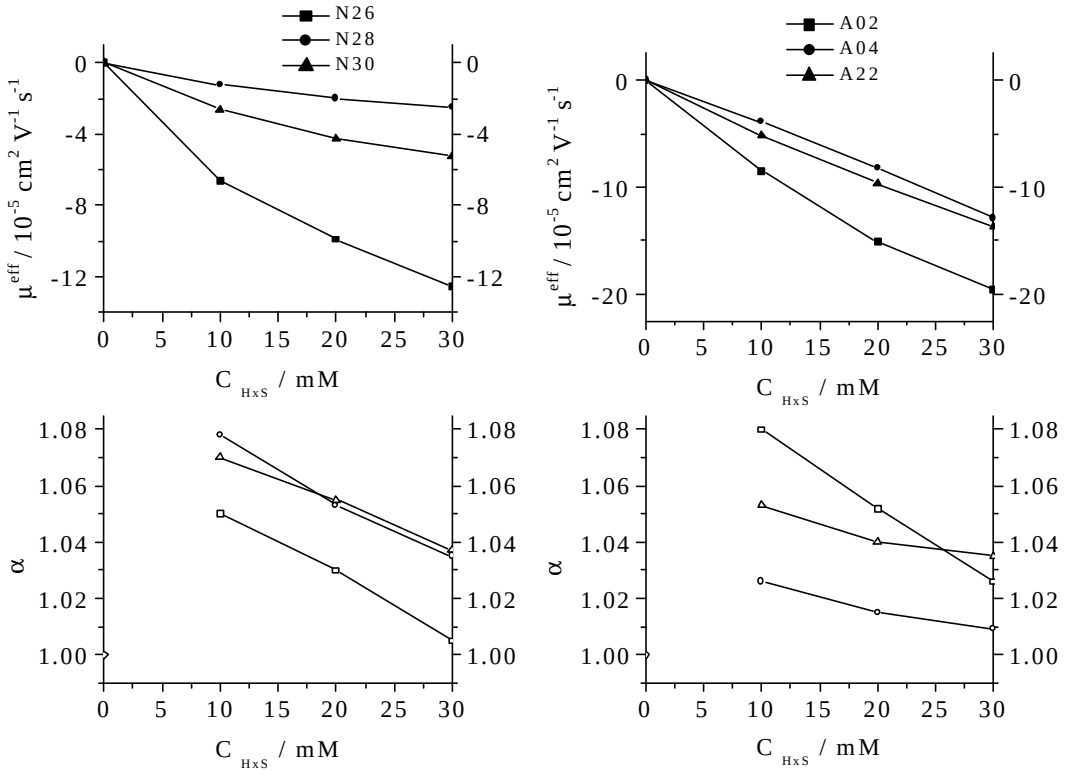

Figure 60. Effective mobilities and separation selectivities for the enantiomers of nonionic and weak acid analytes in pH = 2.5 BGEs with HxS.

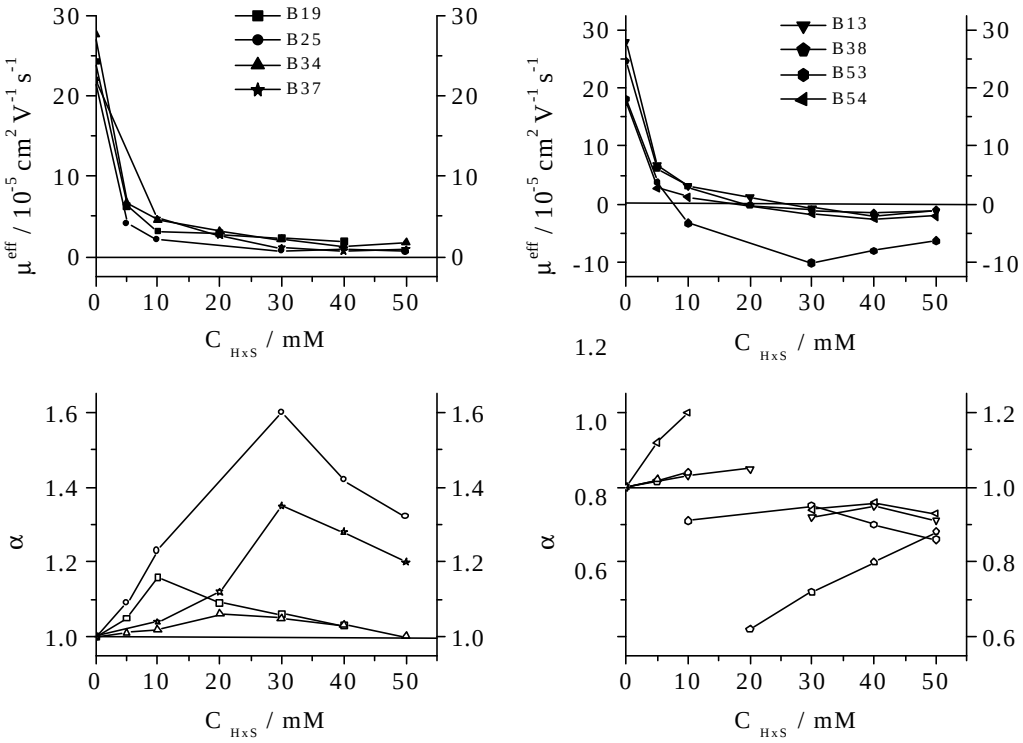

Figure 61. Effective mobilities and separation selectivities for the enantiomers of weak base analytes in pH = 2.5 BGEs with HxS. Weakly binding (left panels) and strongly binding (right panels)**.**

that of the free, monoprotonated weak base analytes and the effective mobility of the weak base analyte band remains cationic, albeit low.

For the strongly binding weak bases, the effective mobilities become anionic as the concentration of HxS is increased (right top panel in Figure 61). However, for this group, the anionic effective mobilities are larger at a moderate HxS concentration than at a high HxS concentration. The cause of the phenomenon is once again the interplay between the increased mole fraction of the anionic analyte - HxS complex and the increased ionic strength that are brought about by the increased HxS concentration [113]. The former of these increases the contribution of the anionic complex to the effective mobility of the band, and its effect is greater at relatively low HxS concentrations, while the latter decreases the effective mobility of the anionic complex and its effect is greater at relatively high HxS concentrations. As expected [113], separation selectivities are larger in the vicinity of the HxS concentration where the effective mobility of one of the enantiomers changes sign from cationic to anionic (right bottom panel in Figure 61).

The interactions between HxS and three of the test weak base analytes, fluoxetine (B18), miconazole (B32) and propranol (B42)were much weaker than with HxDAS [129]. For about 25 % of the test analytes, interactions with HxS and HxDAS were about equally strong. For about one third of the weak bases (alprenolol (B02), aminogluetimide (B03), atenolol (B08), ketamine (B22), methoxyphenamine (B28), metoprolol (B31), norephedrine (B34), oxybutynin (B35), phenylglycinonitrile (B39), pindolol (B41), and synephrine (B61)), the interaction were much stronger with HxS than with HxDAS [129]. Only for analytes, aminogluthetimide (B03), norephedrine (B34), phenylglycinonitrile (B39) and artane (B53) had

higher separation selectivities with HxS than with HxDAS (at an identical BGE concentration, e. g., at 5 mM). The differences must be due to multiple, subtle interplays between analyte structure and both the polarity and size difference of HxS and HxDAS.

The cyclodextrin cavity size also affects the chiral recognition process significantly. Figure 62 shows the effective mobility plots (top panel) and the corresponding separation selectivities (bottom panel) for pindolol (B41) with HxS, HS and OS as the chiral resolving agents. Just as with HxDAS, HDAS and ODAS, the strength of the interactions between piperoxan (B41) and the three CDs also follows the orders OS ≅ HS > HxS.

The peak resolution values (Table 4) depend not only on the separation selectivities, but also on the β values and the magnitude of the effective potential drop. A few typical separations obtained with HxS are shown in Figures 63 and 64. The numbers next to the electropherograms indicate the actual HxS concentrations. Figure 63 shows the separation of the enantiomers of noncharged and weak acid analytes, Figure 64 those of the basic analytes. In general, the peak resolution values are quite adequate, even when the separations take only 10-15 minutes.

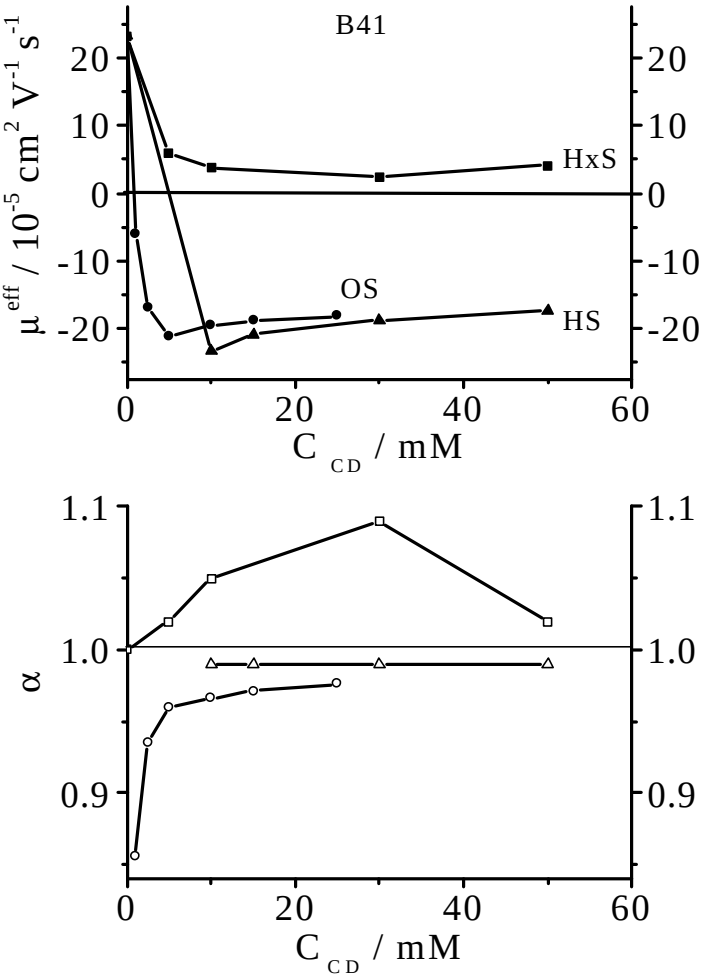

Figure 62. Cavity size effects on the effective mobilities and separation selectivities of the enantiomers of B41 in pH = 2.5 BGEs with HxS, HS, OS.

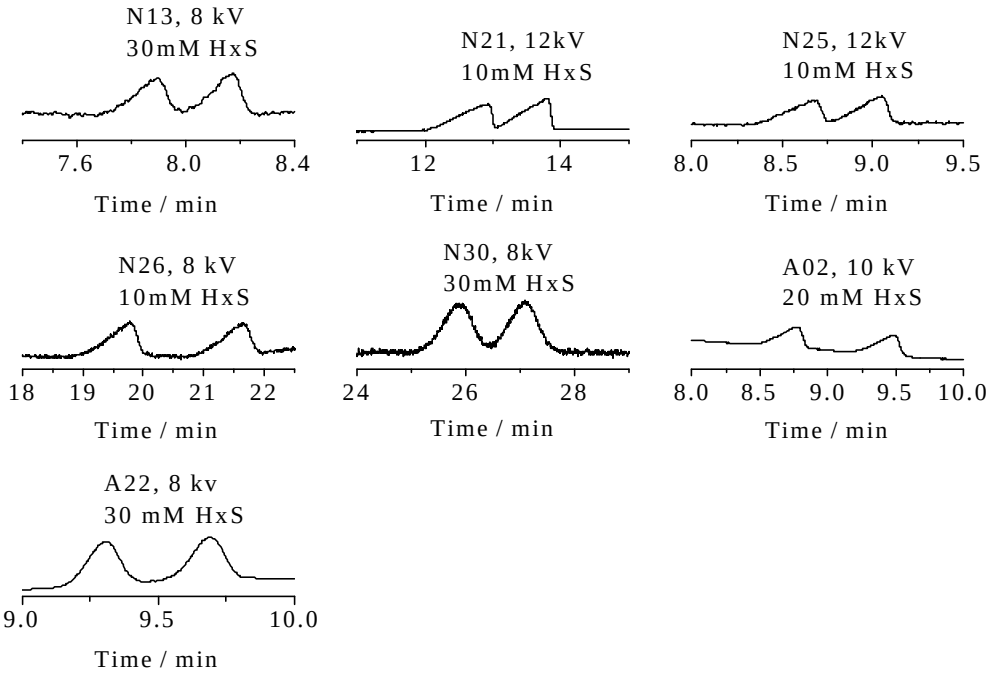

Figure 63. Typical electropherograms of separation of the enantiomers of the nonionic and weak acid analytes in pH = 2.5 BGEs with HxS.

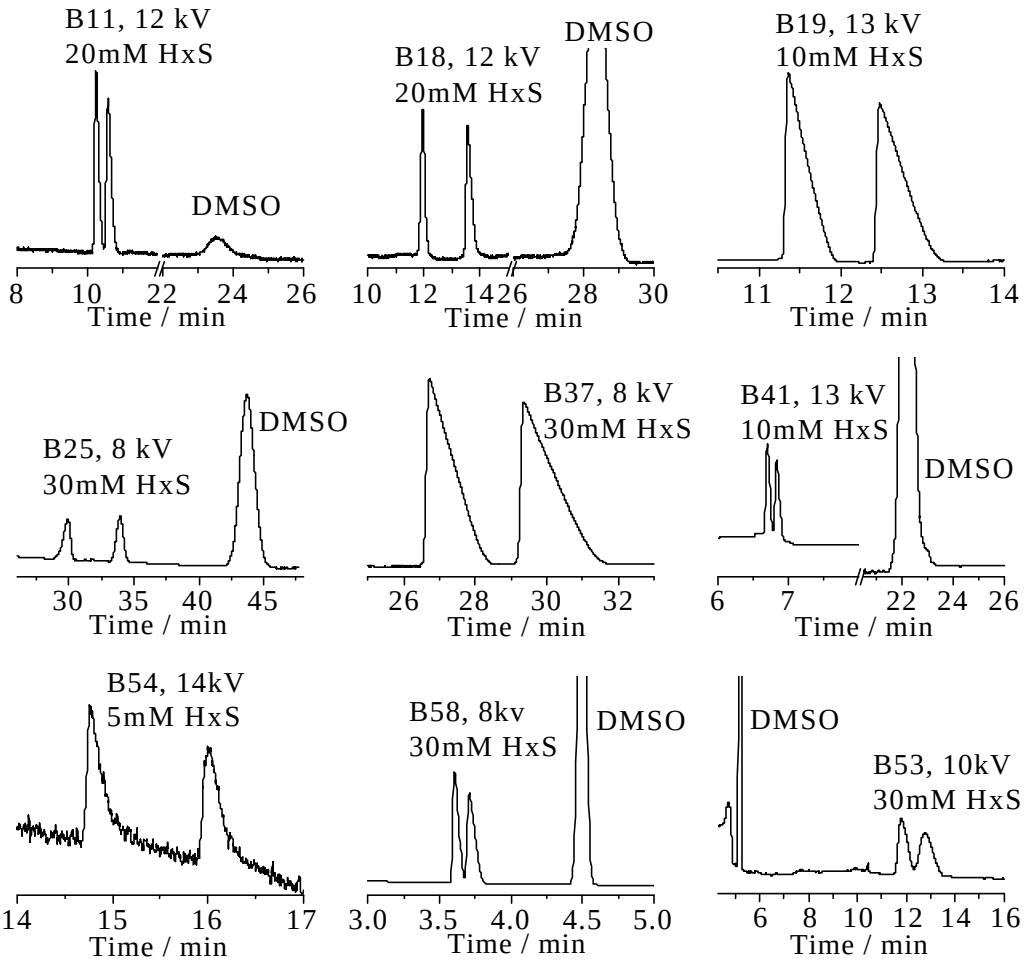

Figure 64. Typical electropherograms of separation of the enantiomers of the weak base analytes in pH = 2.5 BGEs with HxS.

4.2 Separations in High pH BGEs

4.2.1 Experimental Conditions and Methods

All CE separations were carried out in 25 mM ethanolamine which were titrated to pH 9.5 with methane sulfonic acid (MSA). The HxS BEs were prepared by weighing out the required amounts of the sodium salt of HxS into 25mL volumetric flasks and bringing the volumes to mark with the pH = 9.5 stock BGE solution. The other experimental details are the same as described in Chapter III.

4.2.2 Results and Discussion

A series of neutral, weak acid and weak base enantiomers were separated with the pH=9.5 HxS BGEs. Table 5 lists the observed effective mobilities of the less mobile enantiomers, μ, the separation selectivities, α, the measured peak resolution values, Rs, the corresponding dimensionless EOF mobility values, β, and the injector-to-detector potential drop values, U.

4.2.2.1 Separation of the Enantiomers of Nonionic Analytes

For the nonelectrolyte analytes, typical effective mobility and separation selectivity curves are shown in Figure 65. Though the anionic effective mobilities become larger as the HxS concentration is increased, the increase is not as rapid as in the pH = 2.5 BGEs indicating that components of the ethanolamine - MSA buffer compete with the nonelectrolyte analytes for HxS more strongly than components of the H_3PO_4 - LiOH buffer did. However,

Table 5. Separation data in pH=9.5 HxS BGEs. (μ, in 10^{-5} cm^2 / Vs units)

HxS (mM)	0		10		
U (kV)			8		
Analyte	μ	μ	α	β	Rs
N02	0	-1.5	1.00	-34	0
N12	0	-1.2	1.00	-28	0
N13	0	-1.0	1.00	-38	0
N21	0	-7.0	1.00	-7.2	0
N24	0	-0.8	1.00	-33	0
N25	0	-9.8	1.00	-5.2	0
N26	0	-5.0	1.00	-10	0
N27	0	-0.7	1.00	-67	0
N28	0	-1.4	1.00	-37	0
N30	0	-2.3	1.00	-22	0
N34	0	-2.6	1.00	-20	0
N36	0	-1.1	1.00	-29	0
N38	0	-1.5	1.00	-33	0
N39	0	-1.1	1.00	-46	0
A02	-23.0	-30.3	1.00	-1.5	0
A22	-21.1	-24.8	1.00	-1.9	0
A23	-22.7	-27.0	1.00	-1.8	0
A30	-24.0	-25.5	1.03	-1.6	0.9
			1.02		0.8
A31	-20.9	-26.0	1.00	-1.9	0
A36	-23.9	-31.6	1.03	-1.5	<0.6

Table 5. Continued.

HxS (mM)		20				30		
U (kV)		10				8		
Analyte	μ	α	β	Rs	μ	α	β	Rs
N02	-2.9	1.03	-14	<0.6	-3.9	1.06	-8.2	<0.6
N12	-2.0	1.12	-21	<0.6	-2.7	1.18	-12	0.7
N13	-2.0	1.00	-21	0	-3.1	1.00	-10	0
N21	-11.2	1.03	-3.8	<0.6	-14.1	1.03	-2.4	0.6
N24	-1.5	1.00	-27	0	-2.3	1.00	-14	0
N25	-14.2	1.02	-2.9	<0.6	-17.4	1.02	-2.0	0.6
N26	-9.1	1.03	-4.6	<0.6	-12.4	1.04	-2.7	0.6
N27	-1.4	1.00	-30	0	-2.1	1.00	-16	0
N28	-2.2	1.00	-19	0	-3.2	1.00	-10	0
N30	-3.9	1.00	-11	0	-5.8	1.00	-5.7	0
N34	-5.0	1.00	-8.2	0	-6.3	1.00	-5.3	0
N36	-1.9	1.00	-22	0	-2.6	1.00	-7.9	0
N38	-2.7	1.00	-15	0	-4.2	1.00	-7.9	0
N39	-2.0	1.00	-21	0	-2.8	1.08	-12	<0.6
A02	-31.0	1.00	-1.5	0				
A22	-25.0	1.00	-1.8	0	-24.6	1.00	-1.5	0
A23	-27.3	1.00	-1.5	0	-25.9	1.00	-1.2	0
A30	-28.5	1.03	-1.5	1.4	-27.4	1.04	-1.3	4.3
		1.01		0.7		1.02		1.7
A31	-25.4	1.00	-1.8	0	-23.7	1.00	-1.4	0
A36	-31.8	1.03	-1.4	<0.6	-31.1	1.03	-1.1	<0.6

Table 5. Continued.

HxS (mM)		40				50		
U (kV)		6				6		
Analyte	μ	α	β	Rs	μ	α	β	Rs
N02	-4.9	1.09	-5.4	<0.6	-6.0	1.08	-4.0	<0.6
N12	-3.4	1.16	-8.1	0.8	-3.8	1.13	-5.5	<0.6
N13	-4.0	1.00	-6.7	0	-4.6	1.00	-4.1	0
N21	-14.8	1.03	-1.8	<0.6	-15.3	1.02	-3.4	<0.6
N24	-3.1	1.00	-8.4	0	-3.5	1.00	-5.1	0
N25	-18.2	1.02	-1.4	0.7	-18.6	1.02	-1.2	<0.6
N26	-14.3	1.04	-1.9	<0.6	-15.4	1.03	-1.4	<0.6
N27	-2.9	1.00	-7.6	0	-3.3	1.00	-3.5	0
N28	-4.0	1.00	-5.5	0	-4.6	1.02	-3.0	<0.6
N30	-6.9	1.02	-2.9	<0.6	-8.0	1.07	-3.2	<0.6
N34	-7.5	1.02	-3.6	<0.6	-8.1	1.02	-3.2	<0.6
N36	-3.1	1.00	-8.8	0	-3.7	1.00	-7.1	0
N38	-5.2	1.00	-5.2	0	-5.8	1.00	-4.6	0
N39	-3.6	1.14	-7.6	0.7	-4.3	1.14	-6.5	<0.6

Table 5. Continued.

HxS (mM)	0		5			10			
U (kV)	18		12			10			
Analyte	μ	μ	α	β	Rs	μ	α	β	Rs
B02	10.4					2.0	1.19	23	0.9
B03	8.6	-2.4	0.92	-41	<0.6	-5.5	0.93	-7.9	<0.6
B04	12.6					10.1	1.00	4.0	0
B08	10.9					7.1	1.00	5.8	0
B09	11.3					6.8	1.00	6.1	0
B11	1.5	N/A				-3.2	0.75	-14	0.7
B13	14.8	N/A				N/A			
B14	5.9					2.0	1.10	51	<0.6
B18	10.3	N/A				-9.8	0.28	-4.3	8.0
B19	11.2					7.0	1.04	6.4	<0.6
B22	10.0	N/A				-3.5	0.93	-9.5	<0.6
B23	9.0	1.17	1.69	43	<0.6	-0.4	0.64	-117	0.8
B24	7.0	N/A				-2.1	0.95	-20	<0.6
B25	18.0					4.0	1.05	10	<0.6
B37	10.5					6.9	1.00	6.2	0
B39	0.0	N/A				-2.1	1.22	-20	0.7
B46	1.1	N/A				N/A			
B51	8.0					3.9	1.07	11	<0.6
B54	0.0	-9.86	1.25	-5.0	1.0	-10.5	1.20	-4.1	3.0
B58	20.2					9.5	1.03	4.7	<0.6

Table 5. Continued.

HxS (mM)	20				30			
U (kV)	10				8			
Analyte	μ	α	β	Rs	μ	α	β	Rs
B02	-2.7	0.74	-15	0.8	-4.3	0.88	-8.3	0.9
B03	-7.9	0.94	-5.0	0.7	-8.7	0.94	-4.0	1.1
B04	8.3	1.00	4.7	0	6.7	1.00	6.8	0
B08	5.1	1.00	7.6	0	3.7	1.00	8.6	0
B09	4.1	1.00	9.1	0	2.7	1.00	12	0
B11	-5.7	0.89	-6.9	0.9	-7.4	0.92	-4.3	1.4
B13	N/A				-9.7	0.97	-3.2	<0.6
B14	-1.1	0.91	-36	<0.6	-3.9	0.97	-8.1	<0.6
B18	-11.3	0.44	-3.5	10.5	-11.5	0.56	-2.7	12
B19	4.7	1.06	8.1	<0.6	2.5	1.08	16	<0.6
B22	-8.3	0.95	-4.8	<0.6	-10.8	0.96	-3.0	0.7
B23	-2.7	0.79	-14	0.7	-4.5	0.95	-7.3	<0.6
B24	-5.5	0.96	-7.1	<0.6	-7.7	0.97	-4.3	<0.6
B25	1.5	1.16	26	<0.6	N/A			
B37	5.3	1.00	7.4	0	4.2	1.00	11	0
B39	-3.3	1.19	-12	0.9	-4.4	1.23	-7.6	1.1
B46	N/A				-2.1	0.95	-2.5	<0.6
B51	1.2	1.15	29	<0.6	0.5	1.26	127	<0.6
B53	N/A				-5.0	1.07	-6.6	0.7
B54	-11.4	1.16	-3.5	3.3	-12.7	1.12	-2.6	4.3
B58	6.5	1.07	5.9	0.6	4.3	1.12	7.7	0.7

Table 5. Continued.

HxS (mM)	40				50			
U (kV)	6				6			
Analyte	μ	α	β	Rs	μ	α	β	Rs
B02	-1.4	0.65	-19	0.7	-1.2	0.57	-21	10
B03	-8.6	0.95	-3.1	0.8	-7.9	0.94	-3.1	1.2
B04	5.8	1.00	4.1	0	6.0	1.00	3.9	0
B08	3.4	1.00	5.9	0	3.2	1.00	6.2	0
B09	1.6	1.00	14	0	1.8	1.00	12	0
B11	-5.4	0.88	-4.5	0.9	-5.2	0.84	-5.1	1.1
B13	-6.9	0.96	-1.8	0.9	N/A			
B14	-4.3	0.95	-7.7	<0.6	-4.2	0.93	-6.9	<0.6
B18	-10.7	0.47	-2.4	8.3	-10.1	0.34	-2.3	9.8
B19	2.3	1.12	6.7	1.0	2.8	1.06	7.5	0.7
B22	-9.6	0.97	-2.4	0.6	-8.7	0.96	-2.8	0.7
B23	-4.2	0.93	-5.9	<0.6	N/A			
B24	-6.8	0.92	-2.0	<0.6	N/A			
B25	4.0	1.12	1.7	1.3	4.3	1.09	1.5	0.9
B37	4.9	1.00	5.0	0	5.1	1.00	3.5	0
B39	-5.3	1.21	-4.5	0.9	-5.8	1.22	-3.8	0.8
B46	N/A				N/A			
B51	0.9	1.11	28	<0.6	1.53	1.04	16	<0.6
B53	N/A				-6.7	1.06	-3.4	0.6
B54	-12.6	1.19	-2.0	2.0	-13.1	1.23	-1.8	2.8
B58	4.2	1.08	5.7	0.9	4.75	1.05	5.2	0.7

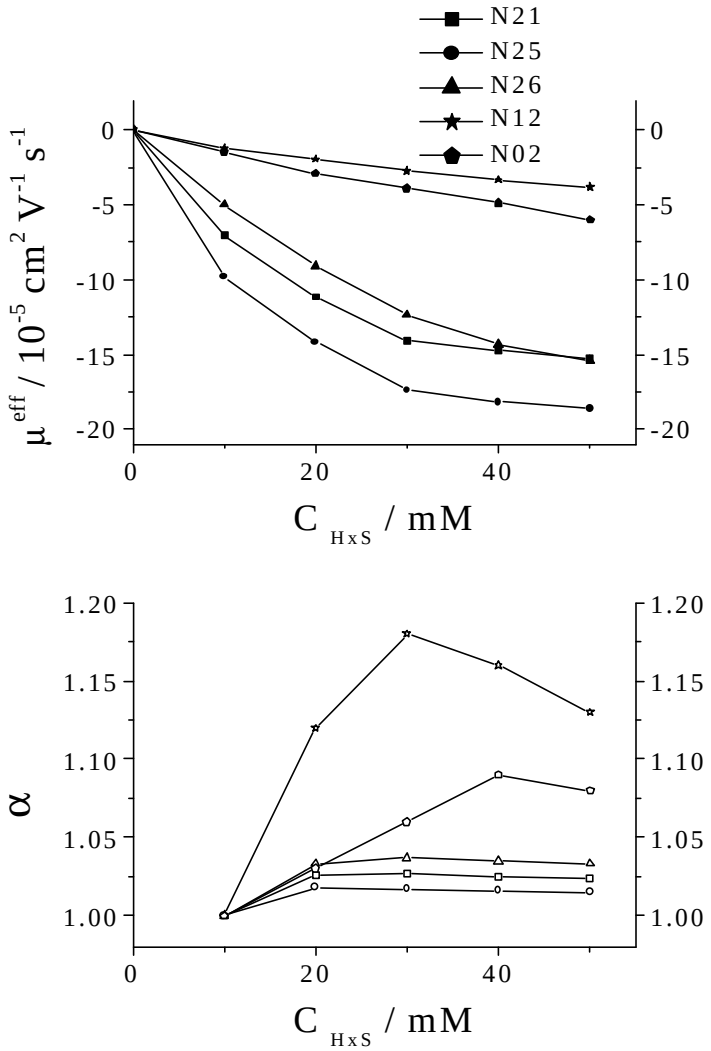

Figure 65. Effective mobilities and separation selectivities for the enantiomers of nonionic analytes in pH = 9.5 BGEs with HxS.

by-and-large, separation selectivities are similar in both BGEs, indicating that there is no preferred BGEs in terms of the pH of the BGE for this set of analytes.

4.2.2.2 Separation of the Enantiomers of Weak Acids

The previous studies have shown that HxS could separate enantiomers in low pH background electrolytes. Due to their limited solubilities, only a few of the hydrophobic, acidic pharmaceuticals could be studied in the low pH BGEs. Though acidic analytes become anionic, and thus quite soluble, in high pH BGEs, their binding to the anionic HxS is expected to be weak. Since HxS is hydrolytically very stable at pH=9.5, it was interesting to investigate the separation behavior of weak acid analytes in the pH = 9.5 BGEs. In the absence of HxS, the effective mobilities of the analytes are (-7 to -29)x10^{-5} cm^2 V^{-1} s^{-1}, indicating that the carboxylic acid groups are fully dissociated. Just as the weak base analytes in low pH BGEs, the anionic μ^{eff} values pass a local maximum as the HxS concentration is increased. The effective mobility trends can be explained by the interplay between the increasing degree of complexation between HxS and weak acid analytes, and the increased BGE viscosity, as well as the increased ionic strength of the BGEs, as the HxS concentration is increased. Increases in the anionic effective mobilities of three of the analytes, trans-2-phenyl-1-cyclopropane carboxylic acid (A02), carprofen (A04) and 2-phenylpropionic acid (A36) were about two times larger than the mobility increases for the other weak acids and about three times larger than the mobility increases for similar-size nonelectrolyte analytes. Flubiprofen (A26) stood out as the weak acid for which the mobility increase uniquely low. Despite the relatively favorable β values and the relatively strong interactions between the weak acids and HxS, only partial peak

resolution was achieved, and only for two of the weak acid analytes.

The pH of the BGE may play a role in the separation of the enantiomers of the weak acid analytes. For some of the weak acid, the enantiomers could not be separated in the low pH BGEs with HxS, but could be separated in the high pH BGEs and vice verse. Figure 66 shows the effective mobility plots (top panel) and the corresponding separation selectivities (bottom panel) for fenoprofen (A22) and 2-phenylpropionic acid (A36) in both the high pH and the low pH BGEs with HxS as the chiral resolving agent. The fenoprofen enantiomers could be separated in the low pH BGE, but not in the high pH BGE, while the enantiomers of 2-phenylpropionic acid could not be separated in the low pH BGE, but could be separated in the high pH BGE.

4.2.2.3 Separation of the Enantiomers of Weak Bases

For weak bases, except B39, B53 and B54, the initial effective mobilities in the 0 mM HxS BGE were still cationic, with effective mobilities from 1 to 20×10^{-5} cm^2 V^{-1} s^{-1}, indicating that the pH was not high enough to completely deprotoned the amine groups in the weak base molecules. As in the low pH BGEs, the weak base enantiomers can also be divided into two groups: weakly binding and strongly binding weak bases. Figure 67 shows the mobility (left top panel) and separation selectivity (left bottom panel) curves for three typical, weakly binding weak base enantiomers, as well as the mobility (right top panel) and separation selectivity (right bottom panel) curves for three typical strongly binding weak

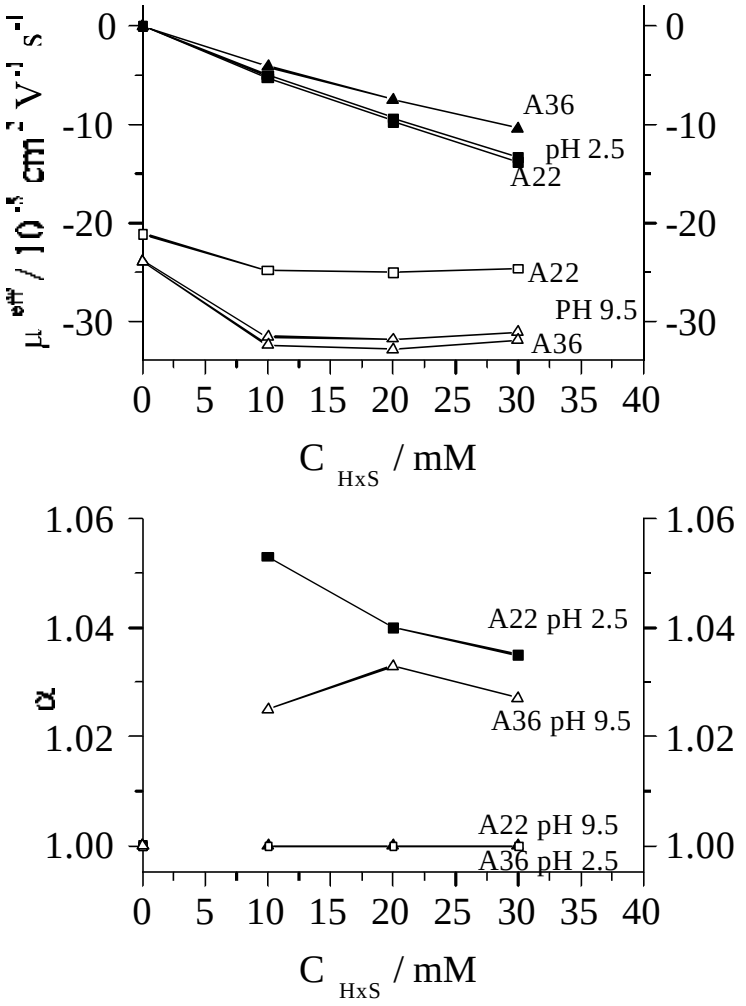

Figure 66. Effects of the BGE pH on the effective mobilities and separation selectivities of the enantiomers of weak acid analytes with HxS.

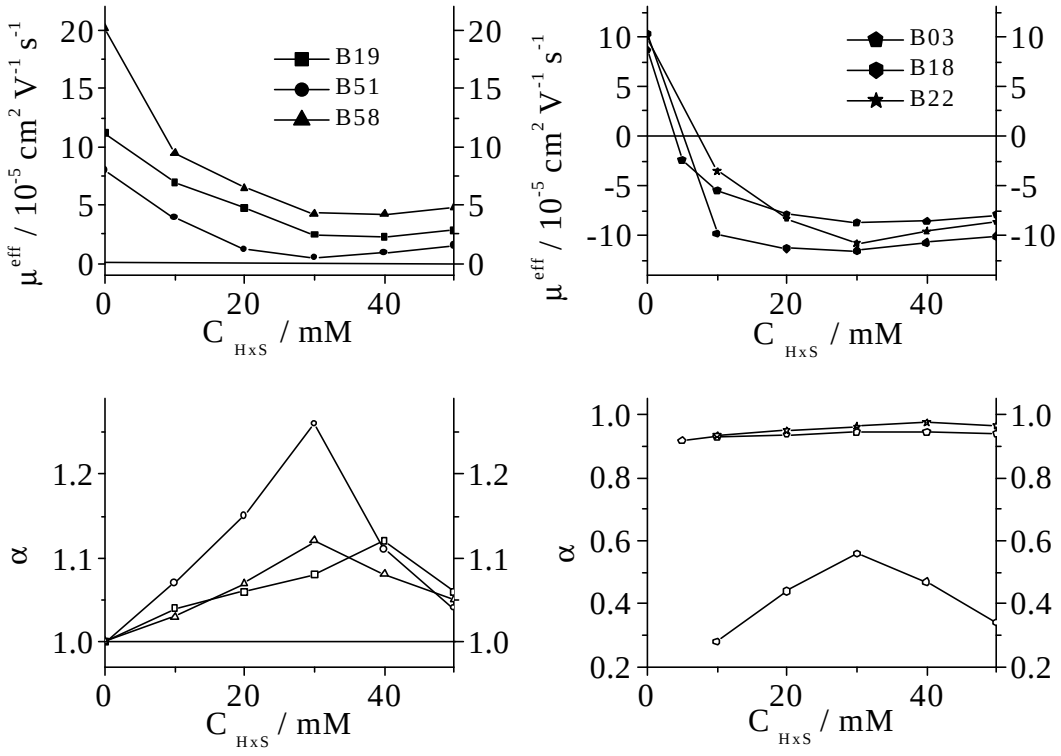

Figure 67. Effective mobilities and separation selectivities for the weak base analytes in pH = 9.5 BGEs with HxS. Weakly binding (left panels) and strongly binding (right panels).

bases. In each case, the initially cationic effective mobility of the weak base is between $9x10^{-5}$ and $21x10^{-5}$ cm^2/Vs.

The type of the CD substituents also affects the separation of the enantiomers of weak base analytes in the high pH BGEs. The complexing strength of tolperisone (B51) with HxS is much weaker than with HxDAS. This can be rationalized by noting that the hydrophobic interactions between B51 and the hydrophilic HxS, are weaker than with HxDAS.

The size of the cyclodextrin cavity also affects the chiral recognition process significantly. Figure 68 shows the effective mobility plots (top panel) and the corresponding separation. selectivities (bottom panel) for chlophedianol (B14) with HxS, HS and OS as the chiral resolving agents. Just as in the low pH BGEs, the strength of the inter - molecular interactions between B14 and the three CDs follow the order: OS ≅ HS > HxS. While at our present level of knowledge the differences cannot be predicted a priori, they indicate that HxS can play a unique role in the CE separation of enantiomers.

The pH of the HxS BGEs also influences the separation of the enantiomers of weak base analytes. Figure 69 shows the effective mobility plots (top panel) and the corresponding separation selectivities (bottom panel) for aminoglutethimide (B03) and bupropion (B11) in both the high pH and the low pH BGEs with HxS as the chiral resolving agent. For both two weak base analytes, the binding strength with HxS is low in the low pH BGEs; but high in the high pH BGEs.

Finally, Figure 70 show some typical electropherograms in the high pH BGEs with HxS. The numbers next to the electropherograms indicate the actual HxS concentrations.

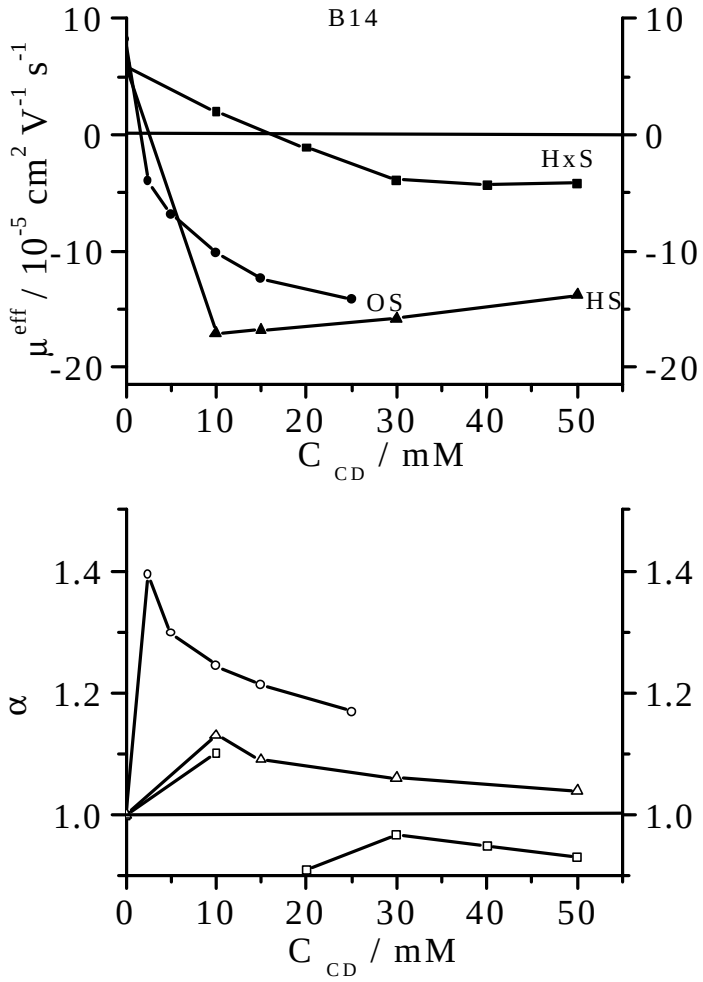

Figure 68. Cyclodextrin cavity size effects on the effective mobilities and separation selectivities of the enantiomers of B14 in pH=9.5 BGEs with HxS, HS, OS.

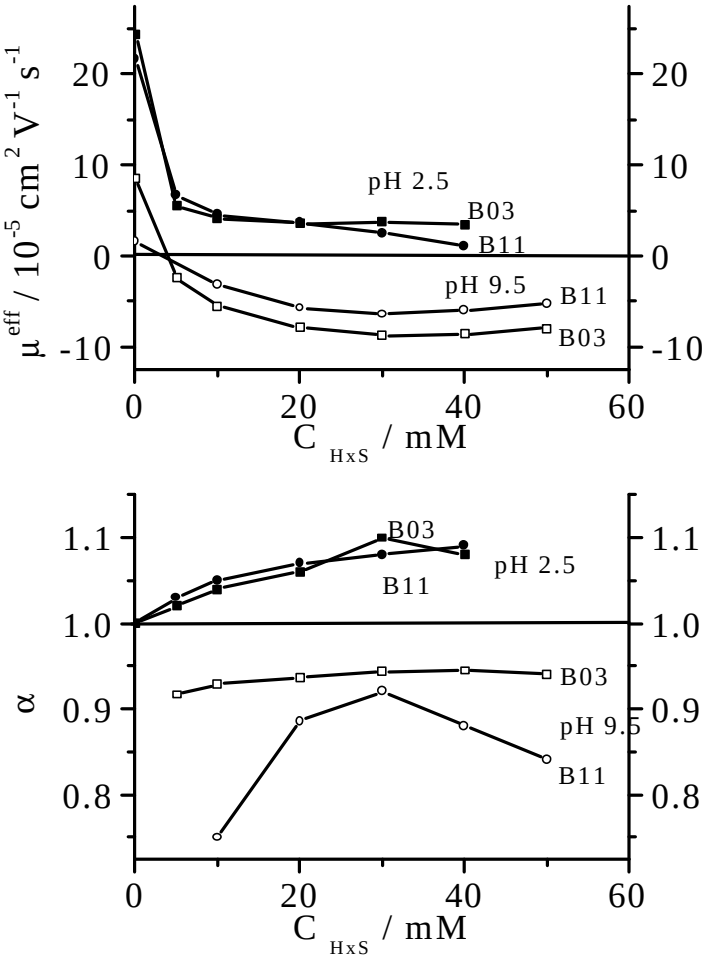

Figure 69. Effects of the BGE pH on the separation of the enantiomers of weak base analytes with HxS.

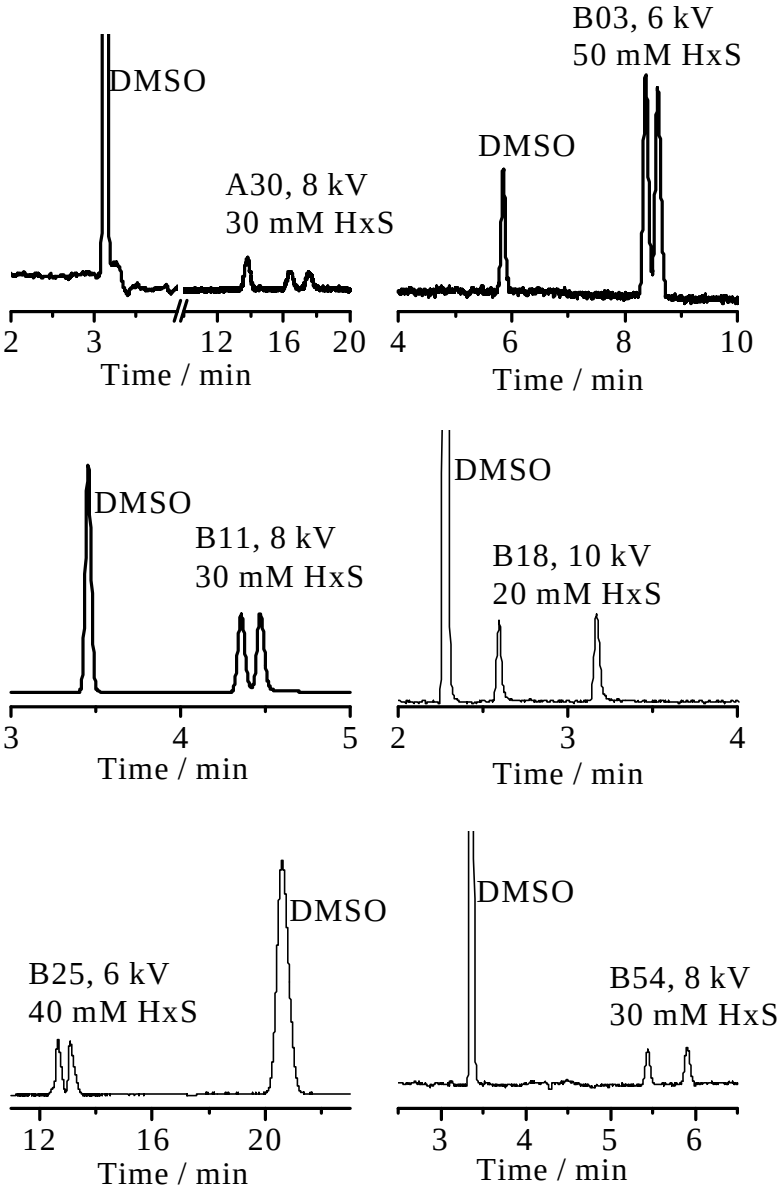

Figure 70. Typical electropherograms of separation of the enantiomers of the weak acid and base analytes in pH = 9.5 BGEs with HxS.

4.3 Summary

The second single-isomer sulfated α-CD, the sodium salt of hexakis(6-sulfo)-α-cyclodextrin (HxS) has been synthesized and used to separate the enantiomers of neutral, weak acid and weak base analytes in both low and high pH aqueous BGEs. The effective mobilities and separation selectivities followed the predictions of the CHARM model of CE enantiomer separations and led to different peak resolution values than HxDAS and its corresponding β-analogues and γ-analogues. The experimental results also show that the inter - molecular interactions of HxS with analytes B18 and B51 are weaker than with HxDAS. Compared to the corresponding β-CD, γ-CD derivatives, HS and OS, the complexing strength of HxS with chiral analytes is much weaker. The pH of the BGE also plays a very important role in the chiral recognition process when HxS is used as the chiral resolving agent.

CHAPTER V

ENANTIOMER SEPARATIONS WITH HxDMS

In order to complete the study of the effect of substituent structure on the separation of enantiomers, hexakis(2,3-di-*O*-methyl-6-*O*-sulfo)-α-CD (HxDMS) was synthesized and evaluated.

5.1 Materials and Methods

Except for the sodium salt of hexakis(2,3-di-*O*-methyl-6-*O*-sulfo)-α-cyclodextrin (HxDMS) which was synthesized as described in Chapter II, all other chemicals were obtained from Aldrich Chemical Company. The low pH BGE was prepared by titrating 25 mM H_3PO_4 with LiOH to pH = 2.5. The high pH BGE was prepared by titrating 25 mM ethanolamine with methanesulfonic acid to pH = 9.5. Effective mobility measurements were carried out within the linear region of Ohm's law using DMSO as the neutral marker. Other details of the experimental conditions were described in Chapter III.

5.2 Enantiomer Separations in Low pH BGEs

A series of neutral, weak acid, weak base enantiomers were separated in the pH = 2.5 HxDMS BGEs. Table 6 lists the effective mobilities of the less mobile enantiomers, μ, the separation selectivities, α, the measured peak resolution values, Rs, the corresponding dimensionless EOF mobility values, β, and the injector-to-detector potential drop values, U.

N/A indicates that the aforementioned values could not be calculated due to either overlap with non-comigrating system peaks or comigration of an enantiomer peak with the neutral marker.

5.2.1 Separation of the Enantiomers of Nonionic Analytes

Enantiomers of eleven of the fifteen nonionic analytes, mostly aromatic alcohols, could be separated with HxDMS, with baseline separations, for seven of the eleven nonionic analytes. The anionic mobilities of the non-charged enantiomers increased monototically with increasing HxDMS concentration as shown in Figure 71 (top panel). The separation selectivity plots (Figure 71, bottom panel) are similar to those obtained for the separation of the enantiomers of nonionic analytes with HxDAS (Chapter III) and HxS (Chapter IV).

HxDMS complexed with all of the nonelectrolyte analytes tested quite strongly. Some of the complexation strength differences can be easily rationalized by considering the structure of the analyte: e. g., of the two γ-butyrolactone, N12 that contains a naphthyl ring complexes much more strongly with HxDMS than N13 that contain phenyl ring. For other analyte pairs, more subtle structural differences still lead to large complexation differences, e. g., 1-phenylpentanol (N25) binds much more strongly than either 2-phenyl-2-pentanol (N26) or 1-phenylbutanol (N21). The effects of the size of the CD in the identically substituted HxDMS, HDMS and ODMS can be seen in Figure 72: the top panels compare the effective mobilities for 1-phenylpentanol (N25) (left panel) and 2-phenyl-2-pentanol (N26) (right panel) with HxDMs, HDMS [104] and ODMS [110] as the chiral resolving agent, the

Table 6. Separation data in pH=2.5 HxS BGEs. (μ, in 10^{-5} cm^2 / Vs units)

HxDMS (mM)	0		10		
U (kV)			12		
Analyte	μ	μ	α	β	Rs
N02	0	-4.3	1.00	-2.8	0
N10	0	-3.3	1.03	-4.5	<0.6
N12	0	-13.7	1.03	-1.2	<0.6
N13	0	-5.1	1.00	-3.0	0
N15	0	-2.8	1.06	-5.4	<0.6
N21	0	-5.0	1.00	-3.4	0
N24	0	-2.1	1.00	-6.2	0
N25	0	-9.5	1.00	-1.9	0
N26	0	-4.3	1.04	-2.8	<0.6
N27	0	-2.8	1.00	-5.2	0
N28	0	-3.0	1.00	-5.1	0
N30	0	-5.5	1.14	-3.0	3.3
N34	0	-3.3	1.00	-3.7	0
N36	0	-2.8	1.34	-5.7	2.2
N38	0	-3.0	1.00	-4.4	0

Table 6. Continued.

HxDMS (mM)		20				30		
U (kV)		11				10		
Analyte	μ	α	β	Rs	μ	α	β	Rs
N02	-7.5	1.01	-3.0	<0.6	-10.4	1.01	-2.9	<0.6
N10	-5.6	1.07	-3.9	0.7	-7.8	1.09	-2.9	0.9
N12	-17.3	1.05	-1.3	3.7	-18.5	1.06	-1.2	4.2
N13	-8.1	1.00	-2.1	0	-10.3	1.00	-2.2	0
N15	-4.5	1.06	-4.7	0.8	-6.1	1.07	-3.6	1.0
N21	-9.1	1.02	-2.5	<0.6	-11.9	1.03	-2.4	<0.6
N24	-3.6	1.01	-6.2	<0.6	-4.7	1.01	-5.2	<0.6
N25	-14.9	1.03	-1.5	1.4	-18.9	1.04	-1.5	2.8
N26	-7.4	1.01	-2.1	<0.6	-9.2	1.01	-3.0	<0.6
N27	-6.1	1.00	-3.2	0	-7.6	1.00	-3.6	0
N28	-5.9	1.00	-3.2	0	-7.3	1.00	-3.8	0
N30	-10.4	1.09	-2.9	1.9	-15.5	1.06	-1.8	2.8
N34	-6.0	1.00	-3.4	0	-7.5	1.00	-3.3	0
N36	-5.0	1.30	-2.5	3.4	-6.4	1.26	-4.3	2.9
N38	-5.1	1.01	-4.4	<0.6	-6.8	1.02	-4.1	<0.6

Table 6. Continued.

HxDMS (mM)	40				50			
U (kV)	8				6			
Analyte	μ	α	β	Rs	μ	α	β	Rs
N02	-12.6	1.01	-2.1	<0.6	-13.3	1.01	-1.8	<0.6
N10	-9.3	1.11	-2.8	2.0	-9.8	1.06	-2.5	0.7
N12	-19.2	1.06	-1.4	10	-19.9	1.06	-1.3	5.6
N13	-11.7	1.00	-2.6	0	-12.0	1.00	-1.9	0
N15	-7.5	1.07	-3.4	0.7	-8.4	1.05	-1.7	2.2
N21	-13.5	1.03	-2.2	0.8	-14.7	1.04	-1.8	1.1
N24	-5.6	1.02	-5.3	<0.6	-6.6	1.03	-3.8	<0.6
N25	-21.9	1.05	-1.4	2.3	-22.7	1.04	-1.1	2.0
N26	-11.1	1.01	-2.7	<0.6	-12.1	1.01	-2.0	<0.6
N27	-8.8	1.00	-2.9	0	-8.9	1.00	-2.5	0
N28	-8.8	1.00	-2.7	0	-9.2	1.00	-2.4	0
N30	-20.5	1.04	-1.4	2.1	-21.8	1.02	-1.2	1.9
N34	-8.8	1.00	-2.4	0	-9.6	1.00	-2.5	0
N36	-7.8	1.24	-3.9	4.7	-8.2	1.22	-3.1	3.5
N38	-8.3	1.02	-3.5	<0.6	-9.5	1.01	-2.7	<0.6

Table 6. Continued.

HxDMS (mM)	0		10		
U (kV)			12		
Analyte	μ	μ	α	β	Rs
NSA^-	0				
A02	0	-10.9	1.03	-1.9	0.7
A22	0	-10.5	1.01	-2.1	<0.6
A23	0	-12.8	1.00	-1.4	0
A26	0	-15.4	1.00	-1.1	0
A27	0	-14.1	1.00	-1.6	0
A28	0	-5.3	1.02	-4.3	0.6
A30	0	-10.4	1.05	-1.8	3.1
		-10.9	1.05		1.1
		-11.0	1.00		0
		-11.0			
A31	0	-6.5	1.02	-3.5	<0.6
A36	0	-4.2	1.00	-5.2	0

* Polarity (-) to (+), NSA^- as secondary EOF marker

Table 6. Continued.

HxDMS (mM)		20				30		
U (kV)		11				10		
Analyte	μ	α	β	Rs	μ	α	β	Rs
NSA^-	-27.5				-26.9			
A02	-17.4*	1.03	-0.2	0.8	-20.3*	1.02	-0.2	<0.6
A22	-16.0	1.03	-2.0	1.2	-20.4	1.02	-1.3	0.6
A23	-17.3*	1.00	-0.1	0	-20.6*	1.00	-0.7	0
A26	-20.4*	1.01	-0.03	<0.6	-24.2	1.00	-1.2	0
A27	-27.9*	1.00	-0.2	0	-25.3*	1.00	-0.9	0
A28	-8.2	1.03	-1.6	1.3	-10.7	1.02	-2.4	2.1
A30	-17.1* -16.4* -14.9* -14.6*	1.04 1.10 1.02	-0.06	2.0 4.4 1.0	-18.2* -17.6* -14.1* -12.6*	1.03 1.25 1.12	-0.2	1.9 3.5 <0.6
A31	-11.5	1.02	-1.4	1.3	N/A			
A36	-8.7	1.00	-1.8	0	-11.0*	1.00	-0.8	0

Table 6. Continued.

HxDMS (mM)		40				50		
U (kV)		8				6		
Analyte	μ	α	β	Rs	μ	α	β	Rs
A02	-22.0	1.01	-1.4	1.0	-22.1	1.01	-1.2	1.4
A22	-23.5	1.01	-1.2	<0.6	-24.2	1.01	-1.2	<0.6
A23	-22.4	1.00	-1.3	0				
A26	-27.5	1.00	-1.1	0				
A27	-22.4	<1.01	-1.3	<0.6	-20.0	<1.01	-1.2	<0.6
A28	-11.8	1.02	-2.0	0.8	-12.6	1.01	-2.1	0.6
A30	-20.5	1.01	-1.5	0.6	-18.0	<1.01	-1.4	0.6
	-20.6	1.00		0	-18.1	1.00		0
	-20.6	1.00		0	-18.1	1.00		0
	-20.6				-18.1			
A31	N/A				-10.5	1.02	-1.8	<0.6
A36	-13.1	1.00	-1.4	0	-14.6	<1.01	-1.3	<0.6

Table 6. Continued.

HxDMS (mM)		5				10		
U (kV)		12				12		
Analyte	μ	α	β	Rs	μ	α	β	Rs
B02					7.7	1.05	1.9	<0.6
B03					10.4	1.04	1.5	<0.6
B08					14.5	1.00	0.8	0
B09								
B10					9.7	1.04	1.3	<0.6
B11					6.9	1.10	2.1	0.7
B13					5.8	1.12	2.6	0.9
B14					8.3	1.09	1.8	0.7
B18	-2.1	0.54	-14	2.4	-6.6	0.63	-2.2	8.0
B20					15.1	1.02	1.6	<0.6
B22					16.4	1.00	1.2	0
B23	-4.9	0.59	-5.8	3.0	-9.4	0.70	-1.5	5.2
B24					-0.7	1.00	-16	0
B25					5.9	1.04	2.1	0.6
B31					12.1	1.00	2.0	0

Table 6. Continued.

HxDMS (mM)	20				30			
U (kV)	11				10			
Analyte	μ	α	β	Rs	μ	α	β	Rs
B02	2.5	1.25	14	1.0	-0.9	0.81	-39	<0.6
B03	-2.3	0.90	-14	<0.6	-7.8	0.95	-4.1	1.0
B08	10.4	1.00	0.7	0	7.5	1.00	4.3	0
B09	6.0	1.00	1.1	0	3.0	1.00	5.4	0
B10	6.0	1.12	2.1	<0.6	3.2	1.34	11	0.9
B11	1.8	1.91	19	2.1	N/A			
B13	-1.0	0.63	-30	0.7	-4.3	0.85	-7.2	1.7
B14	1.6	1.19	16	0.6	-2.3	0.93	-6.9	0.7
B18	-10.8	0.80	-2.7	6.4	-13.7	0.84	-2.5	7.3
B20	8.9	1.06	1.6	<0.6	6.2	1.11	2.2	0.6
B22	12.3	1.00	0.5	0	9.6	1.00	3.7	0
B23	-12.1	0.80	-2.2	11	-13.9	0.84	-2.2	7.6
B24	-3.5	1.00	-7.4	0	-5.8	1.00	-5.1	0
B25	1.1	1.34	20	0.8	-1.0	0.78	-30	19
B31	8.0	1.00	0.6	0	5.7	1.00	4.1	0

Table 6. Continued.

HxDMS (mM)	40				50			
U (kV)	8				6			
Analyte	μ	α	β	Rs	μ	α	β	Rs
B02	-2.5	0.90	-12	<0.6	-4.2	0.94	-6.3	0.6
B03	-8.9	0.96	-3.1	1.4	-10.1	0.96	-2.6	1.4
B08	4.4	1.00	5.8	0	2.9	1.00	8.1	0
B09	1.4	1.00	22	0	N/A			
B10	0.7	1.59	43	0.7	-0.8	0.74	-32	0.6
B11	-2.9	0.67	-10	2.4	-4.8	0.81	-5.6	2.9
B13	-6.5	0.90	-4.5	1.8	-7.6	0.93	-3.4	1.9
B14	-5.4	0.95	-5.1	0.8	-3.9	0.93	-3.4	2.1
B18	-14.9	0.87	-2.0	8.6	-14.3	0.89	-1.8	8.2
B20	5.3	1.08	5.3	<0.6	4.4	1.07	19	<0.6
B22	7.8	1.00	3.6	0	6.3	1.00	3.9	0
B23	-14.8	0.88	-2.0	7.8	-14.0	0.91	-1.8	6.1
B24	-7.7	0.98	-3.9	<0.6	-8.9	0.98	-2.9	<0.6
B25	-2.8	0.83	-11	1.2	-4.2	0.89	-6.1	1.2
B31	3.7	1.00	6.8	0	2.2	1.00	11	0

Table 6. Continued.

HxDMS (mM)	5				10			
U (kV)					12			
Analyte	μ	α	β	Rs	μ	α	β	Rs
B34					16.1	1.01	0.9	<0.6
B35	1.2	1.09	24	1.0	-5.5	0.90	-2.3	1.9
B36	4.1	1.06	7.3	0.9	-0.8	0.86	-17	1.3
B37					6.5	1.00	1.9	0
B38					N/A			
B39					15.0	1.02	0.8	<0.6
B41					6.6	1.00	2.1	0
B42					3.2	1.07	5.9	0.7
B45					10.6	1.00	1.2	0
B46					10.1	1.00	1.2	0
B51					8.1	1.00	1.8	0
B53					-2.9	0.83	-4.2	0.9
B54					-0.7	1.00	-19	0
B56	2.1	1.04	14	<0.6	-6.6	0.97	-2.7	0.7
Z04					2.1	1.33	6.3	0.7
Z06					2.1	1.27	6.9	<0.6

* Polarity (-) to (+), NSA^- as secondary EOF marker

Table 6. Continued.

HxDMS (mM)		20				30		
U (kV)		11				10		
Analyte	μ	α	β	Rs	μ	α	β	Rs
B34	10.9	1.03	0.8	<0.6	8.1	1.04	22	<0.6
B35	-11.2*	0.91	-0.3	2.8	-14.7**	0.93	-1.5	7.1
B36	-5.7	0.95	-3.0	1.5	-9.8	0.96	-2.4	1.4
B37	3.8	1.00	2.1	0	1.2	1.13	9.9	<0.6
B38	3.6	1.11	4.3	<0.6	1.1	1.35	11	0.6
B39	4.7	1.03	2.9	<0.6	-1.3	0.92	-8.8	<0.6
B41	0.2	1.00	47	0	N/A			
B42	-2.3	0.90	-4.8	1.5	-5.1	0.96	-4.8	0.6
B45	5.8	1.02	0.8	<0.6	2.6	1.31	8.5	<0.6
B46	6.4	1.00	0.7	0	4.6	1.07	2.8	<0.6
B51	3.1	1.08	3.4	<0.6	0.9	1.23	40	<0.6
B53	N/A				-9.6	0.98	-2.2	<0.6
B54	-3.1	0.97	-4.2	<0.6	-4.3	1.00	-6.0	0
B56	-13.7	0.98	-2.1	0.7	-18.2**	0.99	-1.4	1.8
Z04	-8.1	0.90	-2.5	1.9	-13.7	0.94	-1.6	3.3
Z06	-9.5	0.82	-1.5	1.5	-18.3	0.87	-1.5	6.4

Table 6. Continued.

HxDMS (mM)		40				50		
U (kV)		8				6		
Analyte	μ	α	β	Rs	μ	α	β	Rs
B34	6.3	1.09	3.8	<0.6	5.3	1.08	4.9	<0.6
B35	-14.8	0.93	-1.8	5.1	-15.0	0.93	-1.6	18
B36	-12.2	0.98	-2.3	1.3	-12.2	0.98	-2.0	0.6
B37	-0.6	1.00	-45	0	-2.1	1.00	-12	0
B38	-1.2	0.77	-32	0.7	-3.1	0.92	-8.2	0.8
B39	-5.7	0.94	-4.2	0.6	-8.9	0.95	-3.0	0.7
B41	-1.7	1.00	-16	0	-3.5	1.00	-7.0	0
B42	-6.7	0.98	-4.0	<0.6	-7.8	1.00	-3.3	0
B45	2.3	1.00	12	0	2.2	1.00	11	0
B46	4.7	1.00	6.1	0	4.7	1.00	5.2	0
B51	-1.0	0.90	-26	<0.6	-3.0	0.91	-8.6	0.8
B53	-11.0	1.00	-2.7	0	-11.4	1.00	-2.3	0
B54	-5.51	1.00	-4.4	0	-6.0	1.00	-4.1	0
B56	-16.6	0.99	-1.8	0.8	-14.8	0.99	-1.7	0.6
Z04	-16.6	0.96	-1.3	5.8	-19.0	0.95	-1.3	6.4
Z06	-22.4	0.91	-1.3	15	-18.0	0.96	-1.3	5.7

** U=11 kV

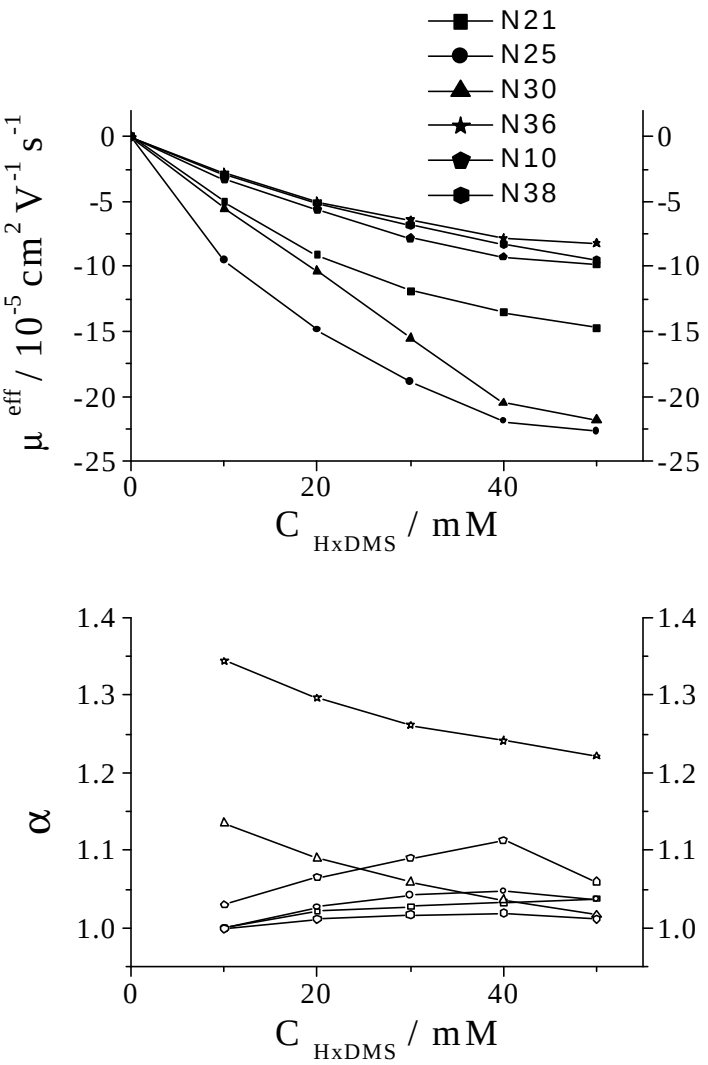

Figure 71. Effective mobilities and separation selectivities for the separation of the enantiomers of nonionic analytes in pH = 2.5 BGEs with HxDMS.

bottom panels show the corresponding separation selectivities. The strength of complexation between 1-phenylpentanol (N25) and 2-phenyl-2-pentanol (N26) and the three CD derivatives decreased in the order of: HxDMS > HDMS > ODMS. Though the selectivities for both N25 and N26 with HDMS are larger than with HxDMS (Figure 72, bottom panel), the Rs values obtained with HxDMS are much larger than with HDMS because stronger complexation with HxDMS leads to more favorable β values (in most of the case, around -1) which, in turn, compensate for the lower separation selectivities and helped peak resolution. Further along the same lines, the enantiomers of methylmandelate (N15), styrene glycol (N24), 1-phenylpentanol (N25), 2-phenyl-2-pentanol (N26), 1-indanol (N36) and 2-phenyl-2-butanol (N38), could not be separated with ODMS [110]; but most of them could be baseline-resolved with HxDMS. The effects of structurally different substituents at the 2,3-positions (for the same CD) are well demonstrated by the behavior of the two γ-butyrolactone in our screening kit: γ-(2-naphthyl)-γ-butyrolactone (N12) and γ-(2-phenyl)-γ-butyrolactone (N13). Under comparable conditions (i. e., about 30 mM resolving agent concentration), the effective anionic mobilities of the naphthyl-group containing N12 range (in 10^{-5} cm^2/Vs units) from about -4, through -5 to -18 with HxS, HxDAS and HxDMS, while the separation selectivities are 1.00, 1.04 and 1.06. On the other hand, the effective anionic mobilities of the phenyl-group containing N13 cover a range of only from about -3, through -7 to -11 (in 10^{-5} cm^2/Vs units) with HxS, HxDAS and HxDMS, while the separation selectivities decrease from about 1.15 through 1.03 to 1.00. Clearly, the differences in the separation behavior are large.

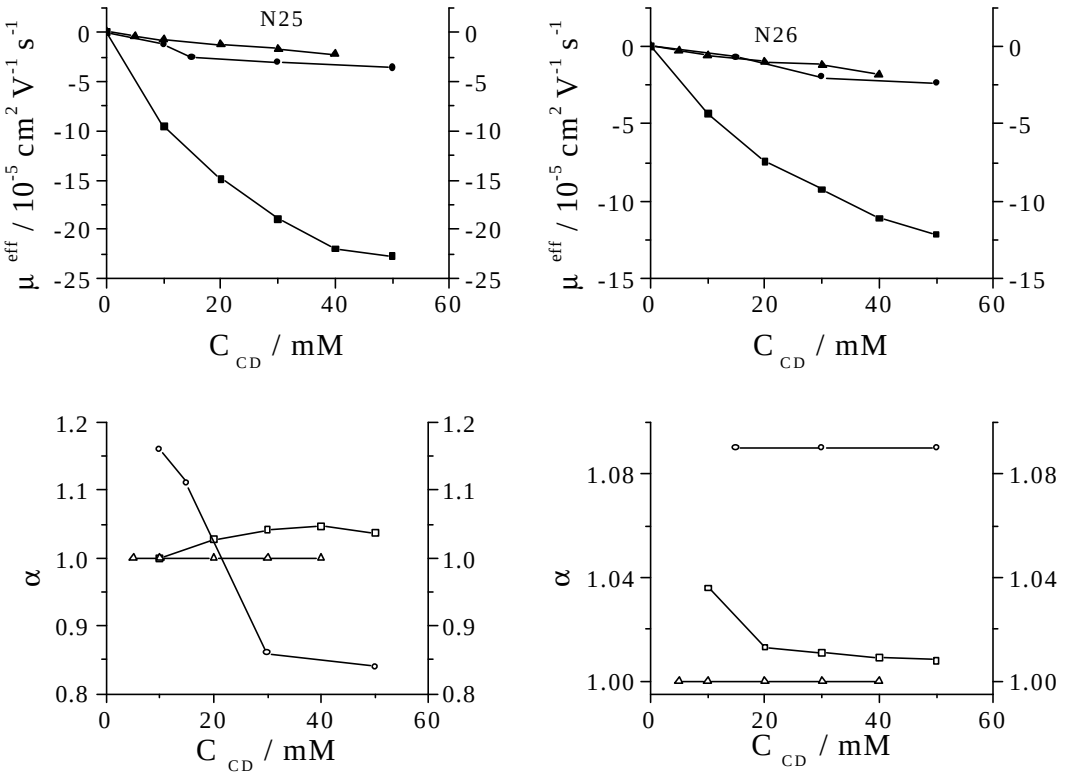

Figure 72. Effects of the cyclodextrin cavity size on the separation of the enantiomers of 1-phenylpentanol and 2-phenyl-2-pentanol in pH = 2.5 BGEs with HxDMS, HDMS, ODMS.

5.2.2 Weakly Acidic Enantiomer Separations

Use of HxDMS as the chiral resolving agent in the pH = 2.5 BGEs for the separation of a set of nine weak acid enantiomers yielded a total of seven separations with $\alpha > 1$. The mobilities of the weak acid analytes in the HxDMS - free BGEs were initially zero. The effective mobility of the bands of the weak acid analytes become increasingly anionic with increasing HxDMS concentration. Separation selectivities observed for the weak acid analytes passed through a maximum at low HxDMS concentrations and are generally between 1.08 and 1.2. Figure 73 shows typical mobility (top panel) and separation selectivity (bottom panel) plots for five of the weakly acidic enantiomers in the low pH HxDMS BGE. Baseline separation was achieved for five of the seven analytes with $\alpha > 1$, in part because the β values were favorable (around -1).

HxDMS also complexed with all of the weak acid analytes tested quite strongly. While the effective anionic mobilities were similar for A28 and A36 that have similar structural features, they were much smaller than the anionic effective mobilities for A02 or A22. The latter can be rationalized by the more extended hydrophobic backbone of both A02 and A22, compared to A28 and A36 (analogously to the case of N12 vs. N13). While separation selectivities for A02 and A22 that had similar mobilities (about -20×10^{-5} cm^2/Vs) in the 30 mM HxDMS BGE were similar (1.02), comparable effective mobilities for A28 and A36 (about -11×10^{-5} cm^2/Vs) were accompanied by quite different separation selectivities (1.02 vs. 1.00).

Just as with the nonionic analytes, the size of the cyclodextrin cavity has significant

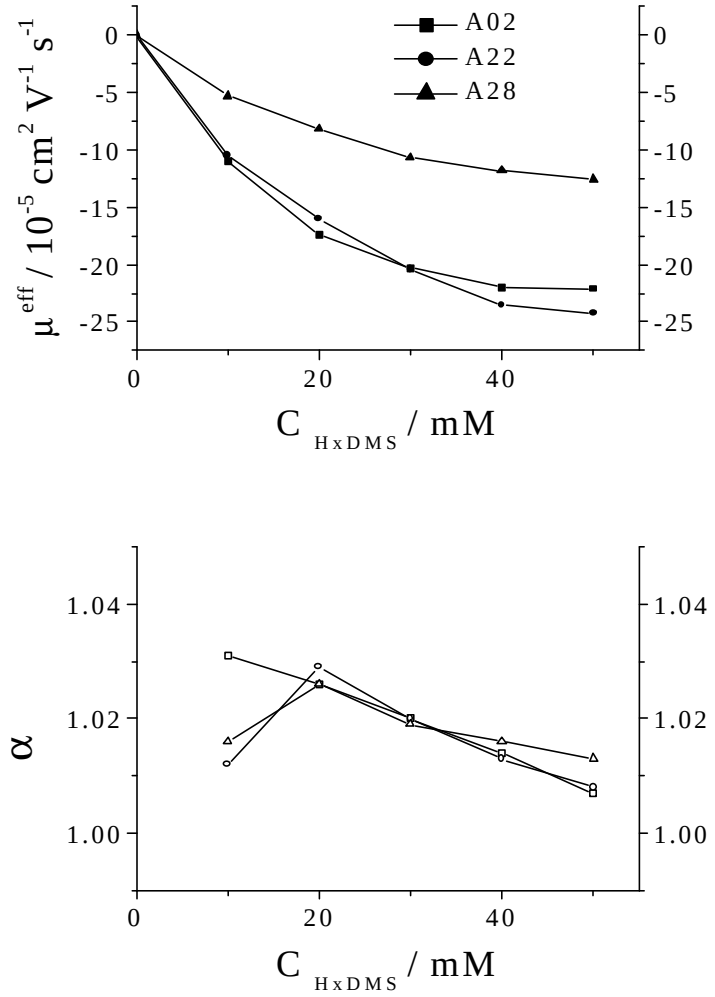

Figure 73. Effective mobilities and separation selectivities for the separation of the enantiomers of weak acid analytes in pH = 2.5 BGEs with HxDMS.

effects on the enantiomer recognition process for weak acid analytes. Figure 74 shows the effective mobility plots (top panel) and the corresponding separation selectivities (bottom panel) for fenoprofen (A22) with HxDMS, HDMS and ODMS as chiral resolving agents in the pH 2.5 = BGE. Unlike the separation trends that were observed with HxS, HS, OS, and HxDAS, HDAS, ODAS, fenoprofen (A22) interact with HxDMS much more strongly than with HDMS and ODMS: the strength of interaction decrease in the order: HxDMS > HDMS ≅ ODMS.

Compared with the other 6-*O*-sulfo-α-CD, HxS and HxDMS interact with A02 and A28 similarly strongly, while HxDAS interact with them very weakly. On the other hand, separation selectivity for A02 is similarly low with HxS and HxDMS (1.03 vs. 1.02), but it is high (1.4) with the weakly complexing HxDAS. For other weak acids, such as A28, separation selectivity is 1.02 with HxDMS, but 1.00 with HxS and HxDAS. These observations, which cannot be rationalized by simple, intuitive structural arguments, further emphasize the need for (and the value of) detailed NMR spectroscopic studies in deciphering the mysteries of enantiomer interactions with sulfated CDs.

5.2.3 Separation of the Enantiomers of Weak Bases

The enantiomers of 24 of the 29 pharmaceutical weak bases were fully or partial separated with HxDMS in the pH = 2.5 BGEs. Just as with the other single-isomer sulfated CDs, the weak base enantiomers can also be classified as weakly binding bases (the effective mobilities did not become anionic throughout the entire HxDMS concentration range studied,

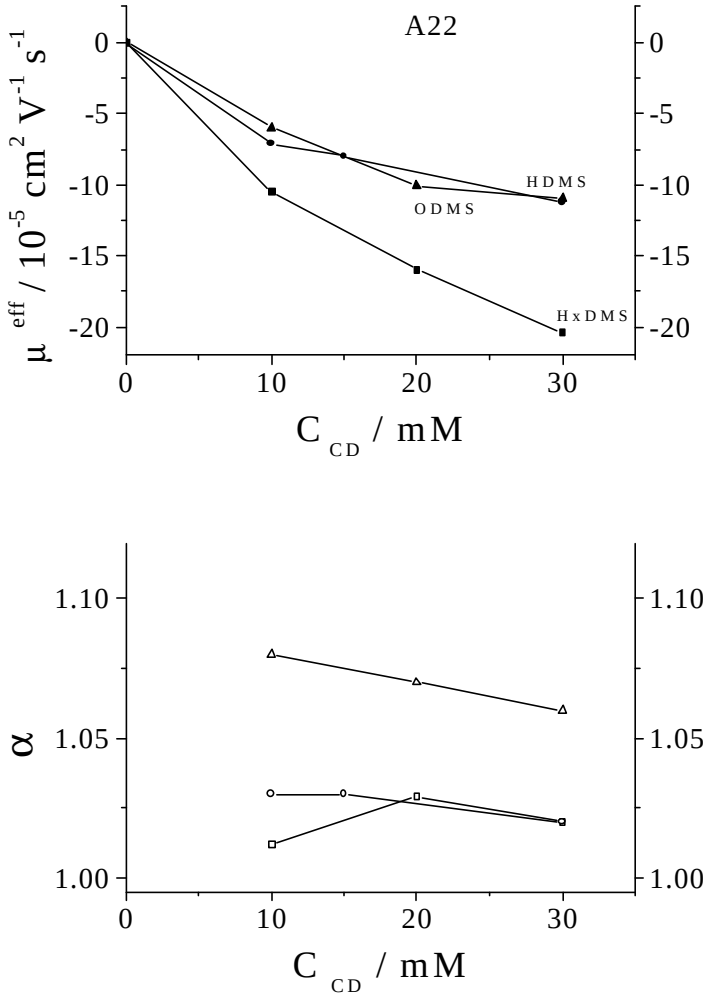

Figure 74. Effects of the cyclodextrin cavity size on the separation of the enantiomers of fenoprofen in pH = 2.5 BGEs with HxDMS, HDMS, ODMS.

0 to 50 mM, e. g., B22), moderately strongly binding bases (the effective mobilities did become anionic but remained close to zero in the HxDMS concentration range studied, e. g., B10), and strongly binding bases (the effective mobilities did become anionic at low HxDMS concentration and passed a shallow local maximum as the HxDMS concentration was increased, e. g. B56).

The effective mobility and separation selectivity curves for two of the weakly binding weak base enantiomers are shown in the top panels in Figure 75. The initial effective mobilities (left top panel in Figure 75) are between 26 and 28 mobility units. As the HxDMS concentration is increased, the mobilities approach zero but still remain cationic due to the effects of both the increased mole fractions of the analyte - HxDMS complexes, and the increased ionic strength and viscosity of the BGE. Separation selectivities (right top panel in Figure 75) go through a maximum value.

The effective mobilities of the moderately strongly and strongly binding weak bases are cationic at low HxDMS concentrations and anionic at high HxDMS concentrations. The middle and bottom panels in Figure 75 show the mobility (left panel) and separation selectivity curves (right panel) for four typical, moderately strongly and strongly binding weak bases, respectively. As the mobility of the slower enantiomer approaches zero, there is a discontinuity in separation selectivity.

The size of the like-substituted cyclodextrin has a significant effect on the separation of the enantiomers of the weak bases as well. For example, while the enantiomers of bupivacaine (B10), bupropion (B11), mepenzolate bromide (B25) and oxyphencyclimine

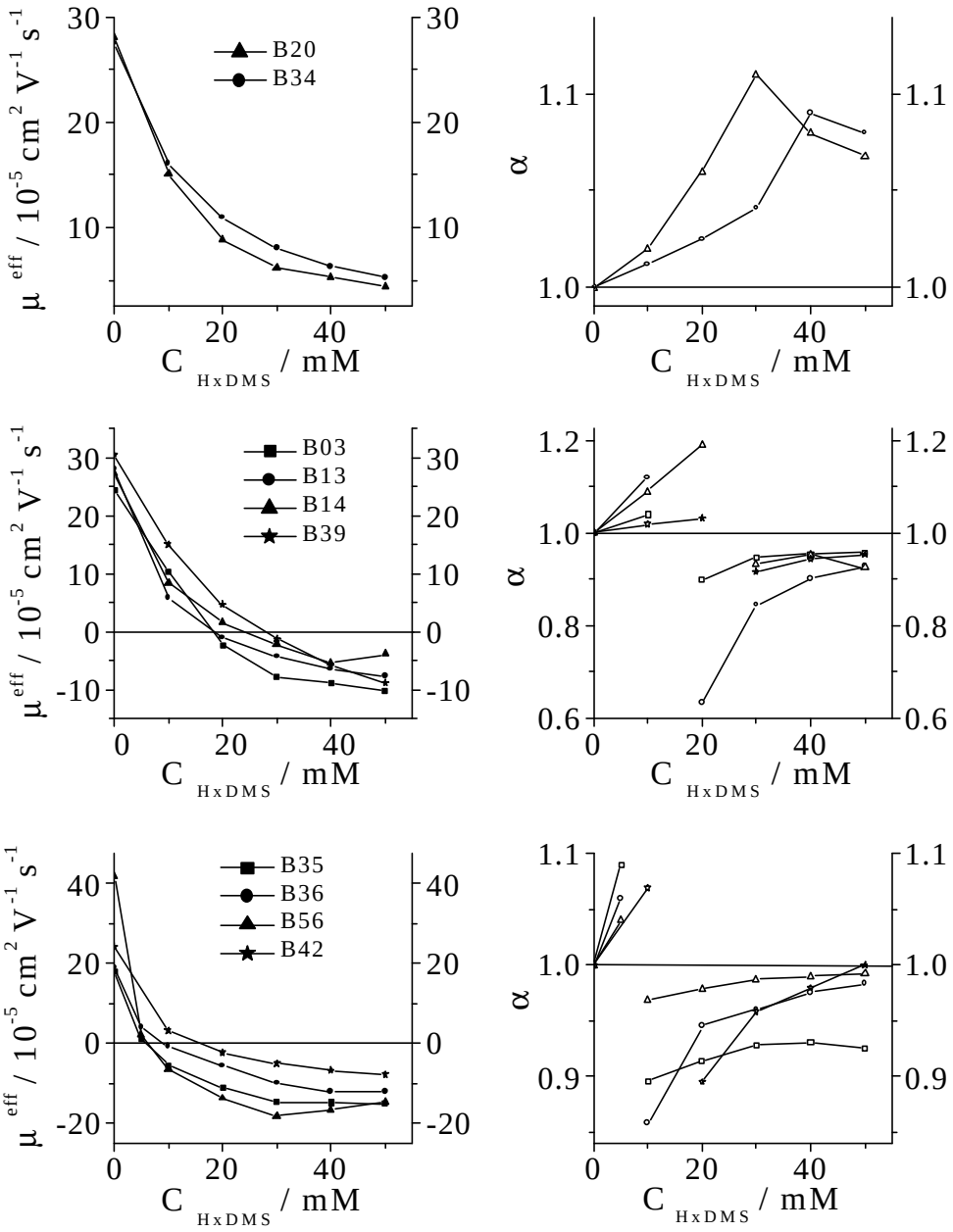

Figure 75. Effective mobilities and separation selectivities for the separation of the enantiomers of weak base analytes in pH = 2.5 BGEs with HxDMS. Weakly binding (top panels), moderately strongly binding (middle panels) and strongly binding (bottom panels).

(B36) could not be separated with ODMS, despite the quite reasonable β value [110], they could all be baseline separated with HxDMS.

The effects of the structure of the 2,3-substituents of sulfated α-CDs on the separation of the enantiomers of the weak bases are typified by Figure 76. Figure 76 shows the effective mobility plots (top panel) and the corresponding separation selectivities (bottom panel) for fluoxetine (B18) with HxDMS, HxDAS and HxS as the chiral resolving agent. The strength of the interactions between fluoxetine (B18) and HxDMS, HxDAS and HxS decrease in the following order: HxDMS > HxDAS > HxS. Similarly, the strength of the interaction between alprenolol (B02), aminogluthetimide (B03), oxybutynin (B35), pindolol (B41) and propranolol (B42) and the sulfated α-CDs decrease in the order of HxDMS > HxDAS > HxS. On the other hand, the effective mobilities in the 50 mM sulfated α-CD BGEs are about equal for atenolol (B08). For norephedrine (B34), the interaction strength is strongest for HxS and weakest for HxDAS, while for phenylglycinonitrile (B39), the interaction strength is strongest for HxDMS and weakest for HxDAS. These observations further demonstrate that there are significant differences between the interaction strengths of the differently2,3-substituted 6-*O*-sulfo-α-CD, but that our current level of understanding, the differences cannot be explained from the structure of the analyte. Detailed NMR studies are desperately needed to find an explanation for the observed differences.

Representative electropherograms obtained for some of the nonelectrolyte, weak acid, and weak bases at low pH are included in Figures 77 and 78, respectively.

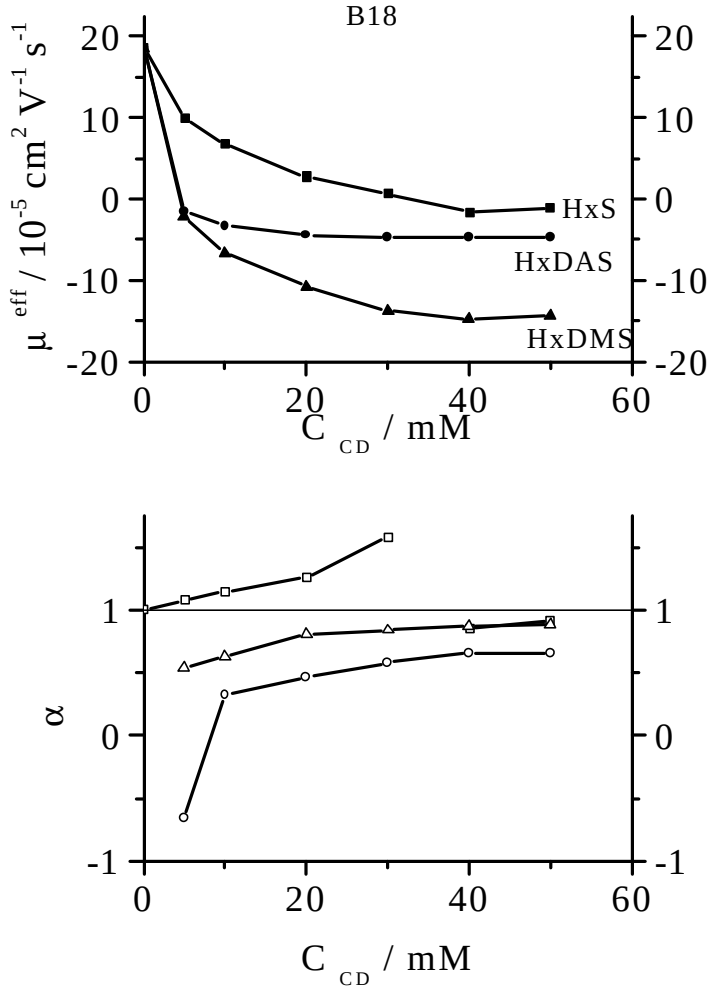

Figure 76. Effects of the type of the CD substituents on the separation of the enantiomers of fluoxetine in pH = 2.5 BGEs with HxS, HxDAS, HxDMS.

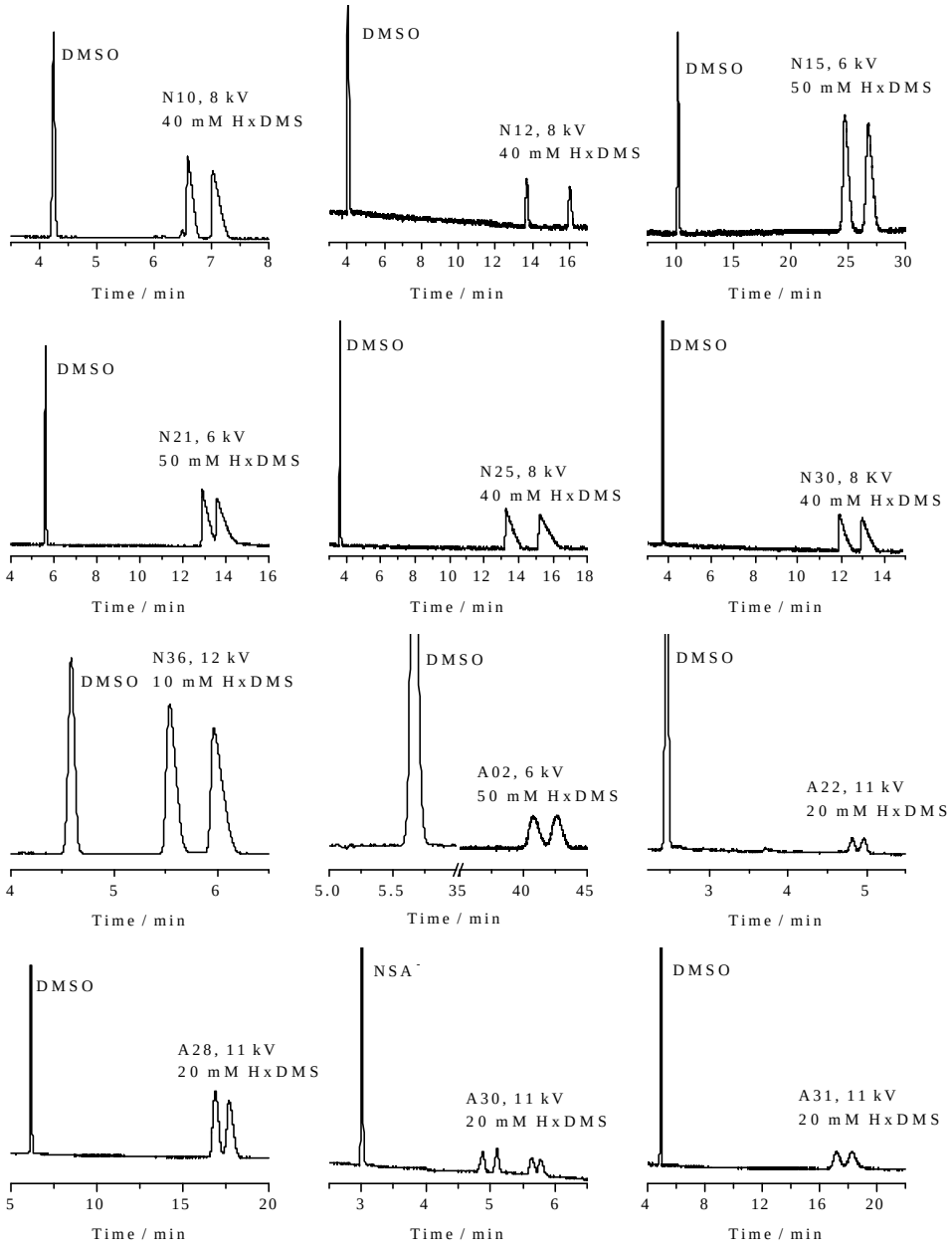

Figure 77. Typical electropherograms of separation of the enantiomers of the nonelectrolyte and weak acid analytes in pH = 2.5 BGEs with HxDMS.

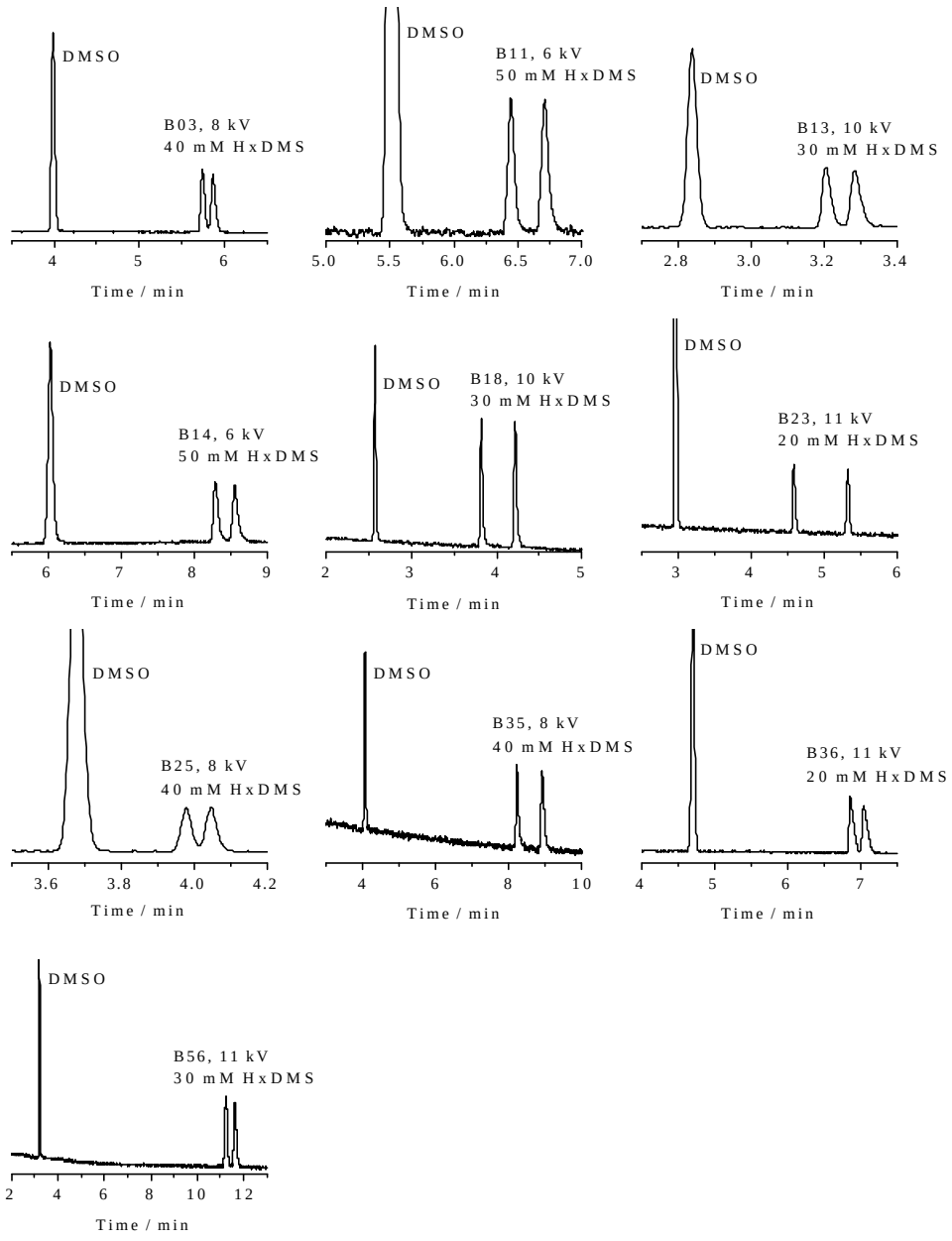

Figure 78. Typical electropherograms of separation of the enantiomers of the weak base analytes in pH = 2.5 BGEs with HxDMS.

5.3 Enantiomer Separations in pH = 9.5 BGEs

The enantiomer of a series of neutral, weak acid and weak base analytes were also separated with HxDMS in pH = 9.5 BGEs. Table 7 lists values of μ (the effective mobilities of the less mobile enantiomer), α, β, Rs, and U in the pH = 9.5 BGEs. Again, N/A indicates that the aforementioned values could not be calculated due to either overlap with non-comigrating system peaks or comigration of an enantiomer peak with the neutral marker.

5.3.1 Separation of the Enantiomers of Nonionic Analytes

The enantiomers of eight of the thirteen nonionic analytes were separated by HxDMS in the high pH BGEs. The anionic mobilities of the non-charged enantiomers increased monototically with increasing HxDMS concentration (top panel in Figure 79). The selectivity plots resembled those obtained at low pH (bottom panel in Figure 79).

The anionic effective mobilities of the nonelectrolyte analytes were almost identical in the pH=9.5 and pH=2.5 BGEs. This behavior is different from what was observed with HxS, with which the effective mobilities in the high pH BGEs were lower than in the acidic BGEs indicating that components of the ethanolamine - MSA buffer competed with the nonelectrolyte analytes for HxS more strongly than components of the H_3PO_4 - LiOH buffer did. Not surprisingly, separation selectivities were almost identical in the low pH and high pH HxDMS BGEs, reinforcing the notion that for this set of analytes, there were no preferred

Table 7. Separation data in pH=9.5 HxS BGEs. (μ, in 10^{-5} cm^2 / Vs units)

HxDMS (mM)	0		10		
U (kV)			11		
Analyte	μ	μ	α	β	Rs
N02	0	-3.2	1.00	-14	0.0
N12	0	-12.3	1.00	-2.8	0.0
N13	0	-4.5	1.00	-10	0.0
N21	0	-4.3	1.00	-11	0.0
N24	0	-1.4	1.00	-33	0.0
N25	0	-8.3	1.02	-4.1	<0.6
N26	0	-3.3	1.00	-14	0.0
N27	0	-2.6	1.00	-18	0.0
N28	0	-2.6	1.00	-18	0.0
N30	0	-5.2	1.20	-6.7	1.6
N34	0	-3.1	1.00	-15	0.0
N36	0	-2.3	1.35	-15	1.1
N38	0	-2.5	1.00	-19	0.0
A02	-23.0	-26.2	<1.01	-1.7	<0.6
A22	-21.1	-24.0	1.00	-1.5	0.0
A23	-22.7	-23.1	1.00	-1.6	0.0
A27	-19.6	-21.2	1.00	-1.6	0.0
A28	-29.1	-27.5	1.00	-1.7	0.0
A30	-24.0	-22.3	1.00	-1.9	0.0
A31	-20.9	-21.4	1.00	-1.8	0.0
A36	-23.9	-23.2	1.00	-2.0	0.0

Table 7. Continued.

HxDMS (mM)	20				30			
U (kV)	11				10			
Analyte	μ	α	β	Rs	μ	α	β	Rs
N02	-6.50	1.00	-4.7	0	-9.4	1.00	-3.3	0
N12	-17.0	1.02	-2.3	0.8	-18.5	1.07	-1.7	5.7
N13	-7.98	1.00	-3.7	0	-10.1	1.00	-3.1	0
N21	-8.0	1.02	-5.0	<0.6	-10.9	1.03	-3.3	<0.6
N24	-3.05	1.00	-12	0	-4.6	1.00	-7.1	0
N25	-14.22	1.04	-2.7	0.7	-19.3	1.05	-1.8	1.6
N26	-7.0	1.01	-4.9	<0.6	-10.4	1.02	-3.0	<0.6
N27	-5.03	1.00	-5.2	0	-6.9	1.00	-4.5	0
N28	-4.88	1.00	-5.1	0	-6.8	1.00	-4.6	0
N30	-10.5	1.13	-3.6	2.4	-15.7	1.07	-2.2	1.7
N34	-5.33	1.00	-4.2	0	-6.9	1.00	-4.6	0
N36	-4.79	1.31	-7.6	2.8	-6.4	1.27	-5.5	3.6
N38	-5.02	1.00	-6.8	0	-6.4	1.00	-4.9	0
A02	-26.3	<1.01	-1.7	<0.6	-26.4	<1.01	-1.3	0.6
A22	-25.5	1.00	-1.7	0	-26.2	1.00	-1.5	0
A23	-23.6	1.00	-1.8	0	-24.0	1.00	-1.6	0
A28	-26.9	1.00	-1.6	0	-26.7	1.00	-1.3	0
A30	-22.0	<1.01	-2.0	<0.6	-21.9	<1.01	-1.5	0.7
A31	-21.9	1.00	-2.0	0	-22.6	1.00	-1.7	0
A36	-22.1	1.00	-2.0	0	-21.9	1.00	-1.5	0

Table 7. Continued.

HxDMS (mM)		40				50		
U (kV)		8				6		
Analyte	μ	α	β	Rs	μ	α	β	Rs
N02	-11.3	1.00	-2.5	0	-12.6	1.00	-2.2	0
N12	N/A				N/A			
N13	-11.0	1.01	-2.7	<0.6	-11.6	1.01	-2.3	<0.6
N21	-12.1	1.04	-2.7	<0.6	-12.6*	1.04	-1.9	1.2
N24	-5.4	1.02	-5.5	<0.6	-6.0	1.03	-3.3	<0.6
N25	-20.7	1.05	-1.6	1.8	-20.8	1.05	-1.2	3.2
N26	-12.6	1.03	-2.6	0.6	-13.2	1.02	-2.0	<0.6
N27	-7.96	1.00	-4.1	0	-8.7	1.00	-2.8	0
N28	-7.97	1.00	-4.1	0	-8.9	1.00	-2.6	0
N30	-18.3	1.05	-1.6	2.5	-19.4	1.03	-1.3	2.4
N34	-7.94	1.00	-4.1	0	-9.0	1.00	-2.8	0
N36	-7.18	1.25	-4.2	4.0	-7.7	1.23	-3.3	5.5
N38	-7.5	1.00	-4.3	0	-8.6	1.02	-2.8	<0.6

*U=5 kV

Table 7. Continued.

HxDMS (mM)	0		10			20			
U (kV)	18		11			11			
Analyte	μ	μ	α	β	Rs	μ	α	β	Rs
B02	10.4	2.7	1.52	18	<0.6	-1.1	0.94	-47	<0.6
B03	8.6	-2.0	0.94	-20	<0.6	-5.9	0.95	-6.9	0.6
B08	10.9	8.0	1.02	4.4	<0.6	6.2	1.04	6.6	<0.6
B10	0.8	-2.4	0.80	-12	<0.6	-5.1	0.85	-8.2	<0.6
B11	1.5	-7.1	0.87	-4.2	1.2	-11.4	0.88	-3.7	2.3
B13	14.8	N/A				-3.4	0.89	-8.4	0.7
B14	5.9	-2.1	0.90	-21	1.4	-5.5	0.95	-8.0	0.6
B18	10.3	-4.7	0.69	-6.6	2.1	-11.4	0.80	-3.7	3.2
B22	10.0	-2.3	0.85	-20	0.6	-6.6	0.86	-6.3	1.5
B23	9.0	-18.2	0.81	-2.4	4.0	-23.5	0.83	-1.8	10
B24	7.0	-5.2	1.00	-6.6	0	-9.9 -10.2	0.99 0.97	-4.0	<0.6 <0.6
B25	18.0	4.9	1.10	9.0	<0.6	1.6	1.33	27	<0.6
B31	10.6	6.2	1.01	7.3	<0.6	4.1	1.03	9.7	<0.6
B34	8.5	5.9	1.02	6.9	<0.6	4.2	1.03	7.5	<0.6
B35	8.5	-17.5	0.88	-2.5	1.2	-22.0	0.89	-1.7	2.8
B36	16.0	-2.2	0.88	-13	<0.6	-7.1	0.94	-5.9	0.7
B39	0.0	-2.7	1.07	-14	<0.6	-4.6	1.06	-9.0	<0.6
B42	10.1	-0.9	1.00	-50	0	-4.6	0.88	-8.8	<0.6
B51	8.0	-2.1	0.88	-20	<0.6	-7.2	0.95	-5.8	0.6
B54	0.0	-4.5	1.14	-7.8	<0.6	-7.2	1.13	-5.8	<0.6
B56	9.9	-9.8	0.98	-4.7	<0.6	-17.0	0.99	-2.5	<0.6

Table 7. Continued.

HxDMS (mM)	30				40			
U (kV)	10				8			
Analyte	μ	α	β	Rs	μ	α	β	Rs
B02	-3.9	0.94	-9.0	<0.6	-6.2	0.96	-4.6	0.7
B03	-7.8	0.95	-5.0	0.6	-9.0	0.95	-3.7	1.1
B08	4.6	1.05	8.0	<0.6	3.9	1.05	8.7	<0.6
B10	-7.9	0.93	-4.1	<0.6	-9.6	0.97	-3.4	0.8
B11	-14.8	0.90	-2.7	3.7	-15.9	0.91	-2.1	5.5
B13	-7.6	0.91	-2.8	1.1	-10.8	0.93	-3.1	0.6
B14	-10.2	0.95	-2.7	0.8	-14.1	0.96	-2.4	0.9
B18	-15.1	0.85	-2.6	3.8	-16.2	0.88	-2.1	4.4
B22	-10.0	0.87	-3.7	3.2	-12.0	0.87	-2.8	3.3
B23	-24.5	0.86	-1.5	15	-24.3	0.89	-1.4	17
B24	-12.4 -12.7	0.99 0.97	-1.9	<0.6 0.8	-14.7 -15.1	0.99 0.97	-2.1	<0.6 0.7
B25	N/A				-2.0	0.77	-16	0.9
B31	2.4	1.05	15	<0.6	1.6	1.07	20	<0.6
B34	2.7	1.05	9.8	<0.6	2.6	1.06	12	<0.6
B35	-22.6	0.90	-1.6	1.1	-22.6	0.91	-1.4	9.1
B36	-10.4	0.96	-2.0	0.8	-11.4	0.97	-2.9	0.9
B39	-6.3	1.05	-5.8	0.6	-7.3	1.05	-4.5	0.8
B42	-7.3	0.89	-2.9	<0.6	-8.8	0.91	-3.6	<0.6
B51	-10.8	0.96	-3.4	0.7	-13.9	0.96	-2.4	0.8
B54	-9.8	1.10	-3.7	<0.6	-12.6	1.07	-2.6	<0.6
B56	-19.9	0.99	-1.8	<0.6	-20.5	0.99	-1.6	0.6

Table 7. Continued.

HxDMS (mM)		50		
U (kV)		6		
Analyte	μ	α	β	Rs
B02	-8.6	0.97	-3.1	<0.6
B03	-9.7	0.95	-2.8	1.1
B08	4.1	1.05	6.2	0.8
B10	-11.1	0.96	-2.4	1.7
B11	-16.1	0.91	-1.7	6.2
B13	-12.0	0.92	-2.2	0.7
B14	-17.6	0.97	-1.6	2.8
B18	-17.1	0.90	-1.7	8.2
B22	-13.9	0.87	-2.0	6.8
B23	-23.2	0.88	-1.3	18
B24	-14.6 -14.9	0.99 0.98	-1.8	<0.6 0.8
B25	-3.6	0.87	-7.8	1.3
B31	1.9	1.06	14	<0.6
B34	2.9	1.05	27	<0.6
B35	-21.8	0.89	-1.2	22
B36	-11.9	0.98	-2.3	0.9
B39	-8.1	1.05	-3.4	1.1
B42	-10.2	1.00	-2.6	0.0
B51	-13.8	0.96	-1.9	1.7
B54	-15.0	1.06	-1.7	<0.6
B56	N/A			

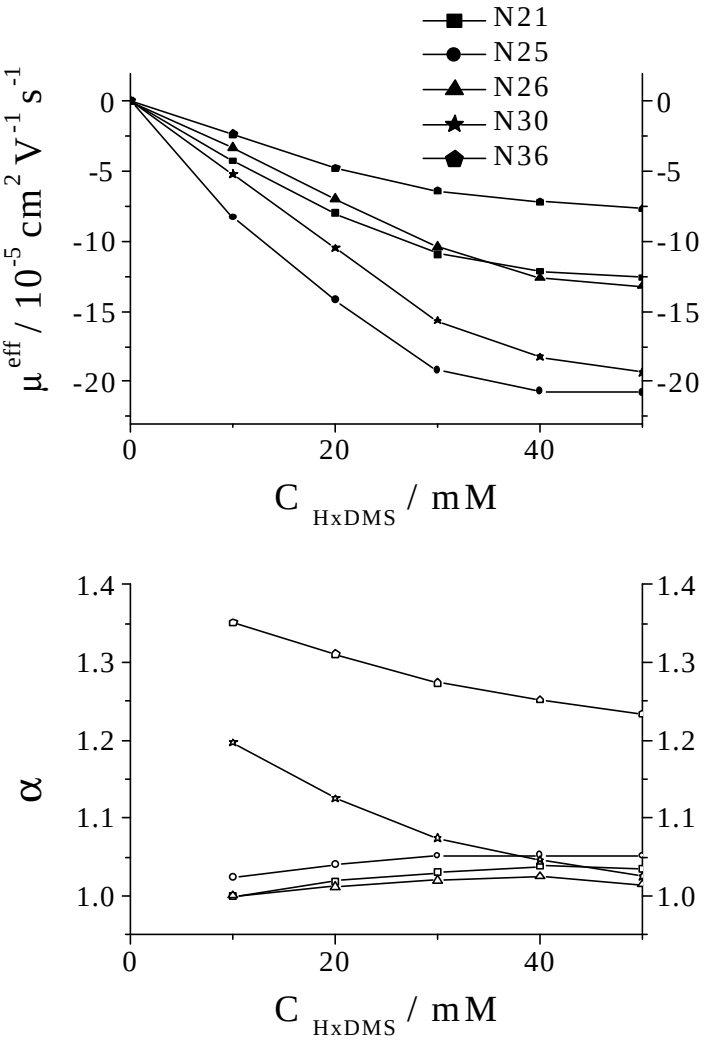

Figure 79. Effective mobilities and separation selectivities for the separation of the enantiomers of nonionic analytes in pH = 9.5 BGEs with HxDMS.

BGE in terms of the pH of the BGE.

Again, just as in the low pH BGEs, the unfavorable β values in the high pH BGEs with ODMS and HDMS system led to unsuccessful enantiomer separations. However, neutral analytes complexed strongly complexed with HxDMS, which led to favorable β values, and good peak resolution values. Figure 80 shows the effective mobilities (top panel) and separation selectivities (bottom panel) for 1-phenylpentanol (N25) in pH = 9.5 BGEs with HxDMS, HDMS and ODMS. The complexation strength between N25 and these three chiral resolving agents follows the order: HxDMS >> HDMS≅ ODMS. Though separation selectivity for N25 with HDMS is bigger than with HxDMS, the Rs values with HDMS are smaller than with HxDMS because the β value are unfavorable(-6 to -15) with HDMS. ODMS did not resolve the enantiomers of N25.

HxDMS performed as a better chiral resolving agent than ODMS: the enantiomers of 1-phenylbutanol (N21), styrene glycol (N24), 1-phenylpentanol (N25), 2-phenyl-2-pentanol (N26), 1-indanol (N36) and 2-phenyl-2-butanol (N38), were separated by HxDMS; but not by ODMS.

5.3.2 Separation of the Enantiomers of Weak Acids

With HxDMS, the anionic effective mobilities of the weak acid analytes typically increased as the concentration of HxDMS was increased, and were higher (or considerably higher) than what was observed with HxS, indicating stronger intermolecular interactions. There were two weak acids that behaved atypically: the effective mobilities of A28 and A30

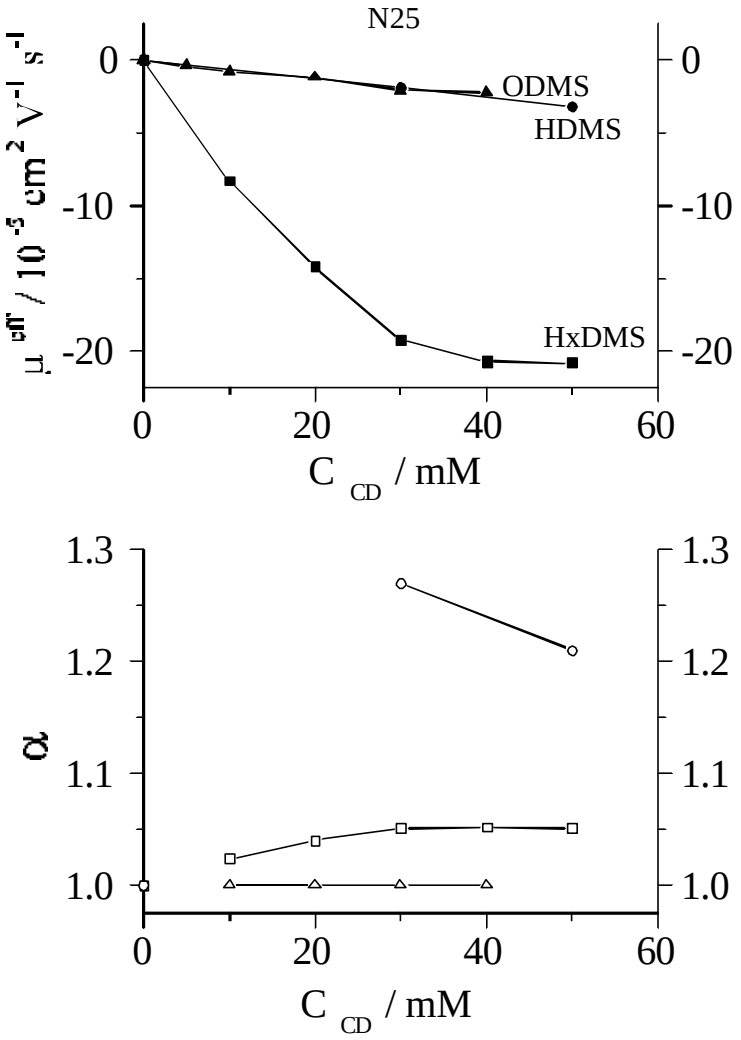

Figure 80. Effects of the cyclodextrin cavity size on the separation of the enantiomers of 1-phenylpentanol in pH = 9.5 BGEs with HxDMS, HDMS, ODMS.

decreased as the concentration of HxDMS was increased, a difference with respect to what was observed with HxS as well. In general, separation selectivities were inferior compared to what were seen in the low pH BGEs. Partial separation was observed for the enantiomers of only two of the weak acids compared to five (A02, A22, A26, A28 and A31) in the low pH BGE's. This behaviors reinforces the notion introduced in Ref. 119 that for weak electrolyte analytes the CE enantiomer separations might be desionoselective or ionoselective, and call for trying the separations in two BGE's with pH values sufficiently far below and above the pKa of the analytes. Again, NMR spectroscopic studies might be able to reveal why separation selectivity became equal to one at high pH, despite the fact that the effective mobilities in the low and high pH BGEs were virtually identical. Although the solubility of the weak acid enantiomers was better in the high pH BGEs than in the low pH BGEs, peak resolution was generally poor due to the unfavorable β values.

The pH of the BGEs play a big role in the chiral recognition process: in the low pH BGEs, the enantiomers of fenoprofen (A22) could be separated, in the high pH BGEs, they could not be separated, similarly to what was seen for HxS in Chapter IV.

5.3.3 Separation of the Enantiomers of Weak Bases

Almost all the weak base enantiomers that we tested showed some measure of separation selectivity with HxDMS in high pH aqueous BGEs. Separations of the weak base analytes with HxDMS in the high pH BGEs were fast because the EOF mobility is considerably high (26-50 mobility unit) due to the increased charge density of the capillary wall. As the HxDMS concentration is increased in the high pH BGEs, the enantiomer bands acquire anionic

effective mobilities at considerably lower HxDMS concentrations than in the low pH BGE. The weak base analytes can be classified into two categories: weakly binding and strongly binding. The left panels in Figure 81 show the effective mobility (top panel) and separation selectivity (bottom panel) curves of three typical, weakly binding weak base enantiomers, while the right panels show the mobility (top panel) and separation selectivity curves (bottom panel) for seven typical, strongly binding weak bases.

Even though the number of enantiomers for which favorable separation selectivities were found in the high pH BGEs is similar to that in the low pH BGEs, separation selectivities with HxDMS were different. Desionoselective and ionoselective separations were observed as well. For example, the enantiomers of four weak base analytes, such as, atenolol (B08), ketamine (B22), metoprolol (B31) and verapamil (B54), could not be separated with HxDMS in the low pH BGEs, but were successfully separated in high pH BGEs.

In addition to the pH effects, differences in the strength of interactions were found for the weak base analytes with the 6-*O*-sulfo CDs that were similarly substituted, but have different size. Significant separation selectivity differences were also found. HxDMS behave as a better chiral resolving agent than ODMS for weak base analytes in high pH BGEs. The enantiomers of following nine weak base analytes, such as, atenolol (B08), bupivacaine (B10), bupropion (B11), ketamine (B22), mepenzolate bromide (B25), metoprolol (B31), norephedrine (B34), oxyphencyclimine (B36) and 2-phenylglyicidonitrile (B39), could not be separated by ODMS in the pH = 9.5 BGEs; however, the enantiomers of all these analytes

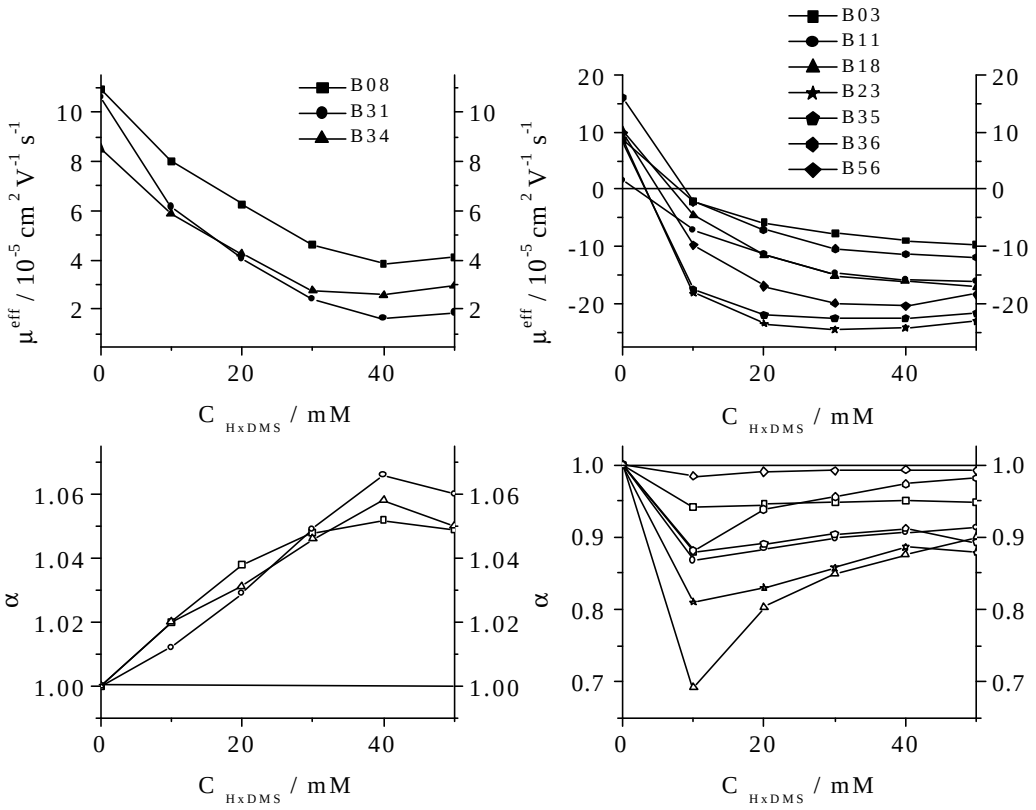

Figure 81. Effective mobilities and separation selectivities of the separation of the enantiomers of weak base analytes in pH=9.5 BGEs with HxDMS. Weakly binding (left panels) and strongly binding (right panels).

were resolved with HxDMS in the pH = 9.5 BGEs. The cavity size of the CDs also affected the separation tendencies. Figure 82 shows the effective mobility plots (top panel) and the corresponding separation selectivities (bottom panel) for ketamine (B22) with HxDMS, HDMS and ODMS as the chiral resolving agents in the pH = 9.5 BGEs. Just as in the low pH BGEs, the strength of interactions between ketamine (B22) and the CD derivatives decreases in the order: HxDMS > HDMS ≅ ODMS.

Just as in the low pH BGEs, The type of the 2,3- substituents of the single -isomer 6-*O*-sulfo α-CDs also plays a role in their interactions with the enantiomers of the weak base analytes in the high pH BGEs. Figure 83 shows the effective mobility plots (top panel) and the corresponding separation selectivities (bottom panel) for tolperisone (B51) with HxDMS, HxDAS and HxS as chiral resolving agents. Tolperisone (B51) interacts with HxDMS very strongly, with HxDAS moderately strongly, with HxS, weakly. A few typical enantiomer separations obtained with HxDMS are illustrated in Figure 84. The numbers under the compound codes show the concentration of HxDAS (in mM) and the applied potential (in kV) used.

5.4 Summary

The third novel, single-isomer, sulfated cyclodextrin, the sodium salt of hexakis(2,3-di-*O*-methyl-6-*O*-sulfo)-α-cyclomaltohexaose (HxDMS), has been produced on the large scale with greater than 98% isomeric purity. It has been successfully used as a chiral resolving agent for the capillary electrophoretic separation of neutral, weakly acidic and weakly basic enantiomers in the pH = 2.5 and the pH = 9.5 aqueous BGEs.

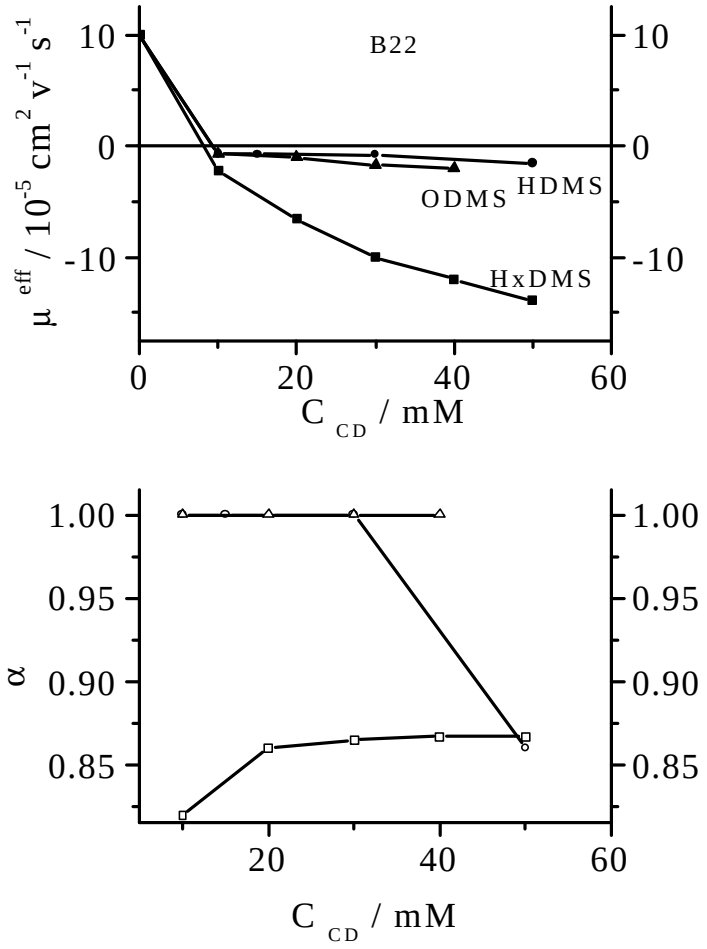

Figure 82. Effects of the cyclodextrins cavity size on the separation of the enantiomers of ketamine in pH = 9.5 BGEs with HxDMS, HDMS, ODMS.

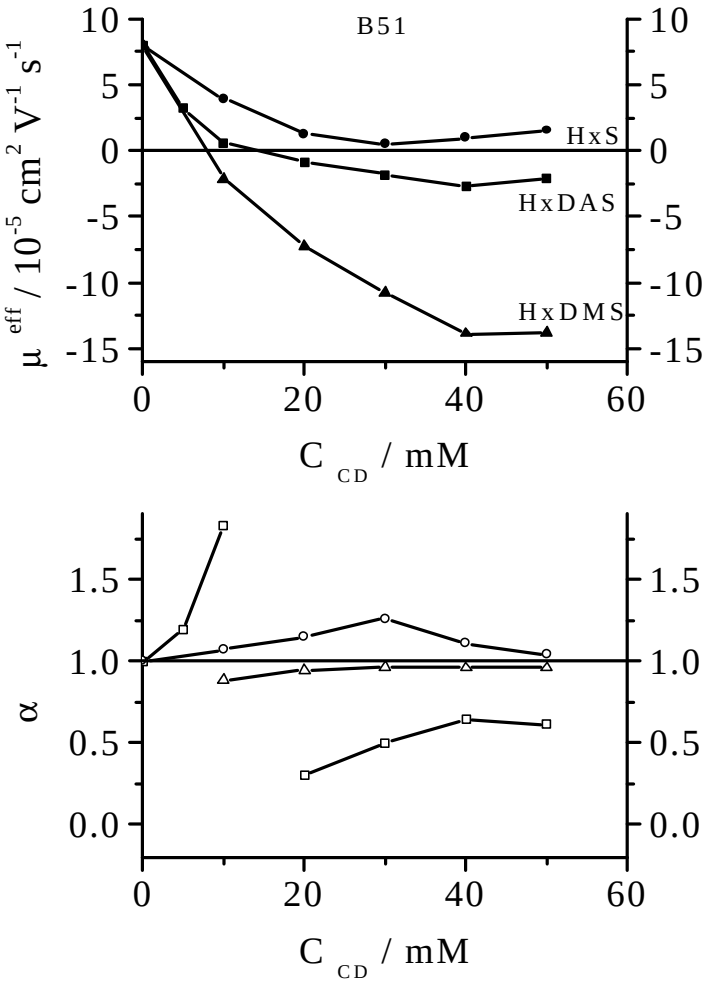

Figure 83. Effects of the cyclodextrin substituent on the separation of the enantiomers of Tolperisone in pH = 9.5 BGEs with HxDAS, HxS, HxDMS.

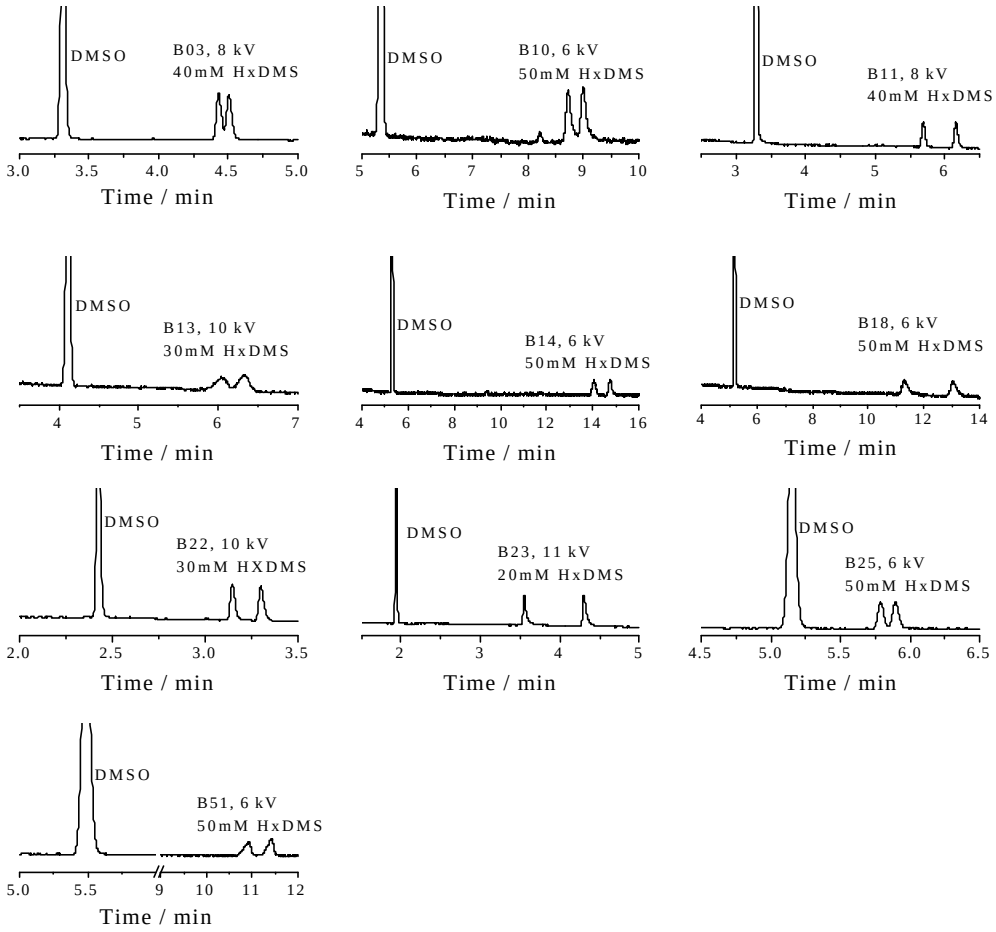

Figure 84. Typical electropherograms of separation of the enantiomers of the nonionic and weak base analytes in pH = 9.5 BGEs with HxDMS.

CHAPTER VI

CONCLUSIONS

The low aqueous solubility of native α-cyclodextrin limits its application as the chiral resolving agent in aqueous BGEs. Charged α-cyclodextrins provide at least two important advantages over neutral α-CDs. First, both neutral chiral analytes and charged chiral analytes can be enantioresolved with charged α-CDs. Second, introduction of ionic groups on the α-CD enhances the solubility of charged α-CDs in aqueous media. Single-isomer charged α-CDs could provide a very reproducible separation system. Since the type of the CD substituents profoundly influences the chiral recognition process, three, pure, single-isomer, 6-*O*-sulfo α-cyclodextrins, the sodium salts of hexakis (2,3-di-*O*-acetyl-6-*O*-sulfo)-α-CD (HxDAS), hexakis (6-*O*-sulfo)-α-CD (HxS), and hexakis (2,3-di-*O*-methyl-6-*O*-sulfo)-α-CD (HxDMS) have been synthesized, analytically characterized and used as chiral resolving agents in capillary electrophoresis. HxDAS, HxS and HxDMS were synthesized on a large scale (500 grams) in greater than 98% purity, through a synthetic scheme which sequentially protects-deprotects the 2,3- and 6-hydroxyl groups of native α–cyclodextrin by using regioselective chemical processes. The purity of each synthetic intermediate and of the final products was determined by either HPLC-ELSD or indirect UV-detection capillary electrophoresis (CE). The chemical and structural identity of each single-isomer intermediate and final product was verified by 1D ^{1}H, ^{13}C and 2D COSY, HETCOR NMR spectroscopy and by high resolution MALDI-TOF MS and ESI-TOF MS. These characterization methods, when interpreted

together, yielded convincing evidence that HxDAS, HxS and HxDMS are isomerically pure and have the expected substitution patterns.

A series of neutral, acidic, basic and ampholytic enantiomers were separated in both aqueous and nonaqueous background electrolytes (BGEs) with HxDAS, HxS and HxDMS using CE. Rapid separations with satisfactory separation selectivity and peak resolution values were obtained for most of the analytes.

Using HxS, HxDAS and HxDMS for the separation of weak base enantiomers in both aqueous (pH 2.5 and pH 9.5) and nonaqueous BGEs (for HxDAS), it was found that most bases exhibited one of two specific mobility trends. The first group was called the group of strongly binding weak bases: their effective mobilities became anionic even at very low HxS, or HxDAS or HxDMS concentrations. The other group was called the group of weakly binding weak bases: their effective mobilities remained cationic over the entire CD concentration range tested.

The anionic effective mobilities of the neutral analytes increase monotonously with increasing concentration of the three CD derivatives. They interact with the sulfated α-CDs weakly which leads to short analysis times. Since most of the weak acid analytes are neutral in low pH BGEs, the separation behavior is similar to those of the neutral analytes.

The use of HxDAS for the separation of the enantiomers of weak base analytes in acidic methanolic BGEs was very successful. Since high potential could be applied, very fast separations were obtained. The β values were favorable for enantiomer separations in methanolic BGEs. This resulted in baseline separations in under 5 minutes, with very low HxDAS concentrations. Many enantiomers were separated both in acidic aqueous and acidic

methanolic BGEs, and showed decreased binding strengths in the acidic methanolic BGEs.

Experimental results show that the separation selectivity depends on (i) the cavity size of the CD; (ii) the polarity of the substituents of the CD; (iii) the structure of the analyte; (iv) the structure of the background electrolyte coion and counter-ion; (v) the type of organic solvent; and (vi) the pH of the BGEs.

(i) Different substituents on the 6-*O*-sulfo-α-CDs lead to significantly different enantiomer separations . The hydrophilic hydroxyl groups, the moderately hydrophobic acetyl groups, and the hydrophobic methyl groups provided different inter-molecular interactions with the chiral analytes. Thus, HxDAS, HxS and HxDMS can provide different enantiorecognition for a large number of chiral analytes and offer complimentary separation selectivities. For example, the enantiomers of halostachin, atenolol, metanephrine, methoxyphenamine, metoprolol, norephedrine, oxybutynin, oxyphencyclimine, piperoxan, pindolol, and propranolol could be separated by using HxDAS as a chiral resolving agent in pH=9.5 BGEs; but, no separation was achieved by HxS. Enantiomer separations were achieved for atropine, chlophedianol, 2-phenylglyicidonitrile, propafenone, quinidine, salbutamol, and scopolamine by HxS in pH=9.5 BGEs, but not by HxDAS. The complexation strength between the analytes and the cyclodextrin derivatives decreased in the order of: HxDMS > HxDAS > HxS.

(ii) The effects of the ring size of the CD on enantiorecognition are also very significant. Pindolol, 2-phenyl-2-butanolol could be separated in pH=2.5 BGEs by using either HxDAS or ODAS, but not with HDAS. The complexation strength of neutral, weak acid and weak base analytes with α-CD derivatives (HxS, HxDAS and HxDMS) were found to be very different from their corresponding β-CD analogues (HS, HDAS and HDMS), and γ-CD analogues (OS,

ODAS and ODMS). The complexation strength of these analytes with β-CD derivatives and with γ-CD derivatives however were similar to each other. For the hydrophilic derivatives and moderately hydrophobic CD derivatives, the complexation strength generally increased in the order of: HxS < HS ≅ OS, HXDAS < HDAS ≅ ODAS. However, for the hydrophobic CD derivatives, binding strength decreased in the order of: HxDMS > HDMS ≅ ODMS.

(iii) The effects of analyte structure on enantiorecognition are also very important. For example, the enantiomers of 2-phenyl-2-butanol and 2-phenyl-2-pentanol could be separated by HxDAS in low pH BGEs; but not those of 2-phenyl butanol. Furthermore, enantiomer separation was achieved for methylmandelate by HxDAS in low pH BGEs, but not for ethylmandelate. Small changes in the analyte structure can also affect the separation trend: for example, Dansyl-leucine binds weakly with HxDAS in pH 2.5 BGEs; but Dansyl-norleucine binds strongly.

(iv) Since different BGEs result in different electroosmotic flow mobilities while affecting analyte properties, the type of the BGE (aqueous/nonaqueous, low pH / high pH) also plays very important roles. For example, the four stereoisomers of labetalol (B24) can be baseline separated in pH=9.5 aqueous BGEs, partially separated in acidic methanolic BGEs, and not separated in pH=2.5 aqueous BGEs with HxDAS. It is not surprising to note that the complexation strength between weak bases and HxDAS is much stronger in acidic aqueous BGEs than in acidic methanol BGEs, because HxDAS is less dissociated in acidic methanol BGEs than that in acidic aqueous BGEs, and because methanol is expected to reduce the extent of inclusion of analyte into the cavity of the CD.

(v) The structure of the background electrolyte co-ion and counter-ion also plays

important roles in enantiomer separations. The anionic effective mobilities of neutral analytes increase as the concentration of HxS or HxDAS or HxDMS is increased in pH=9.5 BGEs (ethanolamine / MSA), but the increase is smaller than in the corresponding pH=2.5 (H_3PO_4 / LiOH) BGEs, indicating that components of the ethanolamine / MSA buffer compete with the neutral analytes more strongly than components of the H_3PO_4 / LiOH buffer.

In conclusion, three novel, single-isomer, sulfated cyclodextrins, the sodium salts of hexakis(6-*O*-sulfo)-α-cyclodextrins (HxS), hexakis(2,3-di-*O*-acetyl-6-*O*-sulfo)-α-cyclodextrins (HxDAS), hexakis(2,3-di-*O*-methyl-6-*O*-sulfo)-α-cyclodextrins (HxDMS), have been produced on the large scale with greater than 98% isomeric purity. They have been successfully used as chiral resolving agents for capillary electrophoretic separation of the enantiomers of neutral, weak acid, weak base and ampholytic analytes in aqueous and methanolic BGEs. HxS, HxDAS and HxDMS have been shown to offer unique mobility and separation selectivity trends as compared to other single-isomer, sulfated CDs.

REFERENCES

[1] T. J. Ward, Anal. Chem. 66 (1994) 633A.

[2] J. McMurry, Organic Chem., Fifth Edition Brooks/COLE, 1999.

[3] W. E. Camp, J. Pharm. Biomed. Anal. 11 (1993) 1167.

[4] FDA Policy, Statement for the Development of New Stereo-isomeric Drugs, Washington, DC, May 1992.

[5] A. M. Abushoffa, M. Fillet, A. C. Servais, P. Hubert, J. Crommen, Electrophoresis 24 (2003) 343.

[6] F. Yasuhara, M. Takeda, Y. Ochiai, Chem. Lett. 2 (1992) 251.

[7] C. Petterson, J. Chromatogr. 316 (1984) 553.

[8] S.C. Chang, L. R. Wang, D. W. Armstrong, J. Liq. Chromatogr. 15 (1992) 1411.

[9] K. Balmer, A. Persson, P. Lagerstrom, B. Personn, G. Schill, J. Chromatogr. A 553 (1991) 391.

[10] C. B. Ching, B. G. Lim, E. J. D. Lee, S. C. Ng, Chirality 4 (1992) 174.

[11] A. Ishikawa, T. Shibata, J. Liq. Chromatogr. 16 (1993) 859.

[12] V. L. Herring, J. A. Johnson, J. Chromatogr. A 612 (1993) 215.

[13] M. Hoshino, K. Yajima, Y. Suzuki, A. Okahira, J. Chromatogr. B 661 (1994) 281.

[14] J. P. McCarthy, J. Chromatogr. A 685 (1994) 349.

[15] C. C. Chen, C.E. Lin, J. Chromatogr. Sci. 33 (1995) 229.

[16] S. C. Sharma, M. B. Evans, S. J. Evans, J. Pharm. Biomed. Anal. 13 (1995) 129.

[17] I. Fitos, J. Visy, M. Simonyi, J. Hermansson, J. Chromatogr. A 709 (1995) 265.

[18] J. B. Esquivel, C. Sanchez, M. J. Fazio, J. Liq. Chromatogr. 21 (1998) 777.

[19] M. Kummer, G. Werner, J. Chromatogr. A 825 (1998) 107.

[20] R. C. Williams, J. H. Miyawa, R. J. Boucher, R. W. Brockson, J. Chromatogr. A 844 (1999) 171.

[21] H. Kanazawa, Y. Kunito, Y. Matusushima, S. Okubo, F. Mashige, J. Chromatogr. A 871 (2000) 181.

[22] S. Hara, A. Dobashi, K. Kinoshita, T. Hondo, M. Saito, M. Senda, J. high Resolut. Chromatogr. 371 (1986) 153.

[23] M. Maftouh, Spectra Anal. 199 (1997) 25.

[24] S. Maver, X. Briand, E. Francotte, J. Chromatogr. A 875 (2000) 331.

[25] D. Wistuba, V. Schurig, J. Chromatogr. A 875 (2000) 255.

[26] S. Fanali, J. Chromatogr. A 792 (1997) 227.

[27] B. Chankvetadze, J. Chromatogr. A 792 (1997) 269.

[28] G. Gubitz, M. G. Schmid, J. Chromatogr. A 792 (1997) 179.

[29] K. Verleysen, P. Sandra, Electrophoresis 19 (1998) 2798.

[30] M. Nielen, Anal. Chem. 65 (1993) 885.

[31] T. E. Peterson, J. Chromatogr. A 630 (1993) 353.

[32] S. Palmarsdottir, L. –E. Edholm, J. Chromatogr. A 666 (1994) 337.

[33] S. Fanali, J. Chromatogr. A 875 (2000) 89.

[34] M. G. Vargas, Y. Vander Heyden, M. Maftouh, D. L. Massart, J. Chromatogr. A 855 (1999) 681.

[35] C. Perrin, M. G. Vargas, Y. Vander Heyden, M. Maftouh, D. L. Massart, J. Chromatogr. A 883 (2000) 249.

[36] S. Fanali, P. Bocek, Electrophoresis 11 (1990) 757.

[37] E. Gassman, J. E. Kuo, R. N. Zare, Science 230 (1985) 813.

[38] M. Acs, Tetrahedron Lett. 41 (1985) 2465.

[39] E. Kuhn, S. Hoffstetter-Kuhn, Chromatographia 34 (1992) 505.

[40] B. Chankvetadze, G. Endrez, G. Blaschke, Electrophoresis 15 (1994) 804.

[41] A. Guttman, Electrophoresis 16 (1995) 1900.

[42] I. Bechet, P. Paques, M. Fillet, P. Hubert, J. Crommen, Electrophoresis 15 (1994) 818.

[43] K. H. Assi, A. M. Abushoffa, K. D. Altria, B. J. Clark, J. Chromatogr. A 817 (1998) 83.

[44] M. Fillet, L. Fotsing, J. Bonnard, J. Crommen, J. Pharm. Biomed. Anal. 18 (1998) 799.

[45] B. Chankvetadze, Trends Anal. Chem. 18 (1999) 485.

[46] B. Chankvetadze, G. Pintore, N. Burjanadze, D. Bergental, K. Bergander, J. Breitkenuze, C. Muhlenbrock, G. Blaschke, J. Chromatogr. A 875 (2000) 455.

[47] I. E. Valko, H. Siren, M. L. Riekkola, J. Microcol. Sep. 11 (1999) 199.

[48] J. H. Knox, I. H. Grant, Chromatographia 24 91987) 135.

[49] V. Pretorius, B. J. Hopkins, J. D. Schielke, J. Chromatogr. 99 (1974) 23.

[50] J. L. Beckers, P. Bocek, Electrophoresis 24 (2003) 518.

[51] Z. Ryslavy, P. Bocek, M. Deml, J. Janak, J. Chromatogr. 144 (1977) 17.

[52] R. H. P. Rcid, J. Chromatogr. A 669 (1994) 151.

[53] J. C. Reijenga, E. Kenndler, J. Chromatogr. A 659 (1994) 403.

[54] J. C. Reijenga, E. Kenndler, J. Chromatogr. A 659 (1994) 417.

[55] W. X. Huang, S.D. Fazio, R. V. Vivilecchia, J. Chromatogr. A 781 (1997) 129.

[56] W. X. Huang, H. Xu, S.D. Fazio, R. V. Vivilecchia, J. Chromatogr. B 695 (1997) 157.

[57] D. W. Armstrong, L. W. Chang, S. S. C. Chang, J. Chromatogr. A 793 (1998) 115.

[58] D. W. Armstrong, K. L. Rundlett, J. Liq. Chromatogr. 18 (1995) 3659.

[59] T. J. Ward, T. M. Oswald, J. Chromatogr. A 792 (1997) 309.

[60] U. B. Nair, D. W. Armstrong, W. L. Hinze, Anal. Chem. 70 (1998) 1059.

[61] D. W. Armstrong, U. B. Nair, Electrophoresis 18 (1997) 2331.

[62] M. P. Gasper, A. Berthod, U. B. Nair, D. W. Armstrong, Anal. Chem. 68 (1996) 2501.

[63] M. Chiari, V. Desperati, E. Manera, R. Longhi, Anal. Chem. 70 (1998) 4967.

[64] E. De Lorenzi, G. Massolini, P. Molinari, C. Galbusera, R. Longhi, C. Marinzi, R. Consonni, M. Chiari, Electrophoresis 22 (2001) 1373.

[65] G. E. Barker, P. Russo, R. A. Hartwick, Anal. Chem. 64 (1992) 3024.

[66] S. Busch, J. C. Kraak, H. Poppe, J. Chromatogr. A 635 (1993) 119.

[67] E. Billiot, J. Macossay, S. Thibodeaux, S.A. Shamsi, I. M. Warner, Anal. Chem. 70 (1998) 1375.

[68] J. T. Smith, Z. El Rassi, J. Chromatogr. A 685 (1994) 131.

[69] M. S. Pena, Y. L. Zhang, I. M. Warner, Anal. Chem. 69 (1997) 3239.

[70] M. Stefamson, M. Novotny, Anal. Chem. 66 (1994) 3466.

[71] R. M. C. Sutton, K. L. Sutton, A. M. Stalcup, Electrophoresis 18 (1997) 2297.

[72] S. Fanali, J. Chromatogr. A 474 (1989) 441.

[73] G. Vigh, A.D. Sokolowski, Electrophoresis 18 (1997) 2305.

[74] B. Chankvetadze, G. Endresz, G. Blaschke, Chem. Soc. Rev. 25 (1996) 141.

[75] K. D. Altria, P. Harkon, M. G. Hindson, J. Chromatogr. B 686 (1996) 103.

[76] A. Nardi, A. Eliseev, P. Bocek, S. Fanali, J. Chromatogr. A 638 (1993) 247.

[77] H. Nishi, J. High Resolut. Chromatogr. 18 (1995) 659.

[78] X. F. Zhu, B. C. Lin, Electrophoresis 20 (1999) 1887.

[79] B. Koppenhoefer, J. Chromatogr. A 793 (1998) 153.

[80] Z. Aturki, C. Desiderio, L. Mannina, S. Fanali, J. Chromatogr. A 817 (1998) 91.

[81] G. Li, X. Lin, C. Zhu, A. Hao, Y. Guan, Anal. Chim. Acta 421 (2000) 27.

[82] B. Chankvetadze, Enantiomer 2 (1997) 157.

[83] T. Schmitt, H. Engelhardt, Chromatographia 37 (1993) 475.

[84] T. Schmitt, H. Engelhardt, J. Chromatogr. A 697 (1995) 561.

[85] S. Fanali, E. Camera, Chromatographia 43 (1996) 247.

[86] F. Lelievre, P. Gareil, A. Jardy, Anal. Chem. 69 (1997) 385.

[87] S. Terabe, Trends Anal. Chem. 8 (1989) 129.

[88] Y. Tanaka, S. Terabe, J. Chromatogr. A 781 (1997) 151.

[89] F. Lelievre, C. Gueit, P. Gareil, Y. Bahaddi, M. Galons, Electrophoresis 18 (1997) 891.

[90] F. wang, M. G. Khaledi, Electrophoresis 19 (1998) 2095.

[91] F. O'keefe, S. A. Shamsi, R. Daray, P. Schwinte, I. M. Warner, Anal. Chem. 69 (1997) 4773.

[92] G. Schulte, B. Chankvetadze, G. Blaschke, J. Chromatogr. A 771 (1997) 259.

[93] C. Dette, S. Ebel, S. Terabe, Electrophoresis 15 (1994) 799.

[94] S. Mayer, V. Schurig, Electrophoresis 15 (1994) 835.

[95] B. Chankvetadze, G. Endresz, D. Bergental, G. Blaschke, J. Chromatogr. A 717 (1995) 245.

[96] B. Chankvetadze, G. Endresz, G. Blaschke, J. Chromatogr. A 704 (1995) 234.

[97] W. Wu, A. M. Stalcup, J. Liq. Chromatogr. 18 (1995) 1289.

[98] A. M. Stalcup, K. H. Gahm, Anal. Chem. 68 (1996) 1360.

[99] J. Szeman, K. Ganzler, A. Salgo, J. Szejtli, J. Chromatogr. A 728 (1996) 423.

[100] E. C. Rickard, R. J. Bopp, D. J. Skanchy, K. Chetwyn, B. Pahlen, J. F. Stobaugh, Chirality 8 (1996) 108.

[101] G. Weseloh, H. Bartsch, W. A. Honig, J. Microcol. Sep. 7 (1995) 355.

[102] J. B. Vincent, D. M. Kirby, T. V. Nguyen, G. Vigh, Anal. Chem. 69 (1997) 4419.

[103] J. B. Vincent, A. D. Sokolowski, T. V. Nguyen, G. Vigh, Anal. Chem. 69 (1997) 4226.

[104] H. Cai, T. V. Nguyen, G. Vigh, Anal. Chem. 70 (1998) 580.

[105] W. Zhu, G. Vigh, Electrophoresis 24 (2003) 351.

[106] W. Zhu, G. Vigh, J. Chromatogr. A 987 (2003) 459.

[107] W. Zhu, G. Vigh, Anal. Chem. 72 (2000) 310.

[108] W. Zhu, G. Vigh, J. Microcol. Sep. 12 (2000) 167.

[109] W. Zhu, G. Vigh, J. Chromatogr. A 892 (2000) 499.

[110] M. B. Busby, P. Lim, G. Vigh, Electrophoresis 24 (2003) 351.

[111] M. B. Busby, O. Maldonado, G. Vigh, J. Chromatogr. A 990 (2003) 63.

[112] M. B. Busby, O. Maldonado, G. Vigh, Electrophoresis 23 (2002) 456.

[113] D. K. Maynard, G. Vigh, Electrophoresis 22 (2001) 3212.

[114] S. Terabe, K. Otsuka, T. Ando, Anal. Chem. 57 (1985) 834.

[115] C. L. Copper, M. J. Sepaniak, Anal. Chem. 66 (1994) 147.

[116] S. G. Penn, D. M. Goodall, J. S. Loran, J. Chromatogr. A 636 (1993) 149.

[117] S. A. C. Wren, R. C. Rowe, J. Chromatogr. 603 (1992) 235.

[118] S. G. Penn, E. T. Bergstron, D. M. Goodall, Anal. Chem. 66 (1994) 2866.

[119] B. A. Williams, G. Vigh, J. Chromatogr. A 777 (1997) 295.

[120] D. H. Russell, R. D. Edmondson, J. Mass Spectr. 32 (1997) 263.

[121] W. K. Russell, D. H. Russell, M. B. Busby, A. Kolberg, S. Li, D. K. Maynard, S. Sanchez-Vindas, W. Zhu, G. Vigh, J. Chromatogr. A 914 (2001) 325.

[122] G. Sheldrick, SHELXL-97 Program for Crystal Structure Refinement, Institut fur Anorganische Chemie der Universtat, Tammanstrasse 4, D-3400 Gottingen, Germany, 1997.

[123] Insight II, Modeling Environment, Molecular Simulations Inc., San Diego, 2000.

[124] K. Takeo, H. Mitoh, K. Uemura, Carbohydr. Res. 187 (1989) 203.

[125] B. A. Williams, G. Vigh, Anal. Chem. 69 (1997) 4445.

[126] W. Friedl, J. C. Reijienga, E. Kenndler, J. Chromatogr. A 709 (1995) 163.

[127] M. S. Bello, R. Rezzonico, P. G. Righetti, J. Chromatogr. A 659 (1994) 199.

[128] E. Kenndler, in M. Khaledi (editor) High Performance Capillary Electrophoresis, Wiley-Interscience, New York, 1998. P. 31.

[129] S. L. Li, G. Vigh, Electrophoresis 24 (2003) 2487.

[130] K. D. Altria, S. M. Bryant, Chromatographia 46 (1997) 122.

[131] F. Wang, M. G. Khaledi, J. Chromatogr. A 875 (2000) 277.

[132] F. Steiner, M. Hassel, Electrophoresis 21 (2000) 3994.

[133] Y. Walbroehl, J. W. Jorgenson, J. Chromatogr. 315 (1984) 135.

[134] K. Sarmini, E. Kenndler, J. Chromatogr. A 806 (1998) 325.

[135] K. Sarmini, E. Kenndler, J. Chromatogr. A 811 (1998) 201.

[136] K. Sarmini, E. Kenndler, J. Chromatogr. A 833 (1999) 245.

[137] I. E. Valko, H. Siren, M. L. Riekkla, J. Chromatogr. A 737 (1996) 263.

[138] I. E. Valko, H. Siren, M. L. Riekkla, Electrophoresis 18 (1997) 919.

[139] H. Cai, G. Vigh, J. Pharm. Biomed. Anal. 18 (1998) 615.

APPENDIX

SYNTHESIS PROTOCOL FOR SINGLE-ISOMER SULFATED a-CYCLODEXTRINS

Hexakis (6-*O*-tert-Butyldimethylsilyl)-a-Cyclodextrin

1. Dry native α-CD in a vacuum oven at 80 C to constant weight.

2. With minimum exposure to air, add 6 L of anhydrous DMF, 444.4 g imidazole and 16.4 g 4-N',N-dimethylamino pyridine (DMAP), to the 24 L three-neck flask. Stir until there is a clear, light yellow solution. While swirling the funnel around, add 1000 g hot, dry α-CD, taken directly from the vacuum oven, through the funnel into the flask.

3. Dropwise adding 1390 mL of anhydrous dichloromethane solution containing 463.5 g TBDS chloride into the flask through the addition funnel. Another batch of 1854 mL anhydrous dichloromethane containing 463.5 g TBDS chloride were dropwise adding at a rate of 1s/drop. The total reaction time was 20 days.

4. Once 6 equivalents of TBDS chloride have been added, monitor progress of the reaction by TLC which use 2.5x10 cm aluminum-backed Silica 60 plates) and 50 :10 :1 $CHCl_3$: MeOH : H_2O as run solvent. Once TLC indicates that the amount of the undersilylated, pentakis(TBDS)-α CD is much less than that of the target compound ($TBDS_6$ α-CD), continue monitoring the reaction by isocratic HPLC.

5. Adding a 10μL sample of the reaction mixture, 2mL dichloromethane and 20μL methanol to a glass vial to quench the reaction by letting it stand for 15 min, analyze the sample by isocratic HPLC, at room temperature, using a 4.6 mm x 250 mm C18 column (5 μm Luna II C18 or Zorbax or similar) and 20 : 80 ethylacetate : methanol eluent at 2mL/min. The total separation time should be less than 20 min.

6. Once the reaction is judged complete, quench it by adding 50mL methanol for each mole of

TBDS chloride introduced in excess of the 6 moles of TBDS chloride per mole of α-CD. Continue stirring the reaction mixture for another hour. Add enough dry dichloromethane to the reaction mixture to bring the ratio of dry dichloromethane to dry α CD to 6mL/g.

7. Washing the reaction mixture with deionized water several times until the imidazole salts were completely removed. Rotovap the dichloromethane solution to dryness.

8. Purify the $TBDS_6$ α CD collected in Step 7 by using methylethylketone as recrystallization solvent (8mL MEKT/g of CD). Heat and reflux until obtain clear solution. Let cool down to room temperature overnight. Filter collect crystal and analyze both the crystals (dissolve 20 mg in 5mL dichloromethane) and the methyl ethyl ketone mother liquor by isocratic HPLC as in Step 5. Typical purity values for the crystal are as follows: undersilylated:< 0.1%, target $TBDS_6$ α CD: > 99.5%, oversilylated: <0.5%.

9. Dry the material in a vacuum oven at low temperature to constant weight. Store the dried material under anhydrous conditions.

Hexakis (2,3-di-*O*-Acetyl-6-tert-Butyldimethylsilyl)-a-Cyclodextrin

1. Dry the pure, hexakis(6-*O*-tert-butyldimethylsilyl) cyclomaltohexaose, $TBDS_6$-α CD in a vacuum oven at 80°C to constant weight.

2**.** Add 400mL anhydrous ethyl acetate, 155mL anhydrous pyridine, and 164mL acetic anhydride to a three-neck flask. While stirring, add, through a wide-bore plastic funnel, 200g dry, $TBDS_6$-α CD. And 11.7g 4-N,N-dimethylamino pyridine (DMAP) as catalyst. The reaction mixture should become clear, and slightly yellow. The temperature will increase to

about 40 C, increase and maintain the temperature of the reaction mixture between 50-55°C, and continue stirring for 10 to 12 hours.

3. Monitor the progress of the reaction. Add a 10μL aliquot of the original reaction mixture and 4mL of methanol to the vial. Analyze the sample by reversed-phase HPLC with a mixture of 20:80 ethyl acetate : methanol as eluent. The total analysis time should be about 15 min. The target material elutes between 8 and 11 min.

4. Quench the reaction by adding 19mL of ethanol once the reaction complete at room temperature. Keeping stir about 2-3 hours.

5. Wash the reaction mixture with deionized water (1:1 volume ratio of water and reaction mixture) three times. And then wash the organic layers with acidic solution which prepared by adding 15.4mL acetic acid to enough water, to obtain the same volume of reaction mixture. Again, wash the acidic organic layer with deionized water several times to neutral. Rotovap the organic solution with the water bath at 50°C to dryness.

6. Using DMF as the recrystallization solvent to purify the crude product obtained in step 5 (1mL DMF/g CD). Heat and regulate the temperature of the solution between 55-60°C. Once a clear solution is obtained, let the solution cool to room temperature to obtain white precipitate product. Filter and collect the solid. Check the purity of the product by HPLC as in Step 3. The purity of the target product should be > 99.5%.

Hexakis (2,3-di-*O*-Acetyl-6-Hydroxy)-a-Cyclodextrin

1. Place hexakis(2,3-diacetyl-6-*O*-tert-butyldimethylsilyl)cyclomaltohexaose, $Ac_{12}TBDS_6$-α

CD, into a vacuum oven and dry it at 80°C to constant weight.

2. Add 800mL dichloromethane (reagent grade) to the one-neck round bottom flask. While vigorously stirring in a well-ventilated hood, gradually add 200g $Ac_{12}TBDS_6$-α CD to the flask and obtain a clear solution. Add 87.8mL BF_3-etherate to the flask. Stir the reaction mixture for 28 hours.

3. Check progress of the reaction by TLC. Use Silica 60 plates and 50 :10 :1 $CHCl_3$: MeOH : H_2O as run solvent yielding R_f = 0.33 for the target component.

4. As soon as the reaction is completed, transfer the reaction mixture into a 4L sep funnel. Add 1000mL of water to hydrolyze BF_3. Carefully shake the funnel for about 5 seconds, then immediately, but carefully relieve the built-up pressure (mostly ethyl ether and dichloromethane vapors). Repeat the shaking and pressure release steps until there is no more pressure build-up.

5. Dissolve 8.74g $NaHCO_3$ in 50mL water. Add the saved organic layer and the $NaHCO_3$ solution to the 4 L sep funnel. Carbon dioxide will evolve as neutralization occurs. Carefully, but thoroughly shake the sep funnel to neutralize the last traces of HF. Separate the phases, save the organic phase and dispose the aqueous phase as waste. Wash the organic layer with 400mL deionized water twice.

6. Concentrate the combined dichloromethane solution on a Rotovap to 1/4 of its original volume. While vigorously stirring, pour the concentrated dichloromethane solution into the beaker containing 700mL hexane to obtain a solid material. Analyze the solid by isocratic aqueous reversed-phase HPLC, at 40 C, using a 4.6mm x 250mm C18 column and a mixture of 52 : 48 methanol : water as eluent at 1.2mL/min. The total analysis time are in 20 min. The overacetylated material elutes before the target, Ac_{12} –αCD.

7. Add 200 mL acetone into a 1 L round bottom flask. Add the solid $Ac_{12}TBDS_6$–αCD collected in Step 6 above to the flask. Place the flask onto a Rotovap and heat it until the solution becomes clear. Distill off 50mL of the solvent, the remaining solution will become a slurry. Allow the slurry to cool to room temperature and filter it to collect the crystals. Analyze the crystals by HPLC as in Step 6. Repeat the crystallization process (step 7) until the purity of the product is > 99.5%.

12. Place the pure Ac_{12} -α-CD into a vacuum oven and keep it at room temperature over night to dryness an store the material in a desiccator.

Hexakis (2,3-di-*O*-Acetyl-6-*O*-Sulfo) - a -Cyclodextrin (HxDAS)

1. Place hexakis(2,3-diacetyl-6-hydroxy) cyclomaltohexaose, Ac_{12} α CD, into a vacuum oven and dry it at 60°C to constant weight.

2. Add 800mL anhydrous DMF and 33 mL anhydrous pyridine to a 2L, one-neck, round-bottom flask. While stirring, slowly add, through a wide-bore, plastic funnel, 400g recrystallized, dry Ac_{12} α-CD. Keeping stir until the cyclodextrin is dissolved. Through a wide-bore plastic funnel, add 310g SO_3-Py complex and let it react for 6 hours at room temperature.

3. Monitor progress of the reaction by indirect UV detection CE. Background electrolyte: 20 mM para-toluenesulfonic acid (pTSA) titrated to pH 3.5 with β- alanine, - to + polarity, 10 kV applied potential, 19/26 cm effective/total length, 25μm I.D., naked fused silica capillary, at 20°C.

4. Prepare a slurry with 344 g of sodium hydrogen carbonate in 440mL of hot water. Transfer

the reaction mixture into a 3 L beaker with a 4" flat stir bar. SLOWLY add the bicarbonate slurry to the stirred reaction mixture until there is no more bubble formation. Keep adding sodium bicarbonate to get a basic solution. Filter-off solid sodium sulfate and excess sodium bicarbonate.

5. Transfer the solution into a 3L, one-neck, round-bottom flask and rotovap the solution to dryness, in a high-vacuum rotovap, at 50°C.

6. Dissolve the solid in a minimum amount of hot water. To as many as required 4 L beakers, add 2.5 L of isopropanol (IPA). While stirring, add slowly 500mL of the reaction mixture to remove any remaining DMF (5mL IPA per 1mL of reaction mixture). Let the solid descend to the bottom of the beaker (this can take several hours). Filter and obtain the solid.

7. Check for purity by CE as in step 4. Check the removal of the DMF by ^{1}H NMR. If needed, repeat Step 6.

8. Dissolve the solid with minimum amount of hot water and rotovap it to dryness in a high-vacuum rotovap at 50°C.

Hexakis (6-*O*-Sulfo) a-Cyclodextrin (HxS)

1. Add 117 g NaOH into a 1L beaker. Place the beaker into an ice/water bath, on a stir plate. While stirring, add 300mL of water. Keep stirring until a clear solution is obtained.

2. Into a 4 L beaker, add 630mL of 50°C deionized water. Place the beaker on a heating/stirring plate. While stirring, add 500g HxDAS. Once the HxDAS is dissolved, slowly add the solution prepared in step 1. Let it stir for 1 to 2 h

3. Monitor reaction progress by CE (indirect UV detection). Background electrolyte: 13 mM TEMED titrated with phthalic acid to pH 5.5, - to + polarity, 10 kV applied potential, 19/26 cm effective/total length, 25μm I.D., naked fused silica capillary, at 20°C.

4. To as many as required 4 L beakers, add 3 L methanol. While stirring, slowly pour 430mL of the reaction mixture into methanol (6.7mL methanol per 1mL of reaction mixture). A white solid forms which is collected by filtration, after it settle to the bottom of the beaker. Filter and obtain solid.

5. Dissolve the solid obtained in step 4 in hot water (2mL of water per 1g solid). Titrate the solution to pH 7 using a calibrated pH meter, by slowly adding DOWEX cation exchange resin in the H^+ form. The solid resin is then filtered from the solution.

6. Precipitate HxS by adding the solution into methanol (4mL of methanol per 1mL of solution). Analyze the solid by CE as in step 3.

7. Dissolve the solid obtained in step 6 in hot water (1mL of water per gram of solid). Precipitate HxS as in step 6, to remove last traces of sodium acetate. Repeat the step if needed it.

8. Place the solid into crystallizing dishes and dry it in a vacuum oven at 60°C, until constant weight is achieved.

Hexakis(2,3-di-*O*-Methyl-6-*O*-t-Butyldimethylsilyl) a-Cyclodextrin

1. Pure heakis(6-O-t-butyldimethylsilyl)cyclomaltohexaose, $TBDS_6$-α-CD, is dried in a vacuum oven at 90°C to a constant weight.

2. In a well ventilated hood, flame dry a 4-L, three neck, round bottom flask equipped with a 4" teflon- coated stir bar, a dry source of N_2 gas at one neck and, at another neck, an oil bubbler with 1" of paraffin oil. The oil bubbler is connected to the reaction flask through a valved adapter with tubulation. The third neck is capped with a ground glass stopper of appropriate size.

3. Weigh 10.43 g of NaH into the above dried 4-L three necks flask, and then cannulate750mL of dried THF to this reaction flask. Lower the reaction flask into a dry paraffin oil bath before proceeding further. In another oven dried, 3-L, round bottom flasks weigh 50-g of $TBDS_6$-α-CD. Canulate 2,000-mL from a septum capped, dried THF container to the 3-L round bottom flask containing the $TBDS_6$-α-CD. Canulate 33.8mL of iodomethane from a septum capped container to the 3-L round bottom flask containing the $TBDS_6$-α-CD and THF. Once the transfer of the reaction solvent is complete, place an oven dried 500mL self- equilibrating funnel equipped with a septum at its fill spout to one of the reaction flask neck. Next, in a smooth motion, place the oil bubbler outlet onto a Liebig condenser and fit the condenser to the reaction flask.

4. Canulate one- fihth of the $TBMS_6$-α-CD/ CH_3I/ THF solution into the self- equilibrating funnel. Equip the Liebig condenser with a recirculating ice water bath. Make certain that the oil bath has a volume large enough to exceed the height of the reaction solvent by a full two inches.

5. While vigorously stirring the hydride/ THF slurry, add the solution from the addition funnel at the rate of a thin but steady stream. Hydrogen evolution will be observed at the oil bubbler in less than 1-2 minutes. During the addition, monitor the rate of hydrogen evolution, the rate

of reflux and the degree of foaming of the reaction mixture. Hydrogen evolution should be stabilized at around 1-2 bubbles every second, reflux should not exceed 1-2 drops per second and foaming should not be so great that the entire surface of the reaction mixture is thickly covered. All of these measures are monitored to ensure that the iodomethane (b.p. 42°C) is not allowed to escape the reaction apparatus. As each funnel is emptied, canulate another portion of the $TBMS_6$-α-CD/CH_3I/THF solution into the self-equilibrating funnel. The addition should be completed in approximately 60 minutes. The reaction will be complete in another 360 minutes and should be monitored rigorously by using a 5μm Luna C18 RP-HPLC column with a 65:35 MeOH : EtOAc isocratic mobile phase at 2mL/min.

6. Once the reaction is judged complete, quench it with the slow addition of 4.4mL of anhydrous ethanol through the addition funnel over a period of 15- to 20 minutes. Allow the quenched solution to continue stirring for another hour.

7. Filter the quenched reaction solution to remove the precipitated NaI. Rotovap the fitrate. The water bath should be kept at approximately 50°C to prevent the formation of an amorphous solid. Beware that the solution bumps violently as more NaI precipitates. Filter as necessary. Once the crude product begins precipitating, continue to rotovap at the specified temperature until no more solvent condenses into the collection vessel. At this point it is safe to increase the temperature to rotovap all of the solvent away.

8. Add 2200 mL ethanol : H_2O (1:10 v:v) mixture to to a 4-L one-neck round bottom flask. Add the crude product (containing trace NaI salt and cyclodextrin impurities) 200 g to the flask through a plastic funnel. Warm the slurry (keep 50°C) for 30 min. Turn off the Varic and let the slurry cool down to room temperature. Filter off the $Me_{12}TBDS_6$ α-CD from the mother liquor

Wash the filter cake while on the funnel with 10mL ice-cooled ethanol : H_2O solvent. Analyze both crystal and mother liquor by isocratic RP-HPLC as step 5.

9. Once the salt was completely removed, then add 475mL ethanol to a 2-L one-neck round bottom flask. Add the $Me_{12}TBDS_6$ α-CD collected in step 8 (about (190 g) to the flask through the funnel. Heating the slurry to reflux for 2 hrs. Turn off the Varic and let the flask cool overnight to form the final crystals. Filter off the $Me_{12}TBDS_6$ α-CD from the mother liquor ethanol. Wash the filter cake while on the funnel with 10mL ice-cooled ethanol. Analyze both crystal and mother liquor by isocratic RP-HPLC as step 5. Typically purity value for the crystal is: target $Me_{12}TBDS_6$ α-CD : >99.6%.

10. Dry the material in a vacuum at temperature 80°C until constant weight. Storied the dried material.

Hexakis(2,3-di-*O*-Methyl)-a-Cyclodextrin

1. In a 4-L polyethylene beaker containing 1.5-L of anhydrous ethanol while magnetically stirring with a 4" teflon coated stir bar. After all $Me_{12}TBDS_6$-α-CD has dissolved (about 1 hour), slowly add, over a period of 20 minutes, 142.8mL of 48% aqueous HF solution. Cover the beaker with aluminum foil and allow to stir 24 hrs. Check the completeness of the reaction by TLC using 2.5x10 cm Silica 60 plates and 50 :10 :1 $CHCl_3$: MeOH : H_2O as run solvent.

2. When the reaction is judged complete, take a 50mL aliquot and place it in a clean, polyethylene beaker. Next, place the reaction flask in an ice bath and allow to cool for half hour. Add a solution of 10mg of phenolpthalein in 1mL ethanol. Quench the reaction by slow

addition of a 5M aqueous solution of NaOH in ethanol over the period of about 1 hour. The quench solution is prepared by dissolving 144.54g of NaOH pellets in 128mL of deionized water. This solution is cooled to room temperature before adding it dropwise to 600mL of anhydrous ethanol. Use the aliquot taken in step 2 to ensure that the reaction mixture is titrated to the proper endpoint indicated by the faintest detectable pink color.

3. Once the solution is quenched, filter the NaF precipitate and wash the filter cake with 3 x 50mL of ice-cold, anhydrous ethanol. Rotovap the filtrate to dryness while filtering the NaF precipitate as needed and properly washing the filter cake. Continue to rotovap in a boiling water bath until dryness.

4. In a 5-L flask add the crude material 80 g to a 320mL of DMF-water (1:1 v:v) mixture and reflux while stirring for about an hour. Then turn off the Varic and add 20mL acetone to the solution, and let the solution cool overnight to get final product. Filter off the Me_{12} α-CD from the mother liquor DMF-water-acetone. Wash the filter cake while on the funnel with 10mL ice-cooled acetone. Continue recrystallization until no more t-butyldimethyl flouride peaks are observed in the ^{1}H- NMR and the product is of desired isomeric purity. Analyze both crystal and mother liquor by using a 5μm Luna C18 RP-HPLC column with a 75:25 MeOH: H_2O isocratic mobile phase at 1.2mL/min with temperature 50°C. Typically purity value for the crystal is: target Me_{12} -α-CD : >99.6 %.

10.Dry the pure material in a 100°C in a vacuum oven to a constant weight. Storied the dried material.

Hexakis(2,3-di-*O*-Methyl-6-*O*-Sulfo)-a-Cyclodextrin

1. Place 120g recrystallized, pure, hexakis(2,3-O-methyl-6-hydroxy) cyclomaltohexaose, $Me_{12}\alpha$-CD, into a vacuum oven and dry it at 60°C to constant weight.

2. Add 500mL anhydrous DMF and 11mL anhydrous pyridine to a 2L, one-neck, round-bottom flask. While stirring, slowly add, through a wide-bore, plastic funnel; 100g recrystallized, dry $Me_{12}\alpha$-CD. Close the flask with a glass stopper and stir until the cyclodextrin is dissolved.

3. Through a wide-bore plastic funnel, add 100 g SO_3-Py complex and let it react for 48 hours at room temperature.

4. Monitor progress of the reaction by indirect UV detection CE. Background electrolyte: 20 mM para-toluenesulfonic acid (pTSA) with 40mM tris(hydroxy)aminomethane (pH 8.3), + to - polarity, 10 kV applied potential, 19/26 cm effective/total length, 25μm I.D., naked fused silica capillary, at 20°C.

5. Prepare a slurry with 143 g of sodium bicarbonate in 175mL of hot water. Transfer the reaction mixture into a 3 L beaker with a 4" flat stir bar. SLOWLY add the bicarbonate slurry to the stirred reaction mixture until there is no more bubble formation. When final solution is basic, filter-off solid sodium sulfate and excess sodium bicarbonate. Rotovap the solution to dryness, in a high-vacuum rotovap, at 50°C.

6. Add a volume of anhydrous ethanol equal to 6 times the amount of water required to dissolve the material. The product will precipitate rapidly. Allow to cool and filter. Repeat the recrystallization with the same minimum volume of water and a 6 fold amount of anhydrous ethanol until DMF is no longer detectable by ^{1}H NMR. To remove Na_2SO_4, dissolve 100g of

recrystallized material in 25mL of deionized water and add 125mL ethanol and filter. Verify the success of SO_4^{2-} removal by indirect UV CE using the same BGE as the used for monitoring the completion of the reaction. This process will reduce the Na_2SO_4 contaminant to approximately 1% by mass. A more complete removal is accomplished by filtration from a 50mM solution in methanol. Once the material is deemed free of all sulfate, DMF and dimethylamine, transfer it to a 5L flask and add 500mL of deionized water. Rotovap the ethanol as its water azeotrope until the product appears completely dry. Check that all ethanol has been removed by ^1H NMR.

VITA

Shulan Li attended Shandong University of Building Material in Jinan, P.R. China, where she received her B.S. degree in 1989 and M.S. degree in 1992 at Shandong University. From 1999 to 2004, she attended Texas A&M University, in College Station, where she received her Ph. D. in chemistry in May 2004.

During her study at Texas A&M University, Shulan Li had four publications in the *Journal of Chromatography A*, and the *Electrophoresis*. She also presented posters on her work at three local conferences. At the 2003 IUCCP symposium, her poster was selected as the best poster in the Analytical Division.